Bulletin 36
Part 3
(of 7 Parts)

THE SHOCK AND VIBRATION BULLETIN

JANUARY 1967

A Publication of
THE SHOCK AND VIBRATION
INFORMATION CENTER
Naval Research Laboratory, Washington, D.C.

Office of
The Director of Defense
Research and Engineering

DISCLAIMER NOTICE

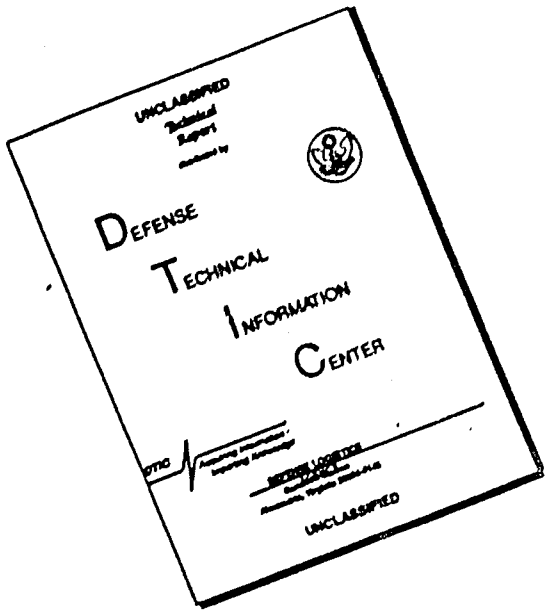

THIS DOCUMENT IS BEST QUALITY AVAILABLE. THE COPY FURNISHED TO DTIC CONTAINED A SIGNIFICANT NUMBER OF PAGES WHICH DO NOT REPRODUCE LEGIBLY.

Bulletin 36
Part 3
(of 7 Parts)

THE SHOCK AND VIBRATION BULLETIN

JANUARY 1967

A Publication of
THE SHOCK AND VIBRATION
INFORMATION CENTER
Naval Research Laboratory, Washington, D.C.

The 36th Symposium on Shock and Vibration was held in Los Angeles, California, on 18-20 October 1966. The U.S. Air Force was host.

Office of
The Director of Defense
Research and Engineering

SYMPOSIUM MANAGEMENT

The Shock and Vibration Information Center

William W. Mutch, Director

Henry C. Pusey, Coordinator

Rudolph H. Volin, Coordinator

Jean B. Goldbecker, Editor

Katherine G. Jahnel, Administrative Secretary

36th Program Committee

William R. Forlifer, NASA Goddard Space Flight Center

Edward H. Schell, Air Force Flight Dynamics Laboratory

George Stathopoulos, Naval Ordnance Laboratory

James M. Taylor, U.S. Army Missile Command

Air Force Liaison

Los Angeles Scientific and Technical Liaison Office, Research and Technology Division, Air Force Systems Command

Lt. Col. Kenneth W. Cook

Arthur E. Kimberly

Bulletin Production

Graphic Arts Branch, Technical Information Division, Naval Research Laboratory

CONTENTS

PART 3

Vibration Testing

PAPERS APPEARING IN PART 1
Part 1 - Confidential
(Titles Unclassified)

PAPERS APPEARING IN PART 5

Analysis and Prediction

PAPERS APPEARING IN PART 6

Data Analysis and Instrumentation

PAPERS APPEARING IN PART 7

Structural Reliability

Design Data and Methods

VIBRATION TESTING

USE OF FORCE AND ACCELERATION MEASUREMENTS IN SPECIFYING AND MONITORING LABORATORY VIBRATION TESTS

G. W. Painter
Lockheed-California Company
Burbank, California

The usual practice of basing vibration test specifications on an envelope of the equipment base acceleration levels experienced in the service environment can often result in excessive levels of overtesting. This results from the large difference between the mechanical impedance of the vehicle structure and that of a fully equalized shaker. A possible solution to the problem is the generation of test specifications that are based on the knowledge of both the accelerations and the forces transmitted to the equipment in the service environment.

Results are presented of a program devoted to the development of improved procedures for defining the vibration levels experienced by equipment attached to flight vehicles and providing realistic laboratory test levels. The program involved the measurement of the accelerations and forces experienced by simulated equipment attached to a vibrating aircraft fuselage. The equipment was later removed from the vehicle, placed on a shaker, and vibrated to a test specification based on an envelope of the acceleration peaks measured in the fuselage. Comparisons were then made of the acceleration levels that a resonant element in the equipment received in the fuselage and on the shaker. The tests on the shaker were repeated with the exception that, at those frequencies corresponding to an equipment resonance, the force transmitted to the equipment base was not allowed to exceed the maximum force developed (at any frequency) when the equipment was attached to the vibrating fuselage. It was found that this procedure largely eliminated the high levels of overtesting introduced by the conventional approach.

INTRODUCTION

Standard methods for specifying laboratory vibration tests often result in subjecting the equipment being tested to a damage potential that is much greater than it will experience in service. The overtesting involved arises from the practice of specifying laboratory test levels on the basis of an envelope of the acceleration peaks measured in the service environment and employing narrow-band equalization to eliminate any spectral notches that may result from equipment antiresonance effects during laboratory testing. This procedure, in effect, causes the shaker to present an infinite mechanical impedance to the attached equipment, while in the

G. W. Painter

service environment the impedance of the supporting structure may in some cases be less than that of the attached equipment.

In a previous paper [1], the author discussed the possibility that this problem could be resolved if the force transmitted to the equipment by the vehicle supporting structure could be measured both in the service environment and during laboratory testing. The suggested force measurements were to be performed in addition to the acceleration measurements normally taken. The referenced paper pointed out that it would be necessary for the force transducers to have very low mass and compliance to preclude the possibility of modifying the dynamic response of the system under study. The design and performance characteristics of an experimental washer type force transducer were described and it was reported that although experimental transducers fulfilled most of the requirements, additional development was required to reduce sensitivity to moment loading.

Efforts to measure both forces and accelerations experienced by equipment attached to a vehicle have continued since the presentation of the previous paper, but further developmental efforts to develop a satisfactory miniature transducer were discontinued when miniature quartz transducers became commercially available.

The present paper is derived from a Lockheed-sponsored program that had the following objectives:

1. To evaluate the accuracy of miniature quartz force transducers when they are used for the measurement of dynamic forces transmitted between equipment and supporting structure in an airplane;

2. To measure the forces and accelerations experienced by equipment attached to a typical vibrating aircraft structure and to determine the degree of overtesting that would be involved if laboratory vibration tests were based on an envelope of the measured acceleration peaks; and

3. To determine the degree of improvement in service environment simulation that can be realized if the laboratory test is correctly based on a knowledge of both the forces and accelerations that exist in the service environment.

FORCE TRANSDUCER EVALUATION

The initial phase of the program was devoted to an examination of the validity of the force measurements that could be obtained in a typical equipment-supporting structure combination. The force transducers used were obtained from the Kistler Instrument Corp. and are shown in Fig. 1. Although the manufacturer of the transducer supplied a detailed performance specification, this information was considered to be not necessarily applicable to the intended application. One would expect, for instance, to be able to reproduce the output versus applied axial force relation specified by the manufacturer if corroborative testing were carried out under idealized conditions which assured that a uniform axial load was applied. The loading conditions that would be imposed in a typical vehicle are complex combinations of moment, shear and axial loading. Other conditions that might affect transducer performance are supporting structure flexibility and attachment point misalignment.

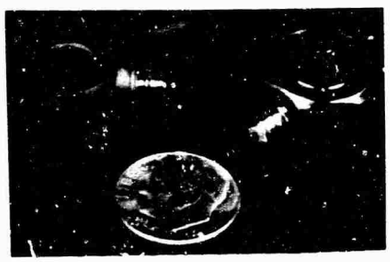

Fig. 1 - Force transducers

To examine the accuracy of the force transducers under loading conditions similar to those just described, the following experimental program was conducted.

A special structure was designed and built to simulate an equipment item. This structure, which will hereinafter be called the "equipment," is shown in Fig. 2. Its basic parts consisted of a base plate and a simply supported beam with a lumped mass in the center. The beam was attached to the base plate at each end through

Fig. 2 - Simulated equipment

flexures. A 15-ft long section of an F-104 fuselage was obtained to simulate a typical aircraft structure. An electrodynamic shaker was attached to the fuselage to provide vibratory excitation (Fig. 3). The interior of the fuselage incorporated a number of brackets for the attachment of various pieces of electronic equipment. One of these was chosen as the supporting structure for the simulated equipment mentioned previously. This bracket is shown in Fig. 4. Figure 5 shows the simulated equipment attached to it.

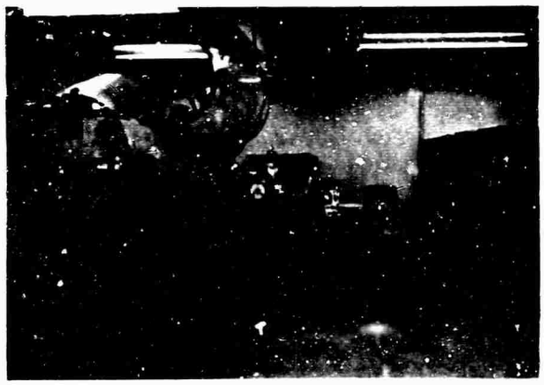

Fig. 3 - F-104 fuselage section with shaker attached

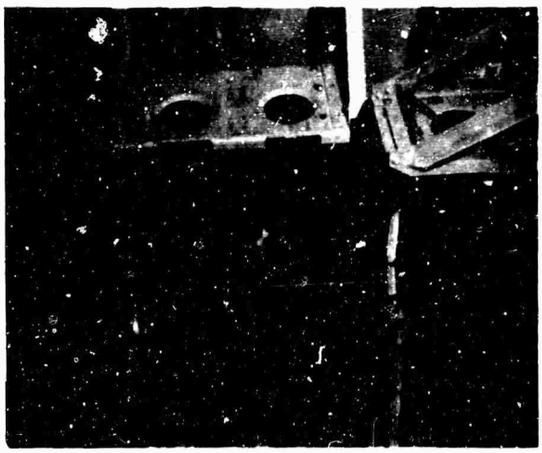

Fig. 4 - Equipment attachment bracket, position 1

Force transducers were placed between the base plate of the equipment and the supporting bracket at each of the four corners. Accelerometers were located at each of the four corners of the base plate, and an additional accelerometer

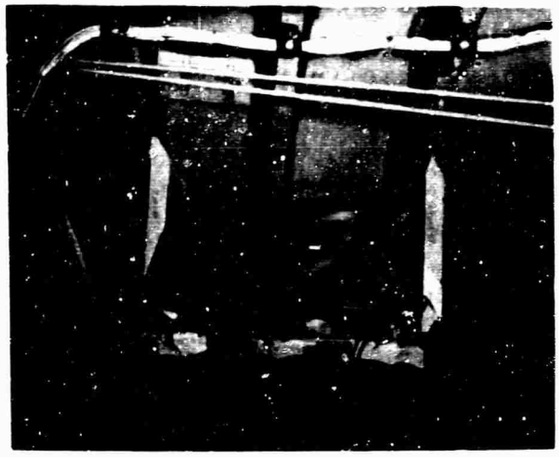

Fig. 5 - Simulated equipment attached to bracket, position 1

was attached on the lumped mass located at the center of the equipment beam.

This arrangement allowed sufficient information to be obtained to allow two independent determinations of the total normal force acting on the base of the equipment. One of these determinations could be made on the basis of the total signal produced by the force transducers. The second could be obtained from the acceleration signals and a knowledge of the equipment masses. Force measurements based on acceleration readings were readily obtained by an analog computer programmed to multiply the incoming acceleration signals by the appropriate constants (representing the base plate and beam masses) and to perform the necessary summing operations.

The force transducer signals were also summed by an operational amplifier. No special care was exercised as to attachment surface condition or bracket flexibility. The conditions were similar to those that would be present in a typical practical application. When the equipment was attached to the supporting bracket, one side of the force transducers pressed against an angle bracket which was only 0.04-in. thick. The surface of the base plate, which was adjacent to the opposite side of the transducers, had a milled finish.

Following the attachment of the instrumented simulated equipment to the support in the vehicle, the fuselage was subjected to a slow sinusoidal sweep vibration excitation and the force and acceleration measurements were plotted versus frequency with an x-y recorder. Typical results obtained are given in Fig. 6. Although both curves in Fig. 6 give the variation

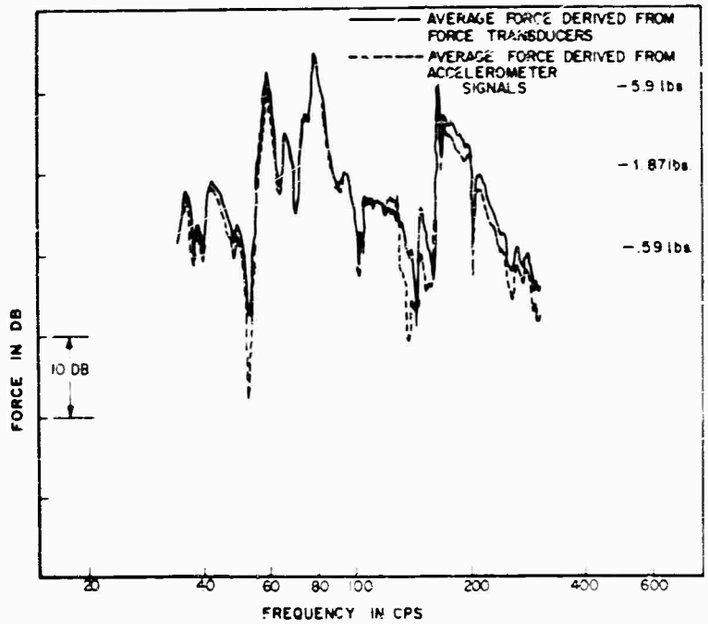

Fig. 6 - Comparison of measured normal force with force computed from acceleration measurements, position 1

of the total normal force (acting on the base plate) versus frequency, one of them was derived from force transducer measurements and the other from acceleration measurements. The agreement between the two curves is considered to be remarkably good and is typical of the correlation between force transducer derived and accelerometer derived data obtained with the simulated equipment attached to the vehicle at various other locations.

PROGRAM PLAN

Once the accuracy of the force transducers had been evaluated, attention was directed to an examination of the benefits force measurement could provide in the formulation of improved laboratory environmental test procedures.

The investigation involved the following steps:

1. The fuselage was subjected to a sinusoidal sweep excitation with the equipment located at various positions. (Details of the attachment locations will be described later.)

2. At each position, the force and acceleration signals were recorded as described above. Of particular interest were (a) the acceleration of equipment base plate based on an average of the four accelerometer readings, (b) the normal force acting on the base plate derived from the sum of the four force transducer signals, and (c) the acceleration of the mass attached to the center of the equipment beam.

3. Hypothetical laboratory vibration test specifications were established for each of the equipment locations. In each case, the test selected was a sinusoidal sweep having a constant acceleration amplitude. The acceleration level chosen was based on the equipment support response in the vehicle and was equal to the value of the major peak base plate response that followed or preceded the antiresonance introduced by the "tuned damper" action of the beam. This procedure is considered to be representative of the practice often followed in generating test specifications.

4. The equipment was then removed from the vehicle structure, placed on a shake table and subjected to the excitation levels discussed in step 3. The equipment was instrumented, as before, with four force transducers located between the equipment base plate and the table and with five accelerometers placed in the positions already described.

5. The acceleration of the mass on the equipment beam was chosen as a measure of the damage potential to which the equipment was subjected. Since the accelerations experienced by the same mass when the equipment

was attached to the vehicle structure were known, it was possible to establish a ratio between the relative damage potential experienced by the equipment on the shaker to that encountered in the vehicle. The ratio of damage potential was named the "Overtest Index." Two different overtest indexes, designated as Type 1 and Type 2, were derived and defined as follows: (a) Type 1 overtest index, $(O.I.)_1$, is the ratio of the maximum acceleration that the resonant element (beam) experienced during the shake table test to the maximum acceleration that it received in the airplane irrespective of frequency; and (b) Type 2 overtest index, $(O.I.)_2$, is the ratio of the maximum acceleration that the resonant element received during the shake table test to that which it received in the vehicle when the exciting frequency was equal to the natural frequency of the resonant element.

6. After completion of the tests during which the shake table was maintained at a constant acceleration amplitude over the frequency range of interest, a second set of tests was conducted. The table acceleration was again maintained at the same amplitude as before except for a narrow frequency band centered at the natural frequency of the equipment beam. In this frequency region, the beam introduced a notch in the table acceleration spectrum. Instead of increasing the command signal to maintain a constant table acceleration amplitude (as was done in the previous tests), a change was made from acceleration control to force control. The input signal to the shaker was adjusted to produce a transmitted force to the base plate which was equal to the maximum force measured (irrespective of frequency) when the equipment was attached to the vehicle structure.

7. Comparisons were made of the damage potentials associated with the two test procedures described in steps 4 and 6.

EQUIPMENT AND VEHICLE CHARACTERISTICS

The simulated equipment used in this investigation has been described in the first section and can be idealized as the vibration system shown in Fig. 7. The beam attached to the base plate behaved as a tuned damper when the exciting frequency was equal to the natural frequency of the beam. Although the base plate itself could be considered as a lumped mass over the frequency range of interest, the mechanical impedance of the composite base plate-supporting structure system was springlike at low frequencies and masslike at sufficiently higher frequencies.

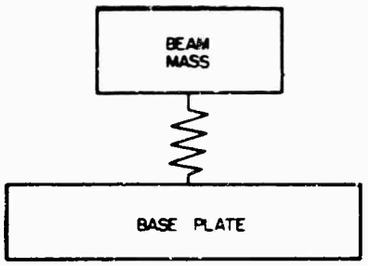

Fig. 7 - Vibration system represented by simulated equipment and supporting structure

The data reported herein were obtained with the equipment located at four different positions on the fuselage. Position 1 was a lightweight bracket on the fuselage interior normally used to support a standard piece of flight hardware. This position was the same as used in the force transducer evaluation program described in the first section. Positions 2 and 3 were on the ring structure of the fuselage. These locations, shown in Fig. 8, were chosen on the fuselage exterior for convenience. Position 4, also on the fuselage exterior, was immediately over the intersection of a highly rigid bulkhead and the fuselage skin. The support at position 1 was by far the most flexible of the four selected. Position 4 was the most rigid and position 2, which was located adjacent to position 4, presented the second most rigid support.

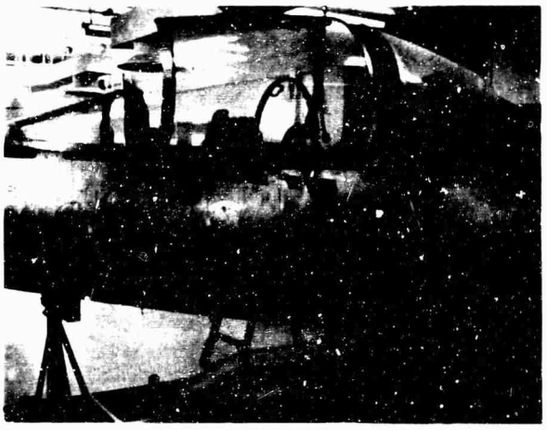

Fig. 8 - Equipment attachment location on fuselage exterior

The results reported here were all obtained with a beam mass of 1.7 lb and a beam natural frequency of 137 cps. The weight of the

base plate was approximately 5 lb. Tests were also conducted using other values of mass and natural frequency. The results from these additional tests do not lead to any modifications of the conclusions reached and, for the purpose of brevity, will not be reported in this paper.

Irrespective of the supporting structure impedance, the beam could be expected to introduce a notch in the base plate acceleration spectrum as the exciting frequency was swept through 137 cps (the natural frequency of the beam). Furthermore, the base plate could be expected to experience peak responses on each side of the notch frequency. Before presenting test results, it will be useful to make certain observations concerning the behavior of an idealized system consisting of a primary simple resonator to which is attached a mass-spring system that can behave as a dynamic damper. Although the support locations cannot be considered to behave as simple resonators over a broad frequency range, the idealization selected is probably valid within the frequency region of interest.

The support can be expected to experience response peaks at frequencies preceding and following the antiresonance (notch) response. The proximity of these peaks to the notch frequency can provide considerable insight into the impedance of the support. If the preceding peak is much closer to the notch than the following peak, it can be concluded that the support is springlike within the frequency range of interest. A masslike support impedance is indicated when the peak support response that follows the notch is closer to it than the preceding peak. If the preceding and following support peak responses are symmetrically located on either side of the notch, the support impedance is damperlike. All other factors remaining constant, the frequency range between the support response peaks becomes greater as the ratio of the tuned damper mass to the effective supporting structure mass is increased.

The observations just cited can be demonstrated analytically, and the reader is referred to the literature for further details [2]. In the present instance these considerations are useful in providing a qualitative evaluation of the beam response at the various attachment locations.

In this regard, attention is called to Figs. 9 through 12 which show the variation of beam and base plate accelerations with frequency at attachment positions 1, 2, 3 and 4, respectively. Position 1, which was considered to be the most typical equipment support, provided a masslike mechanical impedance to the beam system in the vicinity of 137 cps. Here the mass was essentially the 5-lb base plate since the bracket was of very light weight. It can be seen (Fig. 9) that both the beam and base plate peak responses occur approximately 45 cps above the notch frequency. The structure at positions 2 and 3 (Figs. 10 and 11) was springlike in the vicinity of 137 cps as is indicated by the sharp decline in the base plate response as the exciting frequency rose to 137 cps. Position No. 4 (Fig. 12) is seen to have also provided a springlike support impedance.

OVERTEST LEVEL CRITERIA

The problem of defining the relative severity of a laboratory vibration test and of the service environment is difficult. For instance, one does not, in general, know if the damage that the equipment may experience is due to excessive stress, displacement, velocity or acceleration. In the present instance we have rather arbitrarily assumed that the acceleration of an equipment resonant structure provides a measure of the damage potential. The simulated equipment used in the experimental program incorporated such a resonant structure in the beam and the acceleration of the beam was assumed to provide the required measurement of test severity.

It was also necessary to establish a method for choosing the acceleration input level that would be called out in a hypothetical test specification requiring a constant amplitude of acceleration sinusoidal sweep. Since attention was confined to the frequency region that involved the resonant frequency of the equipment and the adjacent peak responses of the supporting structure, it was decided to use the higher of the two peak base plate (support) responses as the input level to be imposed when the equipment was placed on the shake table.

Finally, it was also necessary to provide a basis for quantifying the relative severity of the acceleration experienced by the equipment beam when the equipment was attached directly to a shake table with that imposed by the vehicle. There were obviously an infinite number of frequencies at which the acceleration levels differed but there were two frequencies that were considered to be of particular importance. One of these was the natural frequency of the equipment beam. At this frequency, the beam experienced the peak acceleration when the equipment was vibrated on the shake table. With the equipment attached to the vehicle, the base plate

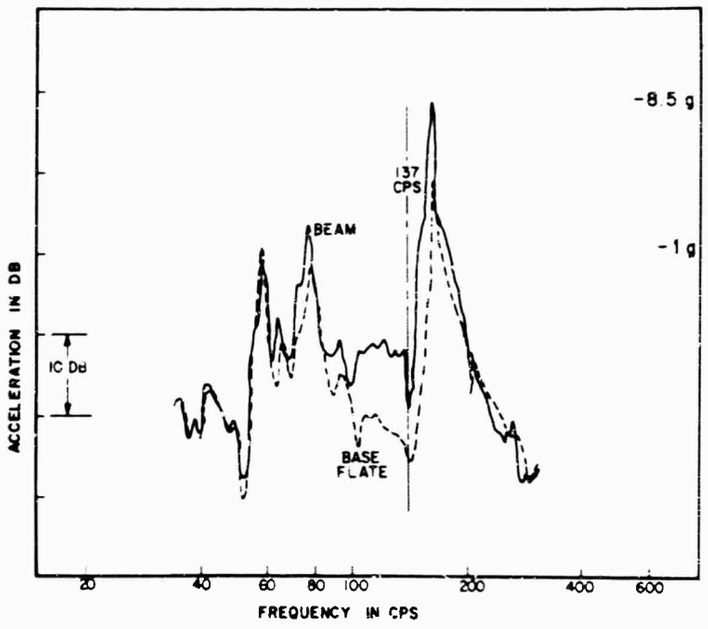

Fig. 9 - Comparison of base plate and beam accelerations, position 1

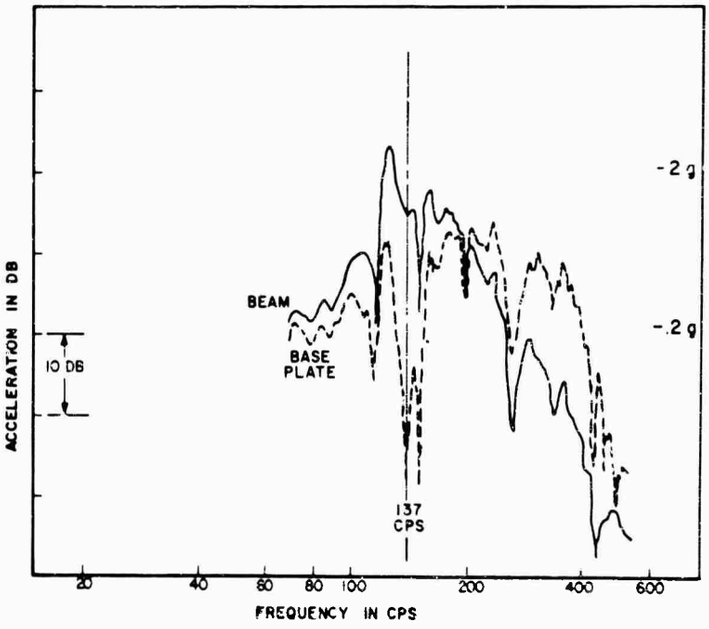

Fig. 10 - Comparison of base plate and beam accelerations, position 2

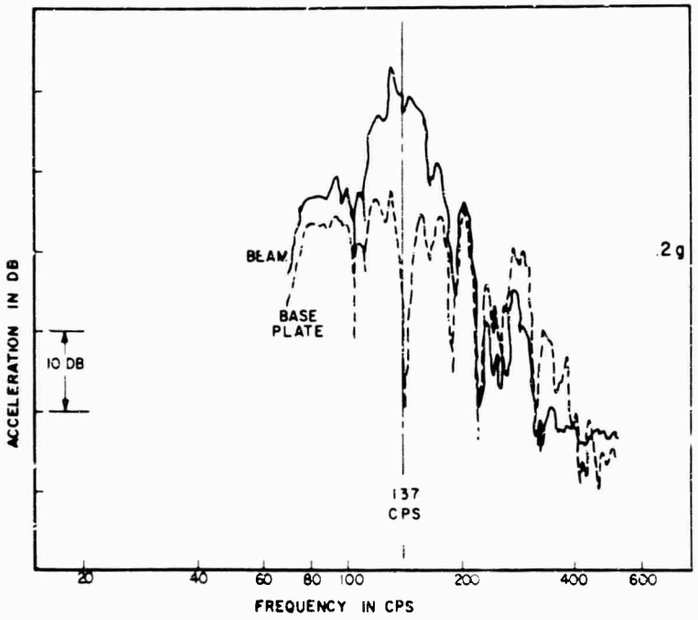

Fig. 11 - Comparison of base plate and beam accelerations, position 3

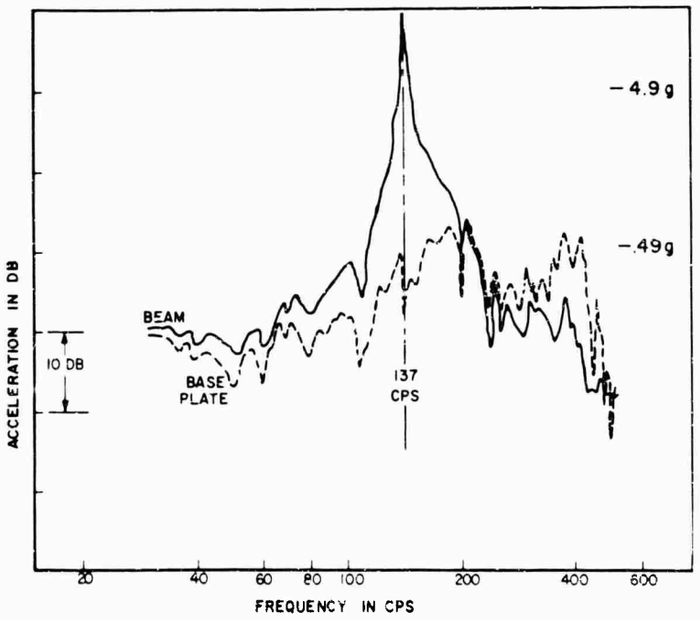

Fig. 12 - Comparison of base plate and beam accelerations, position 4

support assembly experienced an antiresonance notch at the same frequency. The second frequency of interest was associated with the peak response of the base plate-support assembly when the equipment was attached to the vehicle. This was also the frequency at which the beam experienced its maximum acceleration (in the vehicle).

For the shake table tests it was logical to choose the resonant acceleration of the beam as the measurement of test severity. For the simulated service environment tests (equipment attached to fuselage), two values of severity were selected. One of these was the maximum beam acceleration measured, irrespective of frequency. The second was the beam acceleration occurring at the resonant frequency of the beam.

The above measurements allowed two ratios, called "overtest indexes," to be established. A precise definition of these quantities has already been given in step 5 of the section on the Program Plan.

OVERTEST LEVELS

Comparisons of beam accelerations measured with the equipment attached to the vehicle and those produced on the shake table at constant input acceleration amplitude are provided in Figs. 13 through 16. Overtest indexes for the various attachment locations are indicated on the figures.

The greatest overtest levels were associated with position 1 where the Type 1 and 2 indexes were found to be 21 and 1400, respectively. At position 3 (this support was next to position 1 in rigidity) index levels of 10 and 20 were obtained. At the most rigid locations (positions 3 and 4), overtest index pairs of 3, 6 and 2, 3 were measured.

In assessing the significance of these results, it is of interest to note that the highest levels of overtesting were associated with the most typical equipment support structures used. Positions 2 and 4 were highly rigid locations that would rarely be approximated in practice. Furthermore, it is important to remember that the effective mass of the beam was only 1.7 lb. Larger values of mass in the resonating structure could be expected to produce higher overtest levels.

A method for obtaining an approximation of the overtest indexes based on the peak-notch characteristics of the supporting structure and the Q of the resonant element is given in the Appendix.

VIBRATION TESTING WITH FORCE CONTROL

Following completion of the shake table tests at constant amplitude, the merits of a force-controlled test were examined.

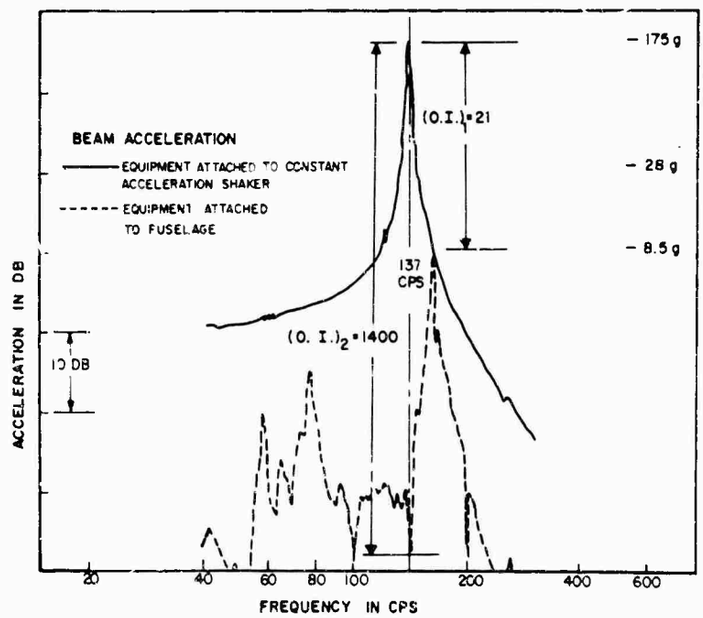

Fig. 13 - Overtest indexes associated with position 1

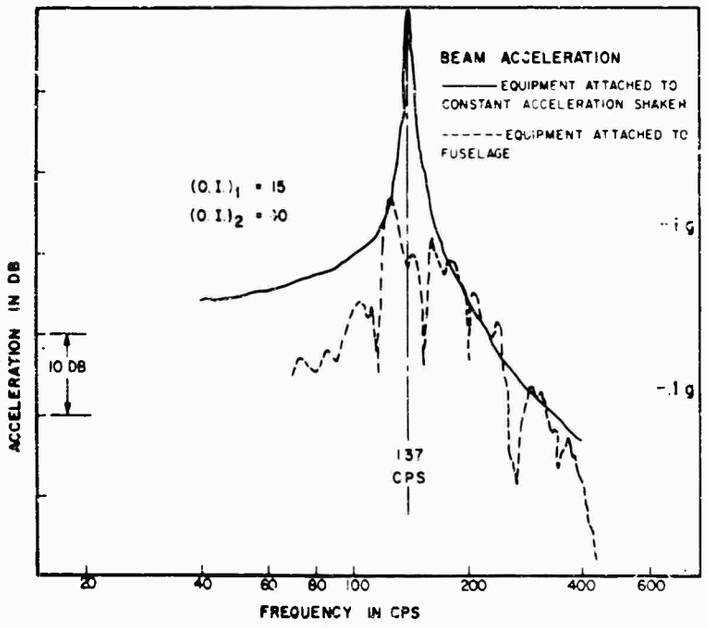

Fig. 14 - Overtest indexes associated with position 2

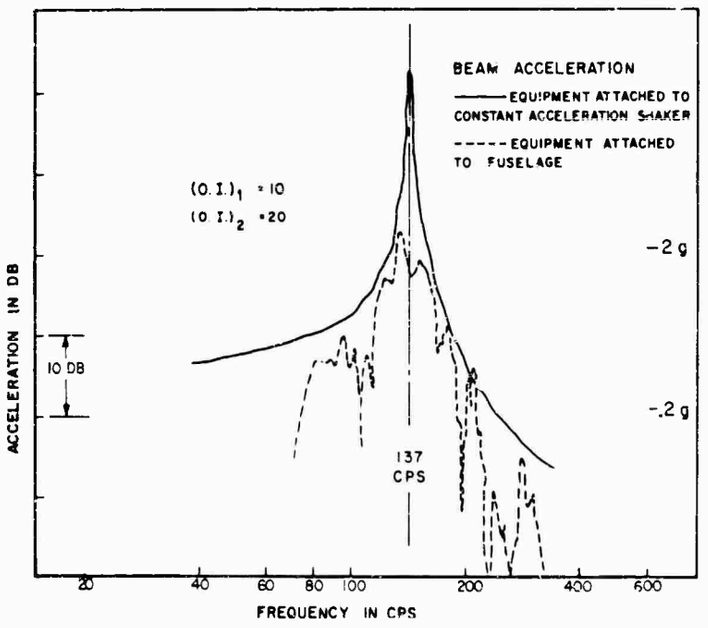

Fig. 15 - Overtest indexes associated with position 3

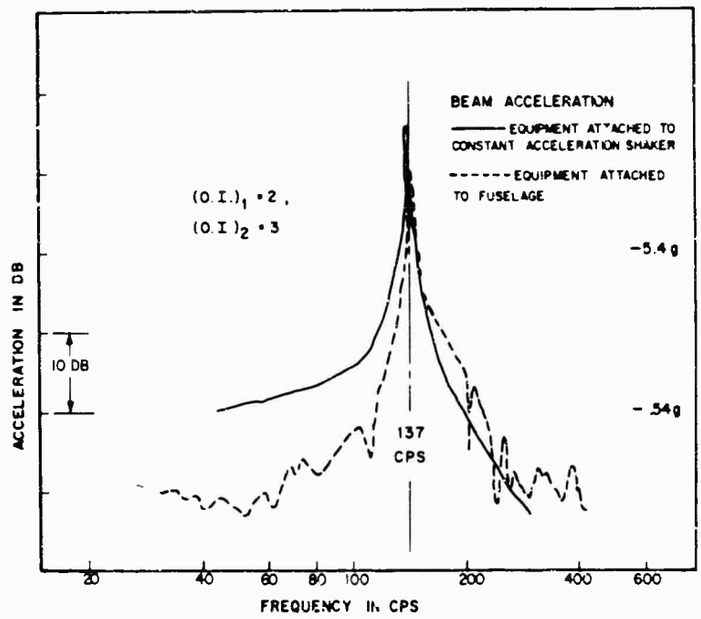

Fig. 16 - Overtest indexes associated with position 4

From the preceding discussion, it is evident that the principal difficulty encountered in constant acceleration testing arises at major equipment resonances. At an equipment resonance, an antiresonance occurs in the table spectrum unless the input signal amplitude is increased to compensate for this effect. In the vehicle, the antiresonance effect always produces a notch in the support acceleration spectrum. It follows that the force transmitted by the support in the vehicle to the equipment will be less than would be transmitted by the shake table.

If the force transmitted by the support in the vehicle is known and if the force transmitted by the shake table to the equipment base can be measured, it is a simple matter to adjust the shaker acceleration in the vicinity of an equipment resonance so as to provide an approximate simulation of the dynamic loads applied in the service environment. In general, maximum dynamic loads that the equipment will experience in the vehicle will not occur at an antiresonance. (If they did occur at an antiresonance, the two overtest indexes would be equal.) To assure that the laboratory shake table test is conservative, the force transmitted by the table at an equipment resonance should not fall below the maximum force measured in the vehicle, irrespective of frequency.

The force-controlled tests, which followed completion of the constant acceleration amplitude tests, were based on the considerations cited above. With one important exception, these tests were similar to the constant acceleration tests. Except at a frequency band in the vicinity of the beam resonance, the table acceleration was maintained at the same constant value as before. As the beam resonance began to occur, a change was made from acceleration control to force control and the table acceleration was reduced to provide a transmitted force that approximated the maximum value measured in the vehicle. As the exciting frequency was further increased and the resonance subsided, a return was made to acceleration control.

The procedure just described could be expected to reduce the Type 1 overtest index to unity. The Type 2 overtest index would be reduced by an amount equal to the change in the Type 1 index. A typical result obtained during a force-controlled test is shown in Fig. 17. Shown here are beam accelerations as measured: (a) in the vehicle with the equipment attached at position 1, (b) during a constant acceleration amplitude shake table test, and (c) during a force-controlled test. The force-controlled test is seen to be conservative but the overtest level at the beam resonant frequency was reduced by a factor of 20.

Figure 18 shows the variation of the transmitted force as measured: (a) with the equipment attached to the vehicle at position 1, and (b) during the force-controlled test. These results provide additional evidence that the force-controlled test was conservative.

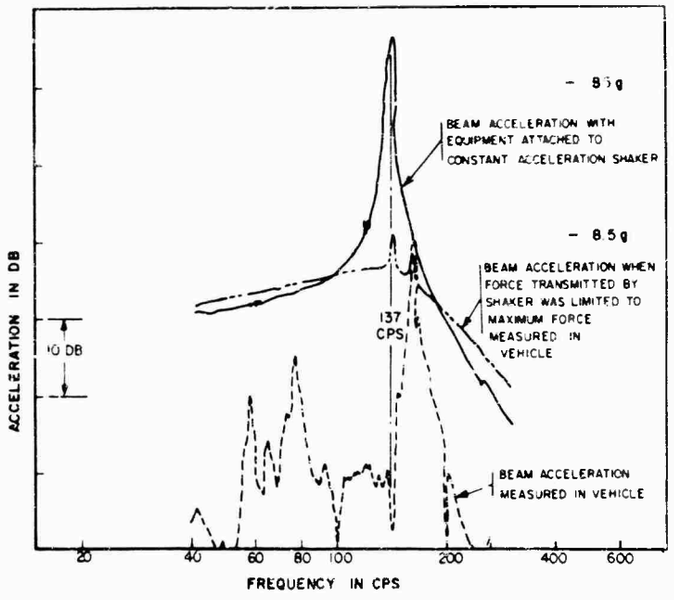

Fig. 17 - Comparison of overtest levels introduced with: (a) shake table acceleration held constant, and (b) force limiting employed at equipment resonant frequency

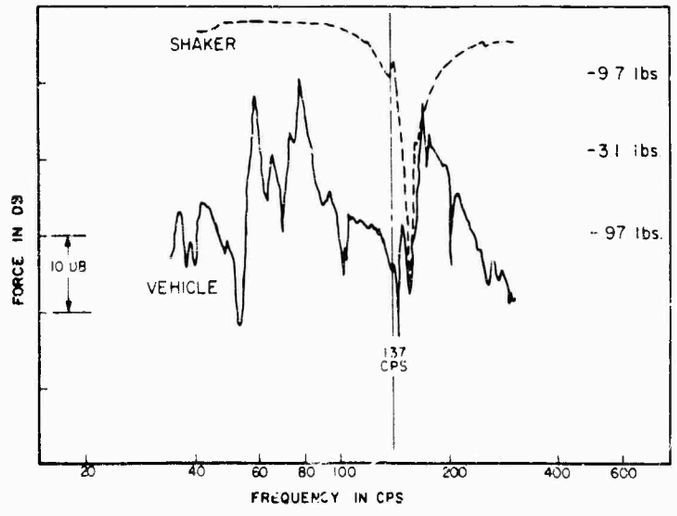

Fig. 18 - Comparison of transmitted normal force measured in vehicle (position 1) with force applied by shake table when table spectrum was notched to limit force at resonant frequency of equipment beam

CONCLUDING REMARKS

This paper has presented a portion of the data obtained during a program designed to examine the feasibility of obtaining and using transmitted force information to provide laboratory vibration tests that are not overly conservative. Due to time and budget limitations, the investigation was confined to sinusoidal rather than random excitation. The reader should be cautious in drawing any conclusions as to what the overtest levels would have been had the excitation been random. It is the author's opinion that the results obtained with random excitation would not have been greatly different if all measurements of power spectral density were obtained with a very narrow-band filter and if narrow-band shake table equalization were employed.

REFERENCES

1. G. W. Painter, "Use of Miniature Force Transducers in the Measurement of Shock and Vibration Environments," Shock and Vibration Bull. No. 34, Part 4, pp. 45-53, Feb. 1965

2. C. H. Powell, "Graphical Treatment of Vibration and Aircraft Engine Dampers," Bookcraft, N.Y.

Appendix

For the idealized system shown in Fig. A-1, it is possible to approximate the Type 1 and Type 2 overtest indexes on the basis of the peak-notch behavior of the support and the Q of the resonant element.

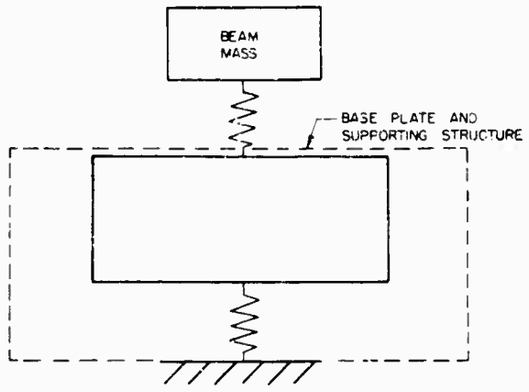

Fig. A-1 - Idealization of equipment vehicle vibration system

The Type 1 overtest index, $(O.I.)_1$, can be determined from

$$(O.I.)_1 = \frac{Q_2}{\left[\frac{\ddot{X}_2}{\ddot{X}_1}\right]_{\omega_p}}, \qquad \text{(A-1)}$$

where

Q_2 = quality factor of the resonant element, and

$\left[\ddot{X}_2/\ddot{X}_1\right]_{\omega_p}$ = ratio, $\ddot{X}_2$ $\ddot{X}_1$, at the frequency (ω_p), where the peak support response occurs.

$\left[\ddot{X}_2/\ddot{X}_1\right]_{\omega_p}$ can be determined from the well-known single-degree-of-freedom transmissibility equation, or

$$\left[\frac{\ddot{X}_2}{\ddot{X}_1}\right]_{\omega_p} = \sqrt{\frac{1 + \left(\frac{\omega_p}{\omega_n Q_2}\right)^2}{\left[1 - \left(\frac{\omega_p}{\omega_n}\right)^2\right]^2 + \left[\frac{\omega_p}{\omega_n Q_2}\right]^2}}, \qquad \text{(A-2)}$$

where ω_n is the natural frequency of the resonant element.

When

$$\frac{\omega_p}{\omega_n Q} << \left|1 - \left(\frac{\omega_p}{\omega_n}\right)^2\right| \quad \text{and} \quad \frac{\omega_p}{\omega_n Q_2} << 1,$$

$$\left[\frac{\ddot{X}_2}{\ddot{X}_1}\right]_{\omega_p} \approx \frac{1}{1 - \left(\frac{\omega_p}{\omega_n}\right)^2} \qquad \text{(A-3)}$$

and, therefore,

$$[O.I.]_1 \approx Q_2 \left[1 - \left(\frac{\omega_p}{\omega_n}\right)^2\right]. \qquad \text{(A-4)}$$

The Type 2 overtest is simply equal to the depth of the support (X_1) notch as measured from the maximum adjacent support response peak.

* * *

FEASIBILITY OF FORCE-CONTROLLED SPACECRAFT VIBRATION TESTING USING NOTCHED RANDOM TEST SPECTRA

Joseph A. Heinrichs
The Martin Company
Baltimore, Maryland

A summary of analyses and results is presented to substantiate the feasibility of using notched random test spectra for force-controlled spacecraft vibration tests. An analytical evaluation of structural loading at the base of the spacecraft caused by application of a broadband environmental acceleration spectrum is made. By using this analytical technique, notching requirements for the broadband test spectrum are established which result in rms structural forces at the spacecraft base that are within the spacecraft's structural design load criteria. Structural loadings of other structural elements of the spacecraft and component acceleration spectra are examined on the basis of the notched spectra and are found to be within design values. The proposed method of notching is considered to be a feasible approach to force limiting when available booster driving force at the spacecraft-booster interface is not known.

J. A. Heinrichs

INTRODUCTION

This paper presents a summary of analyses performed on a spacecraft to show the feasibility of a force-controlled vibration test using notched random test spectra. The introduction of notches into test spectra can be accomplished with available test equipment and is presently being implemented for the environmental test of a complete spacecraft system. The requirement of qualification and verification testing of a new spacecraft to an existing booster contractor's random acceleration spectrum necessitates a force-controlled test to assure compliance with the primary spacecraft design load criteria during the test period. A broadband random test spectrum is defined at the boost vehicle-spacecraft interface in terms of a power spectral density (PSD) envelope of expected environment. Application of this environment by mechanical excitation of the base of the spacecraft is accomplished with a modified Gaussian random distribution in which g-peaks do not exceed three times the root-mean-square (rms) acceleration.

Since the test spectrum is presented as an envelope, statistically derived from previous measured flight data of other payloads, it does not reflect the constraint of having an impedance match between the booster and the new spacecraft at their interface. PSD's of measured vibration environments from which envelopes are constructed contain regions of minimum vibration energy at the major interface anti-resonances and energy peaks at the combined system resonances. This is analytically shown by Kaplan and Petak [1] for a multi-spring-mass model under a constant driving force. The existence and magnitudes of the minimum energy regions will actually be dependent on the available driving force of the booster at the corresponding fixed-base frequencies of the newly installed spacecraft. The amount of driving force over the frequency spectrum is usually unknown and is, therefore, unavailable to the spacecraft test manufacturer. To limit the test spectrum in the spacecraft test, it is proposed to introduce notches into the spectrum

envelope which would approximate the existence of minimum vibrational energy regions at the spacecraft-booster interface. A detailed analytical model of the spacecraft is used to define the interface antiresonance points at which the notches are located. The amount of notching is to be dependent on a compatibility between the produced rms structural forces and the primary structural load design criteria of the spacecraft.

To determine the amount of modification required for a specified spacecraft test spectrum, modal response analyses are performed which evaluate structural loading of the spacecraft when subjected to the test spectrum at the spacecraft base. Notches in the test spectrum are then determined so as to eliminate peaks in the structural force spectral densities and result in rms forces which are compatible with the structural load criteria at the interface. A limiting force spectrum envelope which determines the amount of notching and the location of notches is assumed, having the same shape as the interface acceleration spectrum envelope. The limit loads which can be transferred across the interface and those in the interface structure as defined by the load criteria are used as a basis for notching. After the notched test spectrum is determined, rms stresses and/or loads in those parts of the structure designed to minimum margins of safety are evaluated to assure that their limit loads are not exceeded during the test period. In addition, acceleration spectral densities at various equipment locations resulting from the notched test spectrum are evaluated and compared to the acceleration design environment for spacecraft components.

NOMENCLATURE

$c_n(t)$ Modal coordinate displacement in nth normal mode

g_n Modal damping coefficient in nth normal mode

ω_n Circular frequency of nth normal mode

m Mass

ϕ_n Modal deflection coefficient in nth normal mode

$\ddot{f}$ Acceleration of the fixed base of spacecraft

ω Forcing frequency

C_n nth normal mode modal load coefficient at base of spacecraft in the direction of excitation (force/length)

M_{eq_n} Modal mass in nth normal mode

C_n^P nth normal mode modal load coefficient in the Pth structural element (force/length)

F_n^P Load in the Pth structural element in the nth normal mode

F_T^P Total load in the Pth structural element

Φ_F^P Transfer function, ratio of load amplitude in the Pth structural element to the amplitude of harmonic base acceleration

Φ_A^Q Transfer function, ratio of acceleration amplitude at location Q to the amplitude of harmonic base acceleration

$A_T^{Q_j}$ Total acceleration at location Q in the jth degree of freedom

$\phi_n^{Q_j}$ nth normal mode deflection coefficient at location Q in the jth degree of freedom.

G Gravitational constant

$W_F^P(\omega)$ Spectral density of total load in the Pth structural element (force ^{2}/cps)

$W_f(\omega)$ Spectral density of environmental base acceleration (g^2/cps)

$F_T^P{}_{rms}$ Root-mean-square load

f_L Lower frequency limit in the test spectrum (20 cps)

f_U Upper frequency limit in the test spectrum (2000 cps)

STRUCTURAL ANALYSIS MODEL

To evaluate adequately spacecraft response to the broadband base excitation environment, a detailed structural analysis model is constructed for the prediction of a large number of normal vibration modes. The structural configuration of the spacecraft is presented in Fig. 1 and consists primarily of a glove section (skin-stringer-frame), cantilevered equipment truss, center body, aft body, fixed fins and movable flaps. The spacecraft is covered with a dense nonstructural heat protection material. Three pedestals are used to constrain the spacecraft from its aft bulkhead to the boost vehicle and are designated the support pedestals. A three-dimensional dynamic analysis model of this configuration, consisting of 1800 discrete structural elements, is derived and utilized in the matrix method of obtaining normal vibration

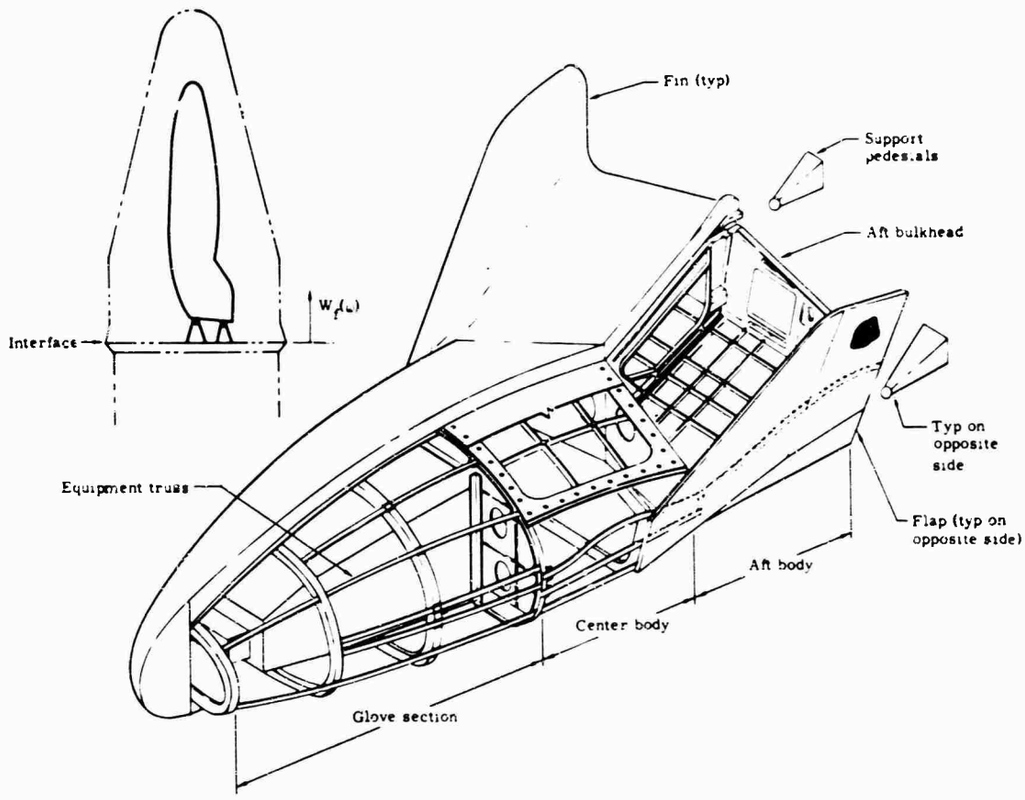

Fig. 1 - Structural configuration

modes [2]. The three-dimensional array of shear panels, tension elements, bending elements and twist elements is depicted in Fig. 2. Masses of the structure, heat shield and internal components are located at discrete points over the model. Motion of the masses is described by 300 degrees of freedom. Each of the support pedestals is represented by a set of three orthogonal reaction elements connecting the aft bulkhead to ground. Outputs from the matrix method of modal analysis consist of modal frequency, modal mass, modal deflection coefficients for each degree of freedom, and modal load and stress coefficients for each of the structural elements. A graphical description of the fundamental Z-direction bending mode is also presented in Fig. 2.

ANALYTICAL METHODS

The objective of the modal analysis is to obtain the rms structural loading at the base of the spacecraft when the structural representation is subjected to the test spectrum. These rms structural loads can then be compared to one-third the allowable base load as given by the spacecraft's design static load factors and the individual pedestal design static loads. The one-third value of allowable loads is used as a criterion to account for applied g-peaks which can be three times the rms value. Determination of loads in each of the 1800 structural elements could also be undertaken; however, the base loading is chosen as the basis for notching the test spectrum.

The modal coordinates' motion equations for a uniform beam subjected to an accelerated base motion can be obtained from the differential equation of classical beam theory and are of the form

$$\ddot{q}_n(t) + g_n \omega_n \dot{q}_n(t) + \omega_n^2 q_n(t) = \left(\frac{\omega_n^2 \int_0^\ell m(x)\, \phi_n(x)\, dx}{\int_0^\ell m(x)\, \phi_n^2(x)\, dx} \right) \frac{\ddot{f}(t)}{\omega_n^2} \,. \qquad (1)$$

This equation has been derived by Shinozuka [3]. For the discrete mass spacecraft model, the modal coordinates' motion equations become

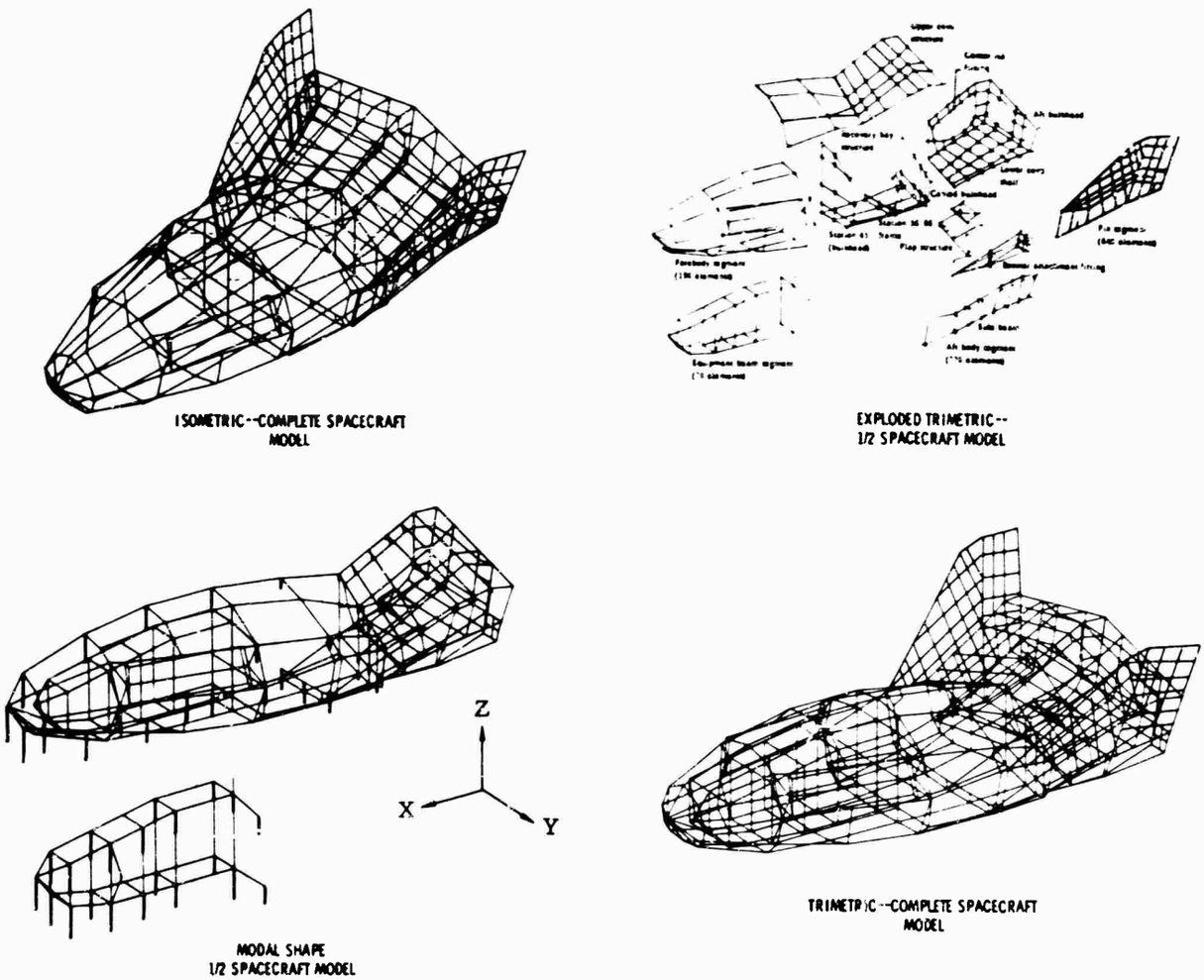

Fig. 2 - Structural analysis model of spacecraft

$$\ddot{q}_n(t) + g_n\omega_n\dot{q}_n(t) + \omega_n^2 q_n(t) = \left(\frac{\omega_n^2 \sum_j m_j \phi_{jn}}{\sum_j m_j \phi_{jn}^2}\right) \frac{\ddot{f}(t)}{\omega_n^2} \quad (2)$$

where the summations are made over the number of degrees of freedom in the spacecraft model. The term

$$\omega_n^2 \sum_j m_j \phi_{jn}$$

represents the modal constraint in the nth mode at the base of the structure in the direction of excitation. This is obtained from the modal results of the spacecraft model by adding the modal load coefficients of the support pedestal elements lying in the direction of excitation. The term

$$\sum_j m_j \phi_{jn}^2$$

represents the modal mass of the nth mode. Equation (2) can also be obtained by the method used by MacNeal [4], whereby a modal model is constructed which has the proper force-displacement relationship for a single coordinate. The model consists of masses sprung from the coordinate by springs, and the values of the springs and masses can be computed from the normal modes with the coordinate constrained to zero motion. The procedure used in obtaining the motion equations by this method is summarized in Fig. 3. The sum of all the sprung masses (M_E) will equal the total mass of the spacecraft, since the system has a rigid body degree of freedom when the base constraint is removed.

Solution of Eq. (2) for harmonic accelerated base motion at the driving frequency ω gives the following relation for amplitude of the modal coordinate to the amplitude of base acceleration:

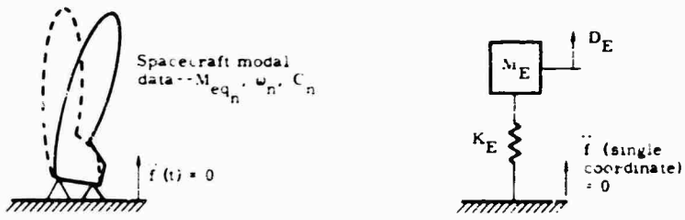

$1/2\, M_{eq}\, \dot{q}^2$ $(1/2\, M_{eq}\, \omega^2 q^2)$ [kinetic energy] $1/2\, M_E \dot{D}_E^2$ $(1/2\, M_E\, \omega^2\, D_E^2)$

$1/2\, Kq^2$ $(1/2\, M_{eq}\, \omega^2\, q^2)$ [potential energy] $1/2\, K_E\, D_E^2$

Cq [root constraint] $K_E\, D_E$

equating the kinetic, potential energies and root constraint results in

(a) $M_{E_n} = C_n^2 / M_{EQ_n}\, \omega_n^4$ (b) $K_{E_n} = \omega_n^2 M_{E_n}$

Equivalent Modal Model

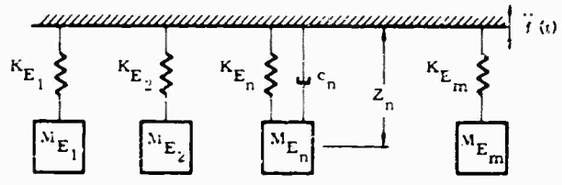

Motion equations for the above system connected to the single coordinate are of the form

$$M_{E_n} \ddot{Z}_n + c_n \dot{Z}_n + K_{E_n} Z_n = - M_{E_n} \ddot{f}(t)$$

Using $C_n q_n = K_{E_n} Z_n$ (equating root constraints)

$$M_{E_n} \ddot{q}_n + c_n \dot{q}_n + K_{E_n} q_n = - \frac{M_{E_n} K_{E_n}}{C_n} \ddot{f}(t)$$

This form of the modal motion equation is equivalent to that of Equation 2

Fig. 3 - Derivation of motion equations (4)

$$q_n(\omega) = \frac{-C_n}{M_{eq_n}\, \omega_n^2} \left[A_n(\omega) + iB_n(\omega)\right] \ddot{f}(\omega) . \qquad (3)$$

where

$$A_n(\omega) = \frac{\omega_n^2 - \omega^2}{(\omega_n^2 - \omega^2)^2 + (g\omega_n \omega)^2}$$

and

$$B(\omega) = - \frac{g\omega_n \omega}{(\omega_n^2 - \omega^2)^2 + (g\omega_n \omega)^2} .$$

The ratio of load in a structural element in the nth mode to the amplitude of base acceleration is obtained by multiplying Eq. (3) by the element's modal force coefficient:

$$\frac{F_n^P(\omega)}{\ddot{f}(\omega)} = \frac{C_n^P q_n(\omega)}{\ddot{f}(\omega)} = - \frac{C_n^P C_n}{M_{eq_n}\, \omega_n^2} \left[A_n(\omega) + iB_n(\omega)\right] . \qquad (4)$$

The ratio of total load in the Pth structural element, based on a modal sum approximation, to the amplitude of base acceleration becomes

$$\frac{F_T^P(\omega)}{\ddot{f}(\omega)} = \sum_{n=1}^{m} \frac{-C_n}{M_{eq_n}\, \omega_n^2} C_n^P \left[A_n(\omega) + iB_n(\omega)\right] = \phi_F^P . \qquad (5)$$

The ratio of total structural acceleration at any of the mass locations to the amplitude of base acceleration can also be similarly obtained. Acceleration is given by

$$\frac{A_T^{Q_j}(\omega)}{\ddot{f}(\omega)} = 1.0 + \sum_{n=1}^{m} \frac{C_n}{M_{eq_r} \omega_n^2} \Phi_n^{Q_j}$$

$$\times \left[\omega^2 A_n(\omega) + \omega^2 B_n(\omega)\right] = \Phi_A^{Q} \qquad (6)$$

The value of 1 is added to the summation if the acceleration is in the direction of excitation and is omitted if the acceleration is not in the direction of base excitation.

Equation (5) is of the form now to be utilized in obtaining PSD's of load from a base excitation environment, given terms of an acceleration spectral density. The load spectral density is given by

$$W_F^P(\omega) = (\Phi_F^P)^2 W_f(\omega) \qquad (7)$$

and

$$F_T^P \text{ rms} = \left(\int_{f_L}^{f_U} W_F^P(\omega)\, d\omega \right)^{1/2} . \qquad (8)$$

ANALYTICAL RESULTS AND DISCUSSION

By using the modal data of the analytical model in Eq. (5), force transfer functions over the frequency range of interest (20 to 2000 cps) are evaluated for the total base forces and pedestal element forces in the directions of the three vehicle axes. A typical transfer function in terms of force squared to base acceleration squared is given in Fig. 4. Peaks in the transfer function occur at the fixed-base spacecraft modal frequencies for those modes having relatively large base modal force coefficients. In all of the evaluated transfer functions, the magnitudes of these peaks decreased in a broad sense with increasing frequency. The summation in the equation is made with the data of the first 35 normal modes which correspond to frequencies below 520 cps. The summation changes insignificantly when made with the data of the first 80 modes corresponding to modal frequencies below 1100 cps. This indicates that total modal forces at the spacecraft base are practically independent of the higher modes of vibration. Based on the sum of the equivalent single harmonic oscillator masses given in Eq. (a) of Fig. 3, 97.5 percent of the tota spacecraft mass is represented by the first 35 modes and 98.3 percent is represented by the first 80 modes. Values of the modal damping coefficient ($2c/c_c$), which are considered to be conservative, range from 2 percent in the fundamental vibration

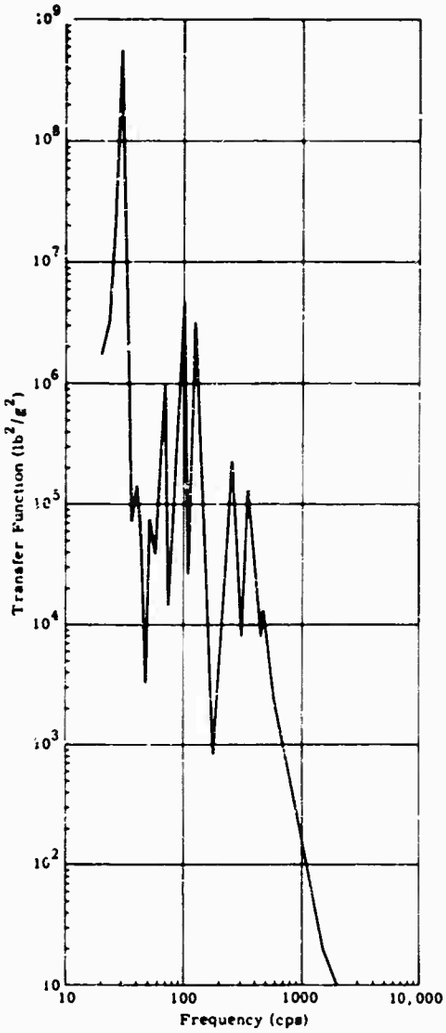

Fig. 4 - Total Y force at spacecraft base to interface acceleration transfer function

mode to a maximum of 10 percent in the higher modes of vibration. (An experimental resonance survey of the spacecraft structure indicated a structural damping coefficient in the fundamental mode of 6 percent.) The magnitudes of the peaks in the transfer functions are expected to be significantly affected with changes in the structural damping coefficient.

Acceleration transfer functions are also evaluated for two equipment locations by using Eq. (6). One of the locations (guidance package) is at the tip of the equipment truss and the other (actuator package) in the aft body section near the spacecraft base. Sample acceleration transfer functions relating the equipment accelerations in the same directions as base accelerations are given in Fig. 5. As is expected, the

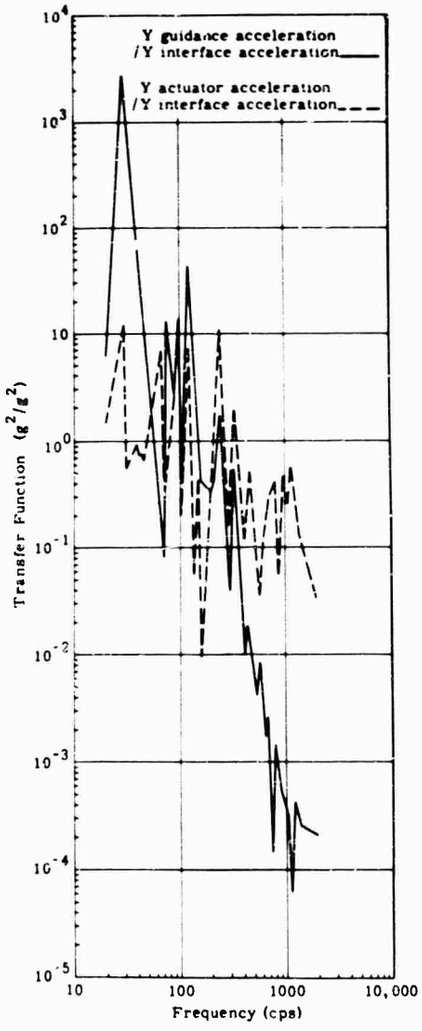

Fig. 5 - Transfer function

high-frequency portion of the acceleration transfer function is lower at the tip structural location than that near the plane of excitation. This result can be substantiated by examining the acceleration at the free end of a cantilevered beam when the driving frequency at the base approaches infinity. The expression for the ratio of free-end to fixed-end acceleration at $\omega = \infty$ is given by

$$\frac{A_{free}}{A_{fixed}} = 1 - \sum_{n=1}^{\infty} \frac{\int_0^{\ell} m(x)\, \phi_n(x)\, dx}{\int_0^{\ell} m(x)\, \phi_n^2(x)\, dx} = 0 . \quad (9)$$

Force spectral densities for the total base loads and pedestal loadings for the excitation applied in each of the three spacecraft axes directions were evaluated using Eq. (7). A typical force spectral density of total force across the interface is given in Fig. 6 and represents an rms force which is approximately 3.5 times greater than one-third of the peak allowable force given by the static loads criteria. To limit the force density to represent an allowable rms force, a limiting force spectrum, assumed to have the same shape as the input spectrum, is positioned with the force spectral density until the area contained within the shape represents an allowable rms force. The assumed limiting corresponds to a shape which would be obtained from a completely rigid structure. The limiting spectrum is shown in Fig. 6 with the contained shaded spectrum representing an allowable rms force. Sharp notches are then introduced into the acceleration spectral density for eliminating the spectral density peaks which exceed the limiting spectrum. Resulting notched test spectra based on each of the considered structural loadings are derived for each test excitation direction. An enveloping notched spectrum in each direction which satisfies all of the loads criteria is then proposed as the test spectrum. Figures 7 and 8 contain resulting notched spectra for two excitation axis directions and are primarily based on satisfying the total allowable loads at the base of the spacecraft. The spectrum in Fig. 7 is seen to be considerably notched between 20 and 30 cps and is caused by the fixed-base spacecraft's fundamental Y-direction bending mode frequency falling in this frequency band.

The fundamental X-direction bending mode frequency falls below 20 cps, thereby resulting in the relatively small notching requirements given in Fig. 8. The required notches are always contained in the low-frequency portions of the spectra, since the lower frequency modes produce the most significant amount of base loading. Because the notches are dependent on the sharp peaks occurring in the force spectral densities, their positioning as load limiters will be sensitive to the actual frequencies (rather than predicted frequencies) at which these peaks occur. It is, therefore, necessary to define the force transfer functions prior to the environmental tests by sinusoidal or random transmissibility testing of the spacecraft. Other structural elements, selected on a basis of minimum design margins, were also examined for rms stress levels produced by the final notched test spectra.

The modal load coefficients in Eq. (4) are replaced by the modal stress coefficients for evaluating the stress transfer functions used in obtaining the stress spectral densities. In all cases, rms stress levels produced by the notched spectra are always below one-third of

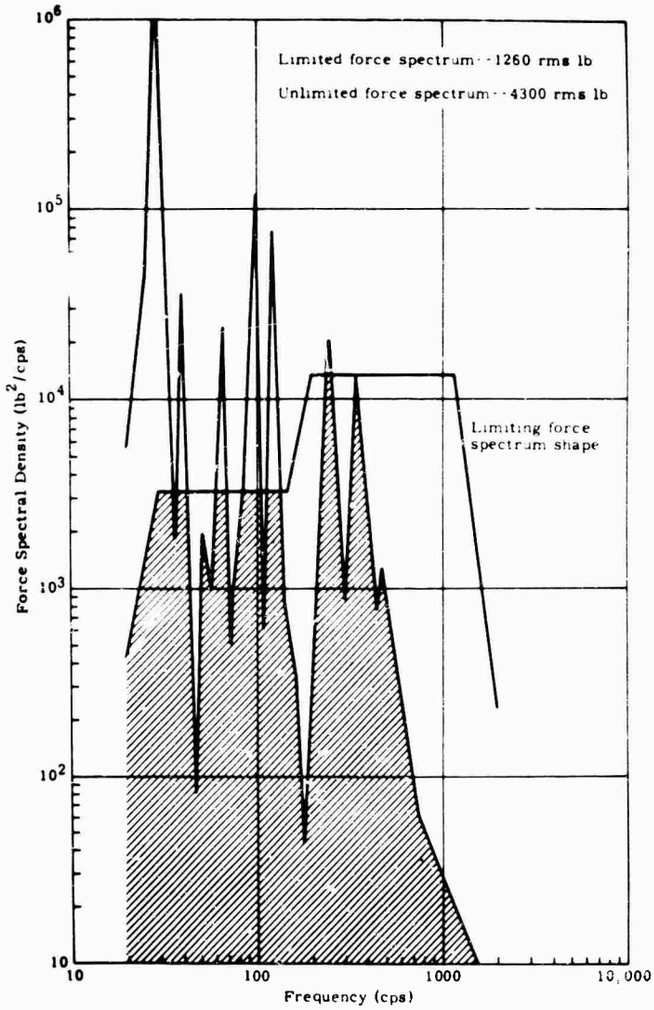

Fig. 6 - Interface force spectral density (notched and unnotched input acceleration spectra)

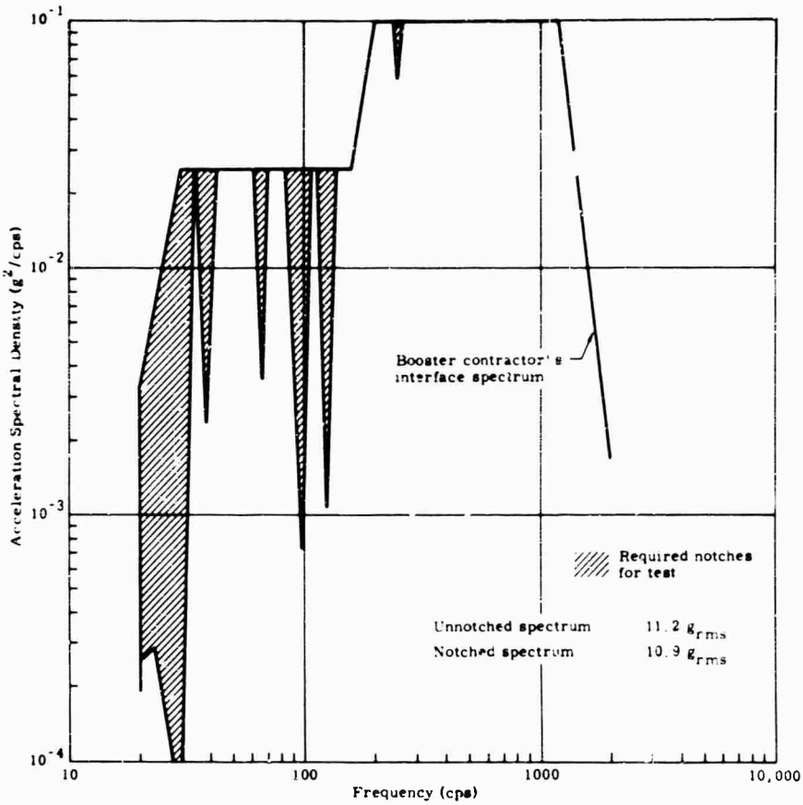

Fig. 7 - Y-direction test spectrum

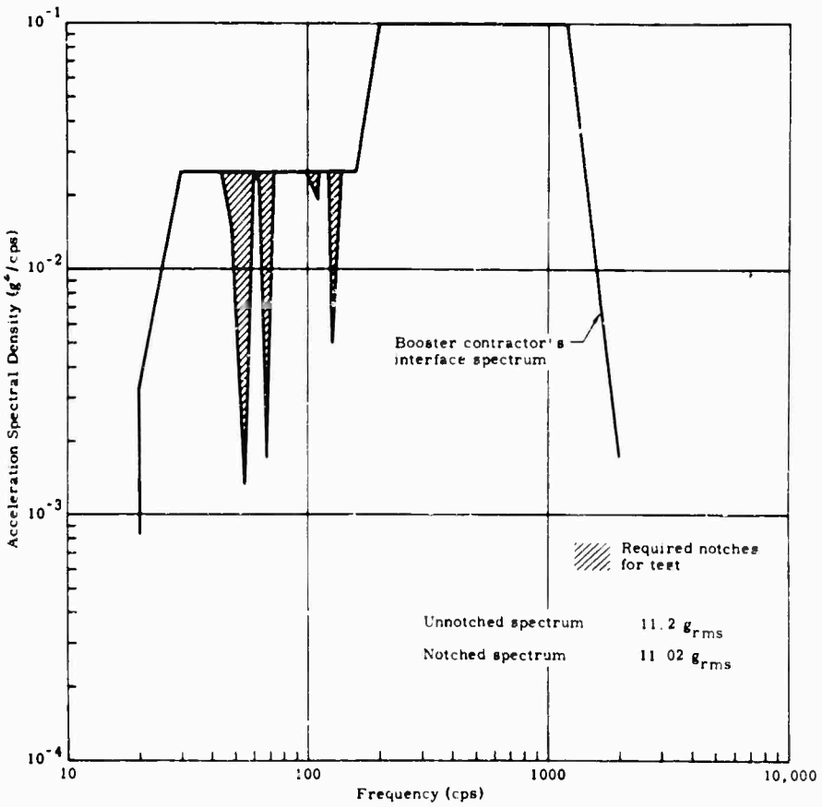

Fig. 8 - Z-direction test spectrum

the design stress levels. Acceleration spectral densities at two equipment locations (guidance package and actuator package) are also evaluated using Eq. (6) and the final notched test spectra. These densities can be compared to that used for component qualification testing to assure that the design environment will not be exceeded during the complete spacecraft testing. Sample acceleration spectral densities are given in Figs. 9 and 10 for the two locations together with the qualification test spectrum envelope.

The envelope is seen to contain almost all of the components' acceleration environment predicted from the spacecraft test. It is noted that the qualification environment envelope is based on the use of measured data from other booster vehicles in the prediction method described by McGregor et al. [5].

CONCLUSIONS

The analyses presented and analytical results show force-controlled random testing of a spacecraft is feasible by the positioning of notches in the test spectra. The notches can be considered the natural attenuations which actually occur at points of high driving impedance at the spacecraft-booster interface. When the amount of the notching is evaluated on the basis that it does not exceed the rms structural design loading at the base of the spacecraft and in the base support structure, spacecraft structural loads and component accelerations are expected to be within design values during the test period. With the assumed method of letting the position and amplitude of notches be based on a limiting force spectrum shape having the same shape as the test spectrum, notching

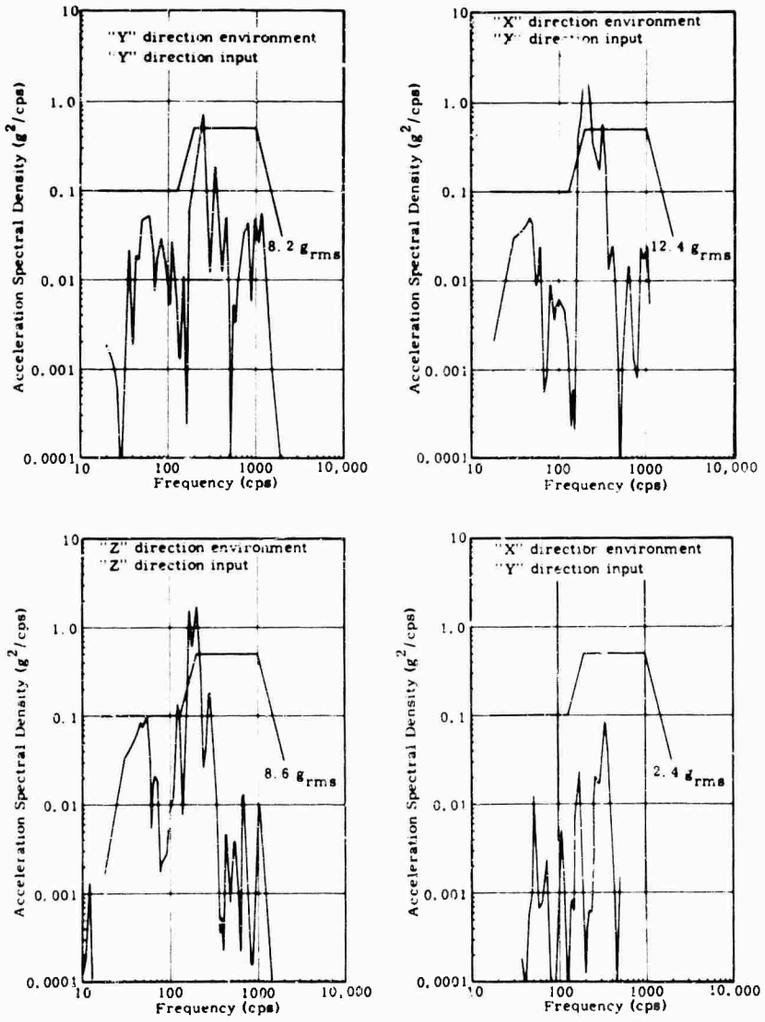

Fig. 9 - Acceleration environment at actuator

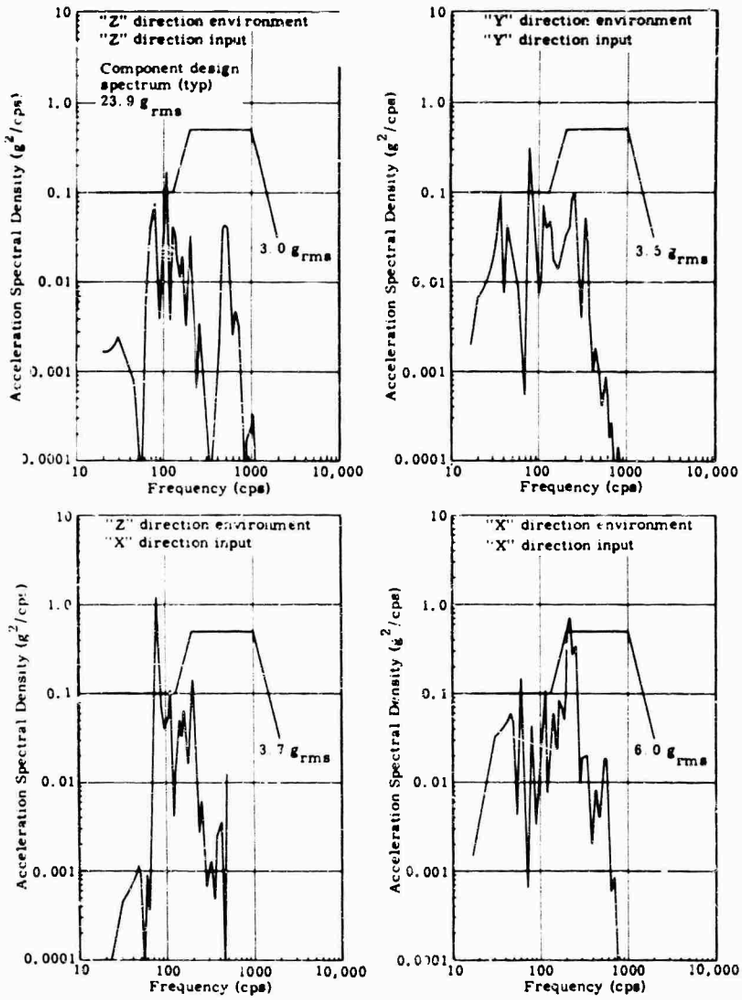

Fig. 10 - Acceleration environment at guidance package

requirements exist only in the low-frequency range of the test spectrum. A more exact method of introducing notches into the spacecraft test spectra would include the use of an available driving force spectrum of the booster; however, these data are generally not coexistent with given test spectra.

REFERENCES

1. R. E. Kaplan and L. P. Petak, "Determination of System Fixed Base Natural Frequencies by Shake Tests," Shock and Vibration Bull. No. 34, Part 3, pp. 95-99, Dec. 1964

2. S. Kaufman and D. B. Hall, "Static and Dynamic Analysis by a Matrix Force Method," Shock and Vibration Bull. No. 34, Part 2, pp. 121-128, Dec. 1964

3. M. Shinozuka, "Random Vibration of a Beam Column," Columbia Univ. Tech. Rept. No. 10, Contract Nonr 266(91), Proj. NR064-470, Oct. 1964

4. R. H. MacNeal, Electric Circuit Analogies for Elastic Structures, Sect. 10.3. John Wiley and Sons, New York, 1962

5. H. N. McGregor et al., "Acoustic Problems Associated with an Underground Launching of a Large Missile," Shock and Vibration Bull. No. 29, Part 4, pp. 317-335, June 1961

DISCUSSION

Mr. Davis (Fairchild Hiller): Wouldn't the notched spectrum that you refer to approximate very closely the unequalized random vibration input that we usually get on a shaker before we equalize it?

Mr. Heinrichs: Usually during equalization you try to match a spectrum and envelope as closely as possible. I don't think that this type of notches occurs in the equalized spectrum shape.

Mr. Forlifer (NASA Goddard Space Flight Center): This notching procedure seems to be based on not exceeding some loads which are derived from a static load criterion, so the whole validity of it hinges on how adequate the static load criterion is. How do you check this?

Mr. Heinrichs: The spacecraft is designed to the static loads criterion and we are trying to perform the qualification test within the design load values. In other words, we do not want to test the spacecraft and then pick it up in pieces.

* * *

COMPARISON OF MARINER ASSEMBLY-LEVEL AND SPACECRAFT-LEVEL VIBRATION TESTS

Peter A. Franken and Terry D. Scharton
Bolt Beranek and Newman Inc.
Van Nuys, California
and
Thomas H. Mack
Jet Propulsion Laboratory
Pasadena, California

Results are presented of a study of vibration data obtained by the Jet Propulsion Laboratory in two series of tests of an electronic assembly from the Mariner C spacecraft. In one series of tests, the electronic assembly was mounted in a conventional vibration test fixture; in the other, the assembly was mounted in the spacecraft. The results of the study can be divided into two categories: those regarding the averaging of large collections of vibration data, and those concerning the differences between assembly-level and spacecraft-level vibration tests. Some recommendations are also given for future random vibration tests of aerospace structures.

P. A. Franken

INTRODUCTION

In the development of the Mariner C spacecraft, the Jet Propulsion Laboratory (JPL) obtained a large collection of vibration data in two series of vibration tests of an electronic assembly. In one series of tests, the assembly was mounted in the spacecraft (Fig. 1); in the other, the assembly was mounted in a test fixture (Fig. 2). In each series, vibration measurements at some 35 positions on the assembly were obtained at several test levels for both random and sinusoidal excitation, along three orthogonal excitation axes.

This paper presents the results of an engineering study of the vibration data obtained in the two series of tests. This study was conducted by Bolt Beranek and Newman Inc., but the data manipulations were performed primarily by JPL personnel utilizing JPL computational facilities. The primary objective of the data study was to compare the vibration environment of the electronic assembly in the spacecraft and fixture series of tests. Differences in both the assembly vibration characteristics and vibration levels between the two series of tests were investigated. A large part of the data study concerned the formulation of different averaging techniques involving averages over uniform spatial regions, similar components, measurement axes, excitation axes, etc.

DESCRIPTION OF ELECTRONIC ASSEMBLY, TEST CONFIGURATIONS, AND VIBRATION DATA

Electronic Assembly

The electronic assembly consists of 20 module boards containing electronic circuitry mounted to a flat chassis plate. The chassis plate (with accelerometers attached) is shown in Fig. 1, and the module boards are shown in Figs. 2 and 3. The chassis plate measures approximately 18 and 20 in. on the sides, and the module boards measure approximately 6 in. on a side.

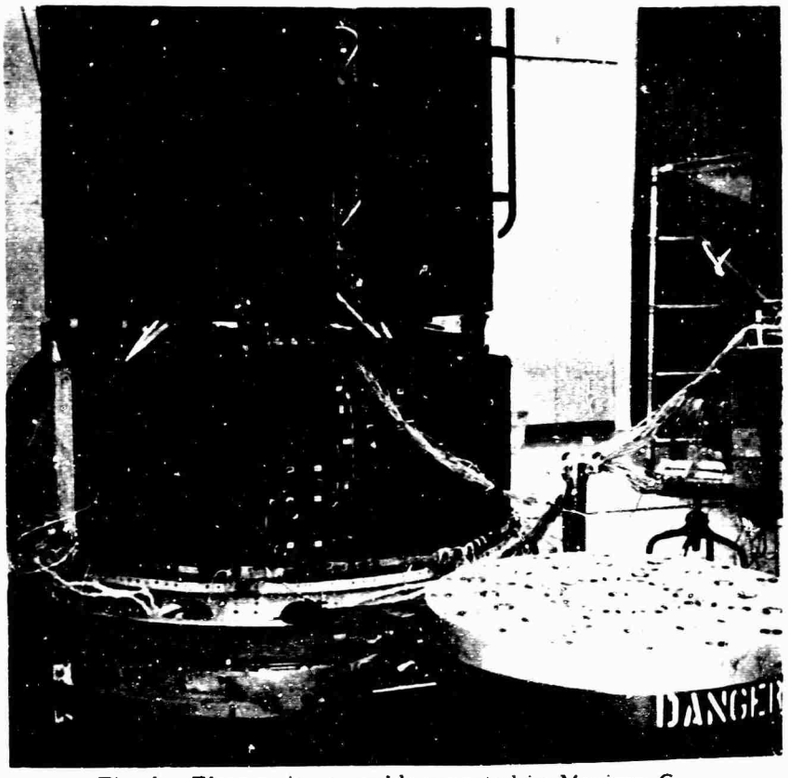

Fig. 1 - Electronic assembly mounted in Mariner C structural test model spacecraft

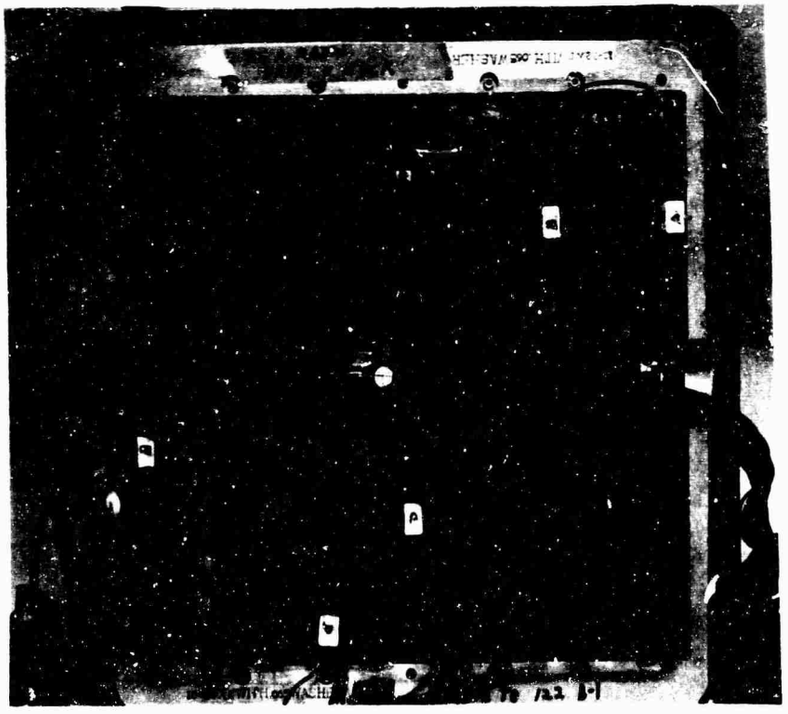

Fig. 2 - Electronic assembly mounted in conventional test fixture

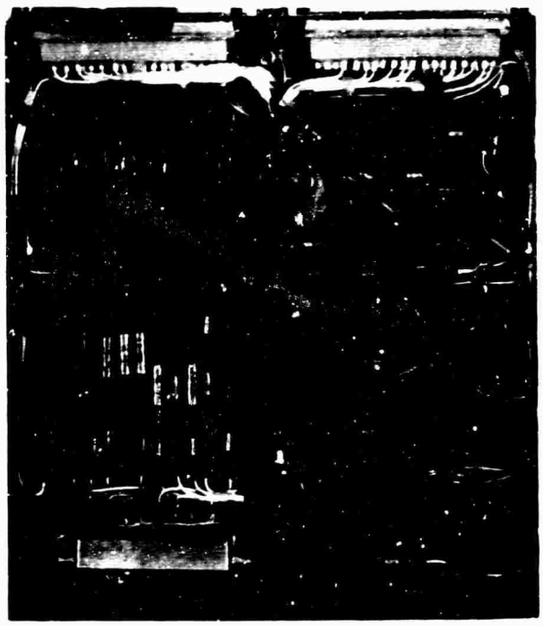

Fig. 3 - Module board from electronic assembly

Accelerometers for response measurement are located close to modules A, B, C, D, and E shown in Fig. 2. For each of these module boards, accelerometers are located in three different regions of the assembly: on the back side of the chassis plate (Fig. 1), on the module board ears where the boards are attached to mounting racks (Fig. 2), and on the face of the module boards (Fig. 3). It should be pointed out that all of these response accelerometers are positioned so as to measure specifically the vibration environment of the electronic components rather than the general vibration environment of the entire assembly. The accelerometers on the chassis plate and the module ears are triaxial, but those on the module boards measure only vibration perpendicular to the boards.

Test Configurations

In the spacecraft tests, the electronic assembly is mounted in the Mariner C structural test model spacecraft as shown in Fig. 1. The spacecraft, complete with adapter, is mounted on a ring-frame-type fixture attached to the mechanical shaker. In the spacecraft test, the excitation levels are controlled by the average response of six accelerometers oriented along each of the three excitation axes and positioned around the circumference of the ring-frame fixture.

In the fixture test, the electronic assembly is mounted in a conventional vibration test fixture as shown in Fig. 2. The excitation levels in the fixture test are controlled by a single accelerometer oriented along each of the three excitation axes and attached to the fixture. Thus, the locations of the accelerometers used to control the excitation levels are quite different in the two types of tests.

Vibration Data

The vibration response data provided by JPL consisted of power spectral density (PSD) plots in the case of random excitation, and amplitude vs frequency plots in the case of sine-sweep excitation. The PSD data covered a frequency range from 100 to 2000 Hz and were plotted vs a logarithmic frequency scale, whereas the sine-sweep data covered a frequency range from 30 to 2000 Hz but were plotted vs a linear frequency scale. The PSD data were also available in digital form so that averaging and other manipulations could be performed automatically.

Data were available for 24 different runs which included low- and high-level random and low- and high-level sine-sweep excitation along three different axes, in both the spacecraft and fixture series of tests. Approximately 48 piezoelectric accelerometer instrumentation channels were recorded for each run. All response accelerometers, except those used for excitation control, were in the same position in the spacecraft and fixture tests.

SUMMARY OF RESULTS

Averaging Large Collections of Vibration Data

The results of the data study can be grouped into two categories. The first category of results concerns methods of averaging large amounts of vibration data to reduce the volume of data and obtain consistent significant trends. This data study resulted from the realization that some sort of averaging was necessary to reduce the volume of vibration data and to bring forth the most important features of the assembly vibration behavior. However, at the onset of the program, we did not know how much sophistication in the averaging techniques would be necessary to bring out the important vibration characteristics and to minimize the noise associated with fine-scale details.

The results of the study indicate that surprisingly little sophistication is necessary for effective averaging. For example, the gross

average spectra (averaged over all spatial regions, measurement axes, and excitation axes), shown in Fig. 4, illustrate many important features of the assembly vibration environment that could not be discerned readily from any single measurement. Our results also indicate that more complex averaging techniques (in which different spatial regions, measurement axes, and excitation axes were treated separately) reveal surprisingly little new information not contained in the gross average spectra of Fig. 4. Thus, it appears that a "law of diminishing returns" governs the results of the various averaging techniques employed. Of course, one might argue that the electronic assembly shown in Fig. 2 is a relatively simple structure compared to other aerospace structures (or in some cases, ensembles of structures) which are of interest in vibration data analysis programs. However, even in cases involving more complex structures, it seems reasonable that the first cut in the data analysis might well be a very gross average of all the data. These gross averages will often suggest examination of individual measurements or formulation of more detailed averages.

It is of additional interest to note that random excitation data were used to compute the average spectra shown in Fig. 4, since the sinusoidal data were not available in digital form. The study indicates that the results of random excitation tests, which are often more realistic than high-frequency sine-sweep tests, can be used efficiently to investigate the vibration characteristics of complex structures.

Differences Between Assembly-Level and Spacecraft-Level Vibration Tests

The second category of results is concerned with understanding the differences in the vibration behavior of the assembly between the fixture and spacecraft tests. Figure 4 illustrates some of the differences in the vibration environment in the two types of test, and Table 1 summarizes the results of a more detailed investigation of the differences.

Referring to Fig. 4, the large peak at approximately 1200 Hz in the average response spectrum for the fixture test is associated with resonance of the test fixture, and thus is not

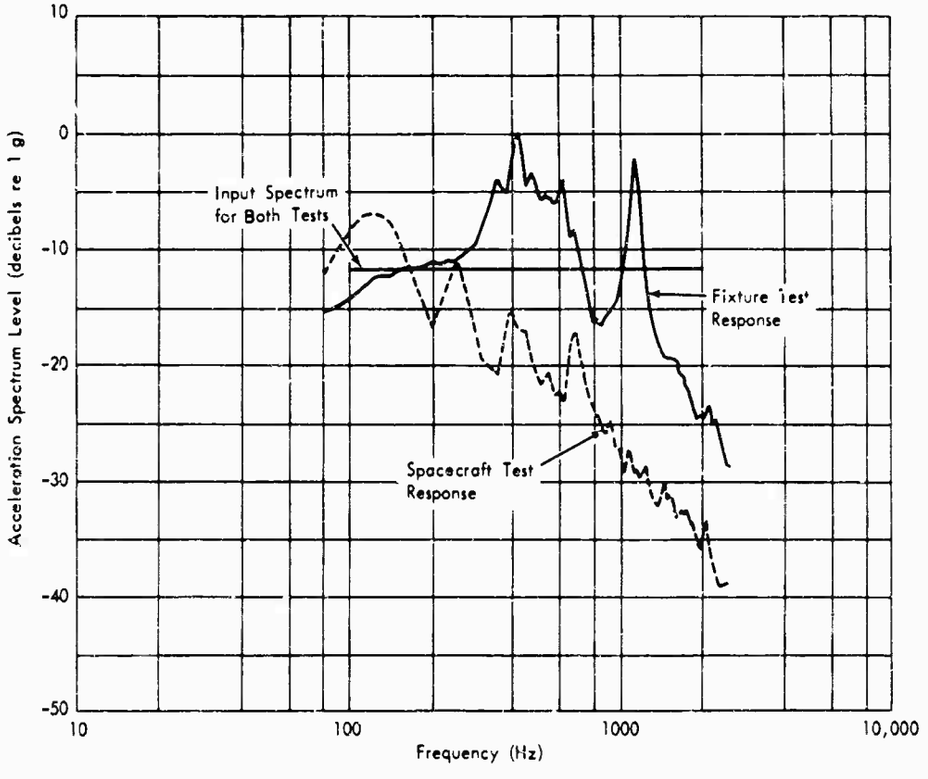

Fig. 4 - Comparison of average response spectra of electronic assembly in fixture and spacecraft random excitation tests

TABLE 1
Comparison of Electronic Assembly Vibration Environments
in Fixture and Spacecraft Tests

Source of Difference	Fixture Tests	Spacecraft Tests
Characteristics	Pronounced fixture resonance	No fixture resonance problems
	Fixture provides coherent excitation	Spacecraft provides relatively incoherent excitation
	Resonant response of module boards governs vibration	Above-resonance response of spacecraft modes governs vibration
	Excitation axis is important except at high frequencies	Excitation axis is relatively unimportant
	Module boards vibrate as rigid bodies at low frequencies, as cantilevers at intermediate frequencies and as a diffuse field at high frequencies	Module board vibration characteristics are similar to those in fixture tests
	Average response is linear with small deviations from linear behavior	Average response is slightly nonlinear with larger deviations from linear behavior than in fixture tests
Levels	High levels at intermediate frequencies	High levels at low frequencies
	Roll-off in response at frequencies above 700 Hz	Roll-off in response at frequencies above 100 Hz
	Relatively large variations in chassis plate response but smaller variations in module board response	Roughly the same magnitude variations in chassis plate and module board response
	Variations in response decrease with increasing frequency	Variations in response fairly uniform with frequency

characteristic of the assembly vibration. In the fixture test the average response spectrum is characterized by six response peaks in the frequency range from 350 to 700 Hz and then a roll-off in response of approximately 12 db/octave at higher frequencies. These six peaks are associated with the fundamental plate-mode resonances of the electronic modules (Fig. 3). The chassis plate (Fig. 1) to which these modules are attached acts to couple these module modes together and split the resonance frequencies apart. It is interesting to note that the 12 db/octave roll-off in the response at high frequencies corresponds to the theoretical result for the response of plate modes excited above resonance by motion of the supports [1].

In the spacecraft tests, the average response spectrum in Fig. 4 indicates that the overall spacecraft modes superimpose on the low-frequency end of the assembly vibration spectrum, and an attenuation associated with the vibration transmission through the spacecraft structure superimposes on the high-frequency portion of the spectrum. The results of more detailed averaging indicate that the direction of the excitation becomes insignificant in the spacecraft-level tests, particularly at the higher frequencies. The results also indicate that at low frequencies the variation in the assembly response is less in the spacecraft tests than in the fixture tests.

The study suggests some recommendations for more realistic fixture-mounted tests of individual assemblies in future spacecraft programs. Figure 4 indicates that future assembly-level tests should have less weight at high frequencies to be equivalent to spacecraft-level tests. The test results also suggest a means of avoiding the problems associated with fixture resonance in future assembly-level tests. In the

spacecraft tests the structure holding the assembly has a complex modal pattern throughout most of the frequency range of interest. This suggests that a comparable "multimodal" mounting be utilized in future assembly-level tests. It is not difficult to visualize such a supporting structure, and some model experiments along these lines have been performed [2]. Additional recommendations for future random vibration tests are contained in the final section of this paper.

DETAILED INVESTIGATION OF ELECTRONIC ASSEMBLY VIBRATION ENVIRONMENT

The vibration environment of the electronic assembly can be explored in more detail by treating different spatial regions, measurement axes, and excitation axes individually in the response averages. The spatial regions considered are the chassis plate, the module ears, and the module boards. No distinction is made among measurements on the five different modules, so in every case the results represent the average vibration environment of all the modules.

Figure 5 illustrates the average response spectra of the chassis plate for different excitation and measurement axes in the fixture random excitation tests. In each case the excitation and measurement axes coincide. The large peak at approximately 1200 Hz occurs only for x-axis excitation. The fact that the 1200-Hz peak is characteristic of one excitation axis in the fixture tests and is absent in the spacecraft tests suggests strongly that this peak is associated with a fixture resonance.

The five peaks between 350 and 700 Hz in the y-axis response of Fig. 5 are very distinct. These peaks are associated with resonance of the fundamental plate-modes of the module boards. (In experiments conducted at JPL, the fundamental mode of a typical module board was found to resonate at approximately 380 Hz.) Since Fig. 5 indicates that excitation normal to the chassis plate is a good exciter of the module modes, the chassis plate must be strongly coupled to the module modes in this frequency range. The multiplicity of peaks between 350 and 700 Hz reflects splitting in the resonance frequencies of the various boards introduced by the chassis plate coupling. The x- and z-axis responses in Fig. 5 indicate that the chassis

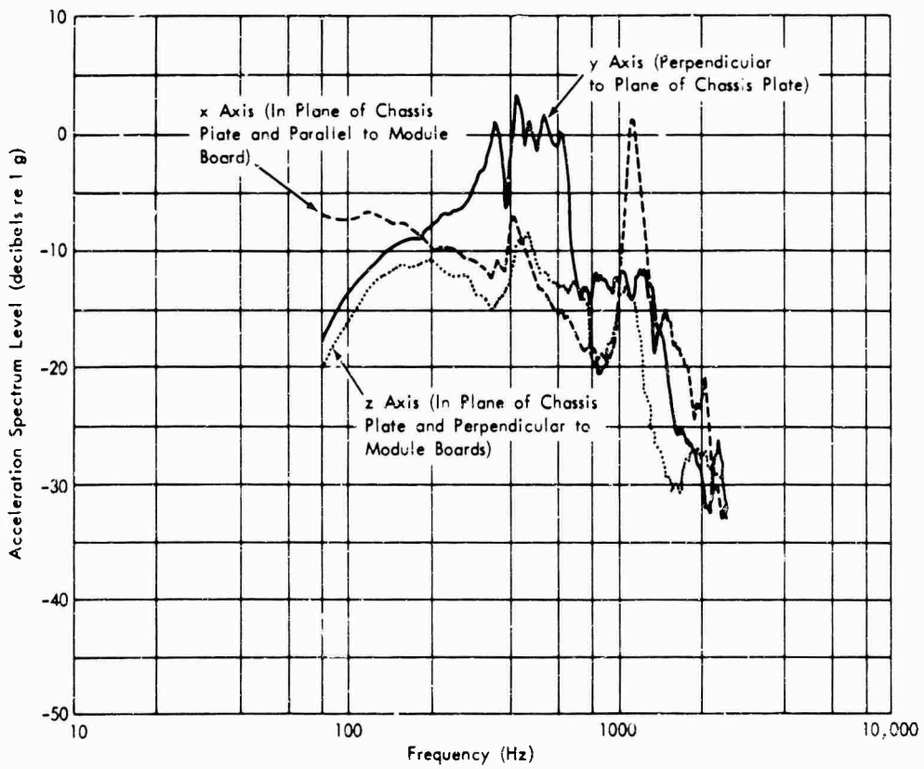

Fig. 5 - Average response spectra of chassis plate in fixture random excitation tests

plate remains stiff in its own plane over the entire frequency range of interest.

Figure 6 shows the average response spectra of the chassis plate for different excitation and measurement axes in the spacecraft random excitation tests. In each case the excitation and measurement axes coincide. Notice that the 1200-Hz peak in the fixture test response is absent in the spacecraft test response. At the lower frequencies, excitation perpendicular to the module boards (z-axis) and perpendicular to the chassis plate (y-axis) are better exciters than excitation in the plane of the module boards and chassis plate (x-axis).

The peak at approximately 100 Hz in the z-axis response must reflect a spacecraft resonance, since the chassis plate is stiff in its own plane. All the response curves in the spacecraft test exhibit several gross low-frequency resonances superimposed on a roll-off in response with increasing frequency. The response of the assembly in the spacecraft tests reflects primarily the above-resonance motion of low-frequency overall-spacecraft modes. The roll-off in the assembly response with increasing frequency can be explained either in terms of high-frequency isolation provided by the "soft" spacecraft mounting or in terms of an attenuation of vibrational energy at high frequencies as one moves away from the base of the spacecraft.

Notice from Fig. 6 that the direction of excitation becomes unimportant in determining the response at frequencies above approximately 300 Hz. This lack of dependence of the response on the excitation axis indicates that at frequencies above 300 Hz the excitation at the base of the spacecraft diffuses in direction by the time it reaches the electronic assembly. Thus, in random vibration tests of complex structures, excitation along a single axis is probably sufficient at high frequencies.

The absence in Fig. 6 of any pronounced response peaks in the 350- to 700-Hz frequency range may appear somewhat puzzling. One might expect the chassis-plate module-board modes, evident in the fixture test response of Fig. 5, to superimpose on the spacecraft response. However, the spacecraft test results indicate that these modes are not excited to any considerable extent in the spacecraft tests. One explanation for the fact that these modes are not excited lies in the possibility that the relatively flexible spacecraft mounting behaves like

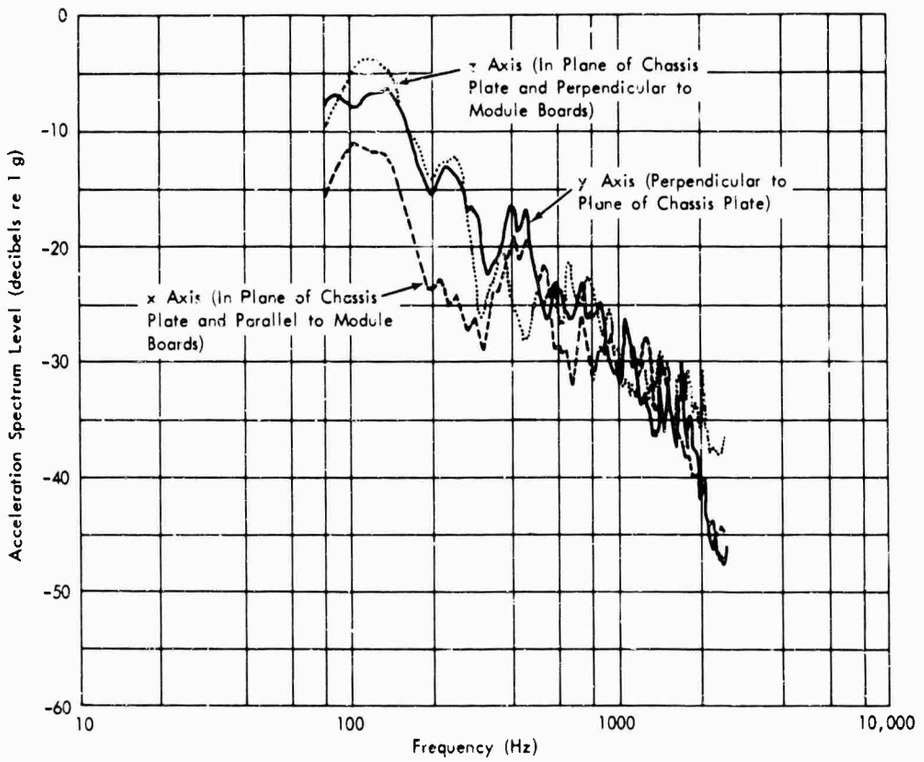

Fig. 6 - Average response spectra of chassis plate in spacecraft random excitation tests

an incoherent excitation source in the frequency range of interest. Previous research [3] indicates that incoherent vibration fields, characteristic of aerospace structures at moderately high frequencies, are inefficient sources of excitation for single-degree-of-freedom systems, compared with coherent vibration sources. (Equation 17 of Ref. 3 shows that the energy transferred from the plate to the connected oscillator is proportional to the average modal energy of the plate. Thus, for a given vibration level on the plate, the energy transferred is inversely proportional to the number of plate modes which contribute to the vibration level of the plate.) The observation that the spacecraft vibration environment is diffuse above approximately 300 Hz lends credence to the incoherent source argument.

Average response spectra at different positions on the module boards show similar characteristics in the fixture and spacecraft random excitation tests. The responses at the three accelerometer positions of Fig. 3 are identical at low frequencies, indicating that the module boards move as rigid bodies. In the frequency range of the module board fundamental resonances, the response amplitude of the module boards decreases as one moves from the tip to the base. The module boards, therefore, behave as if they are cantilevered from the chassis plate. (The module board frames are bolted to the chassis plate and to the mounting racks at the module ears.) It is not difficult to envision a set of modes in which the module boards vibrate like cantilevers, and the chassis plate bending-vibration wavelength determines the relative phase between the motion of the individual modules. At the higher frequencies, the response spectra indicate that the vibration of the module boards is diffuse.

Figure 7 presents a comparison of excitation and response spectrum ratios in the fixture random excitation tests. The flat line at 4.5 db represents the ratio of high-level to low-level excitation spectra, and the response ratio curves represent the ratio of the responses in high-level tests to the responses in low-level tests. Thus, if the system were perfectly linear, the response ratio curves would coincide with the excitation ratio line. When the response ratio curves lie below the excitation ratio line, the results suggest common types of nonlinear behavior such as hardening spring and amplitude-dependent damping. When the response ratio curves lie above the excitation ratio line, the results suggest spurious or unexplained behavior. Figure 7 indicates that the average response spectra (averaged over measurement

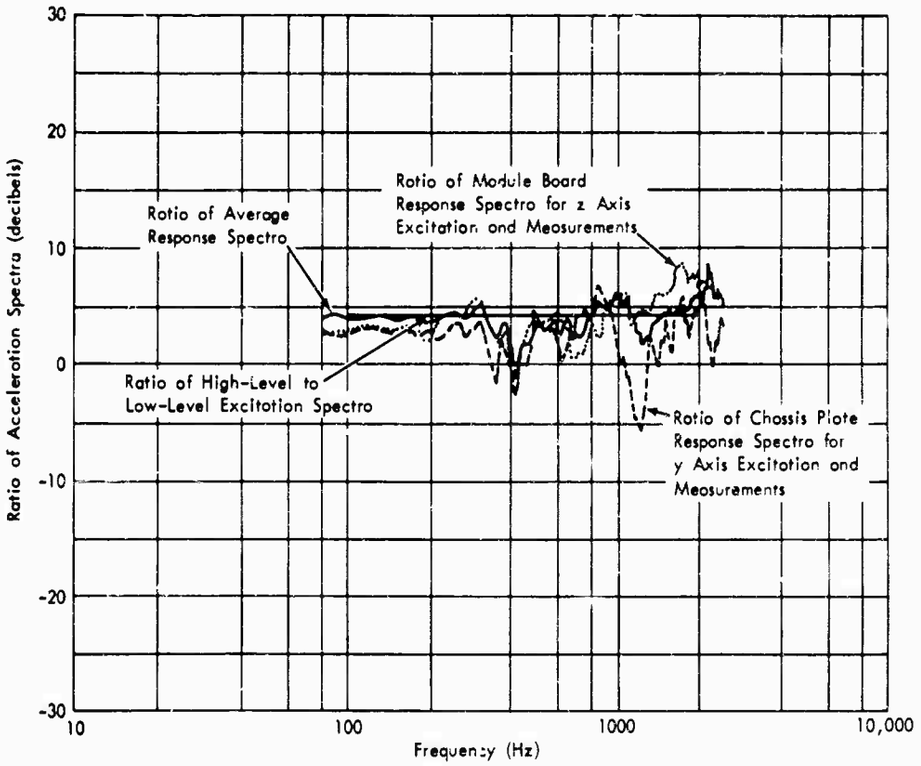

Fig. 7 - Comparison of excitation and response spectrum ratios in fixture random excitation tests

location, excitation axes, and measurement axes) of the assembly behave essentially linearly over the frequency range of interest. In addition to the ratio of average responses, we have also plotted in Fig. 7 response ratios for two particular response measurements which show deviation from the average linear behavior. However, no explanation of these exceptional cases is available.

In the spacecraft test the average response spectra show a slight nonlinear behavior, predominantly in the low-frequency range. This nonlinear behavior in the spacecraft tests at low frequencies possibly reflects the fact that at low frequencies the specified acceleration levels result in relatively large motions in some local regions of the complex spacecraft structure.

To provide an indication of the typical means and extremes encountered, Fig. 8 presents a comparison of the chassis plate response averages and 95th percentile levels between the fixture and spacecraft random excitation tests. The 95th percentile levels are based on a log-normal distribution. The data include different measurement locations, measurement axes, and excitation axes. Figure 8 indicates that the chassis plate response data show considerably less scatter in the spacecraft test than in the fixture test. This result is not unexpected, since previous research [4] has shown that the spatial variation in response is inversely proportional to the number of randomly excited modes which contribute to the response. The result is in the form of a central limit theorem which states that the variance of the sum will diminish inversely as the number of contributing terms. Thus, in the spacecraft test, where a large number of spacecraft modes can couple into the assembly via the flexible spacecraft mounting, the variation in response is small. In the fixture test, where only the rigid body mode of the fixture is excited, the variation in response is large.

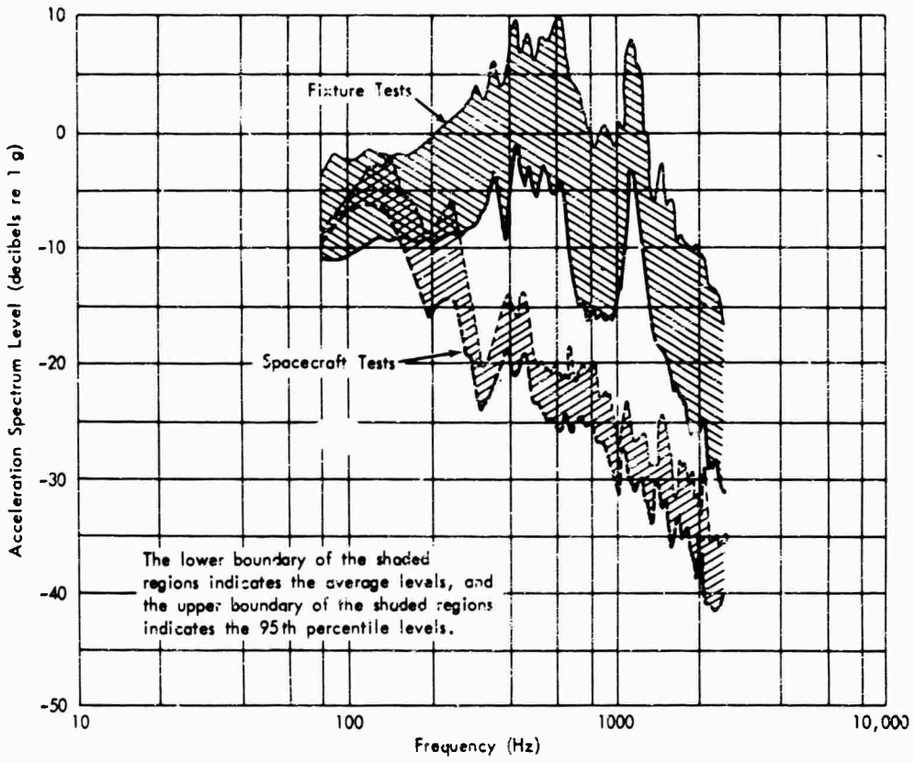

Fig. 8 - Comparison of chassis plate response averages and extremes in fixture and spacecraft random excitation tests

On the other hand, calculation of the means and extremes of the module board response indicates that the response variation in the fixture test is comparable to the scatter in the spacecraft test. Thus, the variation in response in the fixture tests decreases as one moves further into the electronic assembly – away from the fixture.

Figure 9 shows the ratio of the module board average response in the spacecraft test to the average response in the fixture test. The data represent an average over measurement positions and excitation axes. The measurement axis in every case is perpendicular to the module boards. Figure 9 indicates that the response of the module boards in the spacecraft tests exceeds the response in the fixture tests at low frequencies, and hence the fixture tests undertest the assembly. However, at high frequencies (above approximately 200 Hz) the response in the fixture tests exceeds the response in the spacecraft tests, and hence the fixture tests overtest the assembly. It is clear that some frequency shaping of the fixture-test excitation spectrum is necessary to achieve realistic assembly-level testing.

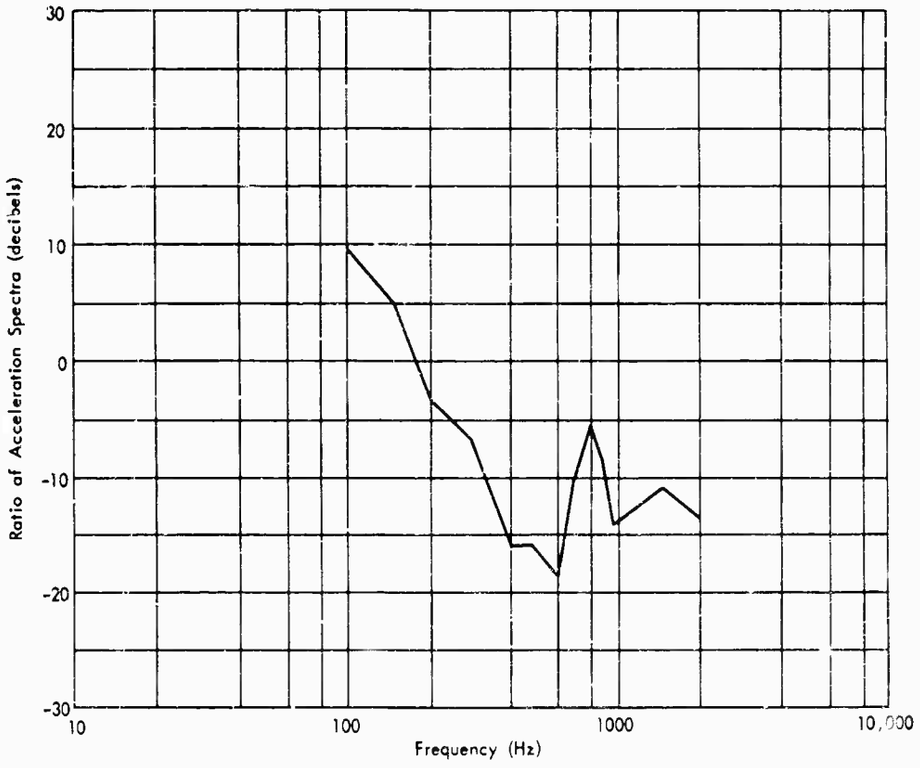

Fig. 9 - Ratio of module board average response in spacecraft tests to average response in fixture tests

The curve in Fig. 9 can also be interpreted as the spectral density levels (in decibels) which must be added to the fixture-test excitation spectrum to achieve identical response of the module boards in the two types of test. The preceding statement is based on the assumption that the spacecraft and assembly behave linearly in the two tests. This assumption seems justified in the light of the small deviations from linearity observed.

It should be pointed out that even though the proposed shaping of the excitation spectrum would produce equivalent response on the module boards in the two tests, the response of the chassis plate might well be higher in the spacecraft test since the chassis plate is a less efficient exciter in the spacecraft tests, where the excitation is incoherent. This example bears out the point that it is usually not possible to simulate the response in every part of a complex structure.

The results of this discussion of the differences in the electronic assembly vibration environments in the fixture and spacecraft tests are summarized in Table 1.

RECOMMENDATIONS FOR FUTURE TESTS

The results of this study suggest the following recommendations for future high-frequency vibration tests of aerospace structure:

1. Develop and utilize multimodal test fixtures or mounting structures to avoid fixture

resonance problems and to provide more realistic excitation sources. In spite of considerable effort to design vibration test fixtures as rigidly as possible, the first bending resonance of conventional fixtures often occurs within the frequency range of interest (approximately 1200 Hz for the Mariner C electronic assembly fixture). As Fig. 4 illustrates, fixture resonance problems can easily result in extremely misleading vibration data. In addition, the coherent source of excitation provided by a rigid fixture is unrealistic and often results in severe overtesting.

The fact that resonance problems and coherent rigid body motion are not characteristic of typical aerospace structure suggests a means of alleviating these problems – design fixtures of light, flexible, multi-modal construction to simulate aerospace structures. We have investigated the use of multimodal fixtures briefly, and the results of our investigation look encouraging.

2. Shape the excitation spectrum in assembly-level tests to compensate for the structural filtering which occurs in spacecraft-level tests and under in-flight excitation conditions. Figure 9 indicates that mechanical vibration transmission through the spacecraft results in amplification at low frequencies and attenuation at high frequencies. These results indicate that assembly-level vibration tests on spacecraft like Mariner C should have increased weight at low frequencies. In contrast, results from other programs, involving the use of mechanical vibration tests to simulate acoustic excitation, indicate that the vibration tests should have increased weight at high frequencies to be equivalent to acoustic excitation. This apparent contradiction points out the necessity of understanding the relative importance of vibration and acoustic transmission paths in future aerospace structures. Some investigations of the vibration and acoustic transmission paths in the OGO and Surveyor spacecraft are in progress [5,6].

3. Exploit simplifications in testing procedures which are afforded by the diffuse property of high-frequency vibrations in complex structures. The results of this study indicate that in many cases the direction or exact location of the excitation source is relatively unimportant in determining the response. These results suggest that in the future it may not be necessary to perform random vibration tests along three different excitation axes – a test along only one axis may suffice. In addition, the possibility of utilizing a number of small mechanical shakers attached directly to the test item should be investigated.

4. Use experimental data from various spacecraft test programs to investigate broadband vibration transmission in complex structures. Although each spacecraft and vehicle is structurally different, we believe that the transmission of high-frequency vibration in complex structures depends largely on a few characteristic properties of the structure.

The results from a large number of programs, involving a wide range of structural configurations, should be analyzed to determine the dependence of vibration transmission on such structural properties as length of transmission path, mass of typical elements, average modal density, and internal damping. The results of such a data analysis program should include both average and extreme values of transfer functions as a function of the most significant structural characteristics. The results would provide guidelines and checkpoints for theoretical work as well as empirical prediction techniques for immediate applicability.

5. Conduct test programs and data-study programs concurrently. The advantages afforded by combining experimental and theoretical efforts in an integrated fashion are well known. Unfortunately, in the case of large programs involving many people and a large amount of equipment, it is not always possible to realize these advantages fully. However, we recommend that preliminary data be analyzed early in test programs to suggest additional and more meaningful tests. For example, one might average together all the preliminary data for a given type of test to obtain a crude picture of the vibration behavior such as that in Fig. 4.

6. De-emphasize high-frequency sine-sweep tests. It is well known that random qualification tests offer several advantages over sine-sweep tests – for example, random tests are less time consuming and usually more realistic. The results of this study indicate that random excitation can also be used in diagnostic tests to uncover the important vibration characteristics of complex structures at high frequencies. Of course, random tests do not provide detailed information available from sine-sweep and relative phase data, but at frequencies much above 200 Hz it is difficult (and usually unnecessary) to determine the exact resonance frequencies and mode shapes of complex structures. To make the most efficient use of test facilities, we recommend that sine-sweep tests of complex structures be avoided in the high-frequency range (above a few hundred Hertz).

REFERENCES

1. Private communication with R. H. Lyon

2. T. D. Scharton, "A New Approach to Random Vibration Fixtures," Bolt Beranek and Newman Inc., 1966

3. R. H. Lyon and E. Eichler, "Random Vibration of Connected Structures," J. Acoust. Soc. Am., Vol. 36, pp. 1344-1354, 1964

4. R. H. Lyon, G. Maidanik, E. Eichler, and J. J. Coles, "Studies of Random Vibration of Coupled Structures," BBN Rept. 967, Appendix 1, p. 28, Eq. 3.12, 1965

5. R. H. Lyon, J. E. Manning and T. D. Scharton, "Analytical Procedure for Determining Random Load Acting on a Spacecraft Due to a Primary Load Acting on an Exterior Structure," 1st, 2nd and 3rd Quarterly Rept., Contract No. NAS5-9601, Bolt Beranek and Newman Inc., June 14, 1965-Feb. 28, 1966

6. BBN letter of June 17, 1966 to A. P. Bowman of JPL, "Proposal to Study Acoustical and Mechanical Vibration Transmission in the Surveyor Spacecraft"

* * *

ACOUSTICALLY INDUCED VIBRATION TESTING OF SPACECRAFT COMPONENTS

Richard W. Peverley
General Electric Company
Houston, Texas

The need for vibration test techniques that provide more realistic simulation of vibration environments, without excessive overtesting, is extremely urgent. The problem of improper impedance matching associated with electromechanical shaker testing has long been recognized. Unfortunately, the use of impedance testing techniques for wholesale qualification testing is not compatible with current spacecraft program budgets and schedules. The approach described utilizes methods of acoustically inducing vibration into simulated structural segments to which components are attached. This technique has received very limited use on early programs. Recently, however, acoustically induced vibration testing was used extensively to qualify Apollo equipment. Approximately 70 components were tested on two distinct structural simulators. One simulator duplicated a segment of the Apollo Service Module radial beam. The acoustic spectrum was shaped to produce vibration levels which satisfied the vibration test criteria. The second simulator was a half section of a service module which was excited by acoustic energy duplicating the "worst case" flight environment. This test program provided an excellent simulation of predicted flight environments plus a reasonable margin of safety.

A description of the use of acoustically induced vibration methods in a mission or space vehicle qualification program and a discussion of the advantages and shortcomings of the methods is also included.

R. W. Peverley

INTRODUCTION

Acoustic simulation has been used as an interim method of determining flight vibration environments. Specifications could be derived from these data and equipment could then be tested on electromechanical shakers. As flight data became available, specifications could be modified to reflect the true mission vibration levels. The addition of man as an integral part of a spacecraft system, however, has created new problems that require a substantial revision of this approach. These problems include the following:

1. A significant number of advances have been made in manned spacecraft structural design techniques and structural materials resulting in lighter weight structure which, very often, is more responsive to acoustic and vibration excitation. Unfortunately, knowledge of vibration analysis and testing methods has not advanced as rapidly.

2. Manned spacecraft often require external devices, such as escape towers and reaction engines, which produce high aerodynamic excitation environments. The higher thrust boosters also produce higher rocket engine noise levels at lift-off, although these higher levels are partially offset by the increased distance from the noise source to the spacecraft.

3. Most spacecraft have little development flight testing and units must often be qualified for the first spacecraft flight.

4. The configuration of many manned spacecraft vary from flight to flight. With the use of lightweight structure, the removal or addition of components can produce significant changes in the vibration response.

5. Rigid schedules often minimize the employment of rigorous developmental vibration testing. Continuous budget adjustments can also result in reduction of some developmental testing. All necessary testing to insure crew safety and mission success is, of course, conducted. Tests that give additional confidence or provide additional insight must often, however, give way to tests more directly concerned with crew safety.

6. Current prediction techniques and electromechanical shaker test methods can contain enough conservatism to produce failures in components that are flightworthy in their natural environment. Some conservatism is, of course, required but should be of a reasonable and known magnitude.

One possible approach to solving these problems is the use of acoustically excited structural segments for both the prediction of vibration environments and for vibration qualification testing. Such a method was used during the Apollo program. Acoustic tests were conducted on a full-scale structure, and the resulting vibration levels were used to derive test criteria. Some vibration qualification testing was then conducted by exciting structural segments with acoustic energy sufficiently high to produce vibration levels equal to the test criteria. This test program demonstrated that this approach has many advantages and should be considered for use on future programs.

This paper presents a general description of the tests conducted and a few examples of the results. The advantages and disadvantages of this approach are also discussed. Since the purpose of the paper is to present an insight into test techniques, many of the important details must be omitted. In addition, some of the more rigorous investigation required to answer some of the open questions is still being conducted.

BACKGROUND

As previously mentioned, acoustic excitation of structural segments has been used extensively as a means of predicting vibration environments but was seldom utilized for qualification testing, although such an approach was proposed several years ago [1]. Some acoustically induced vibration testing was conducted on the Titan program for system level qualification tests with satisfactory results.

A requirement for additional vibration testing of Apollo hardware was generated after the formal qualification program had started and at vibration levels exceeding those used for design and qualification. Thus, some method had to be found to improve the vibration simulation. The dynamic environments and the structural configuration of the Apollo Service Module were such that acoustically induced vibration testing was feasible.

An example of the sound pressure levels measured during Apollo Boilerplate flights and wind tunnel tests is shown in Fig. 1. The data show a scatter of as much as 12 db. A difference of as much as 2 db could be attributed to differences in trajectory and another 2 db to angle of attack. There is no precise explanation for the additional scatter. A spatial average sound pressure level time history for the Apollo Service Module is shown in Fig. 2. The lift-off and Q max sound pressure levels are similar in both spectral distribution and amplitude. The transient near Mach 1 is believed to be associated with a momentary flow separation from the shoulder where the Command and Service Module are joined. The spectrum shape for all the conditions is similar and has a broad peak between 80 and 160 cps with an approximate 6-db roll-off on either end.

A cutaway view of the Apollo Service Module is shown in Fig. 3. The shell is composed of 1-in. thick honeycomb panels. Six radial beams extend inward from the shell to take shear loads. These beams are a web-stringer design made from chem-milled aluminum. The web thickness is 0.018 in. The beams divide the Service Module into six sectors, four containing fuel tanks and two containing equipment shelves. Equipment is also located on forward and aft bulkheads.

It is obvious that this type of structure is highly responsive and that the vibration spectrum can vary greatly from point to point. It is also obvious that the driving point impedance will vary throughout the structure and that the differences in the spacecraft installation and the installation on a shaker head are significant. Thus, acoustically induced vibration testing appeared to be advantageous for this situation.

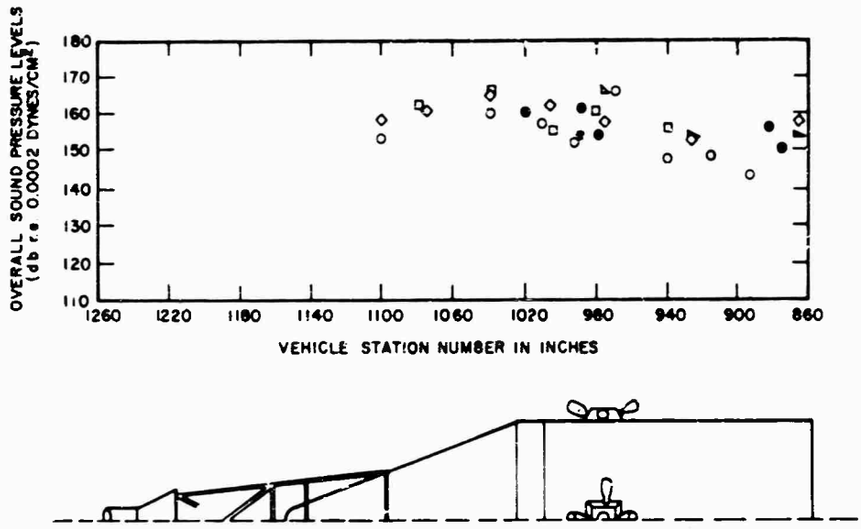

Fig. 1 - Distribution of sound pressure levels on Apollo Command and Service Modules as measured during wind tunnel testing and Boilerplate flights; Mach number 1.55, various angles of attack

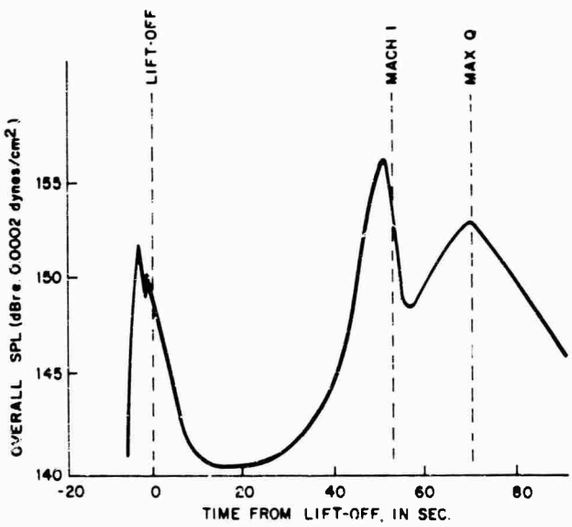

Fig. 2 - Typical rms sound pressure level time history for Apollo Service Module

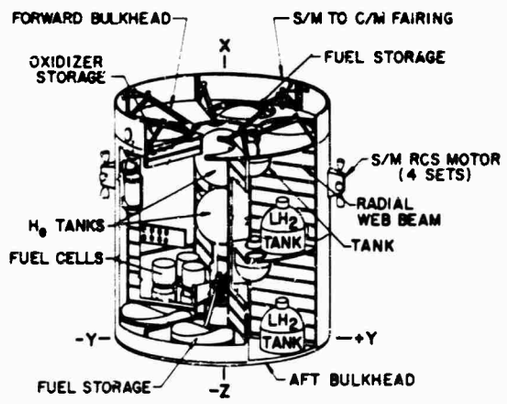

Fig. 3 - Cutaway view of Apollo Service Module

TEST PROGRAM

Two types of tests were conducted. Components mounted on the radial beam were tested on a simulated beam segment at the North American Aviation Space and Information Systems Acoustic Test Facility. All other equipment was tested on a half-segment of an Apollo Service Module (referred to as the 180-deg SM segment) at the North American Aviation, Los Angeles Division Acoustic Test Facility. The 180-deg SM segment was specially fabricated and was geometrically similar to a Service Module cut by a plane through the longitudinal axis. A sketch of this setup is shown in Fig. 4.

At the time the tests were conducted, the vibration specifications had been based on acoustic tests conducted on a full-scale Service Module, which contained only a limited number of mass simulated components. Thus, the data from the acoustically induced vibration qualification tests had to be compared with data from other acoustic tests. As flight data became available, it was possible to assess properly

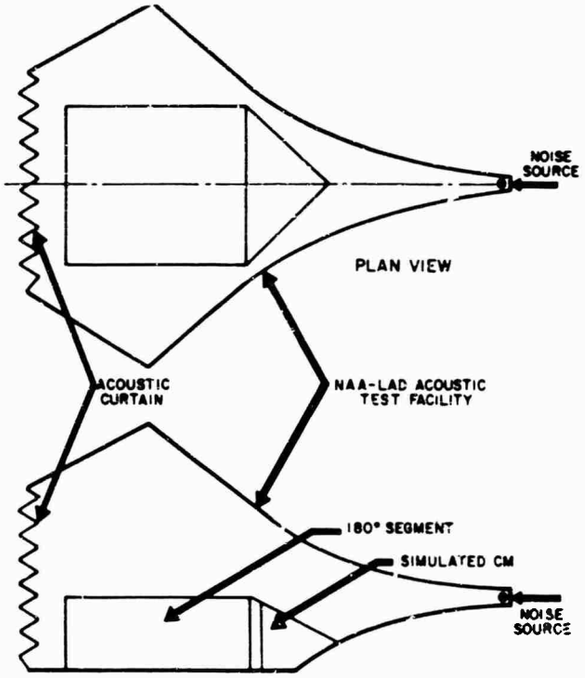

Fig. 4 - Typical test setup for 180° SM segment acoustically induced vibration tests

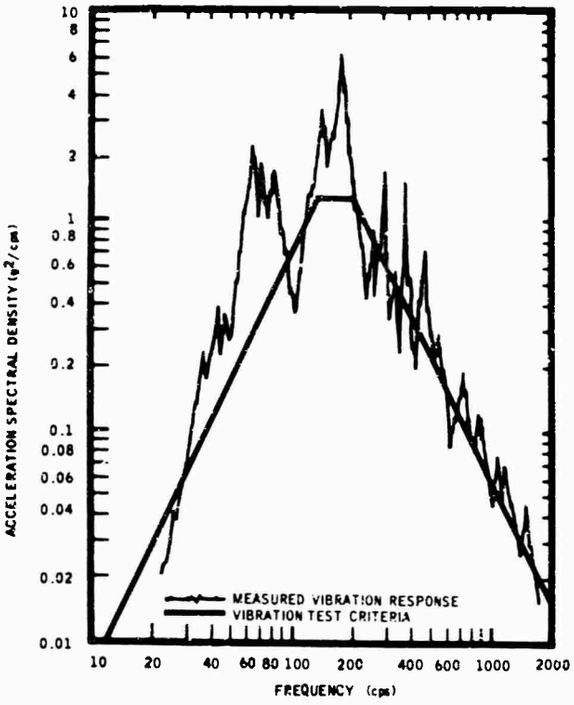

Fig. 5 - Example of vibration levels measured at base of component during acoustically induced vibration test on simulated Service Module radial beam

the conservatism of the test, as is described later in the paper.

Radial Beam Tests

Components normally mounted on the Service Module were tested on a simulated beam segment which contained three shear web panels. The acoustic spectrum was adjusted to produce a beam response equal to the vibration test criteria. Examples of how well the response could be controlled are shown in Figs. 5 and 6. For Fig. 5, the component was mounted to a bracket attached to the beam stringers. The example shown in Fig. 6 was from a large panel mounted between stringers. The data in Fig. 5 show a slight overtest while the data from Fig. 6 compare very well.

180-Degree Segment Tests

The original criteria had been derived from a full-scale structural segment which contained a very limited number of components and was excited by a reverberant acoustic field. Thus, it was necessary to calibrate the 180-deg segment in a plane wave field with essentially the same mass loading. A comparison of vibration measurements taken at identical locations on

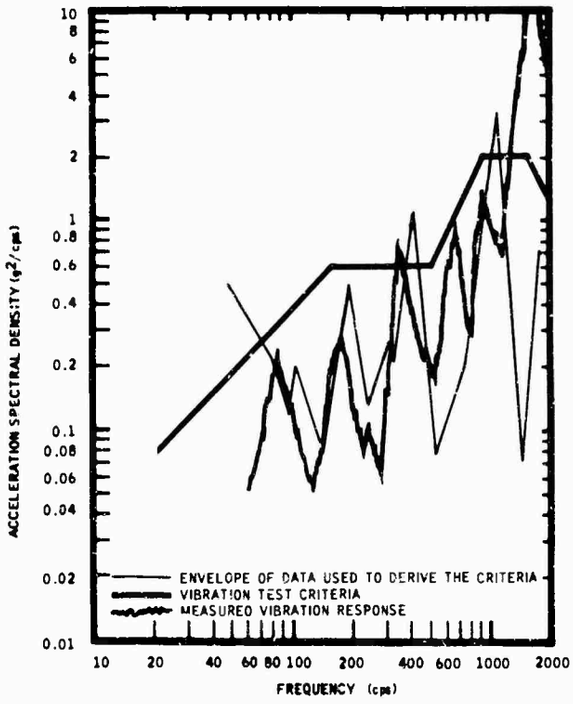

Fig. 6 - Comparison of vibration test criteria and envelope of data used in deriving test criteria compared to data measured at similar location during acoustically induced vibration tests on simulated radial beam

the full-scale test and on the 180-deg SM segment is shown in Fig. 7. The acoustic excitation was at 152-db sound pressure level. The vibration response was duplicated reasonably well except in the neighborhood of 100 cps. It is shown later that this difference is not significant.

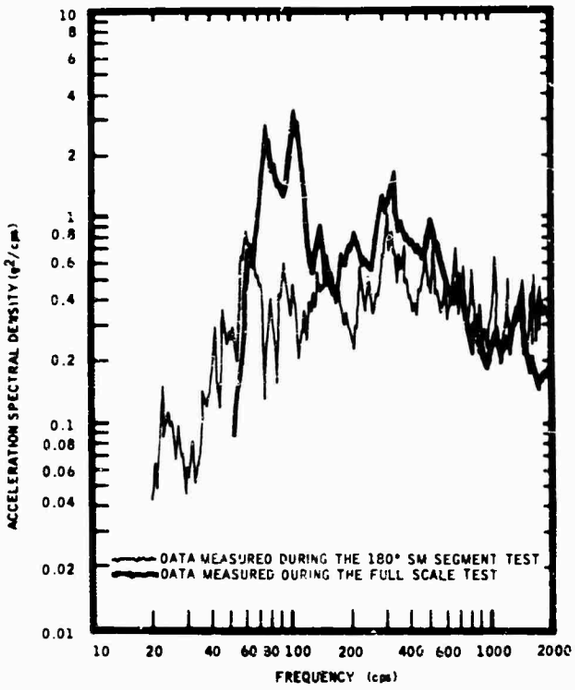

Fig. 7 - Comparison of vibration data measured at same location during 180° SM segment test and full-scale Service Module test that was primary source of data used in deriving vibration test criteria; accelerometers located on forward bulkhead

Components were then mounted in their flight configuration, and the test was conducted. Several tests were made so that equipment could be tested in sets, generally according to subsystem. This approach combined maximum utilization of test facilities with minimum component monitoring problems. Two examples of data are shown in Figs. 8 and 9. In Fig. 8, the addition of the component weight had no significant effect on the response of the bulkhead. In Fig. 9, however, the differences were large. Since the vibration test levels had originally been derived from an unloaded bulkhead, the test criteria would have been overly severe on the component, as shown in Fig. 9.

The tests were generally conducted at an overall sound pressure level of 152 db, which simulated the spatial average aerodynamic noise level at Q max. The time duration was 2-1/2 min. An additional test was also conducted at 156 db for 10 sec to simulate the pressure transient at Mach 1 (Fig. 3).

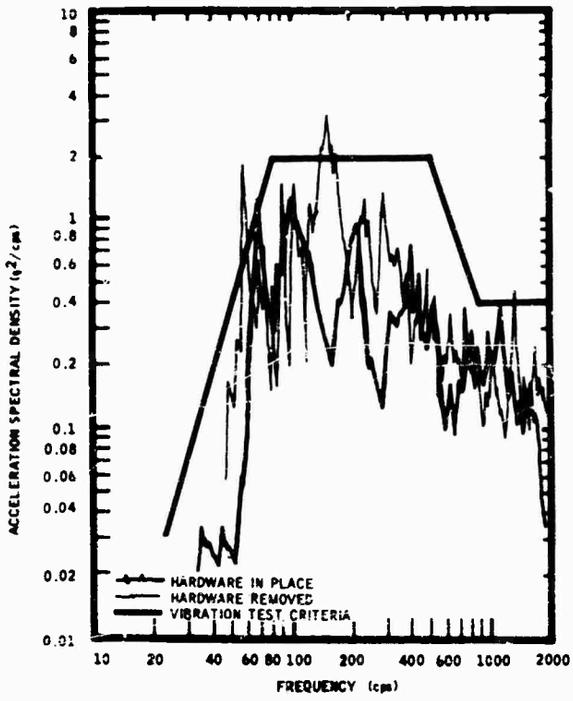

Fig. 8 - Comparison of vibration measurements acquired on 180° SM segment forward bulkhead during test with component in place and during test with component removed

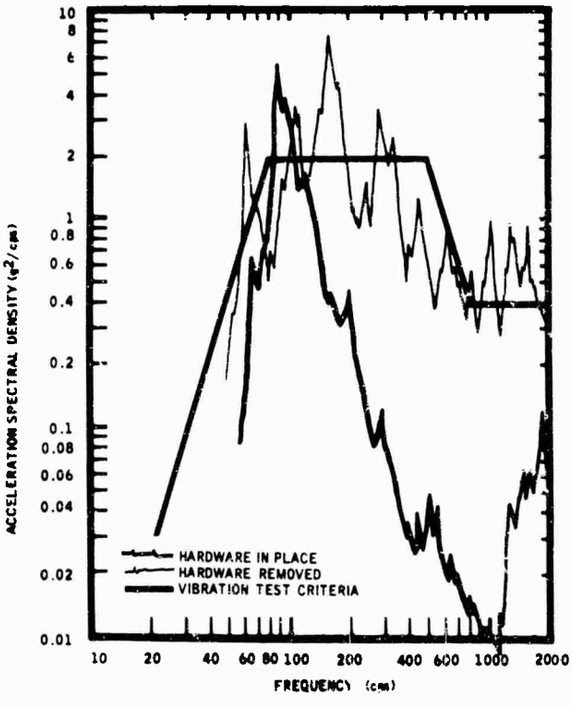

Fig. 9 - Comparison of vibration measurements acquired on 180° SM segment forward bulkhead during test with component in place and during test with component removed

The results were very encouraging. A limited number of failures occurred, although the vibration levels were very high. When failures did occur, it was found that the simulated structure was very useful in searching for a convenient "fix." As a matter of interest, eight components were tested on both the 180-deg segment and on shakers. Four failures occurred during the shaker tests with no failures during the acoustic test. No known vibration failures have occurred thus far in flight.

The data acquired during the first Apollo spacecraft flight were used to determine the degree of simulation during the test. A comparison of data taken at duplicate locations on the outer skin of the Apollo Service Module during flight and during the full-scale ground test is shown in Fig. 10. Obviously, the ground acoustic test provided a more severe vibration environment than occurred during flight. Although the work on these data is not sufficiently complete to provide a conclusive answer, one might suspect that the difference in spatial correlation is the largest factor in producing the different responses. Thus, at frequencies above 200 cps, the acoustically induced vibration test provided a safety factor slightly in excess of 1.5, while below 200 cps the margin was much greater.

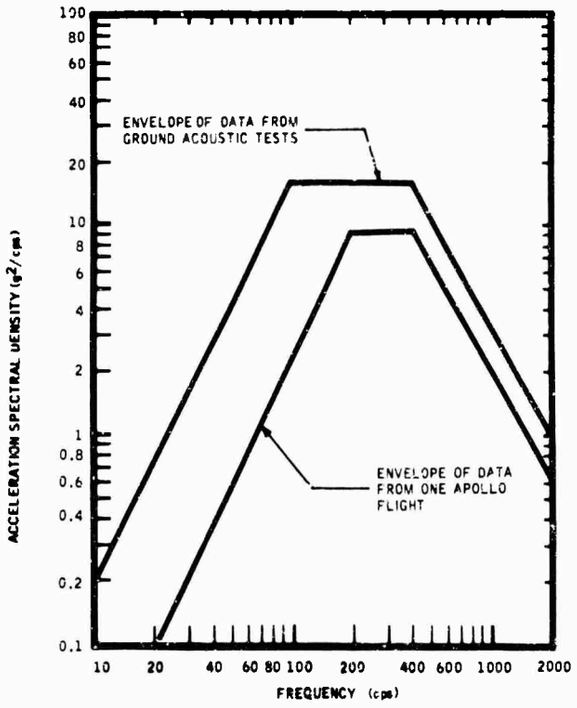

Fig. 10 - Comparison of data envelopes at duplicate points on Apollo Service Module outer shell where data were taken during one Apollo flight and during acoustic test on full-scale Service Module structure

CONCLUSIONS

Some of the advantages of acoustically induced vibration testing are as follows:

1. Accurate duplication of mounting point impedance is the most significant advantage. The problems associated with the impedance mismatching inherent in most vibration qualification testing being conducted today have been widely discussed and are not worth repeating here. The accurate duplication found in this type of test does, however, allow the vibration engineer to determine or specify the test safety margin with some reasonable confidence.

2. The elimination of three-axis testing assures the reduction of fatigue failures that often occur as a result of overexposure. At the same time, the acoustically induced vibration test does assure that no cross-coupling effects have gone unnoticed.

3. The effect of tubing and wire bundles on component response can be determined. In addition, tubings and fittings can also be conveniently tested.

4. Major systems and subsystems can be tested at the same time. Thus, convenience of installation and monitoring is gained and the effect of component outputs on system performance can be accurately determined.

5. Possible structural modification can be tested experimentally where localized responses have produced component failures. Slight changes in component location can also be conveniently investigated.

6. Changes in equipment configuration can be conveniently tested.

7. Components with dual attachment points (such as one end on the skin and one end on the shelf) can be conveniently tested. This situation has always presented a problem on shakers, particularly where the vibration levels at each attachment point are significantly different.

There are several obvious disadvantages:

1. Large test facilities are required. This requirement would preclude final qualification testing being done by a vendor. Tests would be conducted, instead, at the major contractor's facility. Such a situation would require a major change in present methods of writing contracts that include qualification requirements. Perhaps some development testing could be accomplished at lower vibration amplitudes to ferret out weak

design with final qualification testing done at the major contractors. Many possible methods of managing such a contract seem to be feasible, however, and this problem should not present an insurmountable constraint.

2. A better understanding of the differences in aerodynamic versus acoustic loading must be obtained. From the figures, one could conclude that some adjustment in the acoustic spectrum would have provided a constant safety margin. Hopefully, this difference will be better understood in the near future.

3. Some spacecraft do not lend themselves to acoustically induced vibration testing. Such was the case with the Apollo Command Module. This vehicle is not symmetrical; thus, it would not have been possible to conduct a segment test. The cost of constructing a full-scale Command Module for this type of test was also prohibitive. Finally some equipment could not be mounted without removing and replacing the heat shield which required a special fixture which would make such a test time consuming and extremely inconvenient. The Command Module structure, however, is stiffer and less responsive. Thus, the vibration levels were lower and impedance matching (or mismatching as the case may be) did not present such a problem.

Such a test program is not entirely without some risk of over- or undertesting. Comparison of the data from the full-scale acoustic test, flight, and the 180-deg SM segment test showed that some narrow-band peaks were not covered in the test, generally at frequencies above 500 cps. In most cases, these peaks would not have been developed in formulating the test criteria. Although each case requires individual assessment, the risks involved in not including these narrow peaks seem, indeed, to be small and worth taking when considering the amount of overtesting that occurs when all of the notches are filled during a shaker test. Some overtesting can also occur. In Fig. 6, a sharp peak occurred above 1500 cps that was far in excess of the test criteria. Efforts to reduce the input spectrum were futile. This peak was attributed to a local resonance that did not appear in the original data. Such occurrences should be rare and should not compromise the quality of the test.

The results of these tests were encouraging to those involved and were very favorably received by management. Indeed, acoustically induced vibration testing will be conducted as a routine matter on all Apollo Block II Service Module hardware. This experience seems to indicate that acoustically induced vibration testing could also be considered as a routine part of any missile or spacecraft program, where conditions permit.

ACKNOWLEDGMENT

The author is grateful to D. E. Newbrough for assistance in preparing much of the background work presented in this paper.

REFERENCE

1. R. Peverley and H. McGregor, "Missile Component and Vibration Environmental Prediction and Test Methods," IAS Paper 62-48, Jan. 22, 1962

DISCUSSION

Mr. Scharton (Bolt Beranek & Newman): I would like to raise some general questions concerning the relative advantages of acoustic testing versus substitute vibration testing. While it is true that in aerospace vehicles the primary source of excitation is usually acoustic or boundary layer noise, I think electronic equipment in the secondary structure is more efficiently excited by mechanical vibration established on the primary structure. This suggests a possible means of simplifying vibration tests in which the primary excitation was actually acoustic or boundary layer. With this alternate procedure, substitute acoustic testing, a reverberant vibration field is established with small shakers on a shroud or mounting structure as the source of excitation. Using mechanical shakers is, of course, the opposite approach to that you presented. However, it offers several advantages. One, of course, is that mechanical excitation is a lot more efficient than acoustic excitation for most small equipment. Also, in many cases we think that you can actually simulate more realistically the vibration field on a shroud, an adapter or thrust network with mechanical shakers than by plane wave acoustic excitation.

How does your acoustic excitation compare with substitute mechanical excitation with small shakers?

Mr. Peverley: I cannot entirely answer your question because I guess I do not really understand how using shakers is more efficient. As far as we were concerned on the Apollo program, our mechanically induced vibration coming from the Saturn booster structure or from the engines is much less than acoustically induced vibration. The biggest problem we had was how to simulate the correlation in this particular set of tests. We have gone into this much more extensively in tests with the Lunar module and have pretty well determined that the correlation at max Q is random. We have been able to duplicate vibration levels in the laboratory much better than we did here.

Mr. Roberts (Martin Co.): I could not determine whether the first spectrum you showed, which was measured on the spacecraft itself, was indicative of the response vibration or whether it was meant to be the picture of the excitation. Could you comment further on the fact that at lift-off and max Q, the spectrum was all the same?

Mr. Peverley: That was the acoustic spectrum. From the measurements we had, the spectrum characteristics at max Q and at lift-off and during this transonic region were sufficiently similar that we could envelop these to come up with test criteria.

Mr. Roberts: The phenomena associated with the acoustic excitation at lift-off certainly are not the same as those at supersonic speeds.

Mr. Peverley: I agree. Nevertheless, I am showing here the data we investigated. These were measured data from wind tunnel tests, flight, and from a large number of static firings. The spectral characteristics were indeed similar.

Mr. Gorton (Pratt and Whitney Aircraft): These two last papers seem to fit together very nicely. In the first paper I was somewhat tempted to comment, what have we been doing the last two years? Exactly the same recommendation was made in Monterey, that what was needed was a light flexible mounting to simulate properly the real environment. The previous paper gave the impression that no progress had been made. This last paper indicates that maybe progress has not so much been made in testing with acoustic excitation as it has in producing a more realistic mounting of the equipment which gives a better result whether excitation is acoustic or by small shakers. Certainly the mounting is properly simulated in your method.

* * *

REPRODUCTION OF COMPLEX AND RANDOM WAVEFORMS AT VARIOUS POINTS ON A TEST ITEM*

John V. Otts and Norman F. Hunter
Sandia Corporation
Albuquerque, New Mexico

A technique is introduced whereby the Fourier series of any reference waveform can be reproduced at points on or below a test specimen. Any test item-shaker system will have some motion transfer function $H(jw)$ from the exciter input to a response point on the test specimen. Peak notch equalizers with the transfer $H^{-1}(jw)$ are inserted in the system to produce a nearly flat amplitude and phase spectrum for the net system response. In addition, a compensation system is used to improve the low-frequency response. A fast sweep oscillator and a B&K response tracer allow equalization to be accomplished in hours as compared to days for earlier systems.

The test setup, test procedure, and results are presented. Both a mechanical system and an electrical analog are used to illustrate the accuracy of this technique. This capability was developed to reproduce a test specimen's field vibration response in the laboratory. In these cases, the tape record serves as the reference signal. Specific areas of application include simulation of vibration experienced during lift-off of a rocket-payload system, simulation of vibration during ejection from an aircraft, and reproduction of the vibration-time history at the base of internal system components.

N. F. Hunter

INTRODUCTION

Most vibration test specifications are written in terms of a flat motion-controlled input. These specifications are unrealistic since the apparent weight characteristics of the test specimen are ignored. In other words, the test specimen is not allowed to affect its environment as it does in the field. A more complete argument against motion-controlled input is given by Otts [1].

During the past few years, the Vibration Division at Sandia Corporation has been working toward more realistic vibration tests. The primary objective of this work has been to allow for the environmental effects of the test item. As a result, many vibration tests conducted at Sandia Corporation incorporate one or more of the following concepts: g limiting [1], force limiting [1,2], force control of the input [1], and apparent weight simulation of the test specimen's foundation [2]. In addition, several test series have been conducted to derive test specifications experimentally from blocked force tests and apparent weight analyses [3].

A test capability which will further increase the validity of vibration tests is that of reproducing a reference sinusoidal, complex, or random vibration signal at any location on or within a test specimen, where the reproduced and reference vibration spectra are nearly exact in both amplitude and phase All previous attempts to reproduce a reference vibration had been unsuccessful due to our inability to compensate accurately and efficiently for the transfer function from the vibration exciter to the

*This work was supported by the United States Atomic Energy Commission.

control point. The basic instrumentation used to overcome this problem consisted of peak notch equalizers, a fast sweep oscillator, and a response tracer.

DISCUSSION

The vibration history of items being field tested is sometimes recorded on tape. Using this record as the reference signal, similar test specimens and/or components can be subjected to the same field vibration. Of particular interest is the reproduction of short vibration histories such as during ignition and lift-off of a rocket-payload system or during ejection of a specimen from an aircraft.

The reality of this type of test is dependent on the following: (a) the apparent weights of the field unit and those tested in the laboratory should be similar; (b) the apparent weights of the field and laboratory specimen foundation should be similar; and (c) the source of field excitation should be repeatable or representative of the maximum anticipated.

TEST SPECIMEN RESPONSE

Consider the electrical "mobility" analog of the test unit and foundation indicated in Fig. 1. Here the voltages and currents represent the velocities and forces, respectively, at points on the test item. In the field, E_{obs} and I_{obs} are the velocity at and the force driving a point of interest on the test item. Let E_i and I_i in Fig. 1(b) represent the motion and force at the test specimen-foundation interface. Assume that in a vibration test, the field motion E_{obs} is duplicated by a means to be discussed. Now as indicated in Fig. 1(c), E_{obs} occurs across some element Z_z in the test specimen. For similar laboratory and field-tested items, Z_z is duplicated so I_{obs} must be duplicated. For the general test item of Fig. 1(c), the following relations hold:

$$E_i = A\,E_{obs} + B\,I_{obs}. \qquad (1)$$

and

$$I_i = C\,E_{obs} + D\,I_{obs}. \qquad (2)$$

E_{obs} and I_{obs} are known to be the same in both field and laboratory tests; therefore, E_i and I_i, the interface motion and force, will also be duplicated. When motion observed at some point on a field test item is reproduced in the laboratory, all other responses in the item back to the interface will be reproduced. Certain assumptions implicit in this discussion should be noted:

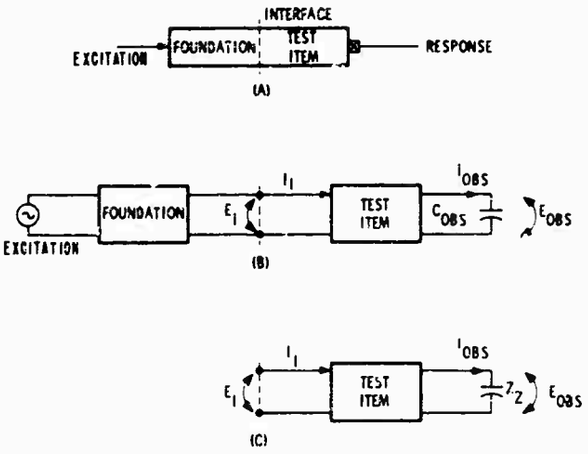

Fig. 1 - (a) Test item and foundation, (b) electrical "mobility" analog of test item and foundation, and (c) electrical "mobility" analog of general test item

1. Field and test units should have similar mechanical parameters such as apparent weight.

2. Field and test inputs from the foundation occur at the same points and may be approximated by a single or averaged input. The foundation apparent weight need not be duplicated if this holds.

3. The system is assumed to be at least approximately linear. Some of these assumptions may be violated in a test. For the case of multiple inputs, it is desirable that the field and test foundations have similar apparent weights. Some field inputs, such as aerodynamic excitation, would be very difficult to reproduce.

BASIC METHOD

For reproduction of field vibration responses, the system shown in Fig. 2 is assembled. Some frequency transfer function $H(jw)$

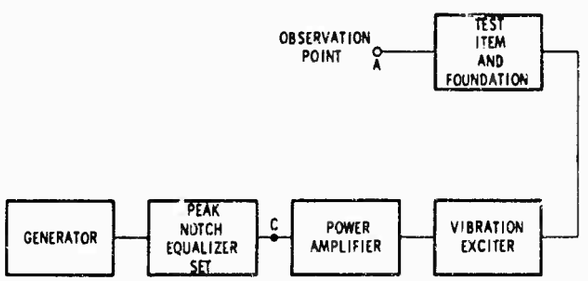

Fig. 2 - System for reproduction of field vibration responses

will exist from C to A through the power amplifier, shaker, foundation, and test specimen system.

The peak notch equalizer set is adjusted to produce the inverse of this frequency transfer function. Then the spectrum from the tape or oscillator input to the observation point at A is flat. Any wave shape introduced at the input will appear at the output since its Fourier spectrum will be reproduced. To verify this method, two experimental setups were used: an electrical "mobility" analog and a mechanical system.

INSTRUMENTATION

The system of Fig. 3 simply substitutes an electrical "mobility" analog for the usual mechanical vibration system. In earlier experiments a setup time of several days was required since the frequency spectrum was observed with a plotter. Numerous adjustments of the peak notch equalizers are necessary when setting up, so many plots had to be made before the final equalized spectrum was obtained. This difficulty was overcome by obtaining a fast sweep oscillator with a maximum sweep rate of 3 dec/sec. With a Bruel and Kjaer Response Tracer, this allows a virtually continuous display of the approximate system spectrum. Setup time is reduced from days to hours. The peak notch units are MB Electronics Model N20 and will synthesize one peak and one notch per unit. Peak and notch frequency are variable from 20 to 2500 cps with maximum response ratios of 100.

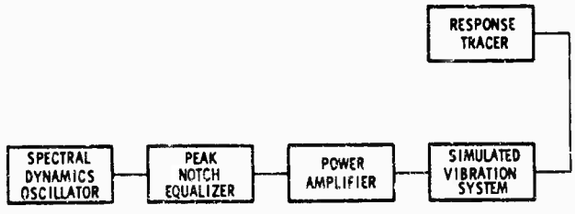

Fig. 3 - Basic analog equalization system

ELECTRICAL ANALOG

The mobility analog of Fig. 4 represents a three-mass two-spring mechanical system. For a constant voltage input the spectrum of this analog includes the two resonant peaks of Fig. 5. After proper adjustment of the equalizers, the overall spectrum in Fig. 6 is flat within ±1 db from 20 cps to 1 kc.

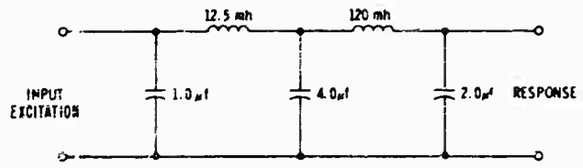

Fig. 4 - Electrical analog of 3-mass 2-spring system

A square wave (chosen because of its availability, large harmonic content, and the ease of noting distortion) is next applied with the oscillator. For a 20-cps input frequency, the waveforms of Figs. 7 and 8 show the effect of equalization on the system. With the system unequalized, considerable distortion of the square wave is evident at the system output. Square wave harmonics with frequencies near the 300-cps system resonance are amplified and are responsible for much of the distortion. Power amplifier output is notable in that it indicates a roll-off in the spectrum below 20 cps, producing a tilt in the square wave. With the system equalized, the output is a much better reproduction of the input though considerable tilt is noticeable in the square wave.

The low-frequency roll-off which produces this tilt cannot be corrected with the peak notch equalizers, since they will not synthesize peaks below 20 cps. This tilt, however, corresponds largely to shifting in phase and reduction in amplitude of the square wave fundamental frequency. With the addition of the tracking filter and summer in Fig. 9, the fundamental lost through the RC coupled amplifiers may be restored. The square wave fundamental is extracted by a tracking filter. Addition of this fundamental of the proper amplitude and phase at the power amplifier input results in a drastic reduction of the square wave tilt. The resultant system waveforms in Fig. 10 show no observable tilt at the output. Some harmonics may be observed riding on the output square wave in Fig. 10, but their amplitude is less than 15 percent of the fundamental. Ordinarily, this low frequency compensation method would be applied to waves whose fundamental frequency is below 50 cps.

As a further check on the validity of wave reproduction by equalization, the rise time and harmonic content of the square wave in Fig. 8 were measured. All harmonics to 2 kc were present in the proper amplitude ratios. The equalized square wave had a measured rise time of 100 μsec, while the rise time at the oscillator output was 0.17 μsec.

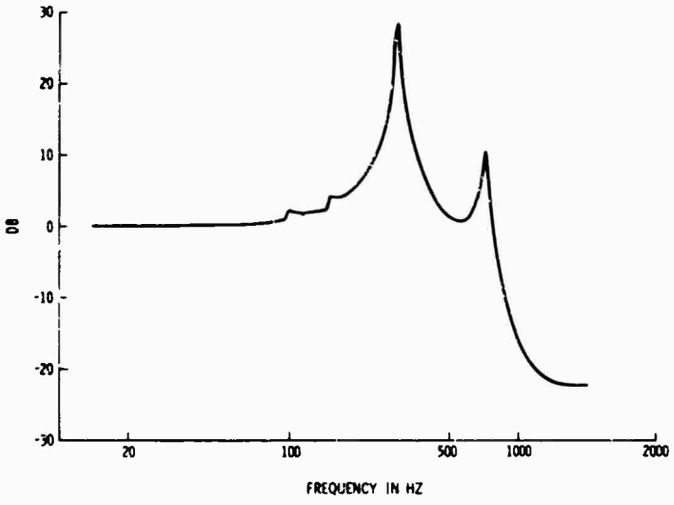

Fig. 5 - Electrical analog spectrum

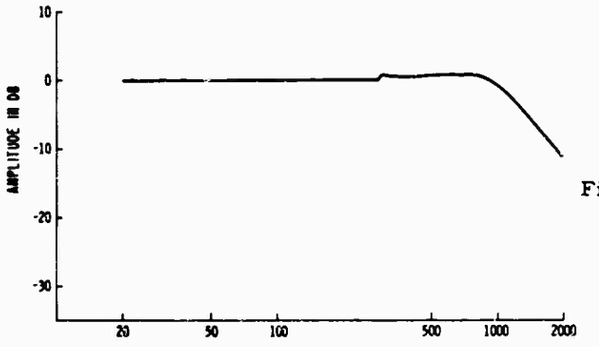

Fig. 6 - Equalized analog spectrum

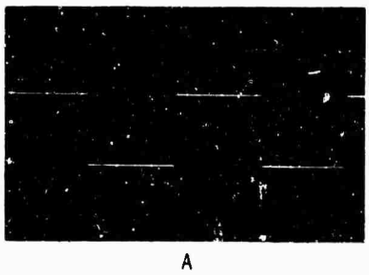

A

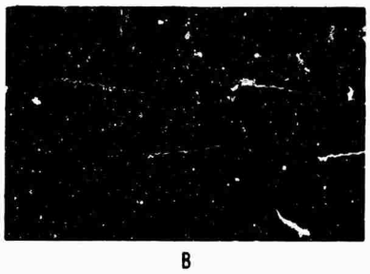

B

C

Fig. 7 - Unequalized analog output: (a) oscillator output, (b) power amplifier output, and (c) system output

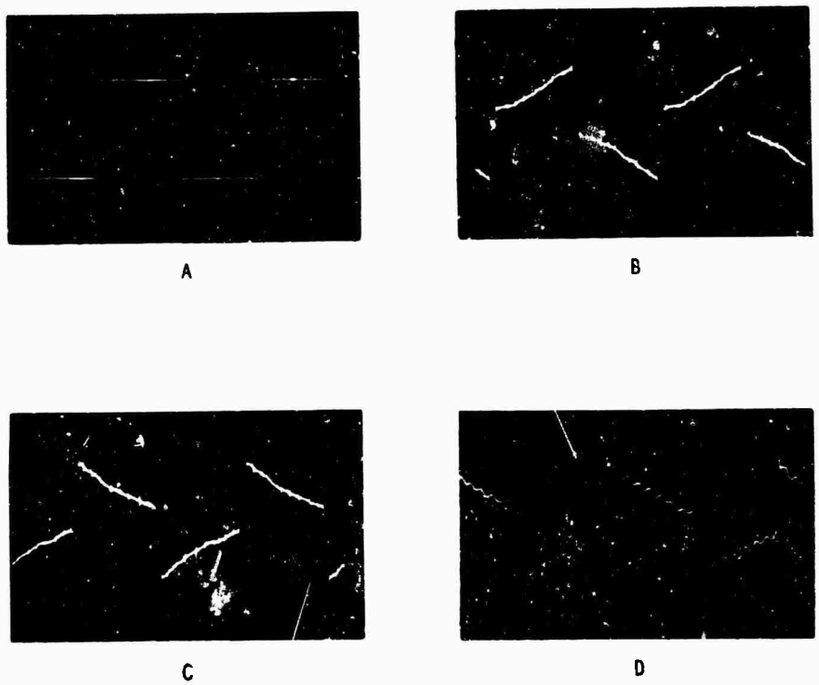

Fig. 8 - Equalized system output: (a) oscillator output, (b) equalized output, (c) power amplifier output, and (d) system response

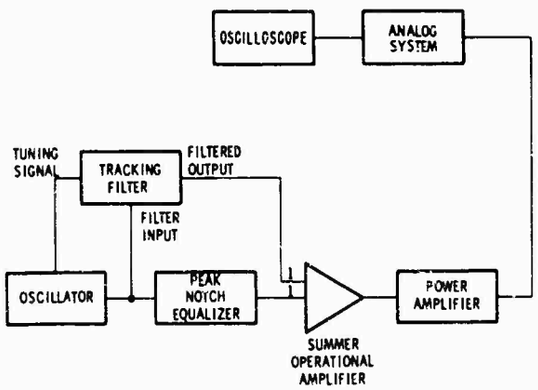

Fig. 9 - Equalization system with low-frequency phase compensation

Equalization will also allow the reproduction of a given random spectrum at some point on a test item. With the system of Fig. 3 equalized to within ±1 db, a uniform random spectrum was reproduced at the system output. Nothing would prevent the reproduction of a waveform composed of both sine and random components.

WAVE REPRODUCTION ON MECHANICAL SYSTEM

Wave reproduction has been performed on a mechanical system. A single-degree-of-freedom mechanical system was coupled to an MB Electronics 1200-lb-force C-10 shaker. Initially the complete system of Fig. 11, including the shaker, had the frequency spectrum of Fig. 12. With two peak notch equalizers, the spectrum of Fig. 13 was obtained. Note that equalization within ±2.5 db was achieved between 20 cps and 2 kc. Considerable data were taken on system performance for square, triangular, and complex inputs. The results for complex waveforms in Fig. 14 are typical. Reproduction is good, though some phase shift of components near 1000 cps may be noted.

LIMITATIONS

Certain inherent limitations in the peak notch equalization method should be realized. Equalization is not perfect. In general, it is difficult to equalize better than ±1 db on any system. Phase and amplitude responses of

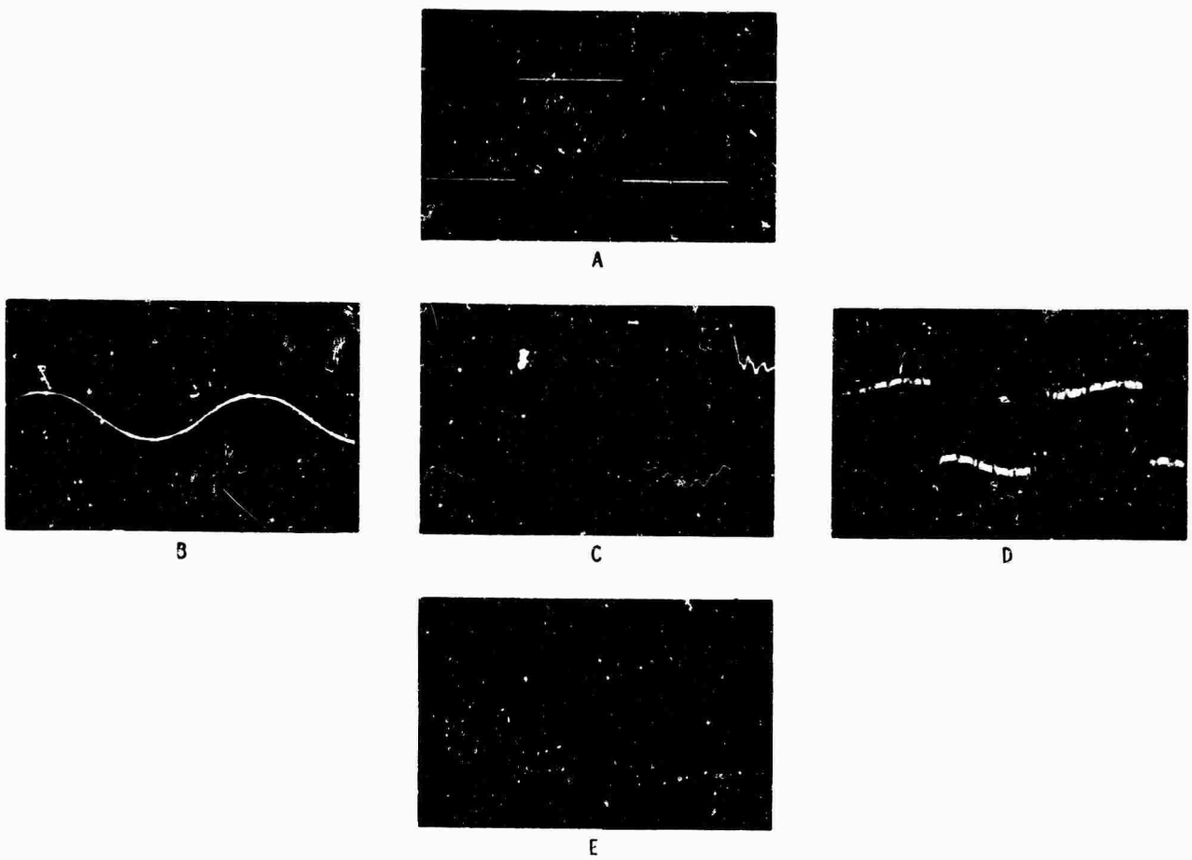

Fig. 10 - System waveforms with low-frequency compensation: (a) oscillator output, (b) equalizer output, (c) summer output, (d) analog input, and (e) system output

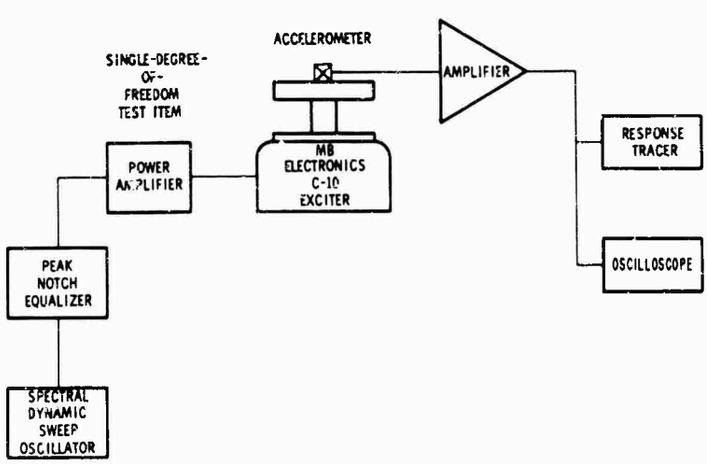

Fig. 11 - Equalization of mechanical system

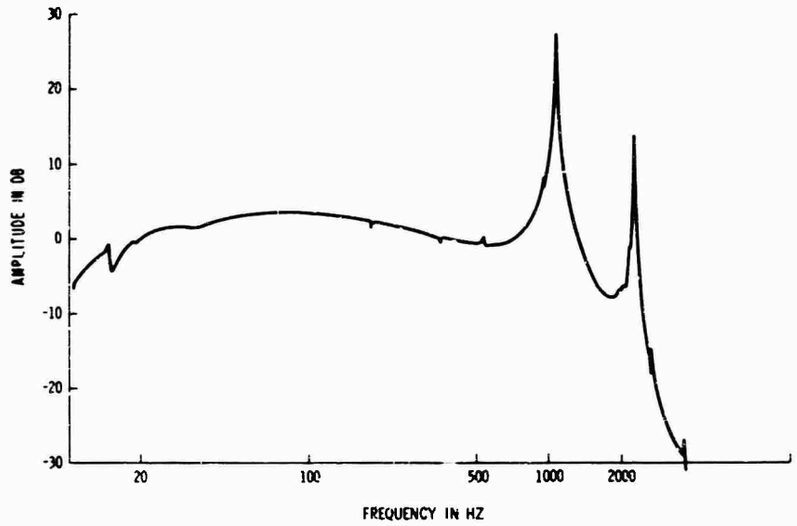

Fig. 12 - Unequalized spectrum of mechanical system

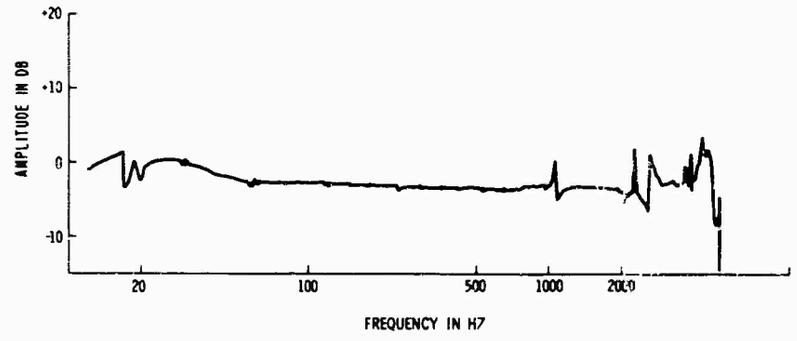

Fig. 13 - Equalized spectrum of mechanical system

mechanical systems are generally not independent, so equalization of amplitude generally implies rough equalization in phase. Phase angles may be 45 deg or more off above 1000 cps, however. The bandwidth over which equalization is possible generally lies between 10 and 2500 cps. A steep roll-off in response is noted at both ends of this spectrum. The MB equalizers use operational amplifiers similar to those found in analog computers. However, differentiators used in equalizer construction tend to produce impulse noise, as is evident in Fig. 10. Still, this method of equalization is far superior to a constant bandwidth equalization.

ACKNOWLEDGMENT

The authors acknowledge the valuable contribution of J. S. Colburn, who developed the instrumentation and techniques used in the mechanical wave reproduction system.

REFERENCES

1. J. V. Ctts, "Force Controlled Vibration Tests: A Step Toward the Practical Application of Mechanical Impedance," Shock and Vibration Bull. No. 34, Part 5, pp. 45-53, Feb. 1965

2. C. E. Nuckolls, "An Approximate Method of Simulating Mechanical Impedance in Vibration Testing," IES Proc., pp. 577-581, 1965

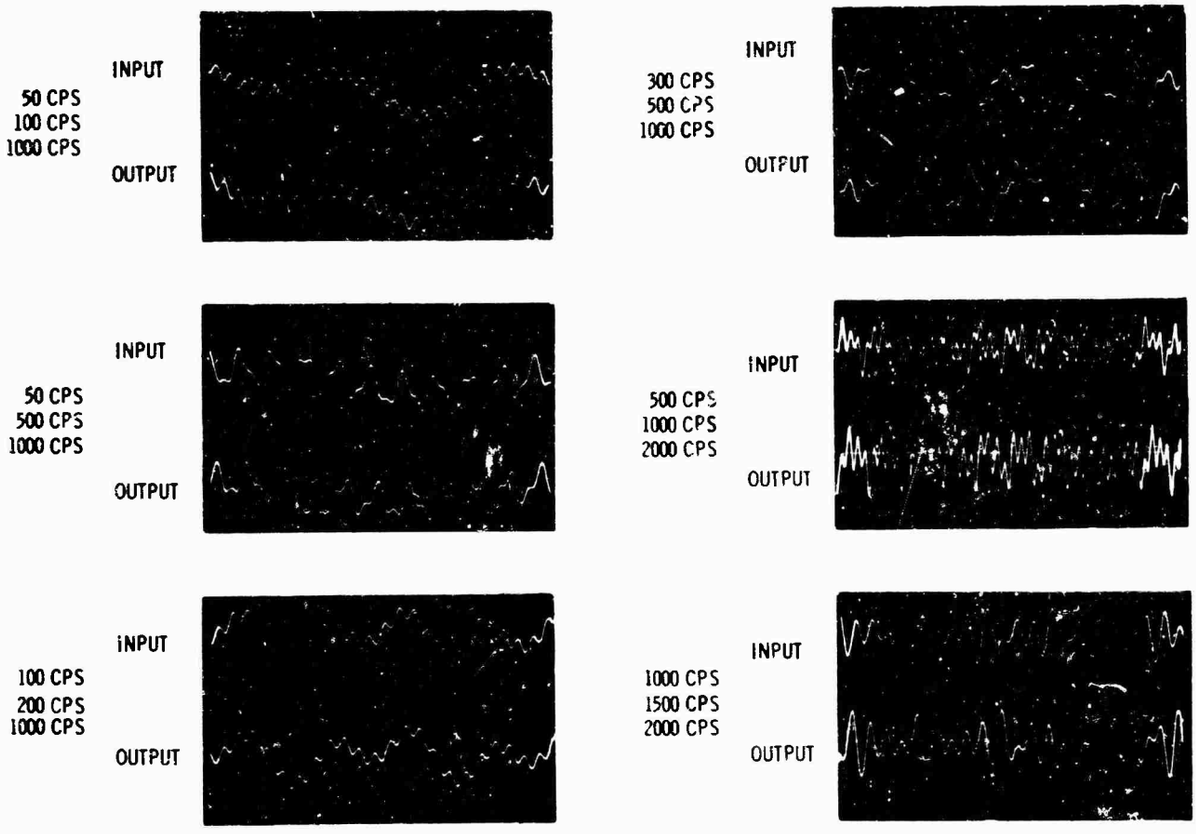

Fig. 14 - Equalized waveforms for mechanical system

3. C. E. Nuckolls and J. V. Otts, "A Progress Report on Force Controlled Vibration Testing," Shock and Vibration Bull. No. 35, Part 2, pp. 117-129, Jan 1966

DISCUSSION

Mr. Rommel (Lockheed-California Co.): You have been looking at transfer functions from a single source to a single output or observation point. Have you investigated the effect produced by multiple sources and multiple output points?

Mr. Hunter: We have investigated multiple input and output points. I should have mentioned in my assumptions that when we neglect the foundation, we assume a single input point. Multiple input points, unquestionably, will make a great difference. The responses will not be the same and, as a first approximation, the foundation in the lab must be as similar as possible to that in the field.

* * *

MULTIPLE SHAKER GROUND VIBRATION TEST SYSTEM DESIGNED FOR XB-70A

R. G. North and J. R. Stevenson
North American Aviation, Inc.
Los Angeles, California

Equipment developed for and employed in the XB-70A ground vibration test, including the 24-shaker vibration excitation system, the 100-channel data acquisition system capable of automatic recording on IBM punched cards, and the low-frequency air vehicle suspension system, are briefly described. Special operating procedures are also described.

R. G. North

INTRODUCTION

The XB-70A ground vibration survey, in addition to being contractually required, was a final proof test of primary importance in determining flight safety, not only with respect to the flutter problem but also with respect to other problems where vibration modes constitute inputs.

Due to the large size, weight, and unconventional configuration of the XB-70A, as well as the broad test program scope and the limited time allotted for the test, special equipment had to be developed to make possible an adequate test. This equipment includes a vibration excitation system, a data acquisition system and an air vehicle (A/V) suspension system. The special multi-shaker vibration excitation system was developed to satisfy requirements for higher power output, full-power output to lower frequencies, a larger number of shakers, and a more highly developed control system and console than could be satisfied by any existing equipment. The data acquisition system was designed to meet frequency response requirements to unusually low frequencies, to provide a recording range compatible with the excitation system when applied to the XB-70A and to record automatically the outputs of 100 vibration pickups installed on the A/V at specified control points. The A/V suspension system was developed to provide A/V supports with very low spring constants so that the natural vibration modes could be measured for conditions providing good simulation of the zero elastic restraints in free flight. Finally all three systems were suitably integrated with appropriate equipment and controls housed in an air-conditioned 35-ft semi-trailer for adequate equipment protection and so that modal excitation, data recording, and on-site data plotting and analysis functions could be efficiently accomplished.

The ground vibration test on XB-70A A/V No. 1 was conducted at the Palmdale Facility of the Los Angeles Division of North American Aviation, Inc., in June 1964 for an elapsed time of 10-1/2 days. The unfueled A/V was tested in five configurations covering three wing tip angles, single and dual hydraulic power, and locked and unlocked flaps. Mode shape and/or frequency measurements and free vibration decay records were obtained for a total of 130 modes.

TEST EQUIPMENT

Vibration Excitation System

While one or two pairs of shakers may provide sufficiently accurate definitions of the flutter significant natural modes in most cases,

they may prove inadequate where greater accuracy is required, structural damping is higher, natural frequencies are closer together, and higher modes are required. Multi-point excitation is the key to greater accuracy and to the ability to cope with more difficult situations. The objective is to tune in or excite only one mode of a structure at a time and to subdue or eliminate response in all other modes. The problem is to determine the excitation force distribution that will accomplish this objective and to develop a method or procedure for establishing the required force distributions for each mode.

In a structure vibrating in a natural mode, at any instant of time the inertial forces are exactly balanced in both magnitude and distribution by the elastic forces. The structural damping forces, by definition proportional to the elastic forces but leading the elastic forces by a 90-deg phase angle, have the same distribution as the elastic or inertial forces. Therefore, the damping forces, like the inertial forces, are distributed in proportion to the product of the mass distribution and the amplitude distribution for the assumed natural mode. To sustain the motion, the energy dissipated by the structural damping forces must be balanced by the energy input from the vibration excitation forces. The distribution of shaker forces should be a mirror image of the distribution of the damping forces, or like the damping forces, the shaker forces should be distributed in proportion to the product of the mass and the amplitude distributions.

Unfortunately this definition of the required shaker force distributions for a given mode requires a knowledge of the mass distribution of the structure being tested. In fact, it is necessary to determine the effective mass at each shaker location and to adjust the relative shaker force output to be proportional to the assigned mass distribution [1]. Obviously, the accuracy of the assigned mass distribution can be no greater than the accuracy of available mass distribution data and, even with exact data, gross approximations are necessary to distribute the total airplane mass to the limited number of shaker locations available with a practical excitation system. In any case, the measured modes should not be dependent on calculated mass data for the structure being tested. A further possible difficulty with the method, as indicated by Lewis and Wrisley [1], is that when the effective mass at each shaker location is not accurately known, it becomes impossible to obtain an in-phase relation of force and velocity at each shaker location with a shaker force distribution proportional to the product of the shaker amplitude distribution and the shaker assigned mass distribution. Under these conditions, adjustments of excitation frequency will, of course, not provide a means of obtaining the desired in-phase condition at all shaker points. This type of impasse is avoided in the method presented here by eliminating the redundancy in the modal tuning criteria. In the present method the shaker force distribution and the frequency for a given mode are adjusted to provide an in-phase condition of shaker force and velocity at all shaker points in a straightforward iteration process described later in the section on mode tuning.

To utilize the above criterion properly, the excitation equipment must provide accurate indications of the phase angle between shaker force and shaker velocity on all channels over the desired frequency range.

A basic property of the shaker power amplifier used is zero voltage phase shift between input and output over the frequency range of interest. Since the current in the output circuit is a measure of the force applied and since at structural resonance the shaker presents a pure resistive load, then at resonance the current and voltage at the output of the amplifier would present an in-phase relationship and the voltage would be a measure of force. The design of the amplifier to present this zero phase shift was such that the output was floating, i.e., could not be grounded, so the current could not be used as a force indication, but then neither could the voltage. But since at resonance they would be in phase, and the amplifier produced zero phase shift between input and output voltage, the input voltage could be used as a direct measurement of force, assuming that it was necessary to sense only phase, not amplitude.

Linear velocity transducers were used to measure the relative velocity between the shaker drive rods and the stationary shaker field coils. This type of transducer has a relatively low output and must feed into a comparatively high impedance to preserve its velocity phase characteristics. Therefore, amplifiers had to be used. Since the amplifiers were simple one-tube devices that introduced 180-deg phase shifts, they also were used in the force (voltage) circuits to preserve the correct relative phase angles. However, since force signal amplification was not required, the inputs to the force amplifiers were greatly attenuated to prevent overloading.

By exhaustive tests on simple single-degree-of-freedom systems, each force and velocity circuit through its indicating circuit

was checked and changed where necessary, until the entire system presented zero phase angle at resonance between force and velocity.

The vibration excitation system developed for the XB-70A includes the following major components:

1. 24 Unholtz-Dickie electrodynamic shakers with a 3-in. stroke and maximum sinusoidal force outputs of 100 lb per shaker;

2. 12 Unholtz-Dickie 250-watt fully transistorized power amplifiers individually capable of driving two shakers to full power over the frequency range from 0.1 to 1000 cps;

3. A velocity coil and mounting hardware for each shaker to measure the relative velocity between the shaker armature and the field coil housing;

4. Shaker drive rods incorporating a telescoping feature and double flexures at each end of the rod;

5. Vacuum pads and vacuum system for shaker attachment to the A/V;

6. 26 shaker stands of varying heights to support the shakers rigidly in close proximity to the attach points on the A/V;

7. Cable slings to provide low-frequency supports for the two vertical tail shakers;

8. A master control unit to provide a variable frequency of excitation at a variable overall force amplitude, together with a long persistence screen oscilloscope for displaying force vs velocity indications for any channel; and

9. Control units for each of the 12 power amplifier channels individually equipped with a 2-in. oscilloscope for monitoring force vs velocity, shaker force (armature current) meter, shaker phase switches, and shaker force control.

Shaker installations are shown in Figs. 1 and 2. Vacuum pads, vacuum lines, electrical cables, velocity coils, telescoping drive rods, rod joint clamps, rod flexures, etc., are shown. The pumps used to supply the vacuum for the

Fig. 1 - Installation of electrodynamic shaker

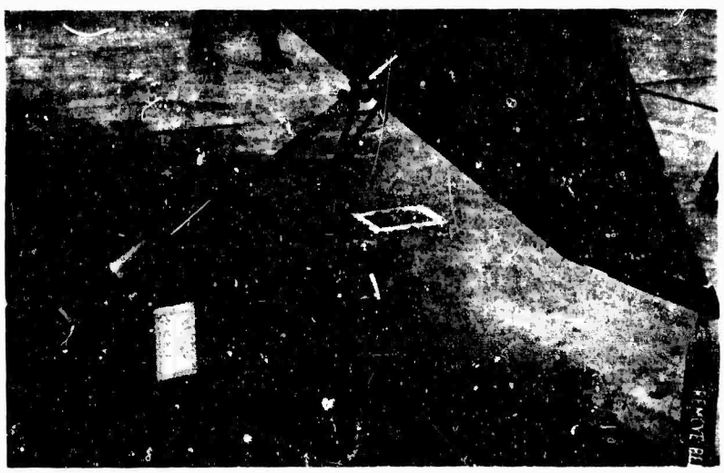

Fig. 2 - Shaker installation on wing tip

shaker attach system are shown in Fig. 3. Figure 4 shows the shaker locations used for a major portion of the testing. Shakers 1L and 1R through 8L and 8R were arranged in eight symmetrically disposed pairs with each pair driven by a single power amplifier. These 16 shakers were used for both symmetrical and antisymmetrical excitation, and conversion from one type of excitation to the other required only the actuation of 8 phase selector switches. The remaining 4 power amplifiers were connected to shakers 9S through 12S for the symmetric case or to 9A through 12A for the antisymmetric case. Thus a total of 20 shakers was used at any one time and conversion from symmetric to antisymmetric drive or vice versa could be accomplished rapidly since it was not necessary to move any of the shaker stand assemblies. Figure 5 shows the interior of the equipment trailer with the excitation console in the left center, the master control panel containing the oscillator, master memoscope, electronic frequency counter, etc. in the rear, and shaker power amplifiers on the right. Shaker stands are shown in Figs. 6 through 10. The shaker stand assemblies are welded steel truss structures designed for high rigidity. The shakers and mounting plates, weighing several hundred pounds each, had to be supported on stands with sufficient rigidity that all natural frequencies would be above 50 cps. The sling supports for the vertical tail shakers, on the other hand, were designed for flexibility (Figs. 9 and 10). The sling cables were long enough to provide frequencies less than 0.2 cps for all shaker rigid body modes except vertical translation. As a further measure to increase the tendency of the vertical tail shakers to remain motionless while driving the vertical tails, ballast was added to increase the shaker weight to approximately 1700 lb per shaker. The shaker drive rods, shown in Figs. 1 and 2, were designed with a diameter-to-length ratio high enough to provide a fundamental lateral bending frequency above 50 cps. Since the required rod diameter increases rapidly with rod length, relatively short rods had to be used to hold the rod weight to a reasonable value.

Data Acquisition System

The simplest and most widely used data gathering systems would probably include a pair of matched vibration pickups, a dual channel oscilloscope, a vibration meter, a suitable switchbox, and an electronic frequency counter. With this equipment, mode shapes are measured by locating one of the pickups as a reference at a point of large response for the mode under investigation and moving the other pickup to various points on the structure, noting at each point the amplitude and the phase, with respect to the reference pickup, on the vibration meter and the oscilloscope, respectively.

Limitations in time allotted for the XB-70A test, the broad scope of the test program, and the large size of the A/V necessitated a highly automated data acquisition system employing a large number of pickups distributed over the A/V at fixed control points. This system, developed for NAA by Gulton Industries, Inc., includes equipment providing the following capabilities:

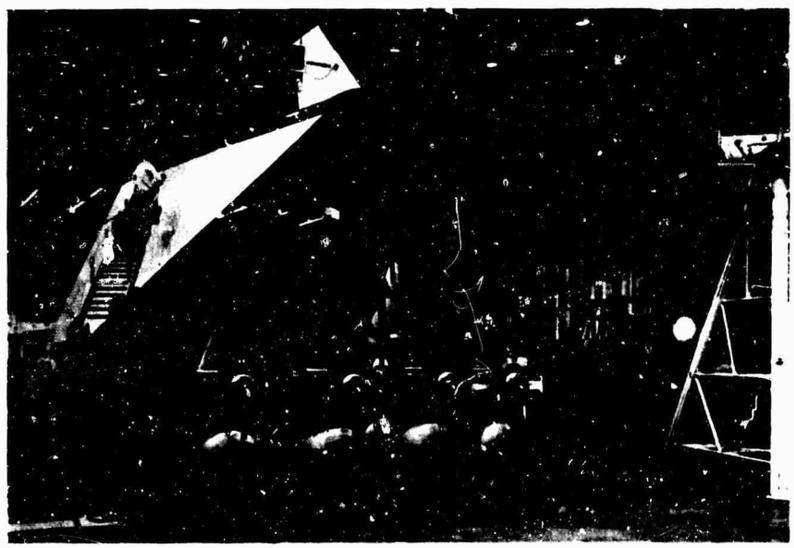

Fig. 3 - Vacuum pumps, shaker attach system

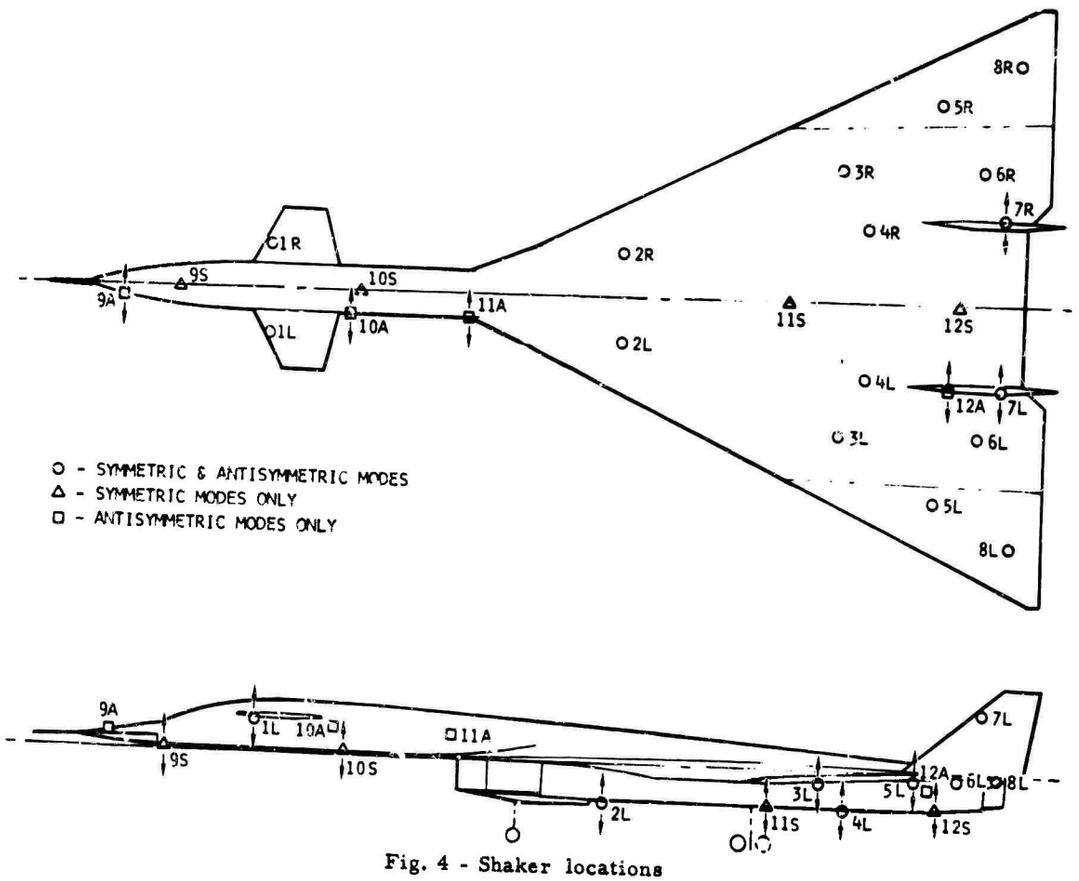

Fig. 4 - Shaker locations

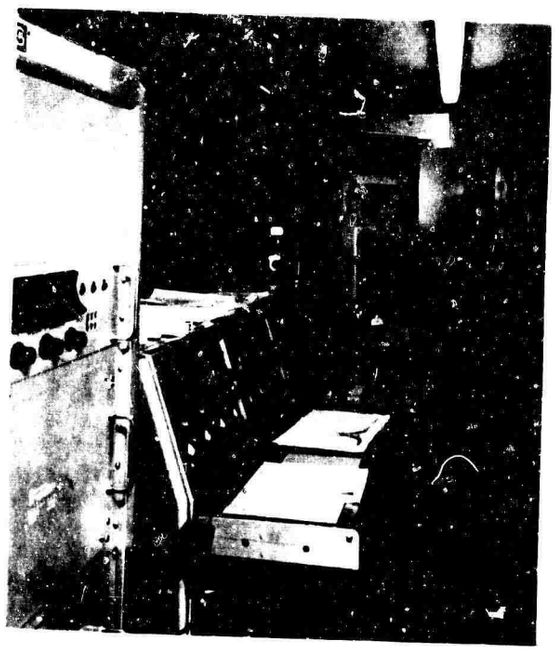

Fig. 5 - Equipment trailer, vibration excitation work area

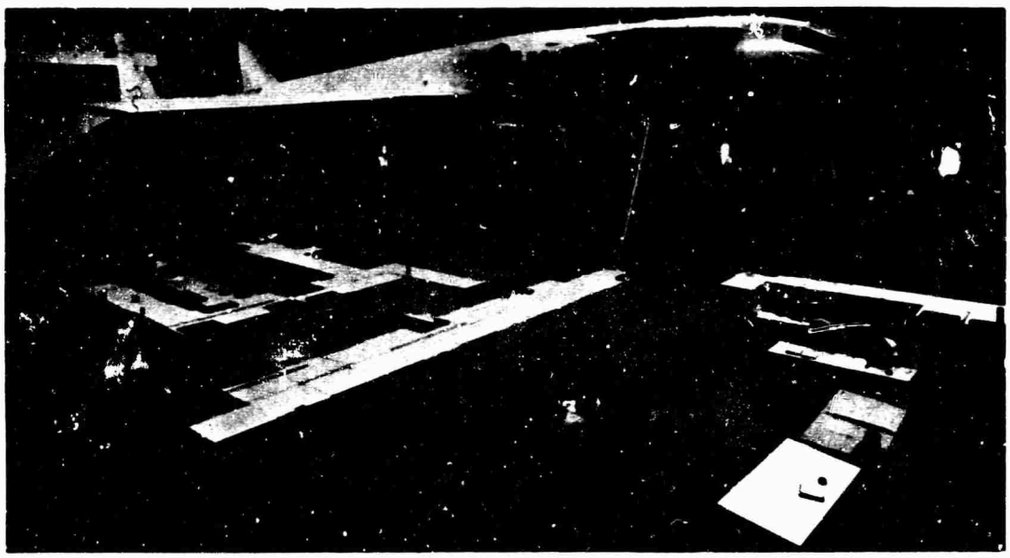

Fig. 6 - Right-hand aft view of test setup

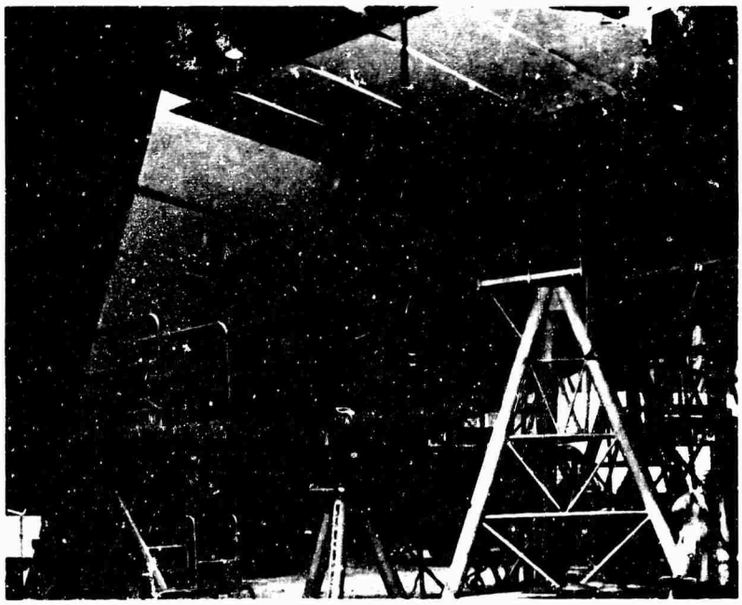

Fig. 7 - Shaker stands under wing, δ_{tip} = 65 deg

1. Automatic digital recording of pickup data at 100 control points on IBM punched cards;

2. Automatic tabulation of mode shape data recorded on the IBM cards for "quick-look" plotting and analysis;

3. Manual data readout on standard meters, primarily as a backup for the automatic system;

4. Simultaneous waveform presentations of the outputs of 32 accelerometers on 2-in. oscilloscopes for rapid pickup gain adjustment and for visual amplitude and phase comparisons;

5. Patch panel facilities for oscillographic or direct writing pen recorder recording of all channels to provide records of the decay of free vibrations, frequency sweep data, and "back-up" mode shape and frequency; and

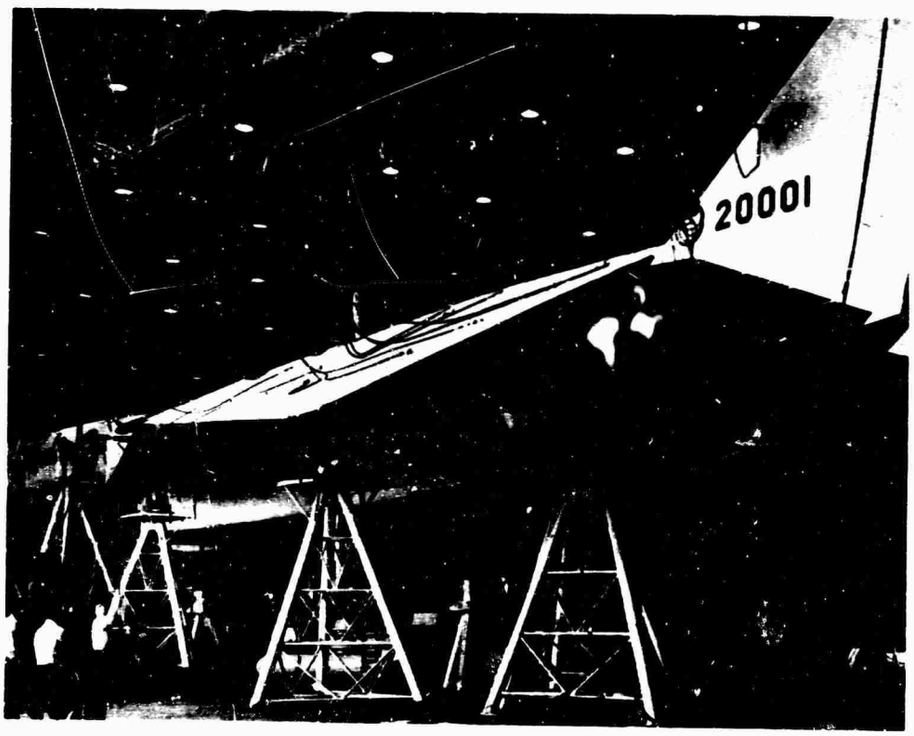

Fig. 8 - Shaker stands under wing, δ_{tip} = 25 deg

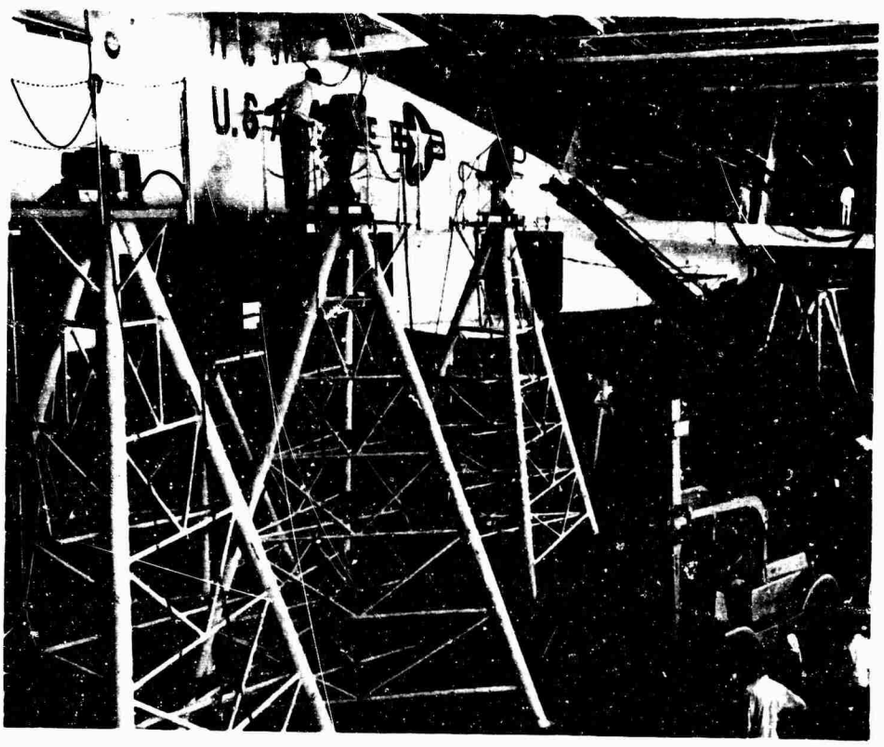

Fig. 9 - Installation of shaker stands

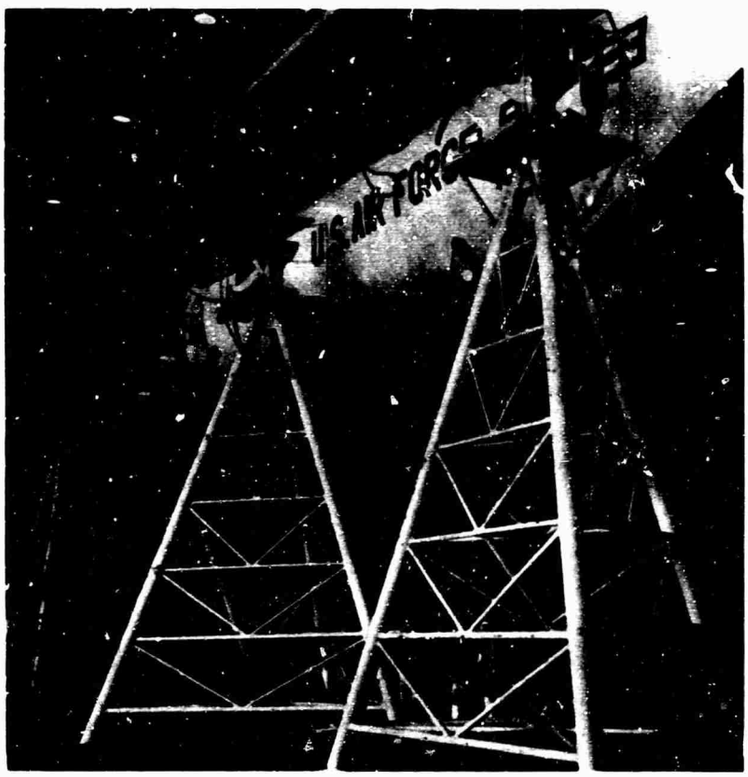

Fig. 10 - Forward fuselage shaker stands

6. Three 8-channel, direct writing pen recorders for recording frequency sweep, modal steady state, and decay data.

High output servo accelerometers were attached with tape at 117 control points located on the A/V as indicated in Fig. 11. At any one time, 100 of the 117 accelerometers were recorded. For example, vertical pickups 1S through 13S were disconnected for the antisymmetric case and lateral pickups 1A through 13A were disconnected for the symmetric case with no loss of data since there is no vertical response of the fuselage centerline in the antisymmetric modes and no side-bending response of the fuselage in the symmetric modes. The 100 pickups recorded at any one time provided detailed mode shape information on the wing-fuselage, canard, canard flap, vertical tail, and elevons. Only a few minutes were required to change from the symmetric to the antisymmetric case and vice versa. Figure 12 shows the data acquisition equipment housed in the trailer. This photograph shows the IBM equipment for punching and tabulating the cards in the left foreground, desks for data evaluation in the left background, power amplifiers in the right background, monitoring scopes, oscillograph mounting racks, and patch panels in the right center, and the data acquisition system in the right foreground. Figure 13 shows three 8-channel, direct writing pen recorders located outside the equipment trailer. These recorders were used in lieu of the oscillograph for the decay records and frequency sweeps because the records were available instantaneously. In addition, the slower available paper speeds made utilization of the envelopes of the unrectified accelerometer traces for the frequency sweeps more practical.

Air Vehicle Suspension System

Ideally, in vibration tests of complete airplanes, free-free modes should be obtained. In other words, it is desired to measure the vibration characteristics of the airplane alone rather than those of the airplane plus arbitrary supports. These free-free modes then are directly applicable to free-flight structural dynamics problems. Excellent approximations of free-free modes may be measured if the airplane supports provide sufficient flexibility. These special supports should be designed to provide natural frequencies in all six airplane rigid

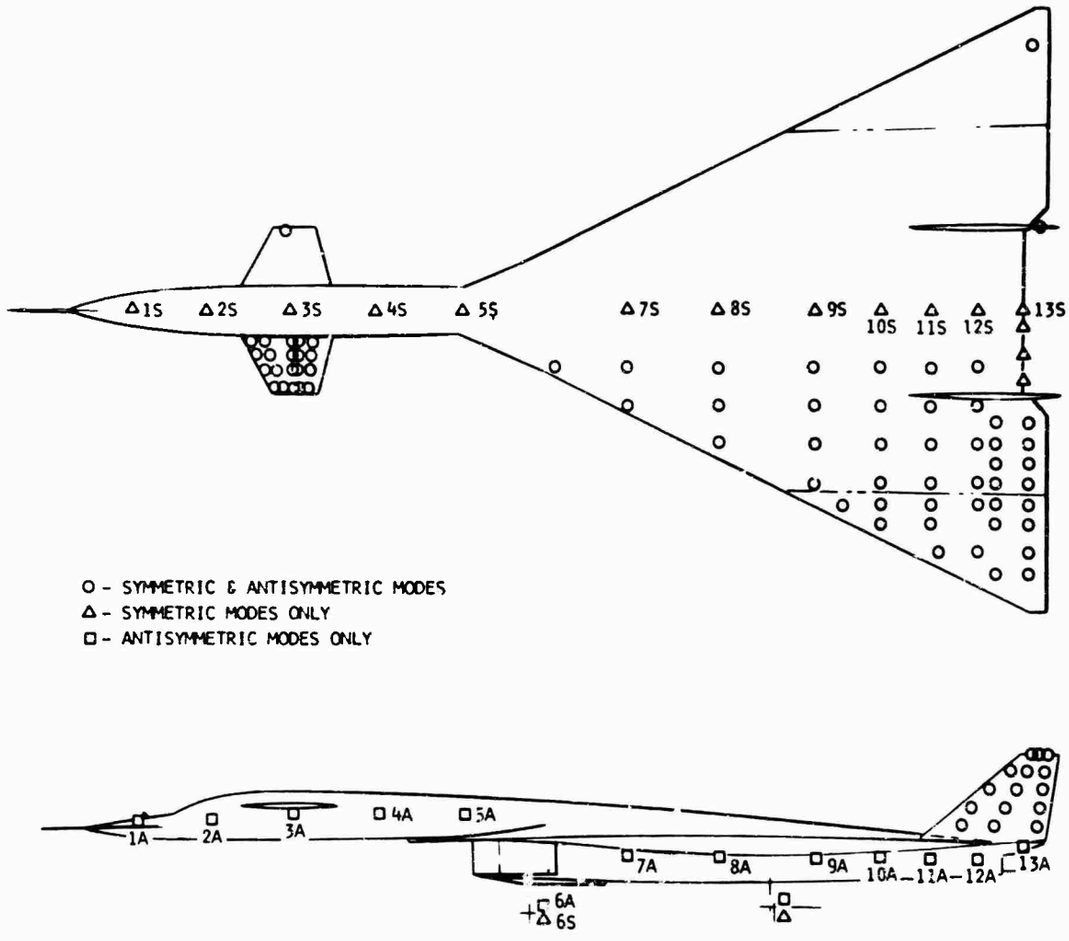

Fig. 11 - Pickup locations

body modes (pitch, vertical translation, fore and aft translation, roll, yaw, and side translation). These frequencies are very low compared with the lowest airplane elastic mode frequencies. In addition, the support stiffness and support sprung mass should be low compared with the A/V mass and stiffness in the vicinity of the support attachment to the A/V, based on an A/V lumped mass and stiffness representation containing a sufficiently large number of values. Satisfying these conditions will minimize the coupling between the artificially introduced finite frequency rigid body modes and the airplane elastic modes. In addition to providing sufficiently low stiffness, the aircraft suspension system should: (a) introduce negligible mass, (b) provide adequate travel within stops of sufficient strength, (c) provide essentially linear spring constants within the available travel, (d) be statically stable, (e) provide low friction or damping, (f) provide adjustable spring constants, (g) allow for simple airplane installations, (h) be free from resonances within the frequency range of interest, and (i) provide adequate strength or built-in fail safety.

Air bags, coil springs, shock cord, and partially deflated tires have been used with varying degrees of success to support airplanes for the ground vibration test. Figure 14 illustrates the principles of operation of a novel and highly successful suspension unit developed by North American Aviation, Inc., for the XB-70A ground vibration test. The A/V suspension system consists of a nose gear unit and two main gear units to support the A/V at the lower ends of the landing gear struts through universal joints. The system was designed to support the A/V maximum gross weight. Each unit can be repositioned on the floor, while supporting the A/V, through a system of skid plates and jack screws. Each of the three units provides adjustable restraints of very low stiffness in the vertical and all horizontal directions. Spring deflections are limited by stops to ±1.0 in. in the vertical and all horizontal directions. A pneumatic spring is used in the vertical

Fig. 12 - Equipment trailer, data acquisition and analysis work area

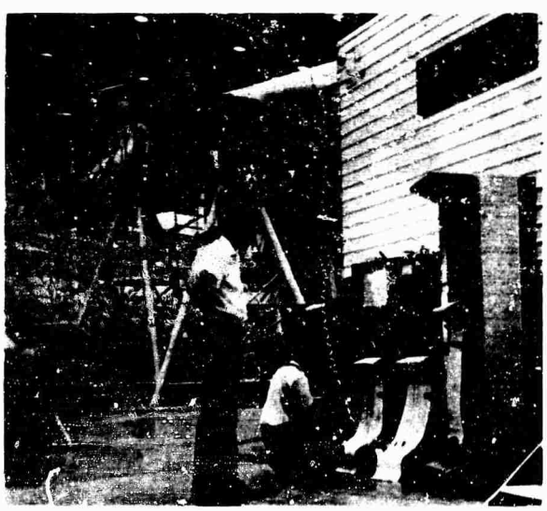

Fig. 13 - Direct writing recorders

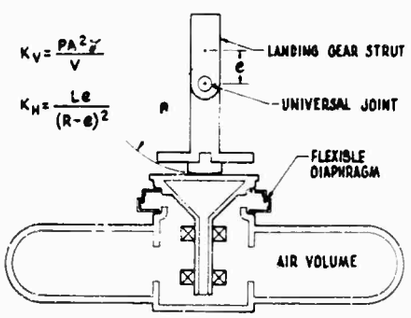

Fig. 14 - A/V suspension unit schematic diagram

direction with dry gaseous nitrogen or air as the working fluid. In the horizontal directions the springs consist of a mechanical universal "rocking-chair" device. In the vertical direction a vertical steel tube attached to the bottom of the loading platform is constrained in bearings to permit it to move only vertically. The A/V is floated in the middle of the range of travel permitted by the stops by inflating the suspension units with the appropriate amount of nitrogen. The vertical spring constant of a suspension unit is given by

$$K_V = \frac{P_a A^2 \gamma}{V} , \qquad (1)$$

where

K_V = vertical spring constant,

P_a = absolute gas pressure,

γ = ratio of specific heats (γ = 1.4 for nitrogen or air),

A = piston area (A = 1520 sq in. based on mean diameter of flexible diaphragm), and

V = gas volume.

A low spring constant is obtained by providing a sufficiently low A-to-V ratio. The spring constant can be adjusted by varying V through the introduction of a relatively incompressible fluid, such as oil, into the integral nitrogen tank. In the lateral and fore and aft directions, low spring constants are provided by a universal "rocking" chair" unit attached to the lower end of the landing gear strut and resting on the loading platform. This device consists basically of a spherical surface which transmits the A/V deadweight reaction to the horizontal loading platform and a universal joint at the end of the landing gear strut, as illustrated in Fig. 14. The spring constant in any horizontal direction at the universal joint is given, for small deflections, by

$$K_H = \frac{Le}{(R-e)^2} , \qquad (2)$$

where

K_H = horizontal spring constant,

L = deadweight reaction,

R = spherical radius of support button lower surface, and

e = eccentricity between universal joint and center of the sphere of radius R.

The horizontal spring constant can be changed in small increments by varying the eccentricity e through screw adjustments. Larger stiffness increments can be obtained by changing the spherical button to one with a different radius R. An overall view of the suspension units installed under the A/V is given in Fig. 15. Figure 16 shows the nose gear installation.

For the XB-70A test configurations, the frequencies of the A/V on the suspension system were approximately as follows:

Vertical translation, 0.40 cps;
Pitch, 0.14 cps;
Fore and aft translation, 0.30 cps;
Side translation, 0.19 cps;
Yaw, 0.05 cps; and
Roll, 0.37 cps.

In all cases the highest frequencies on the suspension system were less than one-sixth of the lowest elastic mode frequencies.

Damping of the suspension units was extremely low in all horizontal directions as a

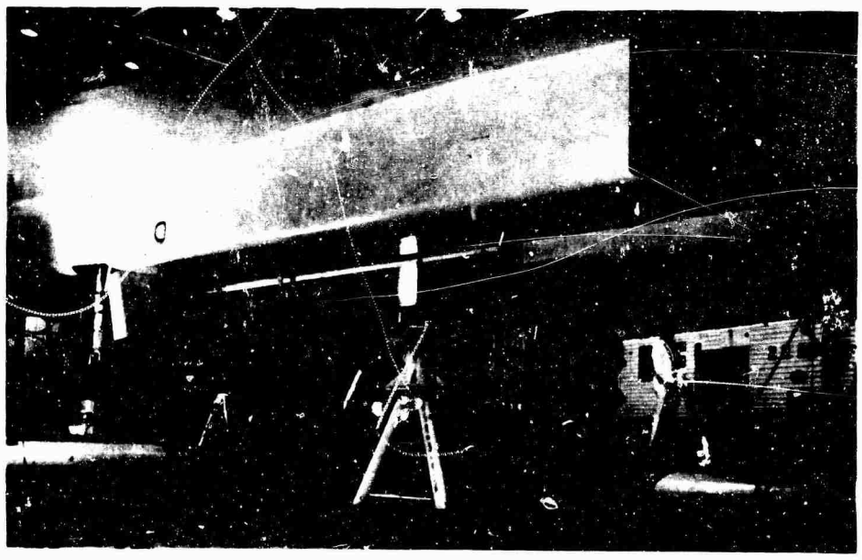

Fig. 15 - A/V suspension system installation

Fig. 16 - Nose gear A/V suspension unit installation

result of the low-friction needle bearings in the universal joints together with the low friction of the spherical buttons. In the vertical direction the damping appeared to be somewhat higher ($g \cong 0.25$) and viscous in nature. However, the vertical damping had no apparent effect on the test or the test results.

OPERATING PROCEDURES

Test Crews

Testing was carried on around the clock by three crews working overlapping shifts. A test crew was composed of seven people, including a test director, and two people for each of the three functions of vibration mode excitation, data acquisition, and data evaluation. In addition, there were supporting personnel for equipment maintenance, suspension system monitoring, A/V configuration changes, moving shakers, etc.

Frequency Sweeps

A single pair of shakers might be used to excite the structure for a frequency sweep and the response recorded from the output of one or two pickups. The objective of a frequency sweep is to vary the excitation frequency slowly to obtain a record depicting the variation of the amplitude of vibratory response vs frequency. From such records, the resonant frequencies related to the various natural modes are determined. These resonant frequencies become the starting points for tuning in the various natural modes. Normally, a sweep using symmetrical excitation is made to determine the resonant peaks corresponding to the symmetric modes, and a second sweep is made with antisymmetric excitation to obtain the antisymmetric modes. The shakers would then be moved to a different location and the sweeps repeated. This process would continue until the wing, fuselage, vertical tail, and horizontal tail had been adequately searched for all modes. The number of these sweeps would also be multiplied by the number of A/V configurations to be tested. In this test, symmetric and antisymmetric sweeps were made for 5 A/V configurations. The frequency of excitation was varied or swept at a logarithmic rate by a constant speed electric motor geared to the oscillator dial. The sweep rate was chosen on the basis of information developed from Refs. 2 and 3 to minimize the time required for the sweeps and still reveal all of the modes over the desired frequency range with sufficiently small errors of frequency. The sweep rate was such that it took approximately 17 min to cover the range from 1 to 10 cps and approximately 12 min to cover the range from 10 to 50 cps or a total of approximately 30 min to cover the total desired frequency range of 1 to 50 cps. To cover wing, fuselage, canard, and

vertical tails by the usual methods would require 40 individual sweeps assuming each component could be adequately searched with only one symmetric and one antisymmetric sweep. At a minimum of 30 min per sweep, this would use up more than 20 hr of valuable test time.

The frequency sweeps conducted during the XB-70A ground vibration tests are of interest primarily for the new technique employed in the use of the shakers. By having all shaker channels operating simultaneously during the frequency sweeps, only 10 frequency sweeps were made, one symmetric and one antisymmetric for each of 5 test configurations, to reveal all of the wing, fuselage, canard and vertical tail modes of interest. The ability to use this method was derived from the simultaneous display of all shaker force vs velocity ellipses. When any of the 12 shaker force vs velocity monitoring scopes showed that the slope of the ellipse was changing from one where the force had a component in phase with the velocity to one where the force had a component out of phase with the velocity (indicating energy was being taken out of the structure rather than being put in), the associated shaker phase selector switch would be changed. With this continuous monitoring, the entire frequency range of interest would be covered with the assurance that all shakers would always be putting energy into the system. During the sweeps, the outputs of 20 accelerometers at key control points throughout the structure were recorded on pen type recorders. Minimum recorder speed was used so that the envelopes of the unrectified traces could be used to indicate conveniently the resonant peaks. Therefore, with many shakers and many pickups continuously exciting and recording the response of each surface, the possibility of not exciting or detecting a mode was effectively eliminated and the time required to perform the sweeps was reduced to less than one-fourth that otherwise required.

MODE TUNING

When only two shakers are used, mode tuning consists merely in adjusting the excitation frequency until maximum response amplitude is indicated on the vibration meter.

However, when multishaker excitation is used the procedure for tuning in a mode is considerably more involved. When a natural mode of a structure is tuned in, the distribution of shaker forces is in proportion to the distribution of the product of mass and amplitude. The distribution of shaker force is then a mirror image of the distribution of the damping forces. Also it follows that the shaker forces are everywhere in phase with the velocities of the motion at their points of application. This latter fact is made use of to tune in the natural modes.

For the XB-70A ground vibration test, a rapidly convergent iteration process was used in tuning in a mode. This procedure had steps approximately as follows:

1. Set system overall force level potentiometer to a sufficiently low value to avoid overdriving the system and turn on the master power switch.

2. Select the master shaker(s) on the basis of calculated modal data for the largest product of local mass and amplitude for the desired mode. Set the phase control for the master shaker for symmetric or antisymmetric as required. Adjust the master shaker force potentiometer to a value of 8 (range from 0-10) and turn on the master shaker(s).

3. Adjust oscillator frequency to close ellipse on memoscope of master shaker(s) at the frequency of the desired mode.

4. Adjust remaining individual shaker force potentiometers to a midrange setting of 5.

5. Using the individual shaker channel scopes for slope indication, set the shaker channel phase selectors of all remaining shaker channels to the same slope-phase relation previously established at the master shaker channel.

6. Turn on each of the remaining shaker channels, one at a time, while adjusting frequency as required to maintain a closed ellipse at the master shaker.

7. Note on the individual channel monitoring scopes which shaker channel has the most open ellipse and adjust that shaker force (potentiometer) in a direction toward closing the ellipse, then readjust frequency to close ellipse at master shaker(s).

8. Repeat step 7 as many times as required to close all ellipses.

9. Check for proper phase on all shakers by turning off each shaker channel in turn and comparing slope-phase relation at the individual monitoring scope with that at the master shaker(s).

10. If the armature current of any shaker exceeds the master shaker current, the former

should be selected as the new master shaker channel and steps 7 and 8 repeated until all ellipses are closed. Armature current for single shakers must be corrected by dividing by 2 for determining the master shaker(s).

11. Using the accelerometer monitoring scopes, note the maximum acceleration at any of the control points. Also note the maximum shaker armature current. Then increase the system force level potentiometer setting until the maximum acceleration corresponds to ±1.0-in. amplitude or 1.0 g (the accelerometer limit) or until the maximum shaker armature current becomes equal to the rated current (100 lb of shaker force), whichever occurs first.

12. Retune mode if necessary by repeating step 7 as many times as required, using the final choice of master shaker channel from step 10.

13. With the outputs of 20 strategically located accelerometers on the structure selected as inputs to the pen recorders, turn on the recorders and turn off the master system power switch. If the decay records of the ensuing free vibration are smooth with no frequency drift or indications of beats, the mode is considered accurately tuned in and the master power switch should be turned on and data recorded.

It should be noted that steps 11 and 12 of this procedure insure that signals of maximum possible strength within equipment limitations will be obtained from the accelerometers so that the recorded data will be of the highest resolution and accuracy.

In most cases the modes could be tuned in in less than 15 min. When more time was spent, the situation was usually one where it was necessary to move one or more shakers before the mode could be tuned in or where no true mode existed for the frequency being investigated.

Data Gathering and On-Site Analysis

In the XB-70A ground vibration test, after the mode was tuned in, the accelerometer amplitude and relative phase (in or out) with respect to a reference pickup were automatically recorded on IBM punched cards for each of the 100 pickups. On an average, automatically punching the original cards, duplicating the cards, and automatically tabulating the data on an IBM typewriter for on-site analysis took from 10 to 15 min per mode. If trouble occurred in the automatic system, the data would be manually tabulated and punched into the cards. Manual tabulation of amplitude and phase information required approximately 30 min per mode.

In preparation for the XB-70A ground vibration test, automatic CRT isometric vector plots of 360 calculated A/V modes were made. These plots were made for the exact test conditions, including suspension system stiffness and mass increments, A/V test weight, test pickup locations (resulting in 97th order matrices in the solutions), three wing tip angles, single system hydraulic restraints on control surfaces, and flaps locked and unlocked. The first 45 symmetric and the first 45 antisymmetric modes of the A/V on the suspension system were computed for four configurations. These configurations included flaps up and locked for each of the three wing tip angles and flaps down for zero wing tip deflection.

During the ground vibration test, manual plots of the amplitude vectors were made on isometric diagrams of the A/V from the tabulated test data as soon as these data were available. Plots of both the automatically recorded and the manually recorded data were made and compared. These plots also were compared with the predicted modes. From these comparisons, judgments were made as to the quality of the measured data, and some idea was obtained as to what modes of flutter significance remained to be tuned in and recorded.

CONCLUSIONS

As a result of adequately detailed and comprehensive equipment development, checkout, and other preparations, the overall system functioned substantially as planned. All test objectives were accomplished within the scheduled test period. The system proved to be very reliable even without allowing for its relatively great complexity. It appeared to be easier to operate than a simple two-shaker system employing "search" pickups for mode shape measurements. The ease of operation is considered to be due not only to the adequacy and the convenient arrangement of controls, but also to the elimination of the "search" operation in the mode shape measurements, the virtual elimination of the need to move shakers, and the division of the overall problem into a number of well-defined jobs for which individual crew members were given advanced training on a full-scale laboratory setup. The provision of three crews working around the clock on overlapping shifts also made the job seem easier by holding personnel fatigue to levels lower than those on the usual one- or two-shift test operations.

The maximum force output of 100 lb per shaker, although adequate, was not sufficient to drive the response amplitude for some modes to the shaker amplitude limit of ±1.5 in. or to the accelerometer overload limit of 1.0 g. However, it is concluded that power requirements were in good agreement with predicted requirements from detailed calculations for each mode.

As anticipated, no resonances of the shaker supports were obtained throughout the test. This was the case for both the rigid tripod shaker supports and the low-frequency pendulum vertical tail shaker supports mounted on bridge cranes from the hangar ceiling. Also it is noteworthy that no resonances of the hangar floor or ceiling were detected over the frequency range of the tests. Consequently, the shaker velocity coils, installed between the shaker field coils and the shaker armature coils, accurately indicated the absolute armature velocity as required for mode tuning.

The novel procedure developed for the frequency sweeps, utilizing 20 shakers simultaneously with a similar number of pickups, made it possible to obtain resonant peaks for the symmetric or antisymmetric flutter significant modes of the entire A/V, for a given configuration, with only one sweep. The benefits of substantial savings in time, increased accuracy (resulting from the use of a distributed force over the A/V), and the virtual elimination of the possibility of not obtaining an indication of all modes of interest were realized compared with the usual sweep methods employing two shakers but requiring about four times as many sweeps.

The iteration procedure developed for adjusting the shaker force magnitude and phase sense of each of the 12 shaker channels along with the excitation frequency to tune in a mode proved to be a rapidly convergent and straightforward operation requiring relatively little time.

The sensitivity and recording range capabilities of the servo-accelerometers were well matched to the capabilities of the excitation system. In other words, for only a minor portion of the modes excited was the excitation system capable of exciting maximum response accelerations in excess of the servo-accelerometer upper limit of 1 g (vibratory acceleration). For all other modes excited, either the 100-lb allowable maximum shaker force (obtained at the master shaker) or the ±1.5-in. maximum aplitude (corresponding to the maximum shaker stroke) was the limiting factor. Thus, for all conditions, the relatively high output and resolution of accelerometers with low maximum g limits, as chosen for the XB-70A system, allowed accurate mode shape data to be recorded — even for the small accelerations near node lines.

In general, the servo accelerometer waveforms were very clean except near node lines when the modal response might be down in the noise level. Although not at all necessary for satisfactory operations, a narrow-band tracking filter could be used to reduce the low noise level further.

The A/V suspension system operated continuously for the 10-1/2-day test duration without any trouble. It is believed that a major portion of the suspension system damping in the vertical direction results from a thermodynamic loss of energy through the walls of the integral air tanks. This loss of energy might be significantly reduced by the application of thermal insulation to the suspension units.

REFERENCES

1. R. C. Lewis and D. L. Wrisley, "A System for the Excitation of Pure Natural Modes of Complex Structures," J. Aeronautical Sci., Vol. 17, No. 11, Nov. 1950

2. G. E. Sanderson and E. A. Bartch, "In-Flight Damping Measurements," OSR-9-0269, Proc. Flight Flutter Testing Symposium, May 1959

3. F. Lewis, "Vibration During Acceleration Through a Critical Speed," APM-54-24, Trans. ASME

BIBLIOGRAPHY

Bisplinghoff, R. L., H. Ashley, and R. L. Halfman, Aeroelasticity, Addison-Wesley Publishing Co., Cambridge, Mass., 1955

Den Hartog, J. P., Mechanical Vibrations, McGraw-Hill, New York

Myklestad, N. O., Vibration Analysis, McGraw-Hill, New York, 1944

Scanlan, R. H., and R. Rosenbaum, Introduction to the Study of Aircraft Vibration and Flutter, Macmillan, New York, 1951

* * *

THE HOW OF HELICOPTER VIBRATION TESTING

Ronald F. McCann
The Boeing Company
Morton, Pennsylvania

Vibration is an ever-present environment in helicopter flight. Ground vibration testing is an inexpensive method of reproducing vibratory motions induced by blade forces. The technique of ground shake testing started from inducing vibratory modes by means of many small exciters attached to fuselage locations with relatively simple instrumentation indicating in- or out-of-phase relationships of velocity pickups vs fuselage location for discrete frequencies. From this, it has evolved into relatively large exciter inputs at the rotor heads with considerable attention paid to instrumentation. With the aircraft suspended by steel springs, frequency sweeps are made from 6 to 20 cps and resonant points are located. Instrumentation allows direct X-Y plotting of phase and amplitude vs frequency with IBM card punch recording of shaker locations, input force, period of frequency, aircraft configuration, phase angle and amplitudes of displacement. It is not the intent in this paper to be all-inclusive but rather to present the history and contemporary approach to ground vibration testing of helicopters at the Boeing Company's Vertol Division.

R. F. McCann

INTRODUCTION

The helicopter is basically a vibration-inducing machine. Vibration and its effects have long plagued the helicopter manufacturer, so vibration reduction has a very high priority in the engineering department. Allied with this, modal characteristics of the fuselage are studied for background information on vibration reduction methods.

A comparatively inexpensive method of obtaining vibration information is the ground shake test. Ground shake testing provides data pertaining to the basic natural modes and forced amplitudes of the fuselage under excitation from electrodynamic vibration exciters. It also allows various methods of vibration reduction to be examined and evaluated before flight.

This report presents the history of ground shake testing at The Boeing Company's Vertol Division with respect to the evolution of test equipment and techniques. Table 1 shows the chronological history of ground shake tests and the specific purpose of each test.

GROUND SHAKE TESTS UTILIZING MULTIPLE SHAKERS

In the early stages of ground shake tests, extensive use was made of the MIT multiple shaker equipment. This equipment consisted of 24 electrodynamic shakers which could be individually or collectively powered, operated, and frequency-, phase-, and force-controlled from a central console. The console included a normalizer, 24 pickup attenuator circuits and a cathode ray oscilloscope. The shakers, capable of 20 lb of force, were used in a frequency range of 5 to 100 cps. Each shaker had a sensitive vacuum tube accelerometer pickup attached to its armature.

The theory on which the equipment operation was based considered that the aircraft

TABLE 1
Chronological History of Ground Shake Tests

Aircraft	Date of Test	Purpose of Test
YH-21	1952	Determine natural frequencies and corresponding mode shapes of the fuselage and natural frequencies of engine as installed.
H-21C	1954	Determine effect of pylon and longeron stiffening on natural frequencies, mode shapes and forced responses.
HUP	1955	Determine natural frequencies and corresponding mode shapes of helicopter fuselage.
H-21B	1955	Simulate reported high-frequency response of the helicopter as experienced in the cockpit area; localize problems and develop suitable remedies.
YH-16	1956	Obtain the natural modes and frequencies of a fuselage which closely simulated the dynamic characteristics of the proposed H-16B; obtain test values which could be correlated with the results of analysis using design data available; by such correlation improve the analysis method so the H-16B fuselage natural modes and frequencies could be reliably predicted.
Model 42	1957	Determine natural frequencies and mode shapes at two different gross weights.
YHC-1A	1960	Determine the longitudinal-vertical and lateral-torsion natural frequencies of the helicopter.
H-21C	1960	Determine vibration characteristics of the helicopter.
YHC-1B	1961	Determine longitudinal, vertical and lateral torsion natural frequencies of gross weights.
HC-1B	1963	Determine the natural frequency and mode shape of the second vertical bending mode for various ballast configurations and gross weights, with and without fuselage stiffening.
CH-113	1963	Determine the longitudinal-vertical and lateral-torsion natural frequencies.
CH-113	1963	Determine the effect of recommended stiffening configuration (fuselage) on the two natural frequency modes.
CH-46	1963	Define the natural modes and forced amplitudes of the helicopter to provide correlative data to support in-flight rotor load and shake tests; evaluate modifications to the modal characteristics of the fuselage resulting from the incorporation of prototype hardware fixes.
CH-46	1964	Obtain basic data from modifications made from fixes resulting from the previous shake test.
CH-47	1964/65	Obtain basic data for the aircraft in various new high gross weight configurations; determine effect of gross weight and center of gravity locations on the aircraft vibration characteristics.

structure was composed of enough appropriately selected discreet and elastically connected masses to allow a satisfactory representation of the required number of higher order modes, and to provide a shaker for each mass at its effective location. Each shaker was then attached to the structure at a selected point and assigned a specifically apportioned mass of structure to be moved. The pickups attached to the shakers provided information relative to the amplitude of each mass section for use in the console circuits to allow selection of the proper mode excitation. Each shaker had a separate control channel, and the console controls provided means for converging on the natural frequency of each "pure" natural mode and adjusting the excitation to provide a force from each shaker proportional to the product of the mass and amplitude at its respective station. The circuits providing this proportioning of shaker force required that a mass-ratio adjustment be made at each shaker control station. This involved listing all shaker locations, together with assigned masses, calling the smallest mass unity, and finding the mass ratio for each other station. The mass ratio was set directly on the calibrated dial for the control channel to which each respective shaker station is attached.

A station selector switch, which could be set to any one of the 24 shakers, connected a voltage signal from the armature control

(Variac) to the Y-axis of an oscilloscope. An integrating circuit displayed the accelerometer output as velocity on the X-axis. Thus, the oscilloscope displayed the phase relationship and proportionality between a particular shaker force and the velocity response of the structure at the point where the shaker was attached. The normalizer was a special feature which automatically modified the velocity signal on the oscilloscope to provide a visual indication of the appropriate force adjustment required to obtain the proper type and slope of Lissajous patterns. This allowed the operator manually to apply a force proportional to the product of an assigned mass and the actual vibration amplitude to any or all shakers while maintaining the same proportionality at a master shaker which vibrated at or near a resonant frequency of the structure.

In the early days of ground shaking, the aircraft was usually suspended from the building structure by elastic cords attached to the rotor heads, thus giving the ship 90 percent vibration isolation (Fig. 1). The shakers were positioned along the fuselage in such a manner as to produce the particular mode of vibration sought after. Weight was added to the rotor heads to simulate the blades and hub mechanism. Ballast was used to bring the aircraft to the desired gross weight. Frequency sweeps were made from 2.5 to 30 cps. For the very low frequencies a mechanical shaker was employed. Testing proved, however, that it was unnecessary to sweep below 5 and above 20 cps. The mechanical shaker proved to be too inflexible for ease of testing, and its use was infrequent thereafter.

GROUND SHAKE TESTS UTILIZING SINGLE OR DUAL SHAKERS

Before 1960, relatively high-force shakers were used only where force levels were beyond those of the smaller MIT units, usually for forced response data.

It became apparent, however, that a closer approximation of the actual flight conditions could be obtained by inducing the excitation of the rotor heads. Other locations such as the nose gear strut were used for convenience during various ground shakes due to the difficulty of hanging shakers and attaching them to the rotor heads. Typical of shakers used were the Calidyne Model 44, Model 58 and MB C-5.

MB velocity pickups were used since they had greater sensitivity at low frequencies than accelerometers. Integrating amplifiers were connected to Brush records equipped with precision step attenuators. Mode shapes were determined by phase relationship of the recorded pickup. As testing progressed, more pickups were used and CEC linear integrating amplifiers were used with a 26-channel CEC oscillograph. The pickups were placed at strategic locations in the fuselage, and in some cases one was used as a probe.

Steel spring banks replaced the elastic cords, with spring rates calculated to obtain rigid body frequencies of the suspended helicopter well removed from the expected flexible mode frequencies.

Excitation was provided at both forward and aft rotor hubs in the following general arrangements:

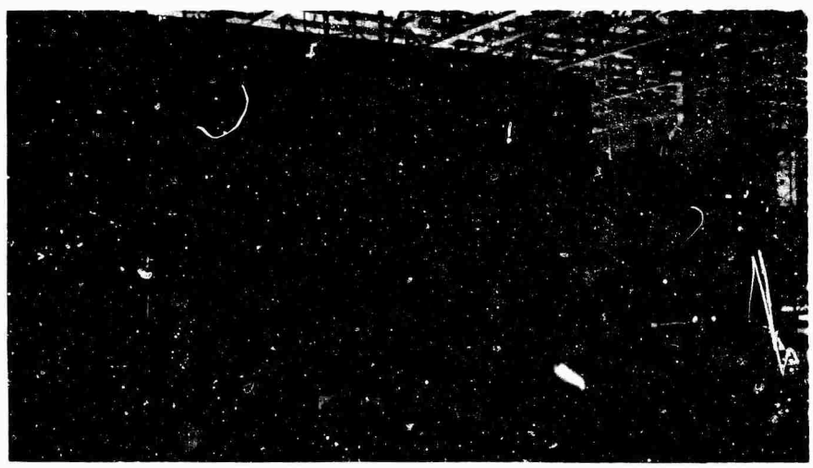

Fig. 1 - YH-21 ground shake test

Position	Mode
Longitudinal	Vertical/longitudinal
Vertical	Vertical/longitudinal
Lateral	Lateral/torsional

Each configuration of the aircraft was tested in this manner.

CONTEMPORARY TEST PROCEDURE

The aircraft is suspended at each hub from a gantry with spring banks having 250 lb/in. deflection per spring (Figs. 2 and 3). Rotor blades are removed and steel plates with lead ballast are used to simulate blade mass.

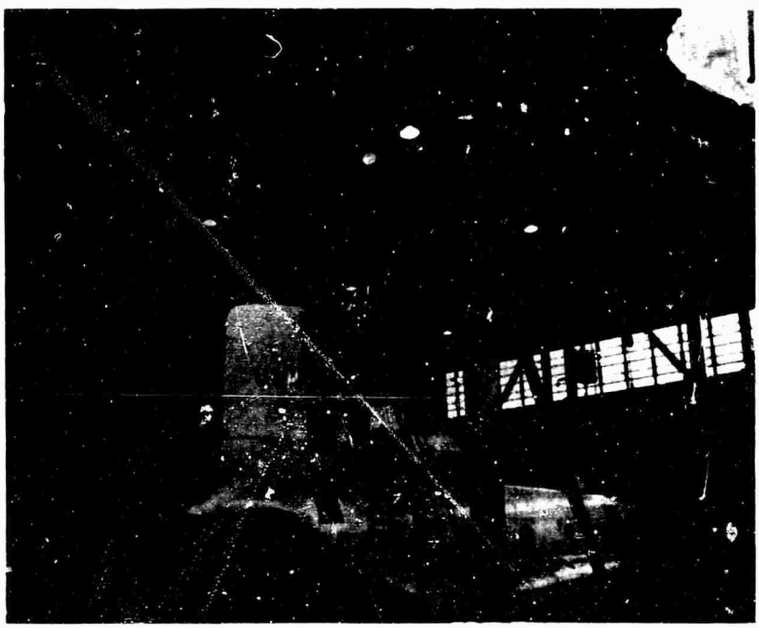

Fig. 2 - CH-47 ground shake test

Single exciter operation is used for longitudinal and lateral conditions, and dual exciter operation is used for vertical and pitch conditions. For vertical tests, the shakers are operated in phase; for pitch tests the shaker forces are applied 180 deg apart, producing a periodic moment at the rotor head.

For each test configuration a continuous sweep is made over a frequency band from 6 to 20 cps, using a logarithmic sweep rate, with a total sweep time of approximately 70 sec. Linear exciting forces are set to 500 lb at 10 cps, and programmed to increase and decrease linearly as frequency increases and decreases. This force is transmitted from the shaker head to the aircraft by a strain-gaged link. The response of this link is used to measure the force applied to the aircraft and is fed back to a servo control and then to a sweep oscillator as a reference signal for automatic control of the exciter force level.

Vibration pickups are located in approximately 100 locations on the aircraft (Fig. 4). Since instrumentation limits recording to one channel at a time, key locations are chosen and frequency sweeps are made for each of these locations. Approximately 11 pickups for each shaker position are used, including cockpit, forward hub (three direction), cabin, aft hub (three directions), and fuel tanks. Prior to recording the instrumentation output, a plot of ramped force input is made while sweeping through the test frequency range. After this is completed, each of the key channels is swept through the test frequency range and the phase angle, referenced to the input force, and the amplitude of displacement is plotted.

Resonant responses, indicated by apparent amplitude buildups, are located and the response of all vibration pickups are recorded at each discrete frequency. Information recorded on IBM cards includes the following: configuration

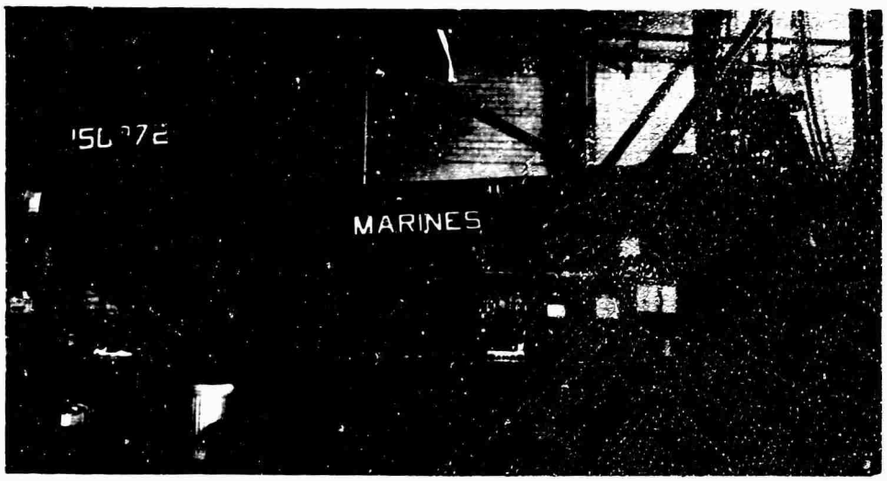

Fig. 3 - CH-46 ground shake test

ARROWS SHOWN ON THE DIAGRAM INDICATE THE POSITIVE DIRECTION OF PICKUPS, WHICH ARE FORWARD, UP AND RIGHT.

THE POSITIVE DIRECTIONS OF THE SHAKER ARE FORWARD, UP AND RIGHT.

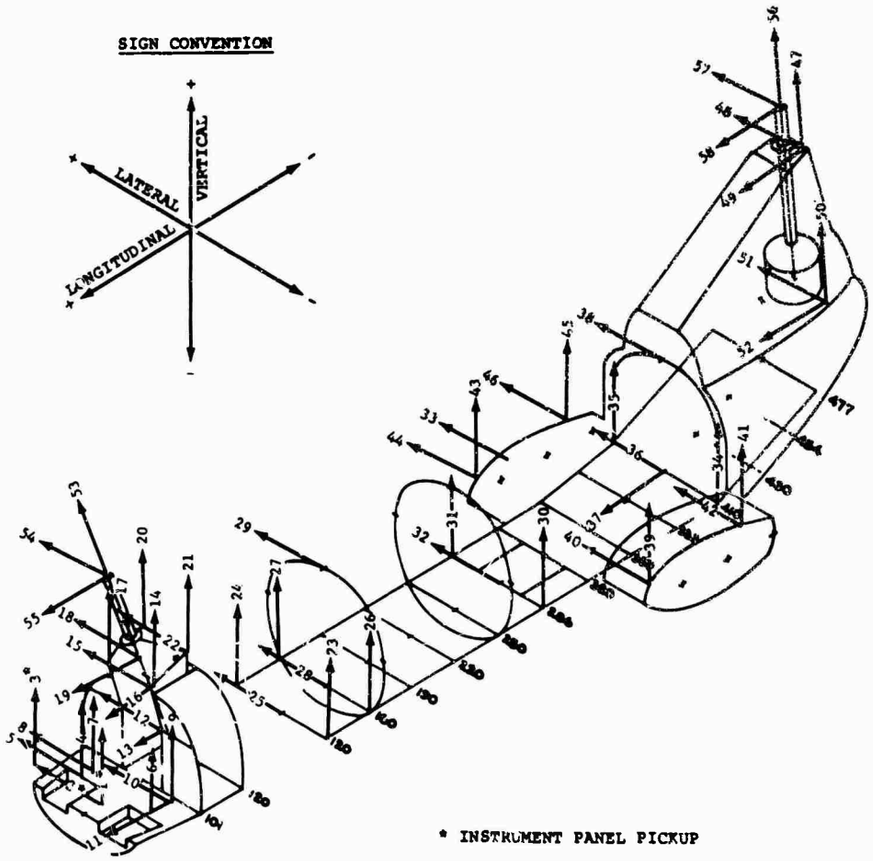

Fig. 4 - Ground shake test vibration pickup locations

code number, exciter location and input direction code number, input force code number, period of the frequency code number, phase angle referenced to force, and amplitude of displacement.

The procedure for dual shaker operation is the same, except for the following:

1. The data system is modified to provide parallel systems for applying a drive signal to two exciters.

2. The force input applied to the test specimen by each shaker is 250 lb at a frequency of 10 cps and straight line ramped to 500 lb at 20 cps. These inputs are applied 18 in. on either side of the rotor shaft for the vertical tests and 18 in. fore and aft of the rotor shaft for the pitch test.

Single and dual shaker locations are shown in Figs. 5 through 11.

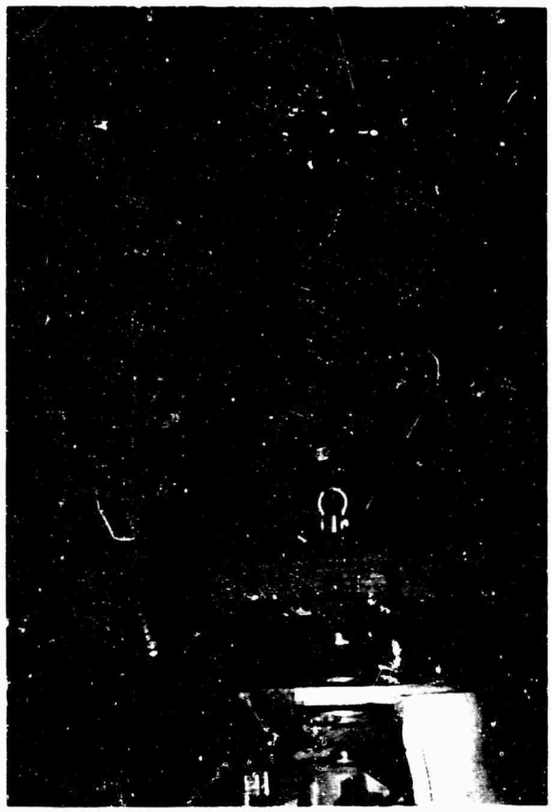

Fig. 5 - Longitudinal shaker position, forward rotor

DATA SYSTEM

The data system consists of the S-400 console, IBM Model 526 card punch, with MB Model No. 124 velocity pickups. The console consists of equipment necessary to originate the sinusoidal input signal, measure and plot responses and furnish the measured modal response of discrete frequencies to the card punch in machine language.

A sinusoidal ac signal is generated by the B&K sweep oscillator and is fed through a power amplifier to the shaker. The amount of amplification is controlled by a force control which is a 2-kilohm one-turn potentiometer. The strain-gaged force link transmits the periodic motion of the shaker head to the aircraft.

The strain gage mounted on the fuse link measures the dynamic strain in the link (using the BA-13) determining the force applied to the aircraft. The output signal from the strain gage is also used to control the input signal to the exciter by feeding it through a servo control and back to the sweep oscillator.

The strain gage signal coming through the CEC Linear/Integrate Amplifier (linear mode) is also injected into a Spectral Dynamics Model SD1012 tracking filter. The tracking filter presents two outputs. The first is a 100-kc phase-sensitive tuned ac signal. The amplitude represents the phase of the force signal and is directed to the phase meter for measuring the phase differences between the force signal and velocity pickup signals. The second output is a dc signal representing the force level. This dc signal is fed to the Y-axis of the X-Y amplitude plotter. The sweep oscillator signal is sent through a frequency meter, which provides a dc signal proportional to the frequency. This signal is used to drive the X-axis of both X-Y plotters.

The velocity pickup signals are fed into a patch panel and into a crossbar scanner. The scanner is an electronic switch which may be operated manually or remotely and can present each of 200 (3-wire) signal channels (one channel at a time) to a common output with a visual channel display and a digital output to the card punch. From the scanner the velocity pickup signal is fed through a CEC Linear/Integrate Amplifier. It is integrated, amplified and fed into a second tracking filter.

The tracking filter again presents two signals. The 100-kc phase-sensitive tuned ac signal has an amplitude representing the phase of the incoming displacement signal and is fed to the phase meter where the difference between

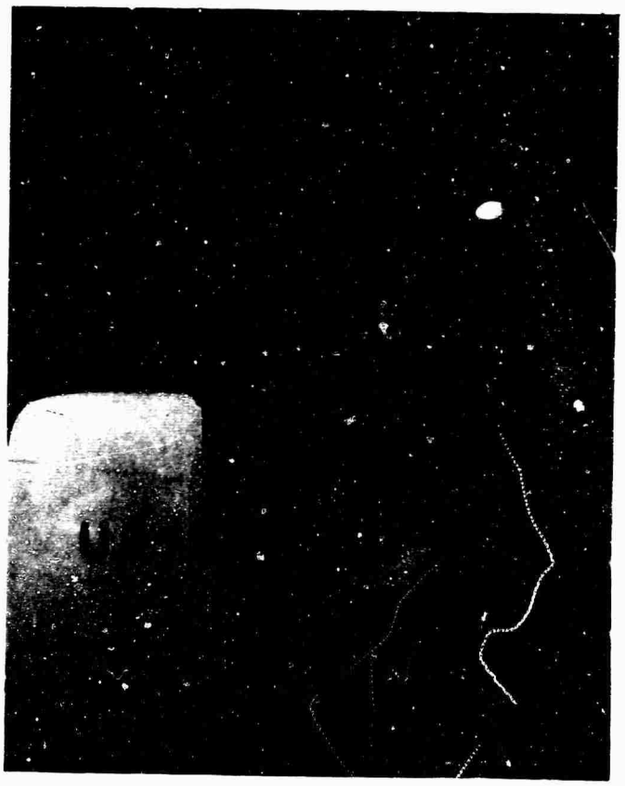

Fig. 6 - Longitudinal shaker position, aft rotor

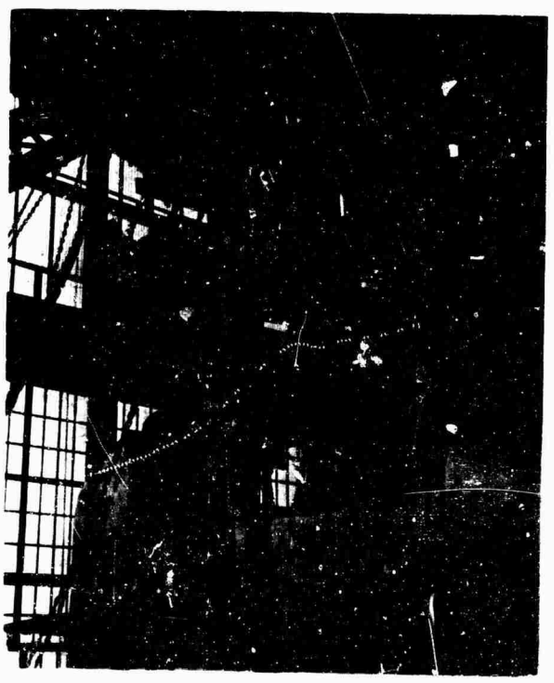

Fig. 7 - Vertical and pitch shaker position, aft rotor

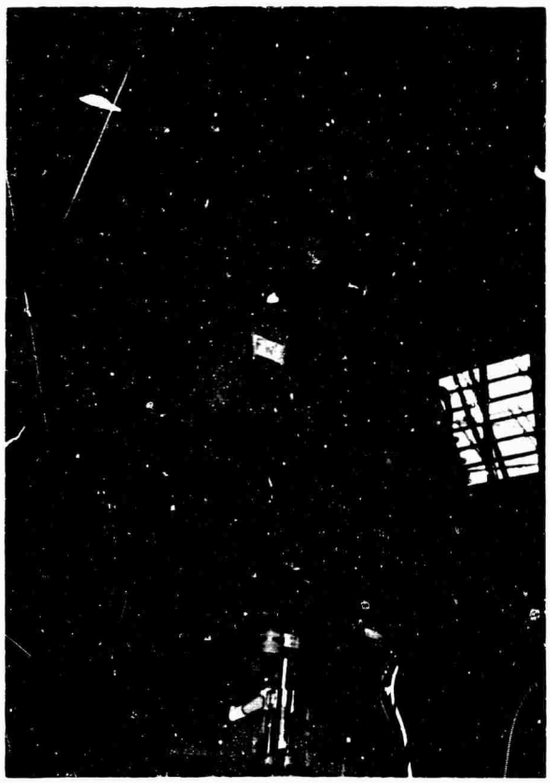

Fig. 8 - Vertical and pitch shaker position, forward rotor

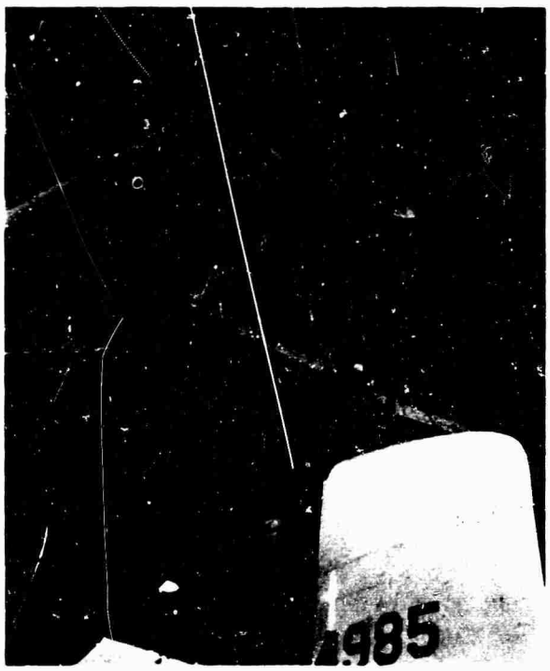

Fig. 10 - Vertical and roll shaker position, aft rotor

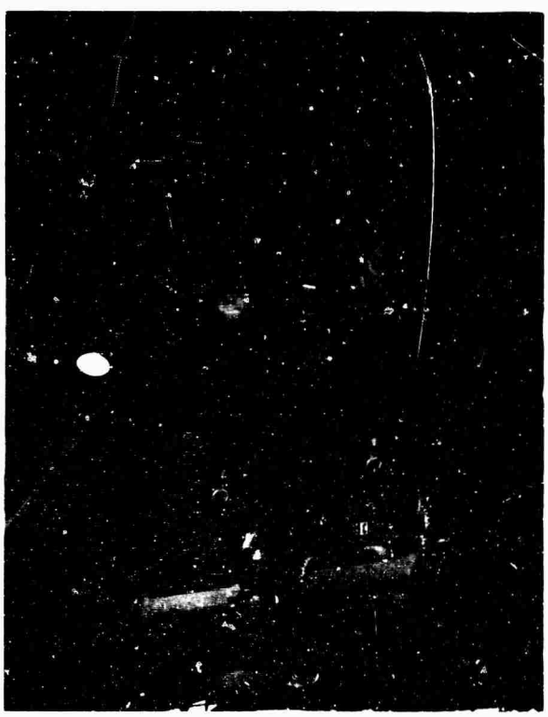

Fig. 9 - Vertical and roll shaker position, forward rotor

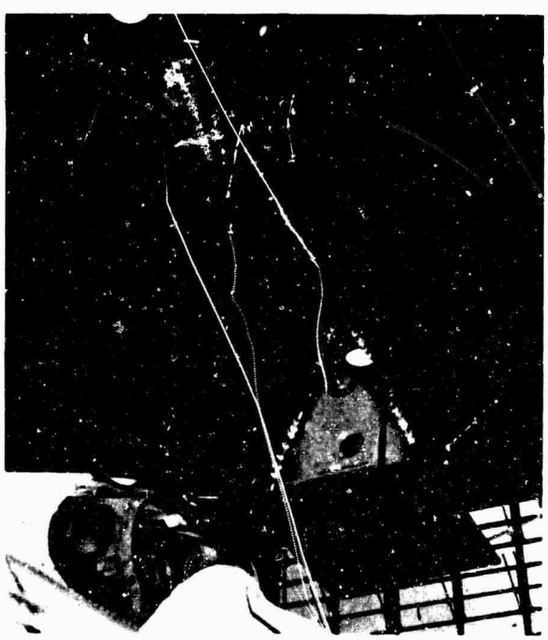

Fig. 11 - Lateral position, forward rotor

this signal and a comparable signal from the force system is measured. This difference is the phase angle by which the displacement lags the input force. The other output is a dc signal representing the amplitude of displacement measured by the pickup. This signal is fed to the Y-axis of the X-Y amplitude plotter during frequency sweeps. It is also fed to an encoder and a Datex translator, which convert the signal to a binary code for delivery to the card punch. The phase meter output is a dc signal fed to the encoder, the translator, and the Y-axis of the phase plotter. This dc signal represents the value in degrees by which the MB signal lags the reference signal and is proportional to the negative of the phase angle.

The sweep oscillator provides an input signal to the Spectral Dynamics Model SD1010. A 100-kc signal is then obtained from a side band of the SD1010 and is used as a common carrier input for both of the tracking filters to slave the tracking units to the excitor frequency.

A program control chassis is provided for controlling tests from one central location. The 28-v dc power supplies the necessary voltage to activate the various relays and switch lights. Also included is a switch and R-Cal box provided for switching between two strain-gaged links and for calibration of the system in conjunction with the BA-13 strain bridge and amplifier network.

Figure 12 shows a diagram of the fuselage response in vertical bending and lateral torsion. Figure 13 shows a comparison between test results and analytical calculations. The signal flow diagram for shaker operation is shown in Fig. 14.

CONCLUSION

By using the ground vibration techniques, the gap between analytical and experimental calculations is closing. Ground shake testing is an effective means for synthesizing vibration levels for certain configuration changes and for evaluating these changes.

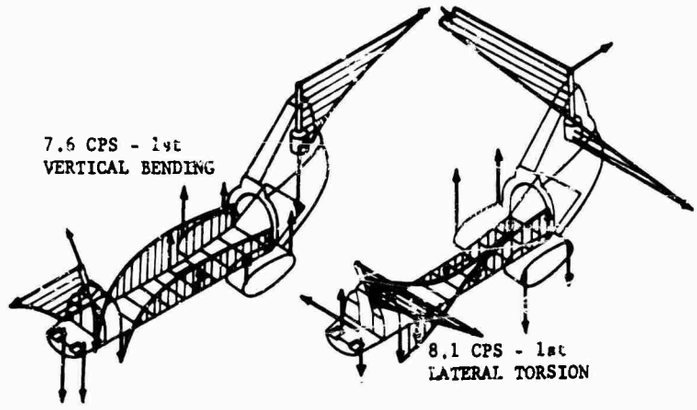

Fig. 12 - Fuselage response to ground shake test

BIBLIOGRAPHY

Gabel, R., "Advanced Vibration Development," Boeing-Vertol Rept. 107M-D-09, 1965

Reed, D., and L. Flippin, "CH-47A Helicopter Flight Vibration, Shake Tests and Noise Level Tests at Increased Gross Weight, Volume 1," Boeing Vertol Rept. 114-T-219, 1966

Robb, J. A., and R. DiTaranto, "Ground Vibration Survey YH-21 Helicopter Fuselage," Piasecki Helicopter Corp. Rept. 22-T-73, 1952

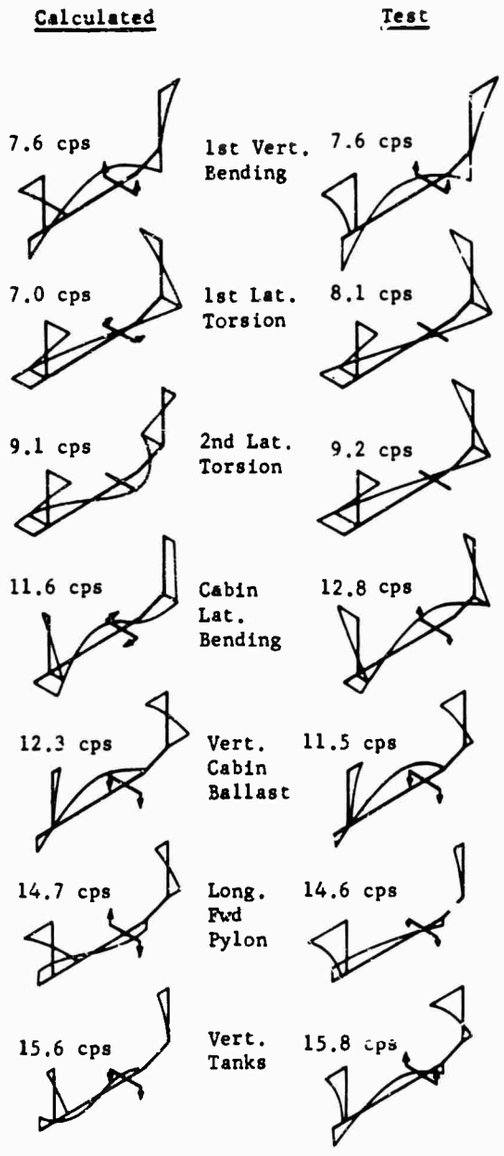

Fig. 13 - Comparison of fuselage natural modes, calculated vs test values

DISCUSSION

Mr. Lyon (Bolt Beranek and Newman): Did your studies give any information on the damping of the modes of vibration?

Mr. McCann: No.

Mr. Rommel (Lockheed-California Co.): In a few years you have gone from using a number of multiple shakers to using two shakers located at the rotor heads. Is this a change in emphasis from the determination of modes to the simulation of the vibratory source?

Mr. McCann: There are two answers to your question. I think the multiple shaker approach is good for obtaining the pure modes, and I think our dynamics people would like to have this. However, we have another problem; the multiple shaker philosophy was more or less set aside when we began to concentrate on the input of the larger shakers to obtain the required force response. I think that we are now economically in a position to use the larger shaker to get the force response, rather than being concerned with modes. Our dynamics

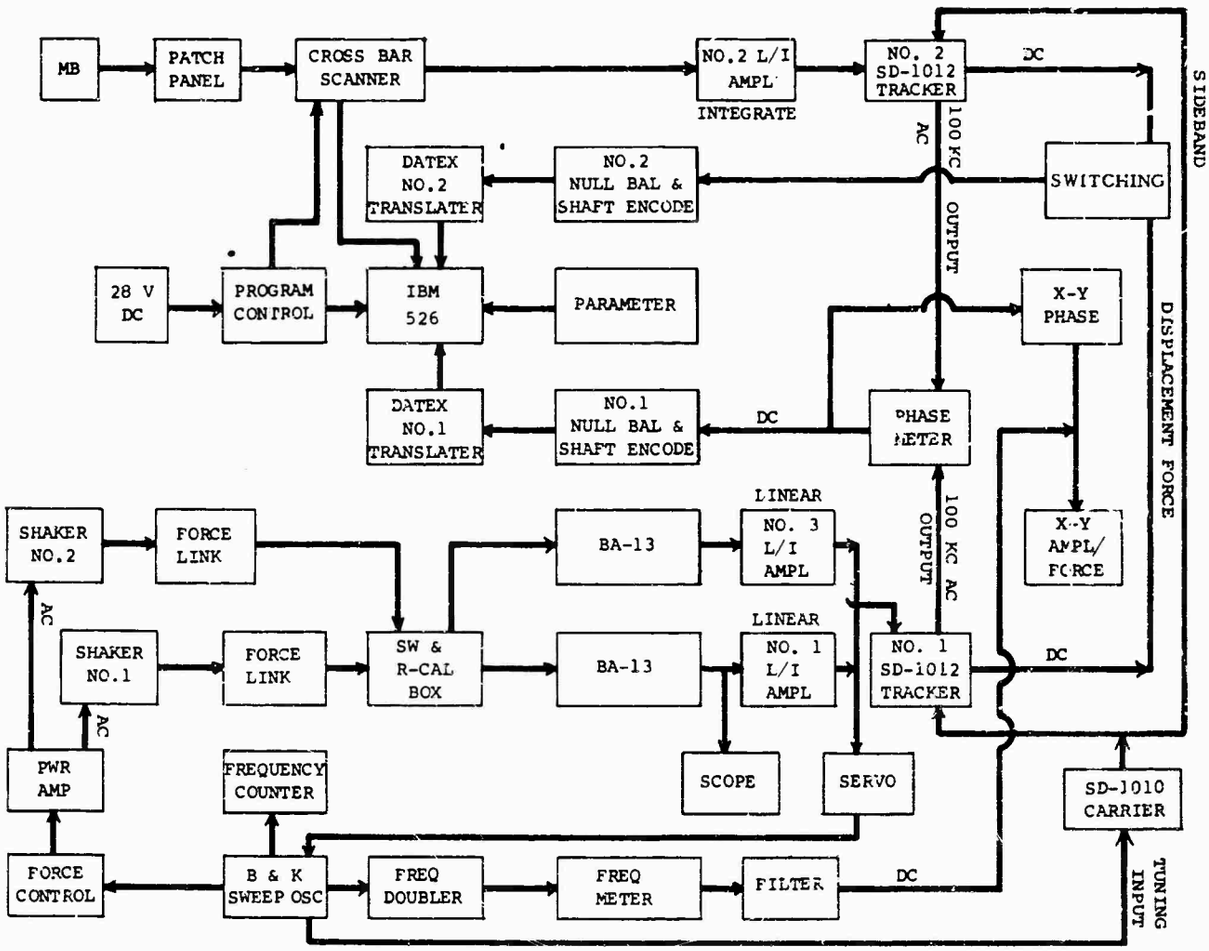

Fig. 14 - Block diagram of ground shake test data system

people are oriented toward the output-per-pound-of-input philosophy.

Mr. Rommel: I feel that the multiple shaker concept is better for the determination of modes as an end in itself but the two shakers that you have, one for each rotor head, is perhaps better from the standpoint of simulating a service environment.

Mr. McCann: This is true. The loads are induced through the rotor heads, giving a better simulation of the actual flight conditions.

Voice: I'm a bit surprised, really at the paper before the last one, to see the multi-shaker systems still being used and talked of in terms of Lewis and Wrisley. I think the reason it seems that you have decreased to few shakers and then returned to using a number of shakers is that 15 or 16 years ago multiple shaker systems were not being used in the right sense. The assumption that the force distribution should be proportional to a local mass times displacement, i.e., proportional to inertia forces, is quite wrong. You should be trying to replace the energy in the system in the same way that it is being dissipated by damping mechanisms, and I deliberately use the plural. There was a paper given about 18 months ago by Skingle from the RAE Farnborough in which he described a system whereby a master exciter of fixed force amplitude and variable frequency utilized a feedback system in which the response phase was used to adjust the excitation frequency until force and response at that point were in quadrature. This was followed by the introduction of secondary exciters, with frequency tied to the first exciter but with the force distribution or the forcing amplitude again varied until the local response was in quadrature. One could then add as many secondary exciters as one liked; of course, the more added, the more energy was input in the way it was being dissipated. Theoretically, and in fact in practice, it has been shown that in the vicinity of the resonant frequency, you can switch the whole lot on and the frequency and force distribution will sort

itself out. You will finish up with a set of exciters and a set of responses all in quadrature. Now, if you measure these forces, you can theoretically, and to some extent in practice, determine the actual damping matrix by calculating the displacement force, a displacement matrix product. Of course, you now have the force distribution used in each normal mode. The one proof that a ground resonance test has been a good one, the proof we generally use, is a check on the orthogonality.

Mr. Forlifer: We appreciate your comments. Of course, there is another school of thought on ground resonance surveys by using one shaker and getting just as good results by good analysis of the data.

* * *

RESONANCE TESTING OF A LIFTINC BODY REENTRY VEHICLE*

G. Sardella and C. L. Riggen
The Martin Company
Baltimore, Maryland

Resonance tests of the Martin SV-5D lifting reentry vehicle were conducted to substantiate experimentally the theoretical treatment used in the calculation of the vehicle vibration mode properties and to measure parameters which are too complex for theoretical treatment such as structural damping coefficient. Tests were conducted for configurations representing boundary conditions for the launch and reentry phases of flight. Tests were performed on a prototype vehicle which, except for the mass and inertia simulation of "black boxes," wiring and plumbing, consisted of the production flight article structure and ablative heat shield. The response of the vehicle under sinusoidal excitation was predicted by the matrix-force method to contain modes which were closely spaced in frequency and deflection patterns which were complex requiring three-dimensional representation. These requirements, in addition to a severe internal space limitation, formed the basis for a test approach which included a unique automatic data processing loop. Typical three-dimensional mode shapes are presented for both of the configurations tested.

INTRODUCTION

The SV-5D is an aerodynamically shaped maneuverable lifting reentry vehicle, weighing less than 1000 lb, which has been designed and is being manufactured by the Martin Company under U.S. Air Force contract as a part of the START (Spacecraft Technology and Advanced Reentry Test) Program. The vehicle, to be launched into suborbital flight by the Atlas SLV-3, is a wingless, V-shaped plane with an airfoil cross section and vertical fin/rudders (Fig. 1). It is constructed using conventional aircraft aluminum structure covered with a Martin-developed ablative heat shield. Aerodynamic control is provided by fixed upper flap surfaces and two movable flaps of beryllium substructure on the underside.

The SV-5D structure required the formulation of a detailed mathematical model to predict static and dynamic properties of the vehicle for the complete spectrum of mission requirements from lift-off through recovery phases. To analyze the vehicle with the accuracy and generality required, it was necessary to represent the structure in its entirety. In addition to the stress-strain analysis and interface loads, the normal modes of this three-dimensional structural representation were computed using influence coefficients by the Kaufman-Hall digital computer program [1,2]. The size and complexity of the model required partitioning of the vehicle into five segments: aft section, equipment beam, glove, recovery bay, and fin/rudder (Fig. 2). The analytical treatment of these segments and the formulation of the composite model is discussed in detail by Skeer and Stein [3].

Modal frequencies and deflection patterns were computed for these boundary conditions: flexible support, rigid support, free-free vehicle, and free-free recovery vehicle. Although each condition was directed primarily towards some particular aspect of the flight profile, the rigid support was one directed particularly for verification by ground resonance testing. Modal deflection patterns were complex and sufficiently numerous that a three-dimensional representation

*This paper was not presented at the Symposium.

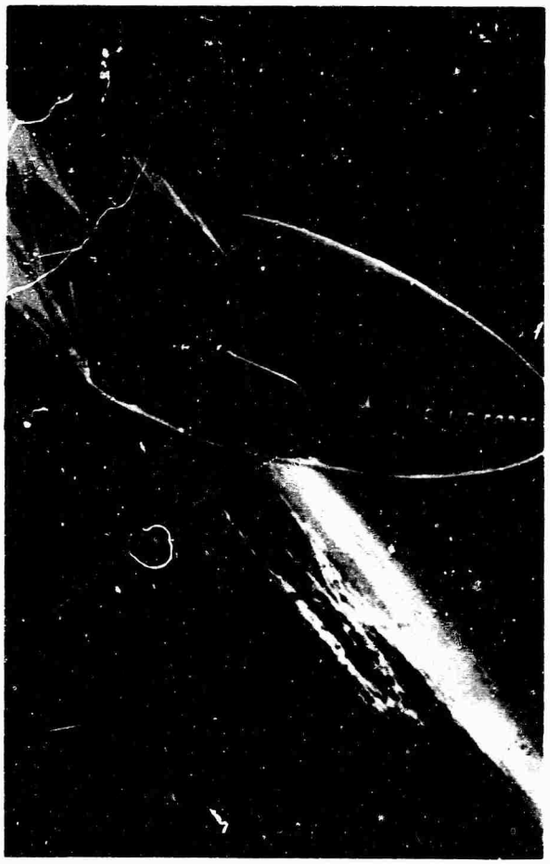

Fig. 1 - SV-5D reentry vehicle

using the Benson-Lehner J-Plotter in conjunction with the Kaufman-Hall digital program was utilized for efficient evaluation of the analytical results.

RESONANCE TEST REQUIREMENTS

Verification of the normal vibration modes of the SV-5D by ground resonance testing was determined necessary to verify previous dynamic calculations, environments, and the dynamic design adequacy of the vehicle. Configurations representing boundary conditions for launch, reentry (free flight), and a rigid cantilever case were selected for test correlation. Examination of the results of the structural analysis revealed a large number of vehicle modes in the frequency range of interest, many of them with complex mode shapes with frequencies closely spaced. Further, a symmetric and antisymmetric mode comparison indicated close proximity of torsion, bending and component modes. It was apparent the separation of the vehicle modal responses would be a difficult task, as would be the identification of the modes.

Definition of the modal responses suggested use of the phase separation technique as developed by Stahle [4,5]. This would permit isolation of individual modes and eliminate the effects of modal interaction in the response. Also, the need for a large number of excitation points, impractical on a vehicle of this size and complexity,

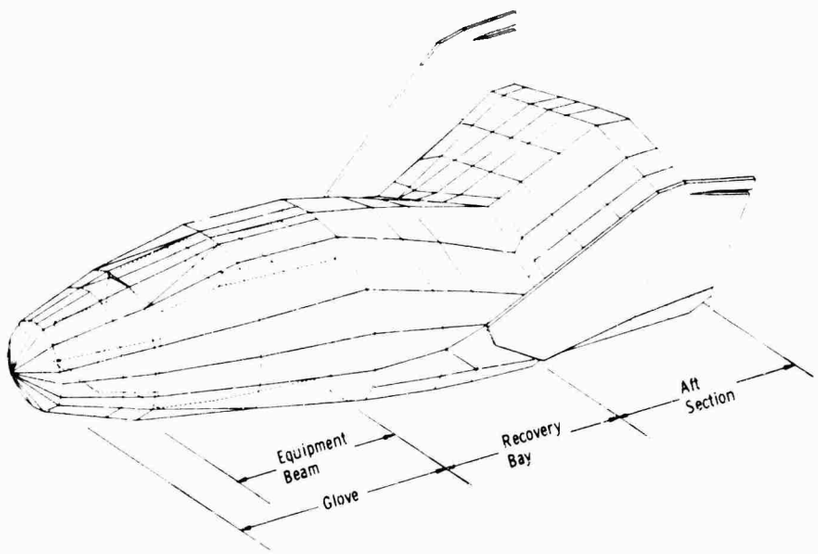

Fig. 2 - Composite SV-5D complex model

would be avoided. This technique would, in addition, provide another means of damping measurement.

Mode shape definition by deflection patterns for the representation of over 400 grid points would require three times that number of accelerometers. This was not only economically unfeasible but also a physical impossibility. It was determined that the internal volume of the vehicle was severely restricted in the areas of primary structure where grid points could be represented by triaxial accelerometers. A compromise arrangement of transducers was determined which combined the economic and physical requirements with the capability of a commercially available component analyzer and signal conditioning equipment. In addition, for direct comparison with analytical mode shapes, three-dimensional mode shape representation was determined as a necessary test requirement.

TEST APPROACH

Test Article

A full-scale test article, structurally identical to the flight article, was utilized to implement the ground resonance tests. In addition to a complete structure including all bracketry for installation of major pieces of equipment, the ablative heat shield identical to its flight configuration was also provided. The test article contained an operating hydraulic system and a recovery system complete with a dummy chute and fittings. All other components were simulated in weight, c.g. and mounting configurations by steel boxes and lead. Weight and c.g. of this vehicle was verified within 0.1 percent using the flight article weight and balance test tool.

Configurations

Vehicle support configurations included the cantilever and free-free conditions. Rigid support was provided by attaching the vehicle aft support points to an arrangement of four Team tables through mating pedestals and an adapter plate (Fig. 3). A two-point suspension by elastic shock cord provided frequencies lower than 2.0 cps for all six rigid body modes in the free-free vehicle horizontal position (Fig. 4).

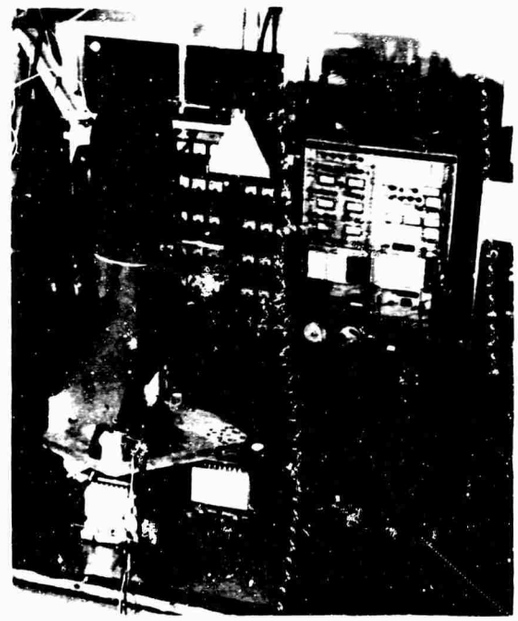

Fig. 3 - SV-5D resonance test cantilever configuration

Fig. 4 - SV-5D resonance test free-free configuration

Several shaker attachment points were provided for symmetric and antisymmetric excitation of the body and fin modes. Access holes were provided in the glove section through the heat shield for shaker inputs directly to the equipment beam. A MB Model C-11 shaker with a relatively light armature of 2.2 lb and a rated force of 50 lb maximum was used for excitation.

Instrumentation-Analyzer System

The proper type and quantity of transducers considered sufficient without relocation to define all anticipated modes were installed in the initial setup. Seven Endevco triaxial (Model 2223) accelerometers and 20 Endevco Model 2235 accelerometers were mounted in single, dual and triaxial configurations at pertinent locations. The small size of the crystal transducer facilitated installation and minimized effects on vehicle response. Acceleration signals were amplified by a selection of charge and voltage type Endevco amplifiers, and these signals were then fed to the component analyzer. Typical setup sensitivity was 3.0 volts amplifier output for 1 g input. An Endevco crystal force transducer attached in series with the shaker rod provided the necessary force signal to the component analyzer. Force level for all surveys and dwells was approximately 5 lb. The complete instrumentation system had a flat frequency response from 5 to 2000 cps.

The component analyzer used in this test is an improved version of the Model 711 waveform analyzer designed and built by Weston-Boonshaft and Fuchs Company. In its function, it allows the detection of resonance frequencies by the known change of phasing when the exciting frequency passes through a resonance. The technique, essentially the same as described in Refs. 1 and 2, provides a precise evaluation of the ratio of real, imaginary and amplitude (total) response to the force amplitude. The analyzer, by Fourier analysis methods, evaluates both the force and acceleration signals and provides over 40 db of noise and harmonic rejection. The following parameters were selected to be printed and punched on paper tape for each of the 40 accelerometer channels during readout:

1. Run number;
2. Accelerometer channel number;
3. Frequency;
4. Phase angle, θ_1 (force);
5. Phase angle, θ_2 (acceleration);
6. Delta phase, $\Delta\theta\ (\theta_1 - \theta_2)$;
7. Force, real;
8. Force, imaginary;
9. Force, total;
10. Acceleration, real;
11. Acceleration, imaginary;
12. Acceleration, total;
13. Acceleration, in-phase;
14. Acceleration, quadrature;
15. In-phase/Force (total), ratio; and
16. Quadrature/Force (total), ratio.

The parameter used for plotting modal patterns was the quadrature/force (total), ratio; the additional items provided a check of any erroneous or questionable points in the modal plotting.

Data Processing

Data processing consisted primarily of removing the punched tape after completion of each resonance dwell and converting to punched cards by a tape/card converter. These punched cards (40 per resonance) were then submitted to the IBM 1130 digital computer. The digital program converted each punched card of raw data into suitable form for the plotting of three-dimensional modal deflection patterns automatically by the Benson-Lehner J-Plotter (Fig. 5). The resulting plot was then placed over an underlay of the vehicle mathematical model for evaluation. This data handling process provided a normalized modal plot in final form within 15 to 30 min after a resonance dwell. This enabled the testing personnel to evaluate readily all "apparent" resonances, since the time-consuming

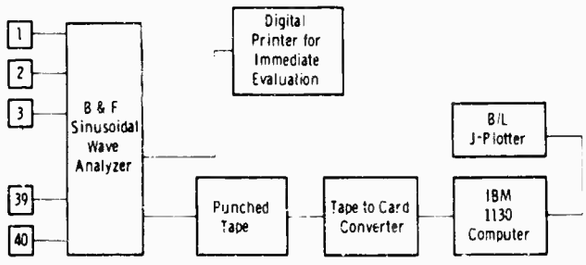

Fig. 5 - Data processing diagram

and expensive hand reduction methods generally employed were eliminated.

TEST RESULTS AND OBSERVATIONS

Testing of the reentry vehicle was limited to the cantilever and free-free conditions. For these configurations, sinusoidal sweeps for resonances were made in the frequency range below 150 cps for the cantilever case, below 200 cps for body modes, and below 500 cps for fin modes in the free-free configuration. Resonances were detected by peaks indicated by the quadrature response for the transducers selected. Approximately 100 resonances were evaluated plus additional evaluations as a result of sensitivity adjustments.

Modal deflections were plotted and evaluated for all significant peaks indicated on each quadrature/force graph. Each mode was identified by deflection patterns through comparisons with the analytical plots. In most cases modes were readily identified in this manner; however, it was found that in the higher modes (above 100 cps, with the exception of the fin) identification by modal deflection plots was not always possible because of the severely limited quantity of transducers. Also, these transducers may, at the higher frequencies, be affected by local resonances, thereby obscuring segments of the mode shape. Verification of the higher modes was, therefore, accomplished by frequency comparisons.

Comparisons of analytical vs test results for some fundamental frequencies are shown in Tables 1 and 2. For both the rigid cantilever and free-free case, agreement of test and analysis in the lower modes was good for the body and flap modes. However, a large deviation occurred in the equipment beam and fin comparison. Examination of the modal deflection

TABLE 1
Comparison of Computed and Test Frequencies, Free-Free Condition

Mode	Mode Description	Frequency (cps)	
		Computed	Test
Symmetric (pitch)	1st Eq. beam bending	78.37	50.3
	1st flap mode	58.15	55.1
	(Not identified)	—[a]	87.4
	1st body bending	95.27	92.3
	2nd flap mode	108.10	—[b]
	Mode No. 5	116.10	114.8
	Mode No. 6	150.60	160.1[c]
	Mode No. 7	156.60	167.7[c]
	Mode No. 8	159.50	147.6[c]
	Mode No. 9	175.10	181.4
	Mode No. 10	205.50	191.3
Antisymmetric (yaw)	Battery bracket	39.00	69.3
	1st flap mode	52.79	54.7
	1st Eq. beam bending	76.69	40.7
	Mode No. 4	108.70	—[a]
	Mode No. 5	111.00	111.3
	1st body torsion	129.00	130.6
	Main hatch	133.90	135.3
	1st body bending	146.50	141.3
	Mode No. 9	156.50	158.5
	Mode No. 10	173.40	169.3
	1st Eq. beam torsion	197.20	202.0
Fin	1st fin bending	46.60	81.1
	1st fin torsion	84.00	133.6
	1st fin camber	134.50	224.6

[a]Not investigated.
[b]No resonance found.
[c]Verified by modal deflection plot.

TABLE 2
Comparison of Computed and Test Frequencies, Rigid Cantilever Condition

Mode	Mode Description	Frequency (cps)	
		Computed	Test
Symmetric (pitch)	1st body bending	11.83	11.3
	1st flap mode	54.50	40.9
	1st Eq. beam bending	79.51	50.3
	2nd body bending	66.75	58.3
	2nd flap mode	107.90	—[a]
	3rd body bending	109.00	—[a]
	Mode No. 7	127.00	—[a]
	Mode No. 8	153.00	—[a]
	Mode No. 9	158.10	—[a]
	Mode No. 10	165.00	—[a]
Antisymmetric (yaw)	1st body bending	29.05	27.3
	Battery bracket	40.19	69.3
	1st flap mode	51.48	—[b]
	1st body torsion	68.30	63.9
	1st Eq. beam bending	76.42	43.6
	2nd flap mode	100.20	—[a]
	Mode No. 7	119.70	—[a]
	Mode No. 8	125.00	—[a]
	Mode No. 9	134.10	—[a]
	Mode No. 10	153.40	—[a]
	Mode No. 11	173.90	—[a]
	Mode No. 12	196.00	—[a]

[a]Not investigated.
[b]No resonance found.

plots for the beam and the fin showed good correlation between test and analysis, thereby verifying these measured frequencies.

An example of the modal deflection pattern and frequency sweeps is presented for a body mode in each test condition. A comparison of analytical vs test mode shapes can be made by Figs. 6 and 7 for the first structural bending mode in pitch (cantilever). For clarity, these plots show the beam response segregated from the body response. Taking advantage of symmetry, only half the vehicle is shown, and for clarity the fin/rudder response is omitted. The correlation of mode shapes is readily apparent by this comparison. A plot of the ratios of in-phase and quadrature acceleration response to total input force vs frequency is presented in Fig. 8 for the pitch accelerometer at the nose of the vehicle. The lowest and most prominent resonance is the first structural bending mode in pitch (cantilever); the second most prominent resonance is the first pitch bending mode of the equipment beam. The smaller resonance was identified as the first flap mode with the actuator system unpressurized (which was not part of the resonance search). A comparison of the analytical

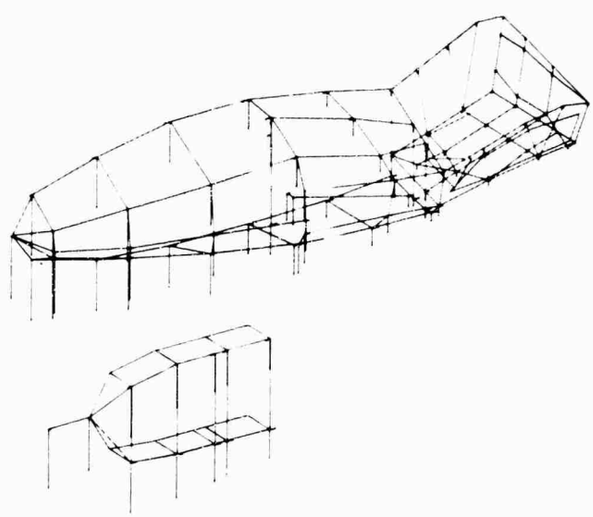

Fig. 6 - Symmetric constrained mode No. 1 (cantilever), first pitch bending of structure, 11.83 cps -- analytical results

vs test mode shapes for the first structural bending mode in pitch for the free-free condition can be made by Figs. 9 and 10. Damping

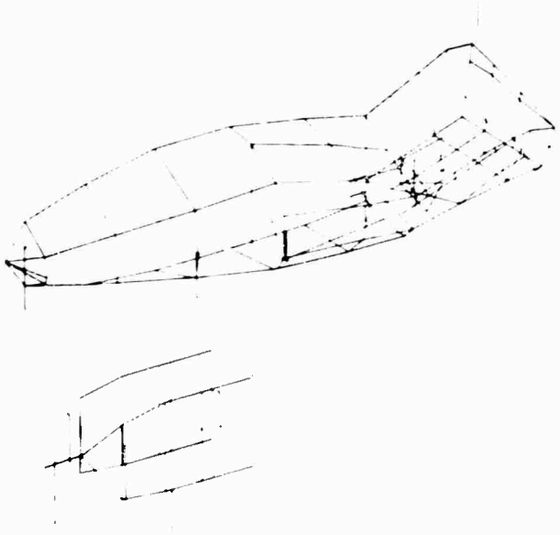

Fig. 7 - Symmetric constrained mode No. 1 (cantilever), first pitch bending of structure, 11.30 cps -- test results

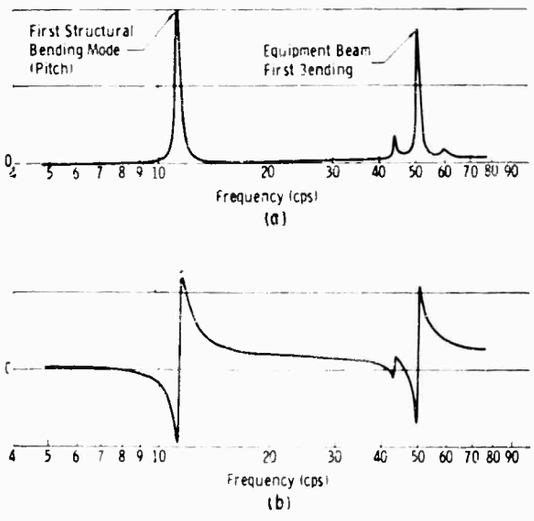

Fig. 8 - X-Y plots of pitch accelerometer response (cantilever condition): (a) quadrature response, and (b) in-phase response

for the lower modes was measured by both the log decrement and the in-phase response peaks. The damping factor γ (defined as $2c/c_c$) was determined to be 0.041 in the first structural bending mode.

In each configuration it was found that all modes of primary interest in the plane under test could be excited by utilizing no more than two shaker input locations; in some cases one

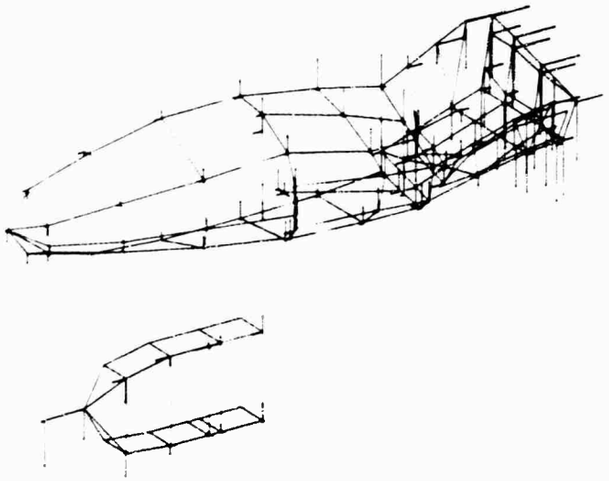

Fig. 9 - Symmetric free-free mode No. 3, first pitch bending, 95.27 cps -- analytical results

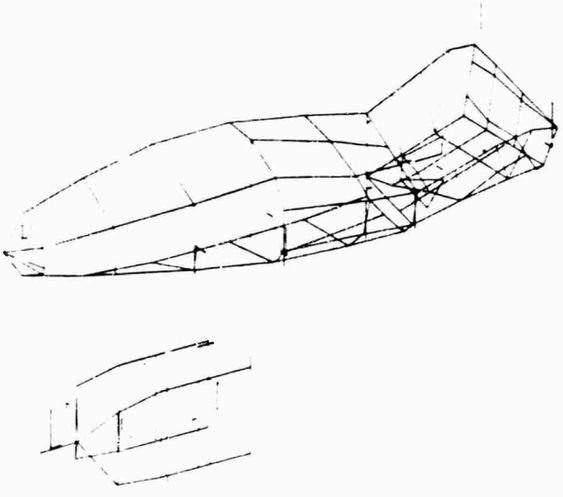

Fig. 10 - Symmetric free-free mode No. 3, first pitch bending, 92.3 cps -- test results

point was sufficient. The force excitation level for most sweeps and resonant dwells was low, on the order of 5 lb. In a few tests the force was lowered to 1 or 2 lb to minimize distortion on the accelerometer signals. The resultant low output signals with some noise did not appear to affect the operating accuracy (±1.0 percent) of the component analyzer. Using the maximum time constant setting, the analyzer can provide an attenuation of 100 (40 db) to a noise frequency only 0.30 cps from the test frequency. Since most of the noise content was further removed from the test frequency, shorter averaging times were selected.

CONCLUSIONS

Results of this resonance test verified the dynamic analysis of the structure for the cantilever (rigid support case) and the free-free conditions. This was evidenced by both the mode shape and frequency correlation. Differences in modal frequencies for the fin and beam were investigated as to probable causes with the following conclusions:

1. Fin – In the analysis of the structure the ablative heat shield was considered nonstructural because of its low modulus of elasticity compared to that of the aluminum substructure. Its effect was not considered sufficient to warrant the additional complexity of the analysis that would be required. It was apparent after the resonance tests that such an assumption may be valid only for the body modes and not for a cantilevered structural segment such as the fin. This was further evidenced by deflection data of the fin with no heat shield under static load which correlated exactly with the structural analysis.

2. Beam – The attachment of the cantilevered beam structure to the bulkhead was determined as the probable cause of the frequency difference. This resulted from the assumption of effectiveness in the estimated lengths of the bending elements at the root. This effect caused analytical frequencies to be considerably higher than the measured frequencies.

The method of data acquisition permitted swift and efficient modal evaluation. This was possible because of the unique features of the component analyzer which permitted a quick resonance search and of the computer/plotter loop which presented the data. All data were available in final form within minutes following the resonance dwell with a substantial manpower saving during the test and for the report effort. Although the verification of the higher modes by mode shape was limited by the measurement arrangement, it was felt that improvement would require not only increases in number but a complete substitution of a subminiature triaxial transducer to improve location effects. Justification of the additional cost would have to be made in light of the value, other than academic, of the higher mode shapes. Improvement in the data loop processing time could be made with a small computer and plotter adjacent to the analyzer; the cost, of course, would also have to be justified in light of the slight time saving.

The log decrement method of determining damping appeared to be the most reliable from the standpoint of repeatability. Peaking on the in-phase response was sometimes found to yield large variations. An average value of damping was determined to be $\gamma = 0.025$ for most of the body modes. For the fin, where the heat shield stiffness effect was greater, damping was found to be $\gamma = 0.055$. It was apparent the damping contribution of the ablator was greatest on the components (fin and panel resonances) rather than having an effect on the overall body modes.

REFERENCES

1. S. Kaufman and D. B. Hall, "Digital Program for Static and Dynamic Analysis of Complex Structures," Martin Co. Rept. RM-136, 1963
2. S. Kaufman and D. B. Hall, "Static and Dynamic Analysis by a Matrix Force Method," Shock and Vibration Bull. No. 34, Part 2, pp. 121-128, Dec. 1964
3. M. H. Skeer and A. L. Stein, "Structural Model of the SV-5D Re-entry Vehicle," Martin Co. Rept. ER-14076, Feb. 1966
4. C. V. Stahle, "A Phase Separation Technique for the Experimental Determination of Normal Vibration Modes of Flight Vehicles," Shock and Vibration Bull. No. 29, Part 4, pp. 30-42, June 1961
5. C. V. Stahle, "Phase Separation Technique for Ground Vibration Testing," Aerospace Eng., Vol. 21, No. 7, July 1962

* * *

SHOCK AND VIBRATION TESTING USING FOUR-SHAKER SYSTEM*

Dean F. Redford
Thiokol Chemical Corporation
Brigham City, Utah

In June 1965, Thiokol's Wasatch Division was awarded a contract to test a LOX vent duct in three different environments: half-sine shock, swept frequency sine vibration, and random vibration. To accomplish test objectives, four-shaker systems were used in conjunction with a wave synthesizer, automatic sine wave vibration control units, and an automatic random vibration control unit.

The shock pulse, as monitored at the shaker heads, was altered by the inductive-capacitive characteristics of the drive system; consequently, the required half-sine pulse was ultimately achieved through successive trials and subsequent adjustment of the wave synthesizer.

The sine vibration environment was initiated and controlled by four automatic vibration exciter controllers. These units were, in turn, controlled by phase control equipment to maintain the four-shaker heads at a zero phase relationship throughout the frequency spectrum of 5 to 2000 cps.

The random environment was achieved with an automatic multi-channel random equalizer-analyzer used with each of the three exciter systems. Each exciter system, loaded with its respective fixture but without the test specimen, was energized until the desired spectrum was attained, at which time the drive signals were recorded on magnetic tape. The three drive signals, contained on parallel tape tracks, were used to drive the individual shakers, while the fourth shaker was driven by the automatic equalizer-analyzer.

Use of the configuration described made it possible to conduct the test with a common spectrum supplied to the specimen from four outputs. Obviously, adding the specimen to the system changed the response characteristics of the fixture-loaded shaker system to some extent. Further, since three of the shakers did not have feedback amplitude control, the random spectrum varied from that of the unloaded system. The fourth shaker was held to specification by the automatic equalizer-analyzer. However, the nature of the specimen was such that the resulting spectrum change was within the ± 3-db limit specified.

D. F. Redford

INTRODUCTION

This paper details the technique used and results obtained in shock and vibration testing of a LOX vent duct used in the S-IVB stage of the Saturn IB and Saturn V launch vehicles. The control system used to perform the tests is described with special emphasis on the method used to achieve the shock and random vibration environment on each of four-shaker systems

*This work was conducted under a contract from the Douglas Missile and Space Systems Division, developers and manufacturers of the Saturn S-IVB stages.

with a single signal source. Data are presented demonstrating the validity of the techniques used.

DISCUSSION

Equipment Description

The test item, a LOX vent duct, had the following configuration:

Specimen weight, 36 lb;
Specimen length, 20 ft;
Specimen diameter, 5 in.; and
Test fixture weight, 1330 lb.

The following vibration equipment (Figs. 1, 2, and 3) was used for the test:

2 Ling Model 249 shakers with Model PP 120/150 amplifiers-fixture (310- and 170-lb load),

1 Ling Model 245 shaker with Model 10/16 amplifier-fixture (30-lb load), and

1 Calidyne Model 177 shaker with Ling Model 15/24 amplifier-fixture (55-lb load).

Control equipment used included:

2 Bruel and Kjaer Model 1029 automatic vibration control units,

2 Bruel and Kjaer Model 1018 automatic vibration control units,

1 MB Electronics Model T589 equalizer-analyzer,

1 Exact Electronics Model 200 waveform synthesizer with Type E plug-in,

1 Chadwick-Helmuth Model 500 phase controller,

4 Kistler Model 568 charge amplifiers,

4 Endevco Model 2242 accelerometers,

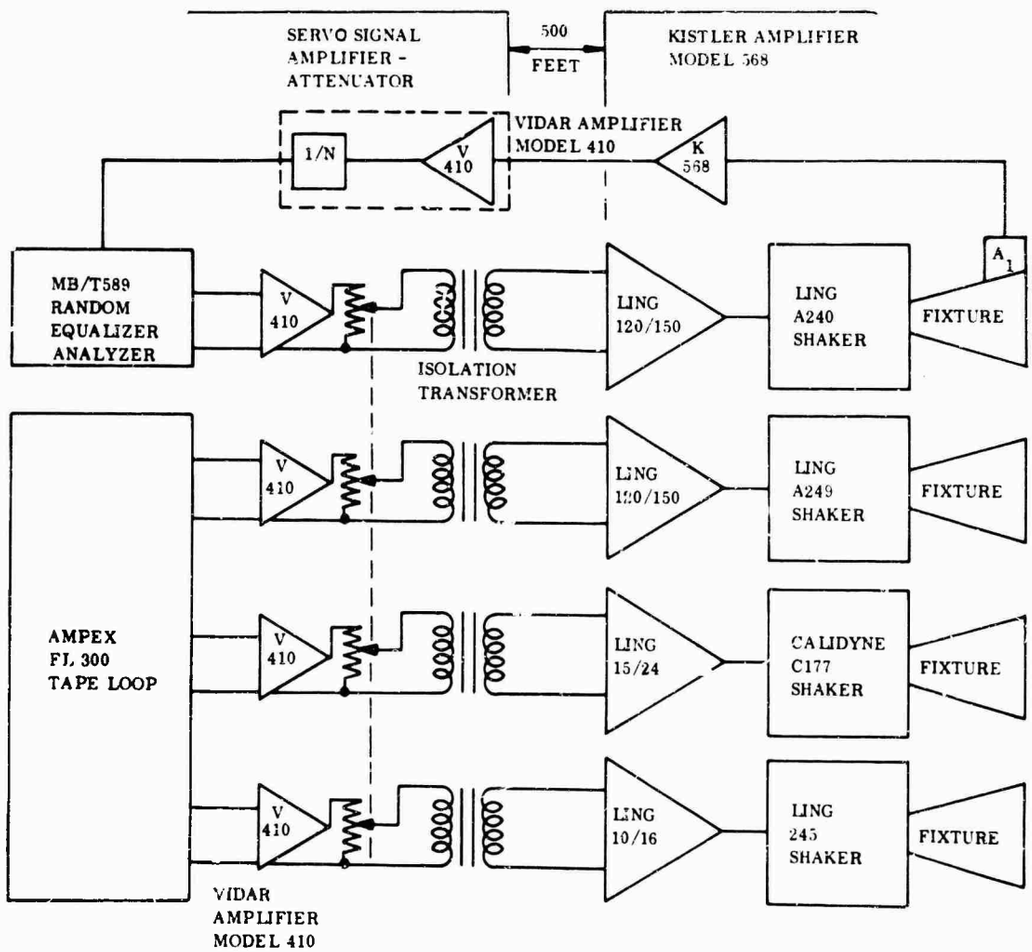

Fig. 1 - Block diagram, random vibration test

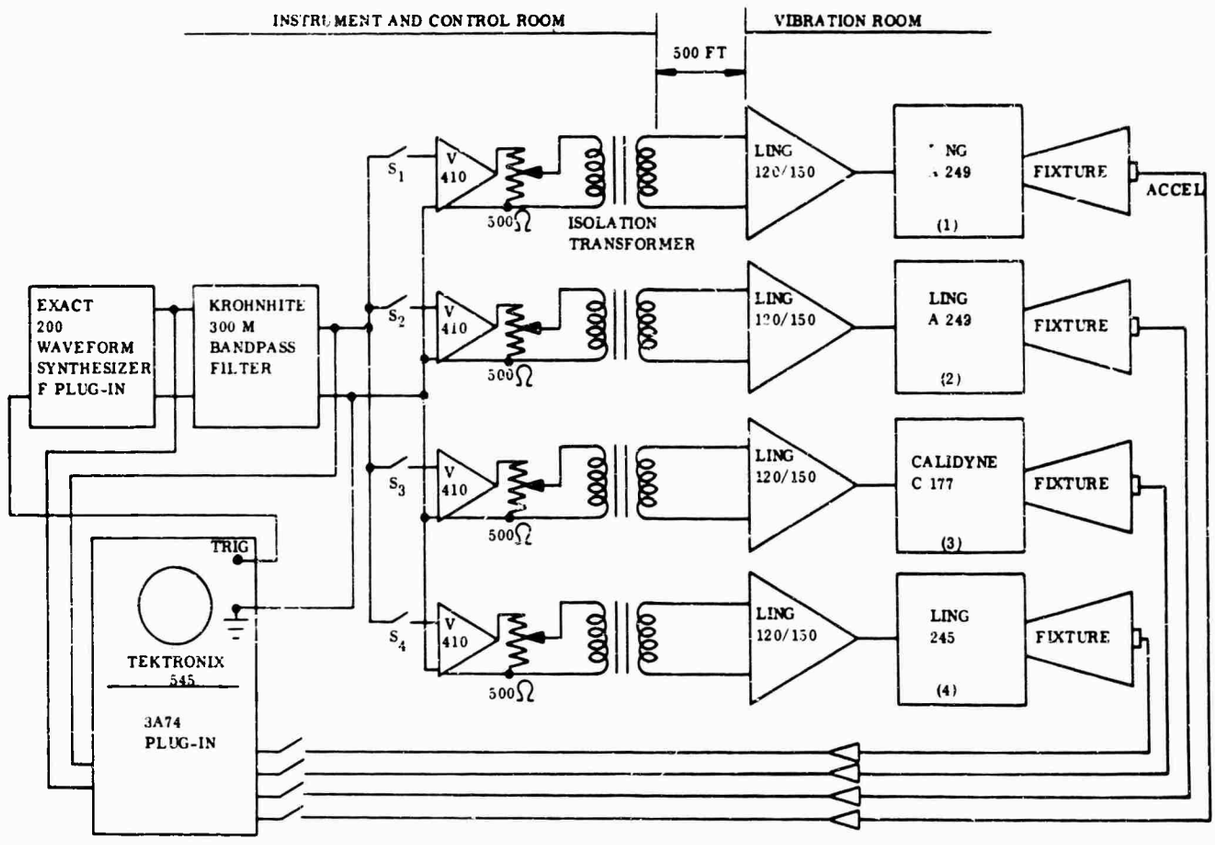

Fig. 2 - Block diagram, shock test

1 Ampex Model FL300 loop tape reproducer, and

4 Vidar Model 400 amplifiers.

Test Arrangement

The test arrangement in the tangential and longitudinal configuration is shown in Fig. 4. The control equipment for sinusoidal random and shock testing is shown in Fig. 5.

The test specimen was installed, wrapped (Fig. 4a), and chilled to -320°F by circulating LN_2 through the duct. The duct was tested in random pulse and sinusoidal environment in this configuration.

Test Procedure

Random Environment – The random environment was produced by utilizing the single equalizer-analyzer to control each of the shakers (loaded with fixture) prior to installation of the specimen. As each shaker system was equalized and controlled to specification, the T589 output signal was recorded on magnetic tape. This information was prepared on a loop tape on parallel tracks so that the drive signal for shaker systems 2, 3, and 4 could be reproduced continuously from the loop tape reproducer simultaneously with the drive signal from the equalizer.

To complete the setup, each of the three indicated shaker systems was driven from the loop tape reproducer while the shaker system's outputs (accelerometer located at the control point) were fed back to the analyzer of the T589. Gains for each system were adjusted until the required spectrum levels were achieved, as monitored at the analyzer output in terms of g^2/Hz. When the required spectrum amplitude was achieved on each shaker system, the specimen was installed, chilled and tested. The results of the test, as monitored at the control accelerometer locations, are shown in Fig. 6.

During the test, shaker system 1 was controlled by the T589 while systems 2, 3, and 4 were driven by the taped signal. As shown by the data, the specification was achieved by using

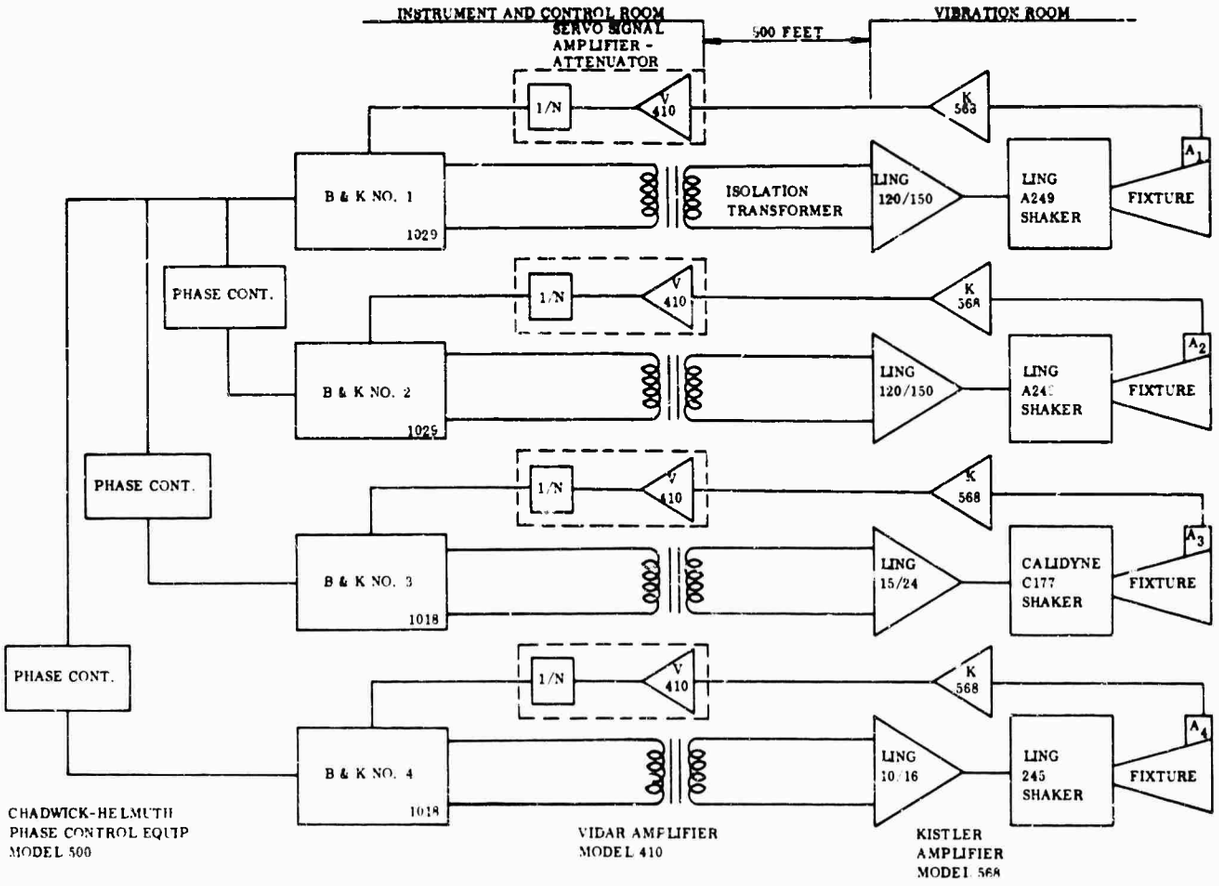

Fig. 3 - Block diagram, sine-sweep test

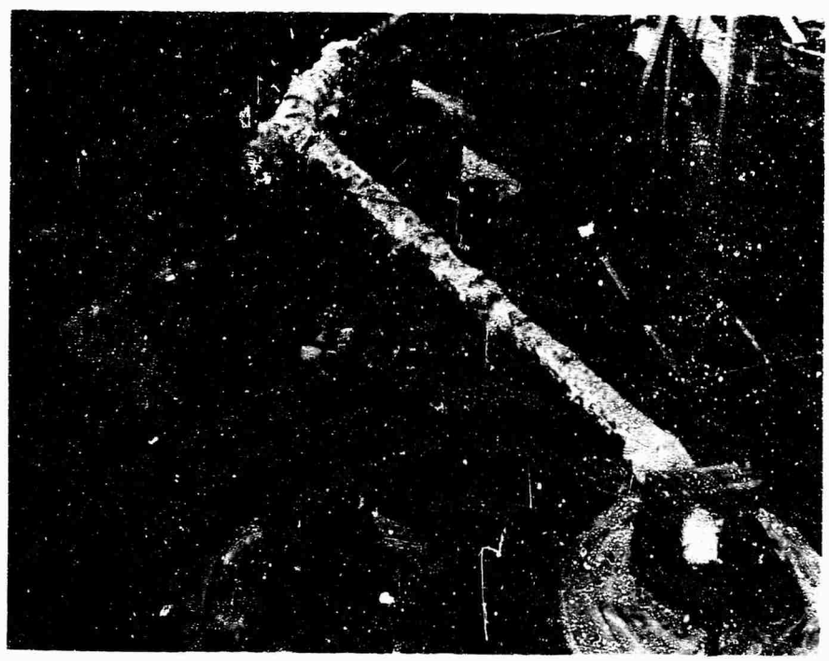

(a)

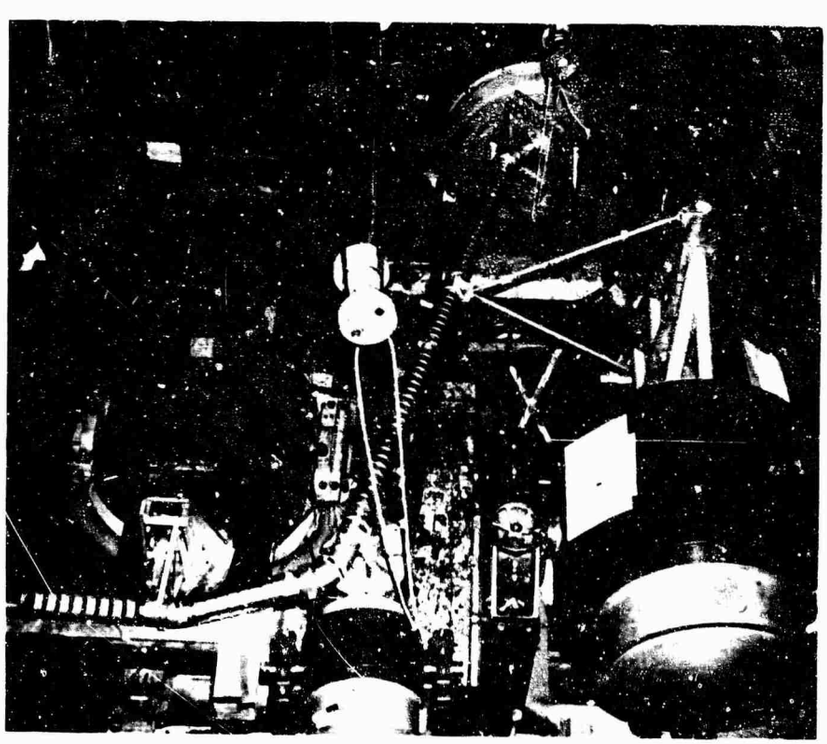

(b)

Fig. 4 - Test arrangement: (a) tangential configuration, and (b) longitudinal configuration

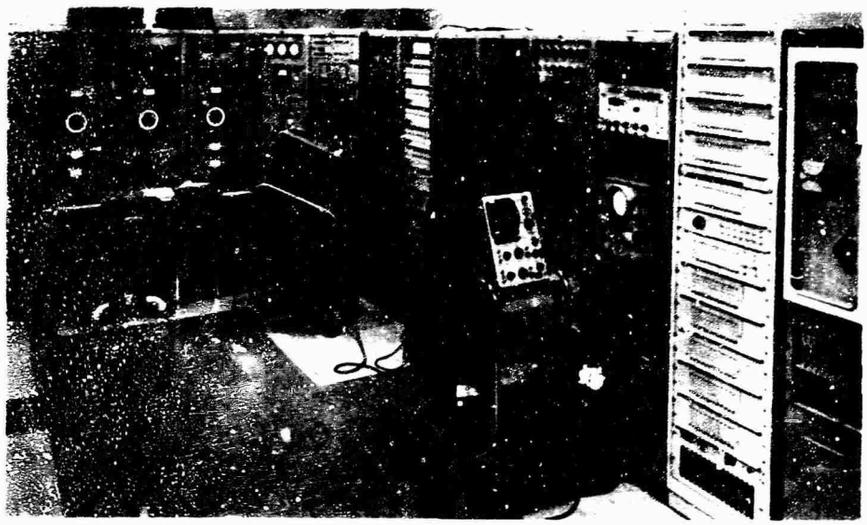

Fig. 5 - Control equipment

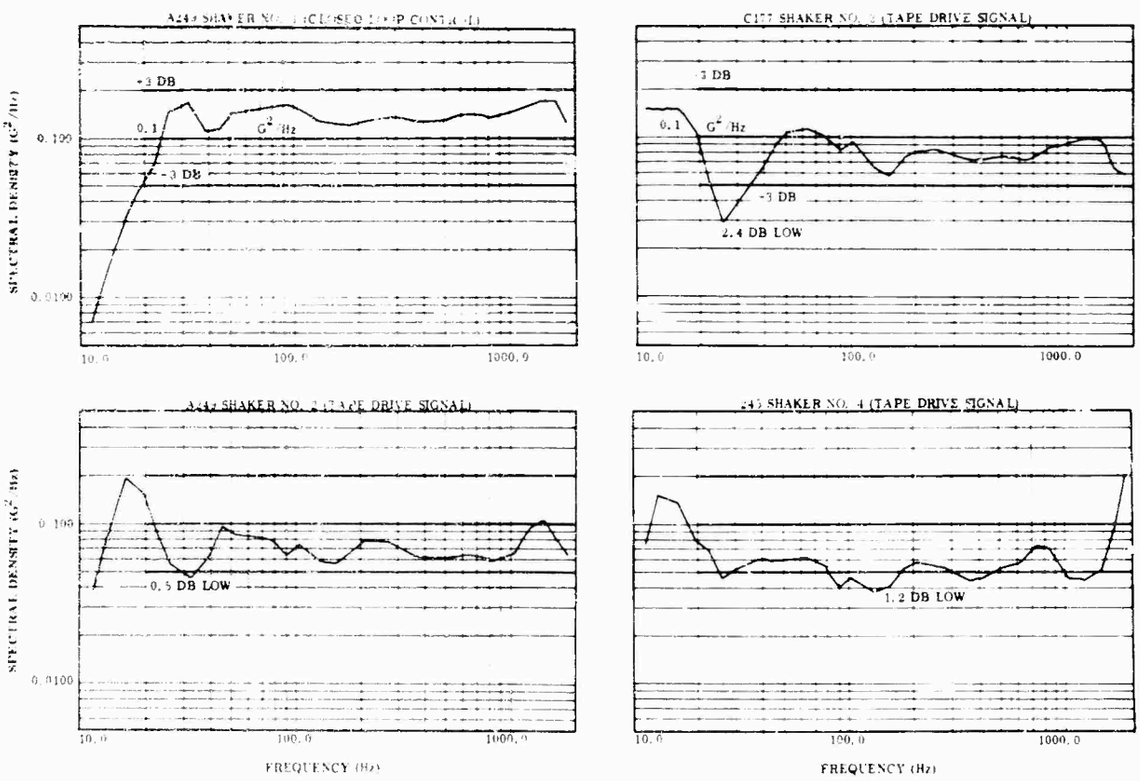

Fig. 6 - Random vibration test results

this method at all points in the spectrum except as noted on the plots. The only serious departure from the specification occurred on shaker 3 (i.e., 2.4 db low at 26 Hz), which was driven by a taped signal.

Shock Environment – The shock environment was reproduced by the method detailed by Hay and Oliva [1]. The waveform synthesizer was used to generate the input pulse which, when differentiated by the shaker system, resulted in the half-sine pulse (Fig. 7). The pulse shape was optimized on shaker system 1 (with fixture attached but without the specimen) and checked on shaker systems 2, 3, and 4. The gains on all systems were set to achieve the required 20-g amplitude. With all systems set for proper level, the specimen was added and the waveform synthesizer was pulsed to complete the test.

Sinusoidal Environment – The sinusoidal environment was controlled by the four Bruel and Kjaer units (Fig. 3). These units were phase controlled by Chadwick-Helmuth phase control equipment. The resulting data from control accelerometers located at each of the four inputs are shown in Fig. 8. Difficulties encountered resulted from the very low level requirements at 5 Hz (i.e., 0088 DA). At these levels the Bruel and Kjaer units demonstrated difficulty in "locking on" to the signal. This was resolved by moving up the frequency scale, locking on the B & K servos and manually repositioning the sweep dial to 5 Hz before starting the sweep.

CONCLUSIONS

Results of the random test demonstrate that multi-point input to long, flexible, lightweight specimens may be achieved economically by taping the drive signals of the second, third, and fourth shaker systems prior to installation of the specimen, thus eliminating the use of multiple input equipment. Although this technique is subject to the shortcoming of open loop control, it can be employed on certain types of specimens with good results.

Results from the shock test show that the technique utilized provides an adequate shock pulse on each of four shaker systems with no time correlation problem. Some degradation in the pulse wave was caused in the third and fourth shaker systems due to imposition of the specimen. This effect would undoubtedly be amplified by a stiffer specimen. However, for certain types of specimens, this technique is completely acceptable.

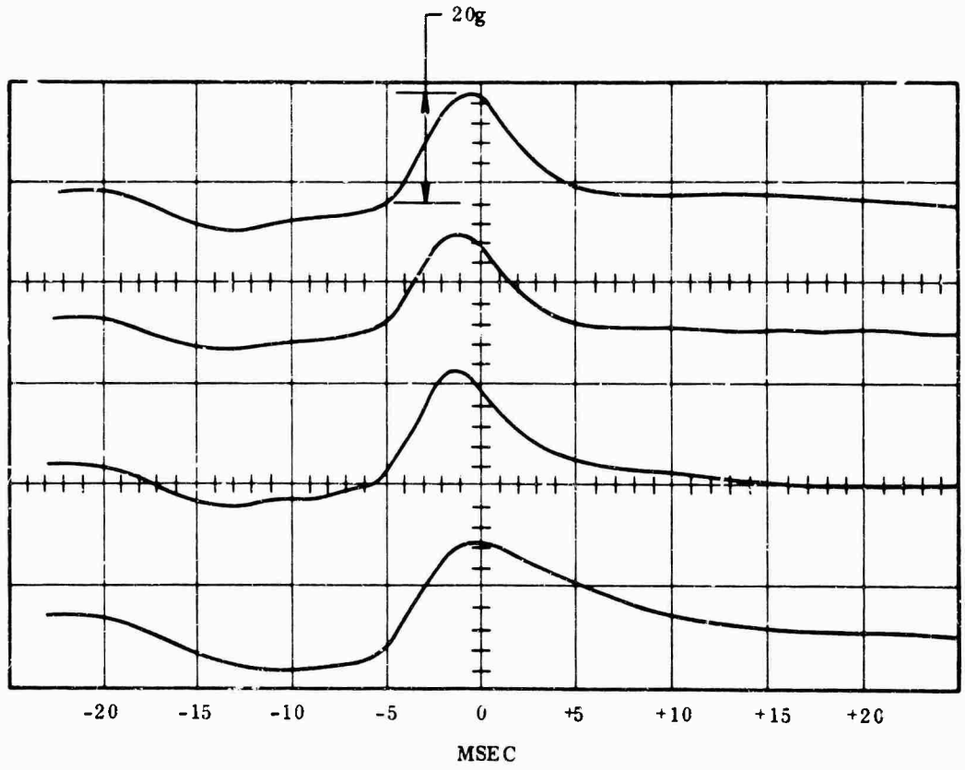

Fig. 7 - Shock test results

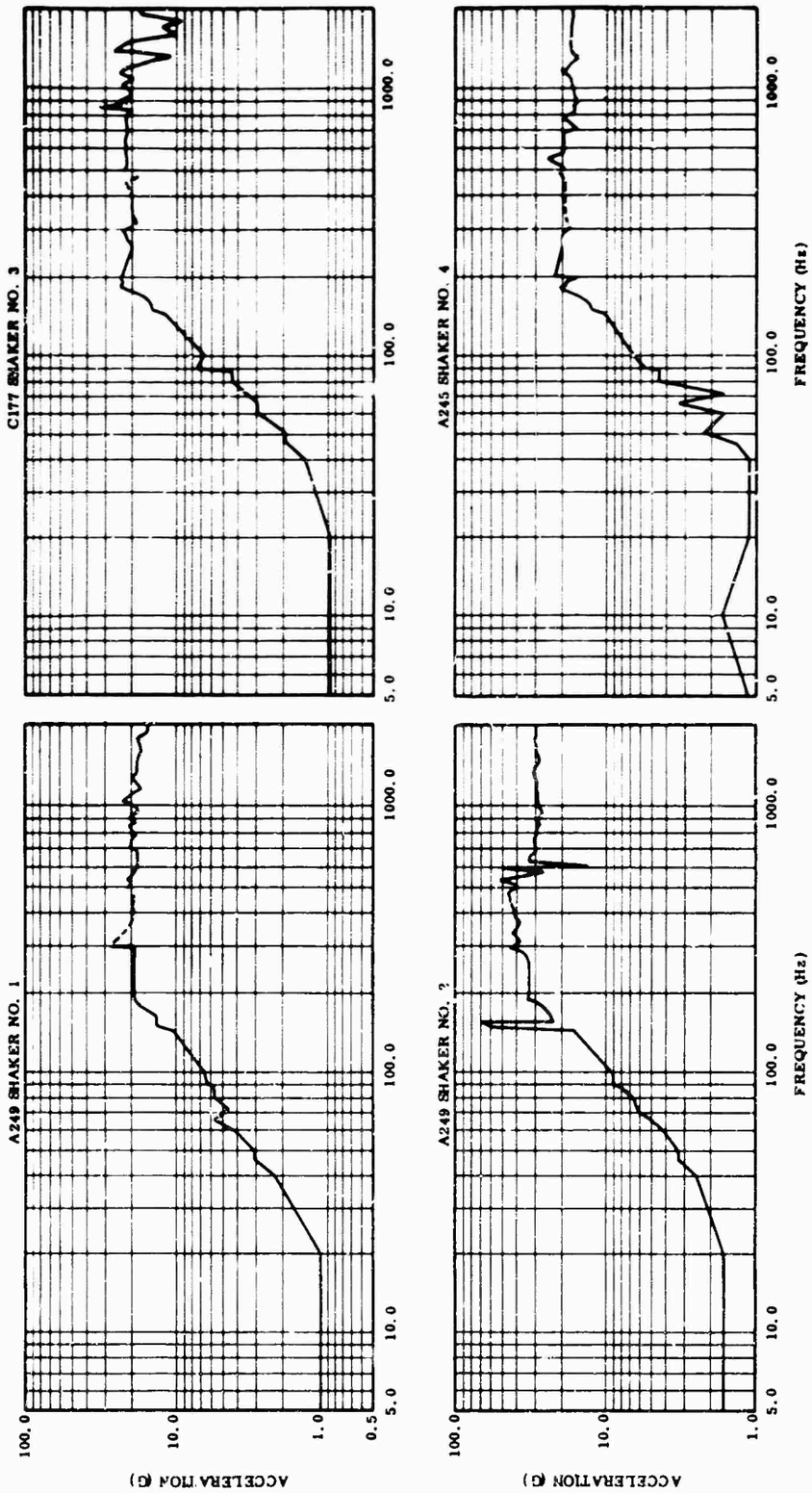

Fig. 8 - Sinusoidal vibration test results

REFERENCE

1. Warren A. Hay and Ralph M. Oliva, "An Improved Method of Shock Testing on Shakers," Proc. IES, pp. 241-246, 1963

* * *

DESIGN TECHNIQUES FOR HORIZONTAL DRIVERS

Fred C. Tolleth
North American Aviation, Inc./Autonetics Division
Anaheim, California

Design requirements, analysis for a large cast horizontal driver (or adaptor) used with a Ling-249 vibration exciter, and pertinent data for use with the design are presented in this paper. The reasoning behind compromises in design is examined so that a particular design may be used for application to other problems. A practical analysis is offered for a single- and two-degree-of-freedom driver and shaker system where the structural members, as individual units and as a whole, employ conclusions derived from unit analysis.

Data recorded during the dynamic evaluation of the driver and shaker units, individually and as a system, indicate the strong points and shortcomings of design. The data obtained are in the form of g's vs frequency plots that reveal various force levels and structural members of the driver in a loaded and unloaded condition. To support the design approach taken here, four other cast horizontal drivers that use different exciter heads but the same techniques of design, which were proven successful, are also analyzed in this paper.

F. C. Tolleth

INTRODUCTION

Fixture design principles are deceptively simple. One can follow all the rules, but still produce a fixture that does not meet expectations. Usually this occurs because of one of the following reasons:

1. The attitude prevalent in the testing industry that a fixture is something which can be manufactured during the test engineer's spare moments, or

2. Failure to take into consideration the whole system during the design procedure.

The purpose of this paper is to dispel some of the confusion which surrounds fixture design in general, and to present a procedure of design for a specific fixture which, with common sense modification, might be applied to a variety of fixture design problems. Attempts to parallel the actual design activity are presented and developed in a logical manner. First, the design parameters are developed for an actual test condition. These requirements are then modified to fit a multitude of tests over a period of time to reduce the cost. After the requirements are determined, the exciter head is examined for mechanical variables. When these have been determined, the design is explained in terms of the overall system, design requirements, and exciter-head characteristics. A simple numerical analysis accompanies each step of the design and is intended to show that compromises within the design are necessary and proper.

To support the idea that fixtures are best designed by people who are specialists in this field, a short description of four other cast horizontal drivers designed by other engineers, but by essentially the same method, is given here. After the design of the Ling-249 horizontal driver is completed, data are given on its performance in the unloaded condition, and an attempt is made to show that if mass is

added properly, the frequency response is reasonably predictable.

This paper is not the last word on design, but is an attempt to show a practical and usable procedure rather than an abstruse mathematical presentation which is often difficult to apply. The purpose here is primarily to give the test engineer, with little or no design experience, a system by which he can design a usable fixture with greater confidence than is usually the case.

DESIGN AND ENGINEERING BACKGROUND

The idea that design engineering and test engineering are separate but related fields of endeavor is not new. The testing industry, however, is only recently revising its attitude which defines the test engineer as an expert in instrumentation, environmental testing, and design. This revision in attitude probably has been brought about because of the realization that testing has increased in complexity, and too few hours remain in the day for the test engineer to complete all the duties required of him. One logical solution to these circumstances is to provide the testing laboratory with a broader base of experience in the form of mechanical and structural design engineers. In this way the test engineer may be relieved of some of the duties which are best fulfilled by people with other specialities. If design engineers are provided as a basic part of laboratory services and work closely with the test engineer, the overall system concept will be taken into account during the design phase. As a result, the intended use and system performance level will improve.

DESIGN DISCUSSION

Most of today's test specifications call for vibration of some level along each of the specimens' three major axes. When this is the case, the choice of designing three fixtures, e.g., one for each axis of vibration to be performed on the head of the shaker, must be balanced against designing one fixture and a horizontal driver. The fixture in the second instance must be designed for use on the shaker head for one axis, and on the slip table for the two horizontal axes. The second alternative, while showing the greatest cost savings, also brings with it the greatest weight penalty, because only two fixtures are designed and built, rather than three. Also in the horizontal axis the exciter head must move the driver as well as the fixture and specimen. By reviewing past test records for specimen weight and test level it also is possible to optimize the design of the driver to work on many tests rather than just the test at hand.

In this discussion the problem is to design a horizontal driver for use with a Ling-249 vibration exciter and PP 120/150 amplifier. This system has a force rating of 30,000 force-lb or 75 g bare table. Its frequency range is from 5 to 2000 cps with a fundamental axial resonance above 2000 cps, where this fundamental axial resonance is defined as a 90-deg change in phase relationship between the driver coil current and table acceleration, measured at the table center. Any attaching structure or horizontal driver must have a fundamental resonance above 2 kc unloaded, because the maximum specification requirement is 2000 cps.

The design weight of the driver is based on the maximum available force and the maximum g-level and specimen weight expected. If 125 lb are allowed for the horizontal driver, the force-pound rating of the shaker in the horizontal mode is reduced from 75 g to approximately 55 g, a reduction of 26.6 percent. The specific test levels for which the driver is to be designed are:

1. Specimen weight = 180 lb,
2. Bandwidth = 5 to 2000 cps, and
3. g-level = 18 rms.

Using the rule of thumb, the fixture should weigh three times the specimen weight or 180 lb × 3 = 540 lb. The total system weight indicated is as follows:

Armature	396 lb
Driver	125 lb
Fixture	540 lb
Specimen	180 lb
Total	1241 lb

To check the system, 28,000 force-lb/1241 lb = 22.56 g was available during the test. Figure 1 shows the g-level attainable with a given specimen and fixture weight combination. It is obvious that for the normal test encountered, the driver would be adequate.

System Design

Reduced to its simplest terms, a horizontal driver is a structural component of the standard horizontal test setup, which will ideally transmit vibration from the exciter head to the text fixture with a force level and

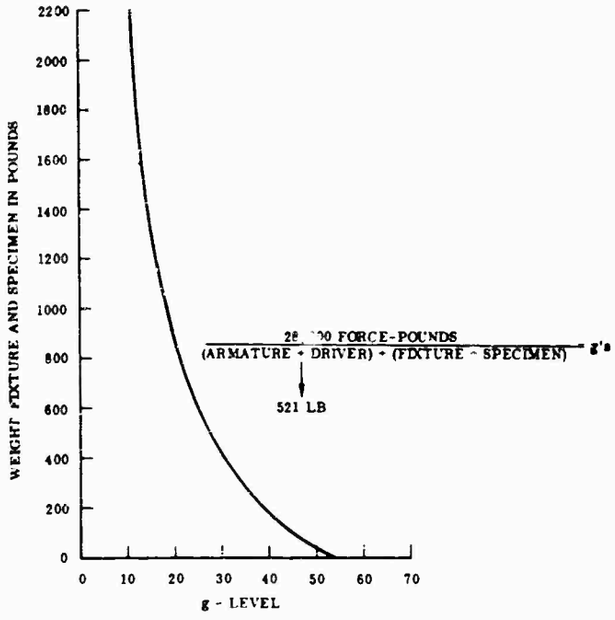

Fig. 1 - g-level attainable with fixture specimen combinations

frequency response of unity throughout the bandwidth of the test. A standard horizontal test setup is shown in Fig. 2a with the components reduced to equivalent masses and springs. The only components of this system considered here are the shaker armature, the armature to driver attach bolts, and the driver. It is not necessary to consider the fixture and specimen at this point, but later it will be necessary to design the driver to fixture interface.

Figure 2b, a two-degree-of-freedom system, is the actual one dealt with in this paper. Diagrammatic representation of damping has been omitted since the damping in a typical mechanical system is usually so small that it has a negligible effect on the natural frequency. Starting with the driver and assuming that the design weight of 125 lb is maximum and that the final hardware will be cast aluminum because of its cost and availability, a substitute structure can be developed. A solid cylinder whose length is approximately the distance from the center of the armature to the outermost attach bolt and whose diameter is large enough to satisfy the 125 lb design weight will be 13 in. long and 11 in. in diameter. Applying Hooke's law to the cylinder, an axial spring rate can be estimated as

$$k_d = \frac{AE}{L} = 73.07 \times 10^6 \text{ lb/in.}$$

Using this spring rate in this expression for a single-degree-of-freedom system of the driver alone gives

$$\omega_n = \sqrt{\frac{k_d g}{W}} = 15.033 \times 10^3 \text{ rad/sec}$$

and $f_n = 2394$ cps, which exceeds the desired limit of $f = 2000$ cps. Now the spring rate of the attach bolts must be taken into account. Assuming that it will be necessary to use at least 20 of the 21 available bolts and that their length will equal their diameter, Hooke's law may be applied again:

$$k_b = \frac{nAE}{L}$$

where n is the number of bolts and the bolts are a parallel spring system. This yields

$$k_b = 235.2 \times 10^6 \text{ lb/in.}$$

Because the mass of the attach bolts is much smaller compared to the total mass of the system, the mass of the bolts may be neglected. In Fig. 2b, k_d and k_b are springs in series and may be combined to yield K_D so that

$$K_D = \frac{(k_b)(k_d)}{k_b + k_d} = 55.749 \times 10^6 \text{ lb/in.}$$

If the portion of the total system, including only the driver and attach bolts, is again checked as a single-degree-of-freedom systems, it will give

$$\omega_n = \sqrt{\frac{K_D g}{W}} = 13.12 \times 10^3 \text{ rad/sec},$$

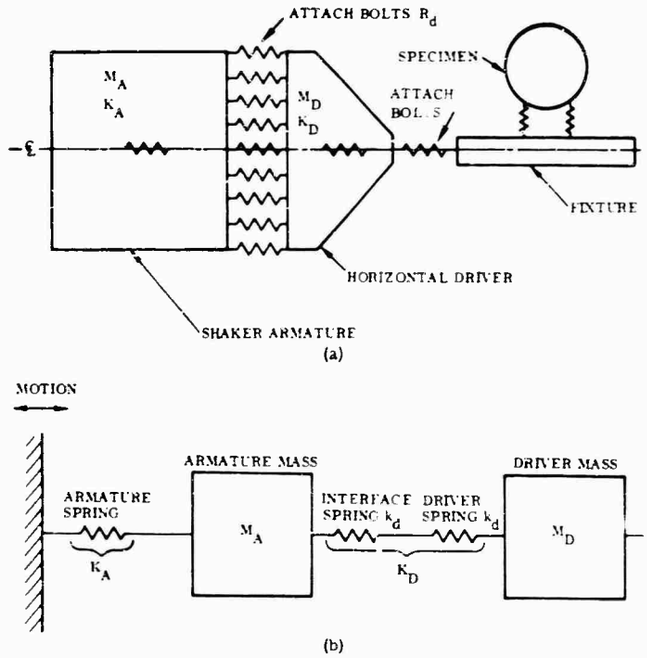

Fig. 2 - Spring and mass diagram of standard horizontal test setup

so f_n = 2088 cps, which approaches the required 2000 cps. Now it is necessary to develop a mechanical spring rate or K_A for the shaker armature. Assuming that the mechanical resonance is above 2000 cps, as the manufacturer states, let f_n for the armature equal 2000 cps. Then,

$$\omega_A = 12.571 \times 10^3 \text{ rad/sec},$$

$$2000 \text{ cps} = \frac{1}{2\pi}\sqrt{\frac{K_A g}{W}}.$$

and evaluating for K_A, $K_A = 164.00 \times 10^6$ lb/in. Based on the substitute driver cylinder and the assumed mechanical spring rate of the armature, it is now possible to estimate the resonant frequencies of the system by evaluating the expression

$$\omega^2 = \left(\frac{\omega_A^2 + \omega_D^2 + \frac{K_D}{M_A}}{2}\right) \pm \sqrt{\left(\frac{\omega_A^2 + \omega_D^2 + \frac{K_D}{M_A}}{2}\right)^2 - \omega_A^2\omega_D^2},$$

where ω is the natural frequency of the system, ω_A is the natural frequency of the armature subsystem and ω_D is the natural frequency of the driver subsystem.

The two frequencies of the total system are approximately f_{n_2} = 2706 and f_{n_1} = 1774 cps. The 2706-cps estimate will be of no concern since it is above the test bandwidth. The 1774-cps resonance for the shaker-driver system will cause difficulty during the test unless the available 125 lb allowed for the driver can be arranged in such a fashion that it will yield a spring rate greater than that which was calculated for the substitute cylinder. During a random test, this frequency will not be a severe problem, but during sine and combined sine and random tests, their resonant frequency may cause problems for the test engineer if the q of the system at this frequency is high.

Detail Design

To lay out the actual driver, the exciter-armature response characteristics should be investigated. A shaker was instrumented with an accelerometer at each attach bolt as shown in Fig. 3. Each diametral section A, B, C, and D is also plotted in Fig. 3 with the abscissa in inches and the ordinate in q. The plot is for the greatest q throughout the frequency range from 5 to 2000 cps. The maximum q occurred at 1550 cps with the phase angle greater than 90 deg but approximately equal to all attach bolts or accelerometer locations.

A study of Fig. 3 indicates that acceleration levels are higher at the outer edges of

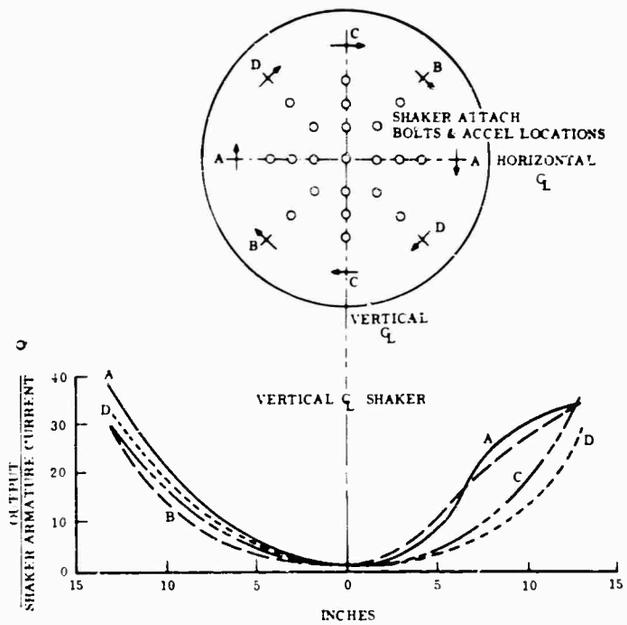

Fig. 3 - Relationship between attach bolt pattern and shaker displacement at resonance

the shaker armature. A main design consideration is to reduce the large vibration amplitude at the output face of the shaker to constant output at the face of the driver. Other design considerations are manufacturing process and material choice. The material choice is limited to either magnesium or aluminum because of weight. The manufacturing processes available in fixture design for these materials are limited at present to weldments and sand castings.

Designing and manufacturing with either material involves basically the same considerations for either manufacturing process. Both materials can be cast, welded or formed. Because internal stresses are set up during welding, both materials require stress relief after welding. In the casting process, however, the cost of heat treatment is minimal and is done as a matter of course. The big advantages of casting either material is that the designer can eliminate most discontinuities in the structure which would cause failure in a weldment. Also, the designer can include more complicated shapes in the design if required, with little or no increase in cost.

The selection of material is most important. Although cast magnesium fixtures generally have better damping characteristics than aluminum castings, the cost is greater. Because the casting shrink rate is in the same range for both materials (from 0.100 to 0.188 in./ft), the driver can be designed for aluminum and cast from either aluminum or magnesium if proper care is taken by the designer. If this is done, the magnesium driver will weigh less, and have about the same fundamental frequency because the ratio of the modulus of elasticity to density is essentially the same for both materials. Here, the driver was cast of aluminum rather than magnesium because the in-house foundry pours aluminum only.

All the design information is now available and an engineering sketch or layout is made which includes all the structural members located in the proper relationship to the shaker armature structure. Each structural member now is properly sized for weight and stiffness, assuming that each is a free structure and not connected to any other element of structure. Because fixture design is design for stiffness rather than strength, each individual unit of the driver should have a geometrical shape such that the highest free-free resonant frequency is obtained for that piece of structure's allotted portion of the total driver weight. This procedure has been purposely oversimplified and is really not as straightforward as it appears. All of the independent units interact and any decision involving one unit necessarily influences all other members of the driver to a greater or lesser degree. Basic decisions are made and checked against the influence on the other members to see their effect, and then the

process is repeated until the design is satisfactory. For this reason, the actual design is a lengthy process of iteration.

Figure 4 is a four-view photograph of the completed Ling-249 horizontal driver after the design and manufacturing processes were completed. The driver consists of three basic types of structural components, plates, gussets and beams; the driver is designed so that it is symmetrical about both the vertical and the horizontal centerlines. Since this is the case, only one of each type of structural component need be analyzed. Figure 5 is an exploded view of the driver showing only the three basic types of structure placed above the Ling-249 shaker armature in their proper location. The beam and its resonance is estimated with the expression:

$$\omega_n = A\sqrt{\frac{EI}{L^4}},$$

which can be reduced to

$$f_n = 9180\,\frac{hA}{L^2}.$$

where A is a constant based on its mode of support, the effective length L is 13 in. and h is its thickness, so that f_n = 1216 cps, which is low. This should cause no concern since in reality it is supported along its entire length by gusset No. 2. Therefore, its f_n should be higher than indicated.

Gusset 2A can only be loaded axially; therefore, its resonance is estimated by

$$\omega = \sqrt{\frac{K}{M}}$$

where $K = AE/L = 16.36 \times 10^7$ rad/sec. Taking an average A for the length L,

$$f_n = \frac{1}{2\pi}\sqrt{\frac{K_g}{W}} = 2393 \text{ cps}$$

which is about where the fundamental frequency should be. Gussets 2B and 2C are basically flat plates supported on two edges as shown in Fig. 6.

If the shaded portion of the plate is removed, the effect will be to raise the frequency, because if half of the mass is removed, e.g.,

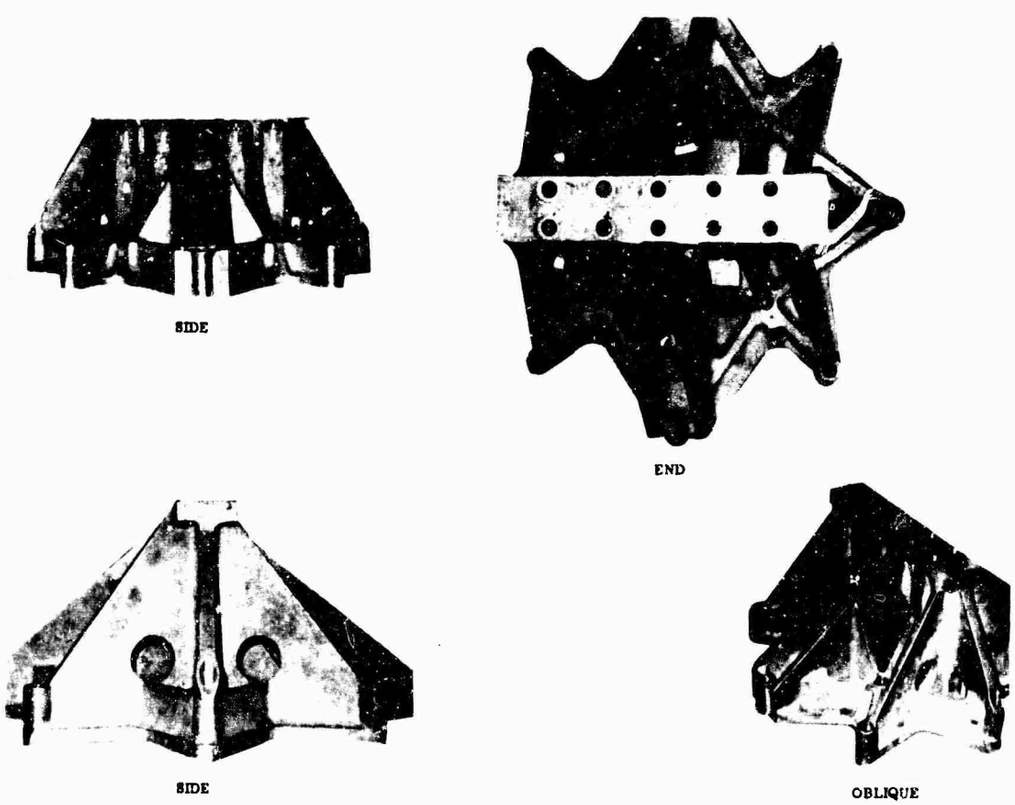

Fig. 4 - Four views of L-249 horizontal driver

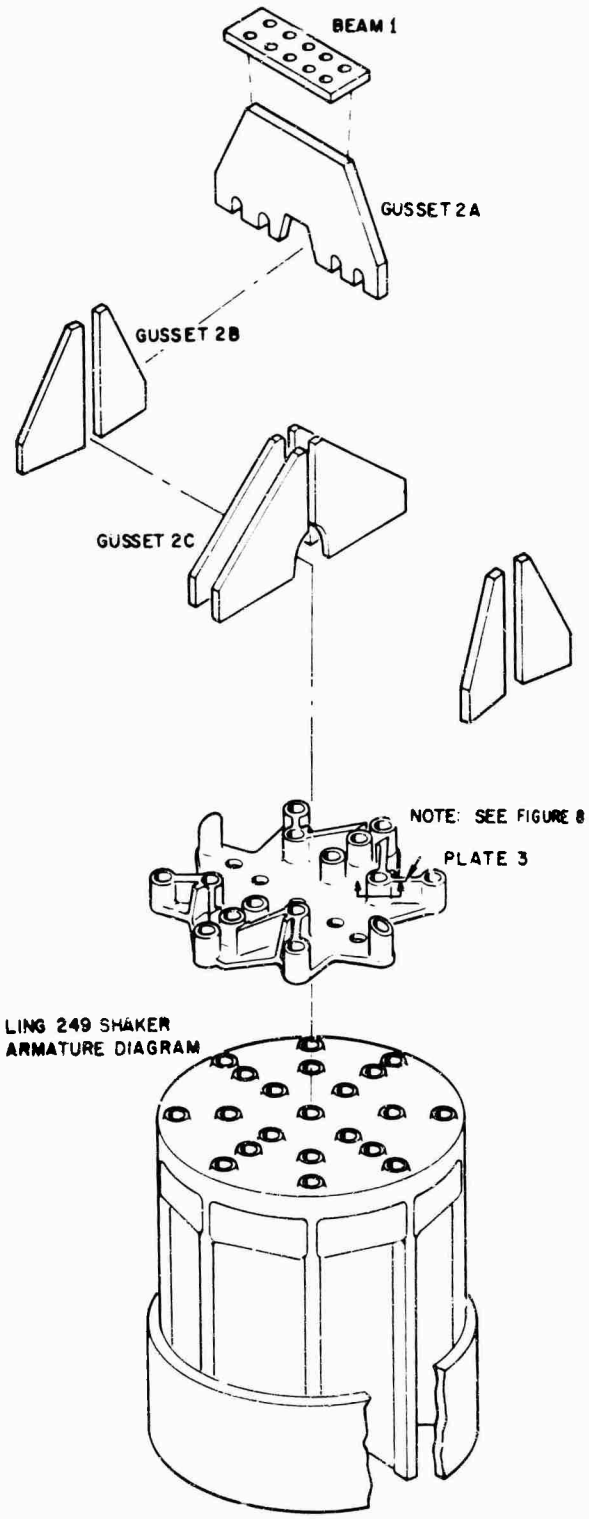

Fig. 5 - Exploded view of driver

that mass which contributes least to the stiffness, the stiffness is doubled and the frequency is increased. Evaluating the following expression for frequency,

$$f_n = 9600 \frac{Kh}{L^2} ,$$

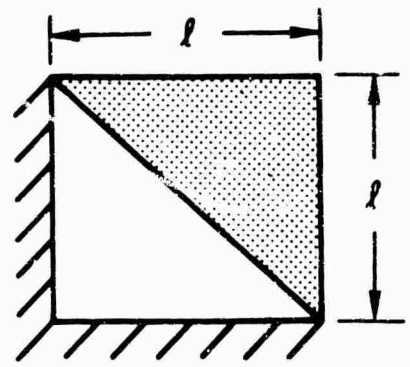

Fig. 6 - Beam-plate analogy

where to allow for the reduced mass, this K is assumed to be equal to K for a plate clamped at all four edges. Then f_n = 1820 cps, which is a good approximation.

Plate No. 3 as shown in Fig. 5, of course, is supported by all the upright gussets and ribs and consequently may be estimated as an equivalent circular plate clamped around the outer edge because the plate will be stiffened by a portion of the upright gussets. Thus, it will be equivalent to a flat plate about 2.5 in. thick, evaluated as

$$f_n = 9600 \frac{Kh}{b^2} = 2130 \text{ cps} .$$

which is probably high. The foregoing computations complete the rough calculations for individual structural components, and generally all that is necessary for most fixtures.

Placement of primary components of structure are of major importance, and generally, the basic rules which must be followed are:

1. The complete structure should be a symmetrical unit about both horizontal and vertical centerlines to insure dynamic balance, since a symmetrical structure will have associated with it a lesser number of excitable natural frequencies.

2. Components of the fixture must transfer load with a limited amount of eccentricity to limit any secondary bending effects.

3. Only those structural members should be used for which direct load paths can be demonstrated, e.g., removal of members which offer no structural rigidity.

For the Ling-249 horizontal driver considered here, these rules have generally been followed. Gusset 2A picks up the force from the shaker horizontal centerline and transfers it directly to the output face of the driver. Gussets

2B accomplished the same function for the vertical centerline and also offer lateral support to 2A. Gusset 2C which is placed midway between 2A and 2B, at a slight angle, performs the same job as 2A and transfers the force to the driver output face from the remaining shaker-driver attach bolts not covered by the other gussets (Fig. 5).

The driver structure as a unit is symmetrical about both the horizontal and vertical centerlines, and all components are loaded in a symmetrical manner. The removal of all extraneous structural members has not been strictly followed here. The short beam which ties the two adjacent 2B gussets together (Fig. 4) transfers no load but helps these gussets work as a unit. All the base material which lies outside the outer bolt circle is a gross violation of the above rules and serves no useful purpose. The base plate has been stiffened with a 3-in. upstanding leg between the attach bolts and the gussets, and really serves no useful purpose except to satisfy the plate frequency estimate previously mentioned. All the remaining structures satisfy the three basic rules of design.

Particular attention also must be paid to the armature-driver interface and the driver-fixture interface. The considerations here are: (a) the bolts must be torqued to the maximum permissible preload, (b) the natural frequency of the fastener system must be adequate, and (c) the fixture structure must be rigid enough to transfer the load.

Figure 7 is a two-view diagram of a typical detail for these interfaces which has proved satisfactory. The fasteners at the armature-driver interface have already been mentioned and found satisfactory; the estimated structural rigidity was shown to be sufficient. There remains the attach bolts at the driver-fixture interface. Here, there is sufficient space to install 10 1-in. diameter bolts with a working length of 3/4 in. Solving the expression

$$f_n = 15,200\ d \sqrt{\frac{n}{WL}}$$

for W, letting f_n = 2400 cps, gives the total fixture plus specimen weight which might be added to the armature-driver system (remembering, of course, that now the system consists of armature, driver, fixture, and specimen, plus two additional springs for attachment). Therefore, $W = 2.929 \times 10^3$ lb, which is well within the range of the exciter head shown in Fig. 1.

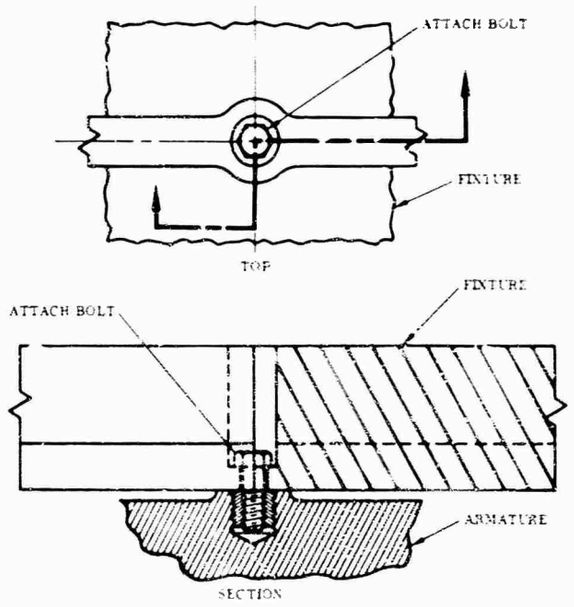

Fig. 7 - Two-view diagram of typical detail

Ling-249 Horizontal Driver Data

Figure 8 is the load vs deflection curve for the Ling-249 driver. The dashed line is the substitute cylinder used in estimating the system resonant frequencies. The solid line is the load vs deflection curve for the completed driver after two years of continuous use. Notice that the actual driver spring rate curve is a slightly hardening curve or nonlinear and that the spring rate tends to increase. This is probably due to material characteristics. In any event, the actual spring rate slope is greater than that of the equivalent cylinder, which is a good approximation for design purposes. It accounts for the actual increase in the system, since the actual driver spring rate is less than estimated and the driver spring rate is much higher than estimated. Figure 9 shows four g vs frequency plots and the output of the control accelerometer. These g vs frequency plots were taken from positions as shown in the figure at a test level of 5 g rms. The control accelerometer is located midway between the center bolt and the outer attach bolt ring of the shaker as shown in Fig. 3a.

The plots in Fig. 9 indicate that the f_{n_1} of the system (which includes armature and driver) occurs where predicted by the analysis presented previously. It also illustrates graphically the dilemma faced by the designer: how to raise the frequency of the system above the upper bandwidth limit of the test without using all the force available. In the case presented

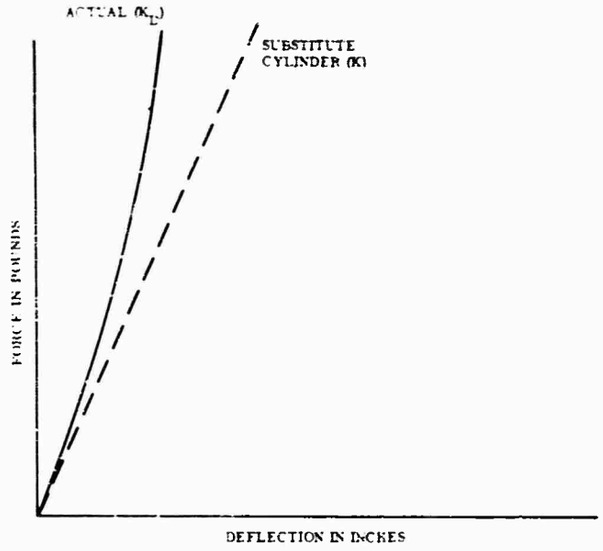

Fig. 8 - Load vs deflection curve for L-249 driver

here, this is patently impossible. The first resonant frequency of the system is shown about 1750 cps, which is very high for a 2000-cps test bandwidth. When the specimen and fixture are added to the system, the frequency will decrease. Further study of the data indicates two outstanding characteristics of the system:

1. Even though the mass of the system was increased 31.5 percent, the frequency of the two-degree-of-freedom system was greater than the one-degree-of-freedom system. This means that the mass was added to the system in the correct manner.

2. The output across the face of the horizontal driver is constant, and there is no "rippling" or unsymmetrical force being delivered to the fixture.

Other Designs

Figures 10, 11, 12, and 13 are photographs of horizontal drivers which were designed for other vibration exciter heads. Each of these fixtures were designed essentially by the same method as presented here and by design engineers specializing in dynamics. Even though in each case the driver and the exciter head were different, the dynamic evaluation showed that the response along the output face of each driver was predictable and uniform. All of these horizontal drivers have been in use for at least three years and have proven the value of the system design concept.

SUMMARY AND CONCLUSIONS

When using the system design approach, the design considerations are:

1. All masses and springs of the system must be considered in setting the unit design limits.

2. Each unit of the system may have its fundamental frequency estimated as a single-degree-of-freedom system.

3. The mass of the attachment bolts may be neglected in estimating system frequencies.

4. Damping may be neglected while estimating the overall system frequencies.

5. Detail mechanical variations of the shaker must be considered in the fixture design.

The basic detail design considerations are:

1. The structure should be a symmetrical unit about both horizontal and vertical centerlines.

2. Components of structure must transfer load with a limited amount of eccentricity.

3. Only those structural components for which a direct load path can be demonstrated should be included in the design.

4. All attach bolts should be torqued to maximum permissible preload.

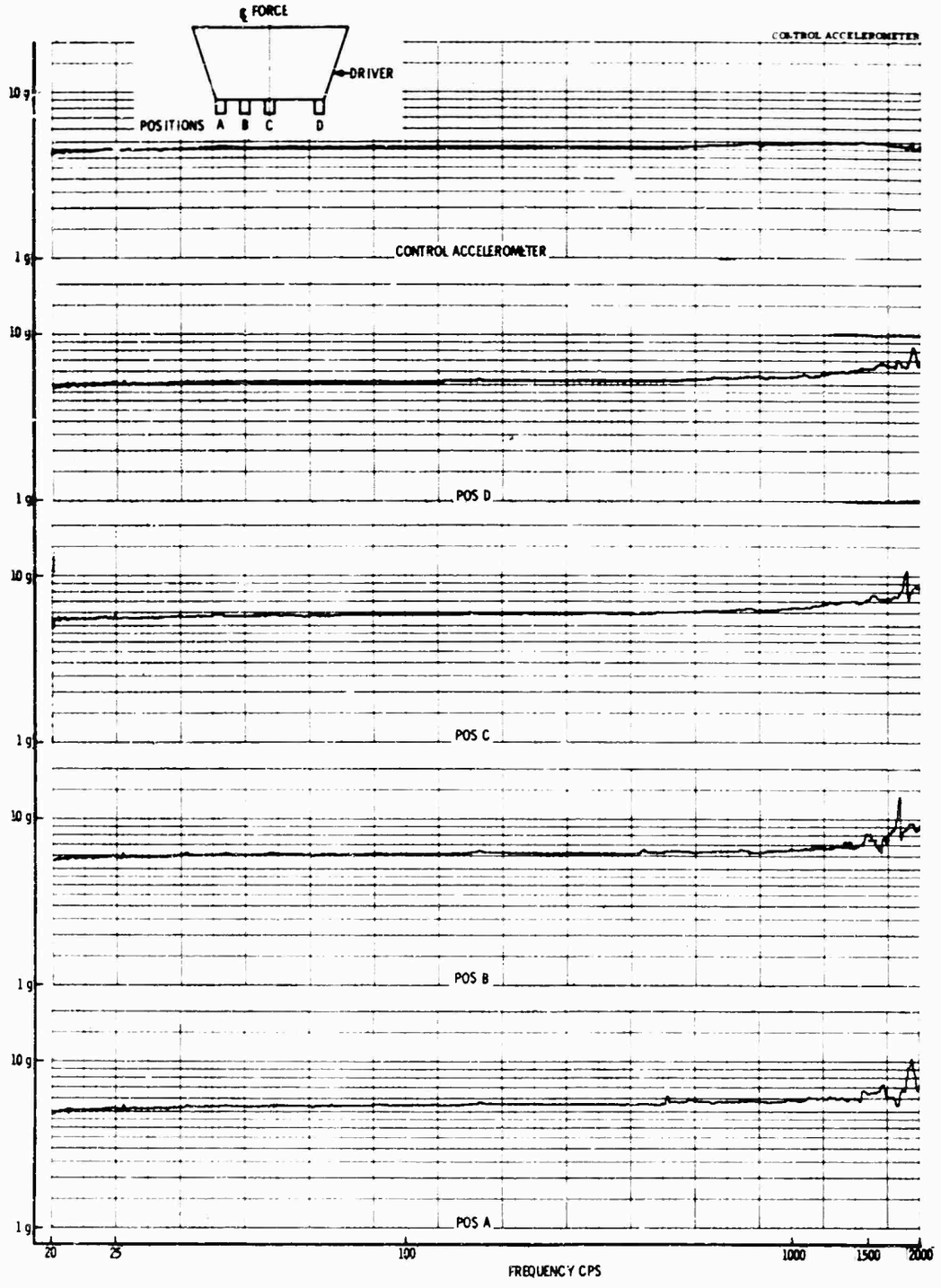

Fig. 9 - Four g's vs frequency plots and output of control accelerometer

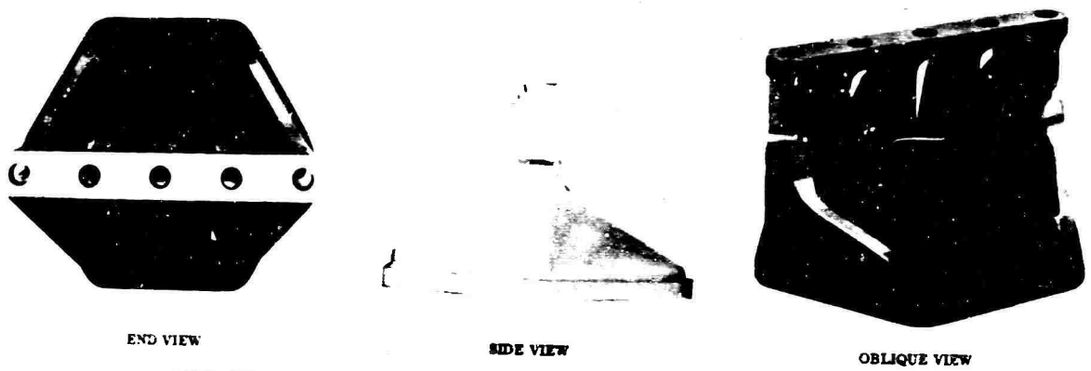

END VIEW SIDE VIEW OBLIQUE VIEW

NOTE: This is a cast aluminum driver which weighs eight pounds and is six-inches long. The driver attaches to the shaker, using all of the attach bolts available. The output face of the driver has provisions made for five 1/2-inch diameter bolts for fixture attachments.

Fig. 10 - C-10 horizontal driver

END VIEW SIDE VIEW OBLIQUE VIEW

NOTE: The driver, manufactured of cast aluminum alloy, is 9-1/2-inches long and weighs 33 pounds. This driver has provisions made for ten 1/2-inch bolts across its output for fixture driver attachment. The driver is bolted to the shaker armature using only 10 of the bolts available.

Fig. 11 - C-25 horizontal driver

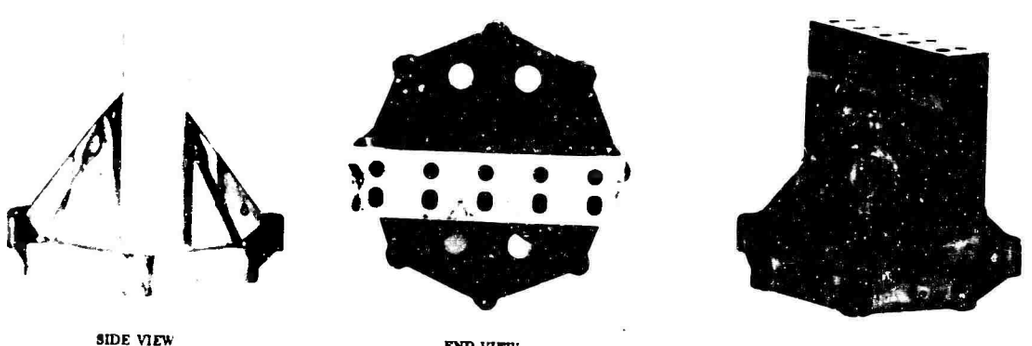

SIDE VIEW END VIEW OBLIQUE VIEW

NOTE: The L-300 driver shown here weighs 31 pounds, is cast of aluminum alloy and is 10-inches long. This driver attaches to the shaker armature using 14 of the 18 bolts available and the output face of the driver has provisions made for ten 1/2-inch diameter bolts for driver fixture attachments.

Fig. 12 - L-246 horizontal driver

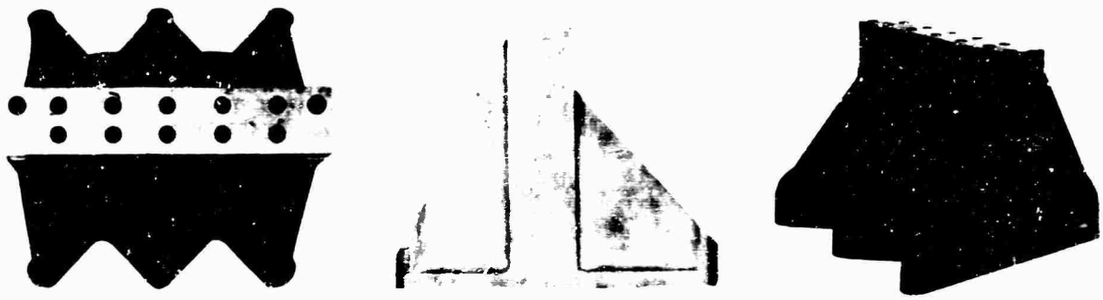

END VIEW SIDE VIEW OBLIQUE VIEW

NOTE: The driver shown here weighs 31 pounds is 9-1/2-inches long, and is cast of aluminum alloy. The driver attaches to the shaker armature using 14 of the 16 attach bolts available The driver is attached to the fixture using ten 1/2-inch diameter bolts shown on the output face of the driver.

Fig. 13 - L-300 horizontal driver

The method of considering the total system to define design parameters is a practical fixture-design approach. The data taken at the output face of each driver clearly demonstrate that an experienced designer, when armed with the simple analysis presented here, is able to apply his design experience to the considerable advantage of the testing laboratory. Although in most cases he may not be able to raise the frequency of a system to the extent desired, he certainly should be able to improve its output characteristics.

ACKNOWLEDGMENTS

The author acknowledges with thanks the support of his colleagues and, in particular, the efforts of W. A. Reagan who designed the C-10 and C-25 drivers shown herein, D. Gonzalez who designed the Ling-249 driver which appears here, and C. Cowl who ran the shaker and driver evaluation test and gathered most of the data on which this paper is based.

BIBLIOGRAPHY

Harris, C. M. and C. E. Crede, Shock and Vibration Handbook. McGraw-Hill, New York, 1961

Curreri, John R., "Fixture Design Notes," MB Electronics Vibration Course Seminar, 1960

Klees, G. T., "Beam Vibrations," Machine Design, 1960

Klees, G. T., "Plate Vibrations," Machine Design, Vol. 32, No. 26, pp. 139-141, Dec. 22, 1960

Curreri, John R., "Vibration of Structures," IES Tutorial Lecture Series, 1966

Cobb, B. J., "Preloading of Bolts," Product Eng., Vol. 34, No. 17, pp. 62-66, Aug. 19, 1963

Klees, G. T., "Fastener Vibration," Machine Design, 1960

* * *

FLIGHT LEVEL VIBRATION TESTING OF A LIFTING BODY REENTRY VEHICLE*

R. McCaa and M. Matrullo
The Martin Company
Baltimore, Maryland

The vibration testing of spacecraft to the levels of the booster interface spectrum while supported by "rigid" fixtures is deemed unrealistic in that structural failures may be induced which would not occur on the more compliant support of the booster. Limiting of the shaker input forces at the vehicle support points to design limit loads precludes this type of failure. Random vibration tests conducted on the PRIME SV-5D lifting body utilized this force limiting approach and the techniques employed are described.

INTRODUCTION

The objectives of the flight level vibration test of the PRIME lifting body vehicle project were to demonstrate the integrity of the structural design and the adequacy of the reentry heat shield when exposed to broadband random vibration at the predicted flight levels. In addition, the test was used to verify procedures and techniques to be employed during acceptance vibration testing of the flight articles. Figure 1 shows the test article mounted for pitch axis vibration.

The test specification required the limiting of the force input to the reentry vehicle – booster interface fittings, and proposed notching of the input acceleration spectrum as a means of reducing the force at frequencies where high peaks occurred. This requirement was included because the spacecraft was subjected to the booster interface spectrum which was considered unrealistic for these tests. Loads in excess of the support point limit would undoubtedly be induced at the cantilever resonant frequencies of the spacecraft, whereas the impedance of the booster structure would not permit these high forces to occur in actual flight.

To meet this requirement, force gage pedestals were designed to support the vehicle at its three aft bulkhead interface mounting points (Fig. 2).

Each axis of random vibration was preceded by low-level sinusoidal vibration tests to obtain force and acceleration transmissibilities throughout the frequency range of interest.

Fig. 1 - Engineering test article mounted for pitch axis vibration test

*This paper was not presented at the Symposium.

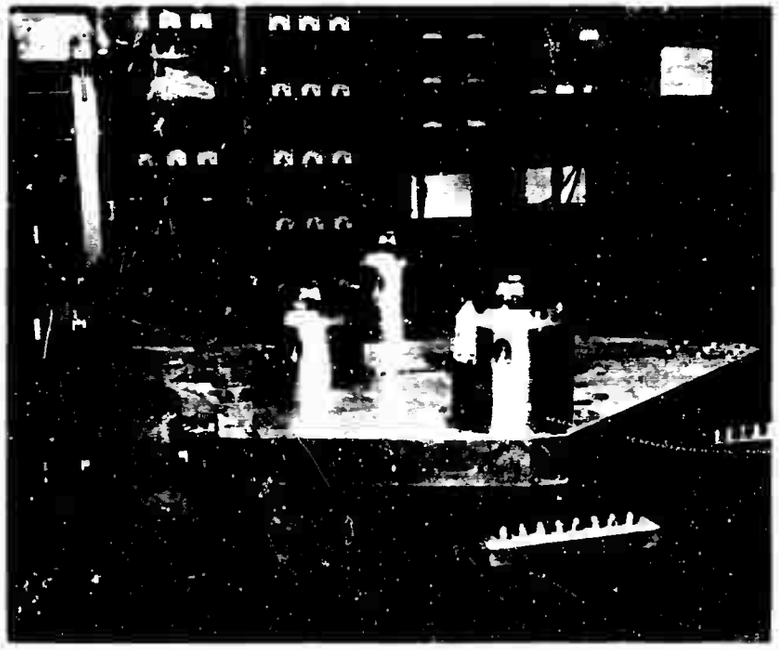

Fig. 2 - Force gage pedestals mounted to receive test vehicle

TEST SPECIMEN

The specimen employed during the engineering test program was identical to the flight articles with respect to structure and ablative heat shield and included all bracketry for installation of major components. Production hardware provided with the test article included a complete hydraulic actuator-flap system, main parachute container (with dummy chute), drogue cannister (with dummy chute), and fin-mounted antennas. Dummy hardware was included to simulate the installation and mass of other major equipments. The complete test article, when subjected to a weight and balance check prior to test, had the same weight, c.g., and mass moments of inertia as did the flight articles.

FORCE MEASUREMENT

Description

Input forces to the vehicle were measured at the vehicle interface attachment points using pedestals designed at the Martin Company, Baltimore. The pedestals consisted of three Endevco Type 2110 impedance heads or Type 2106 force transducers, placed at 120-deg intervals on an 8-in. rigid cylindrical base. Only the force measuring portion of the impedance transducers was used. The sensitive axes of the transducers were oriented at an angle of 50 deg from the horizontal and projected to an apex above the gages, at which point the vehicle was attached by a single bolt to a steel header. The transducers were sandwiched between the header and cylinder and preloaded to a compressive force of 5500 lb. The vehicle attachment point was a ball-type fitting, and the steel header was machined to accept it. This ball and socket connection minimized the effects of bending moments at the vehicle attachment points (Figs. 1, 2, 3).

The orthogonal components of force were then obtained from each of the gage outputs and combined with like components from the other gages to obtain the total X, Y and Z components for each of the pedestals. The individual force components were obtained by adjusting the coefficients of summing circuits to correspond to the magnitude of the respective forces of a unit vector as determined by the angle of the gage axis relative to the vehicle. The total X, Y, Z forces to the vehicle were then obtained by electrically summing the components of each pedestal.

Calibration

The primary purpose of the pedestal was to convert the forces transmitted through it to the vehicle into its orthogonal components. An

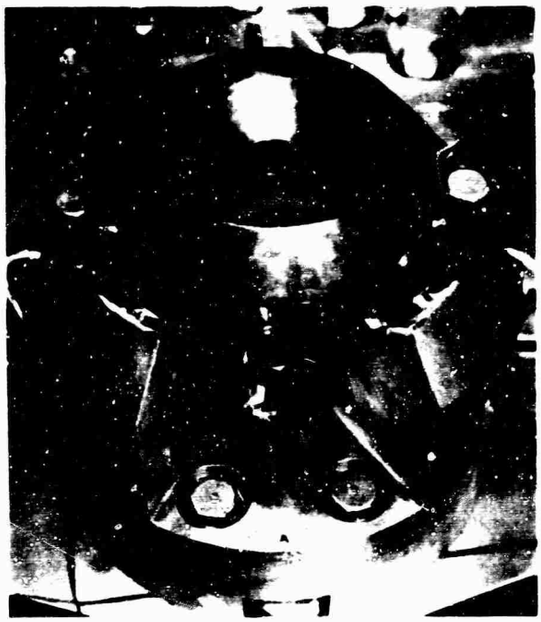

Fig. 3 - Close-up of force gage pedestal

evaluation of the pedestal was performed to verify this capability and calibrations obtained to transform pedestal output into its force coordinates. Vibratory forces were applied to each of the coordinate axes and the sensitivity of the individual gages was determined for forces in each of the three planes.

The coordinate forces were applied by mounting a dead mass on the pedestal and vibrating the system on an electrodynamic shaker while monitoring the acceleration of the mass. The relationship of force equal to mass times acceleration was then applied to determine the force. It was essential that the vibrating frequency was sufficiently removed from any system resonances since this would give a false indication of the actual force acting through the gage. Transmissibility plots for each of the pedestal's axes were obtained to define the resonance-free calibration frequencies.

For proper summation of instantaneous forces within the pedestal, it was essential that no resonances existed within the pedestal or at least did not exist within the frequency range below 200 cps. Most of the damaging force components to the vehicle were determined through analysis to exist in this range of frequencies. A ratio of force to acceleration for each plane of vibration was obtained to determine the existence of resonances, if any. This was done by summing the forces for a given axis of excitation and dividing this result by the acceleration as measured on a dead mass placed on the pedestal. The acceleration was held constant by using the accelerometer mounted on the mass to also control the shaker table on which the assembly was mounted. The ratio of force/acceleration was continuously obtained throughout the 20- to 2000-cps frequency range with the use of the automatic transmissibility plotter. The results of this check indicated that no local resonances existed within the pedestal throughout the primary range of interest. A resonance would have resulted in a variation of the ratio of force/acceleration since the phase relationship of the signal out of each gage would vary, causing improper summing. Gage sensitivities obtained through calibrations did not vary by greater than 10 percent for forces in each of the coordinate planes. The sensitivities were used to normalize the outputs of all gages so that each pedestal had output sensitivities of 1 volt (rms)/1000-lb peak force in each of its coordinate axes.

Application

During the vibration tests the pedestals were mounted on an MB Model C-210 shaker for vertical axis excitation and on a slippery plate using Team Corporation hydrostatic bearings (Models 1-914 and 2-914) for lateral excitation. The vehicle was connected to the pedestals through its adapter attachment points so that all forces were transmitted to the vehicle through the pedestals. The electrical outputs for all force components from each pedestal and their combined forces were made available for monitoring at a summing panel. Three true rms voltmeters calibrated for force were used to monitor the force limits which were to be observed during both the sine and random vibration tests. These forces were also recorded on magnetic tape. The reference input acceleration was an average of the accelerations appearing at input points to the pedestals. An accelerometer was located at the base of each pedestal and the outputs of the three were averaged using an MB Model N681 signal averager. In addition to serving as a reference for transmissibility plotting, this signal was also used to control the shaker output. Averaging was performed by sequentially sampling each of the accelerometer signals and combining them into a new signal. This method of averaging was used for both sine and random vibration testing.

TEST PROCEDURE

Prior to each axis of random vibration, a transmissibility test was conducted as an aid in predicting response peaks and the frequencies

at which they would occur. The test consisted of a slow sinusoidal sweep from 20 to 2000 cps at a maximum input amplitude of 1 g peak. Data provided during this test were force transmissibilities (ratio of force to average input acceleration) at the center support, one outboard support, and the summation of all three supports. Through the use of the force gage pedestals and their associated summing network, it was possible to obtain these transmissibilities oriented in the vehicle's system of coordinate axes. In addition, acceleration transmissibilities (ratio of response acceleration to average input acceleration) were obtained from nine component mounting locations. Figures 4 and 5 present typical force and acceleration transmissibilities.

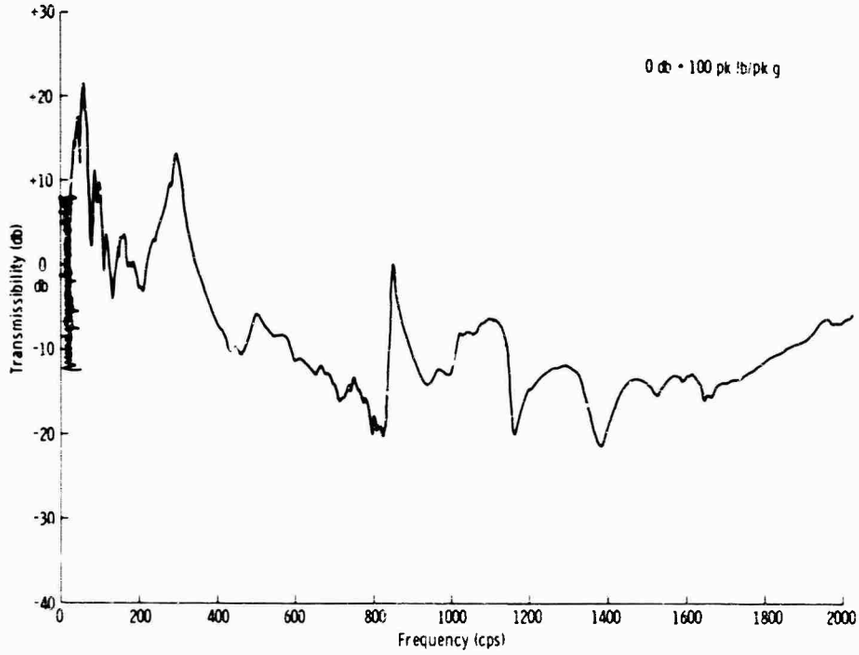

Fig. 4 - Typical force transmissibility (input force/average input acceleration)

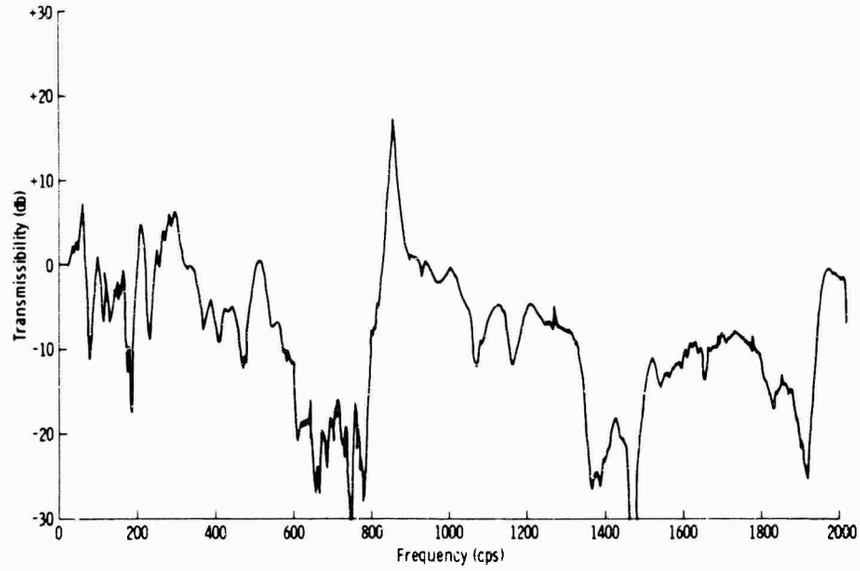

Fig. 5 - Typical acceleration transmissibility (response acceleration/average input acceleration)

The random test was conducted in two parts: a launch phase with an overall level of 11.2 g rms and time duration of 3.0 min and a reentry phase with an overall level of 10.7 g rms and time duration of 5.0 min. The spectrum shapes are presented in Fig. 6.

Three support point forces were specified as critical in each axis of excitation, and 110 percent of their values could not be exceeded during equalization or the actual test. These outputs were read on true rms meters which had been calibrated in force units, thereby providing continuous monitoring during all phases of testing. Short duration trial runs were made at the 20, 60 and 80 percent g rms levels to establish that equalization was being achieved and that the force limits were not being exceeded. During equalization runs at all levels, as well as the full level tests, the outputs of all the instrumentation were recorded on magnetic tape. In addition, the average input acceleration and the three critical forces in each axis were provided to a tape loop recorder. When the critical forces approached a marginal status, a 10- to 20-sec tape loop was recorded for immediate spectrum analysis, thus disclosing the frequency at which a notch was to be inserted into the acceleration spectrum.

The flight article acceptance tests are to be carried out in the same general manner as the engineering test. However, since these tests are designed to uncover latent defects and not to qualify structure or equipments, the overall levels will be reduced to approximately 50 percent of those imposed on the engineering test article. Data acquired from the engineering tests provided a means to limit support point forces by introducing notches into the specified launch spectra to be employed during flight article tests. A typical notched acceptance test spectrum is shown in Fig. 7.

One other significant difference between the engineering and flight article acceptance tests is the use of a time-varying g rms level launch reentry profile. For each axis of excitation, both the launch and reentry spectra will be equalized and recorded on tape loops. These in turn will be recorded on a tape reel while varying the g rms level as shown in Fig. 8. When the taped profile is completed, it will be incorporated into a combined systems test, thus exposing the flight article to a complete simulated flight in each orthogonal axis.

RESULTS AND CONCLUSIONS

The results of the test were favorable since the primary objectives were achieved; i.e., no failures were incurred by the vehicle structure or ablative heat shield. In addition, the procedures and techniques employed during the test

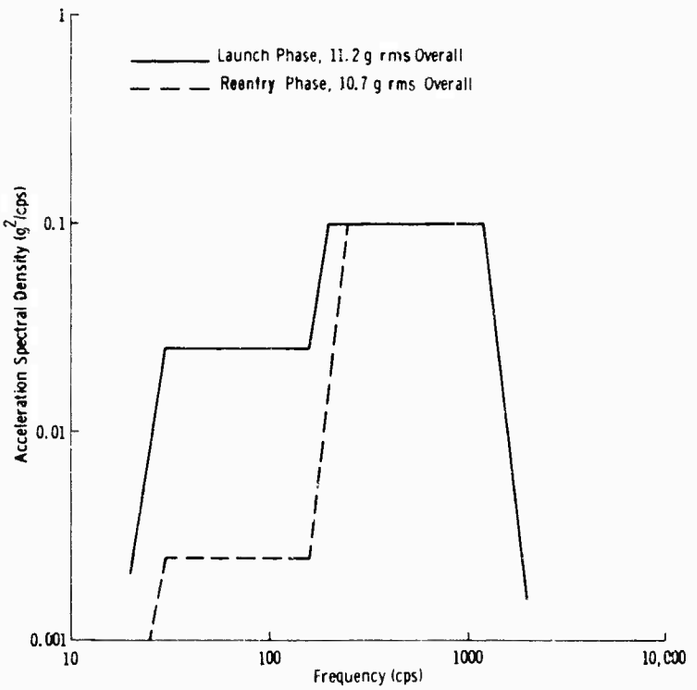

Fig. 6 - Random vibration spectra applied to engineering test vehicle

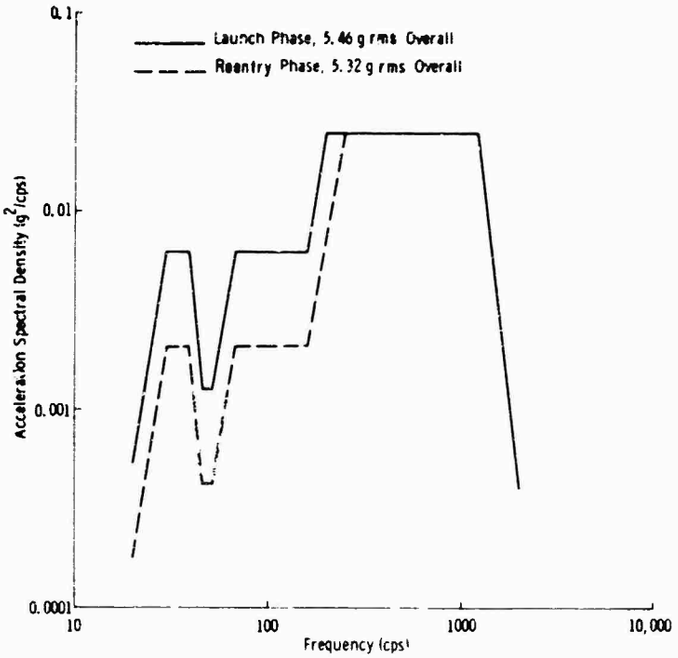

Fig. 7 - Typical random vibration spectra for flight article acceptance tests

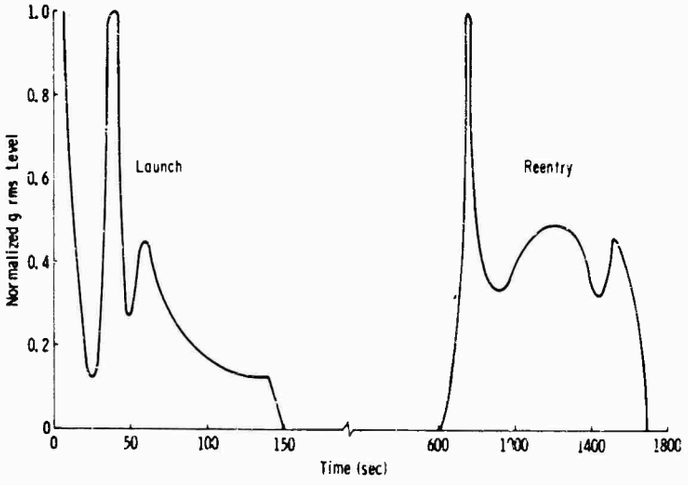

Fig. 8 - Time-varying overall g rms profile

were shown to be effective, and it is believed that they can be used for the flight article tests with a minimum of modification.

It is concluded that the transmissibility tests were of value in the verification and updating of analytical results before proceeding into the more hazardous random vibration testing. Also, for high-level vibration testing of spacecraft, the limiting of support point forces is shown to be feasible and practical. The force gage pedestals provided a means of resolving the vehicle input forces into coordinate components for direct monitoring. Without this capability the design limit loads would certainly have been exceeded, permitting unrealistic structural failures to occur.

* * *

HYDRAULIC EXCITER COMBINED ENVIRONMENT TESTS

Edwin J. Skolka
NASA Goddard Space Flight Center
Greenbelt, Maryland

The combination of vibration and sustained acceleration is especially difficult to produce in a laboratory test and, until recently, has been avoided because of the complex nature of the facility required. These two environments were investigated by operating a 5000-lb force rated hydraulic vibration exciter on a 20-ft diameter centrifuge. Test parameters included a range of exciter table mass loads and variations of vibration and sustained acceleration levels. These parameters were evaluated for two different actuator thrust axis orientations with respect to the centrifuge rotational plane. The exciter test frequency spectrum was from 20 to 500 cps. Performance of the exciter-centrifuge system was determined by measuring exciter acceleration waveform distortion, response characteristics of the centrifuge, and exciter cross-axis acceleration effects.

Test data indicated that the interaction of exciter harmonic content with resonances generated in the centrifuge system produced high levels of exciter acceleration distortion. Increases in sustained acceleration levels produced higher acceleration waveform distortion for frequencies above 150 cps. At lower frequencies, resonances of centrifuge equipment and hydraulic system components distorted exciter input signals and consequently the output waveform.

E. J. Skolka

INTRODUCTION

A test facility designated as the Launch Phase Simulator (LPS) under construction at the NASA Goddard Space Flight Center (GSFC) will have the capability of simulating the combined effects of sustained acceleration, mechanical and acoustic vibration, and altitude variation to which an unmanned spacecraft is subjected during launch [1]. This improved simulation will permit a more thorough evaluation of design features necessary to insure reliability of spacecraft under launch conditions. Better evaluation will aid in reducing overdesign for ruggedness at the expense of effective spacecraft weight without increasing the risk of underdesign and resultant failure.

The current practice in environmental testing is to conduct a series of individual tests usually consisting of single environmental conditions or, at best, simple combinations of such conditions. The combination of vibration and sustained acceleration in a laboratory test of a complete spacecraft is especially difficult and, until recently, has been avoided because of the inherently complex nature of the facility required. Significant effects can be produced by a combination of stresses due to such factors as steady-state structural deformations which modify vibration response characteristics, binding or friction in mechanisms causing erratic responses under vibration, and additive steady-state and vibratory accelerations overstressing both structure and components.

The vibration system required for the LPS will operate on the end of a centrifuge arm and will be subjected to dynamic loads generated by the rotating centrifuge structure. Mechanical, electrodynamic, and hydraulic exciters were considered for use on the LPS. Advantages of hydraulic exciters over competitive systems

led to the selection of a hydraulic vibration system for the LPS. The major advantages are greater force/weight ratio, low-frequency capability, large displacement, exciter table positioning capability, and lower cost.

To obtain combined vibration and sustained acceleration information and experience, a research program was initiated by the Structural Dynamics Branch of the Test and Evaluation Division at GSFC to evaluate a hydraulic exciter on a 20-ft diameter centrifuge. For this investigation, the exciter was oriented and operated in two positions, with the thrust axis parallel and perpendicular to the longitudinal axis of the centrifuge arm. This was done to simulate LPS thrust and transverse modes of vibration. Determination of the optimum exciter orientation when subjected to sustained acceleration was based on the following performance parameters:

1. Acceleration waveform distortion as a function of frequency,

2. Centrifuge response to exciter vibration, and

3. Exciter cross-axis (cross talk) acceleration effects.

These parameters were chosen not only to provide exciter performance data but also to determine the effect of vibratory input on the centrifuge. The information obtained and the techniques developed in this combined environment test are presently being applied to the LPS design and will be utilized in its operation.

EQUIPMENT DESCRIPTION

An hydraulic exciter system consists basically of one or more exciters, hydraulic power supply, servoamplifier, and a signal source [2]. The exciter's output element, the actuator, is a double-acting piston whose area and drive rod are sized according to the force and stroke required of the exciter. The hydraulic power supply includes motor, pump, accumulators, reservoir, heat exchanger, and other accessories to insure a smooth flow of fluid power. Motion of the hydraulic actuator is controlled by an electrohydraulic servo valve responding to signals from the servoamplifier.

The hydraulic exciter selected for this combined environment test was MB Electronics Corporation Model HC 50-80-1 equipped with a special Type 2 Model HV-80 servo valve. Figure 1 shows the exciter mounted on the basket of the 20-ft diameter centrifuge with the actuator

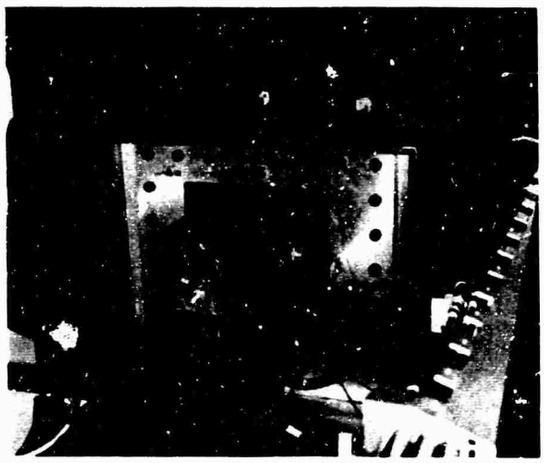

Fig. 1 - Hydraulic exciter on 20-ft diameter centrifuge

thrust axis parallel to the longitudinal axis of the centrifuge. The exciter had a force rating of 5000 lb, actuator velocity of 80 ips, a 1-in. double amplitude stroke, and weight of approximately 500 lb (including 8 lb for the actuator piston). The two-stage servo value contained a pilot spool and a power spool. Using an adapter plate, this valve could be oriented 90 deg with respect to the actuator body, thus providing two mounting configurations for any given thrust orientation. The exciter frequency range was dc to 500 cps. As shown in Fig. 2, the input signal was generated by an oscillator. This signal was transmitted to the servoamplifier where it was combined with actuator feedback, power spool feedback, and 1000-cps (nominal) dither. The dither signal served to overcome actuator and power spool stiction. The combined drive signal, after amplification, was applied to a small electrodynamic exciter driving the first stage spool of the two-stage servo valve. The pilot stage (or hydraulic preamplifier) transformed electrical variations into variations of fluid flow, which were reproduced by the second stage power spool (or hydraulic amplifier) and directed to the actuator. Actuator velocity was proportional to fluid flow and varied directly with the electrical input signal. Figure 3 depicts an operational schematic view of the exciter.

A rotary joint was required to transmit hydraulic power from the power supply to the exciter mounted on the centrifuge. The rotary joint, manufactured by Schaevitz Engineering, was capable of transmitting hydraulic flow of 35 gpm at 3000 psig. The joint was rated at a maximum rotational speed of 140 rpm. Figure 4 illustrates the hydraulic rotary joint supported from the centrifuge pit ceiling.

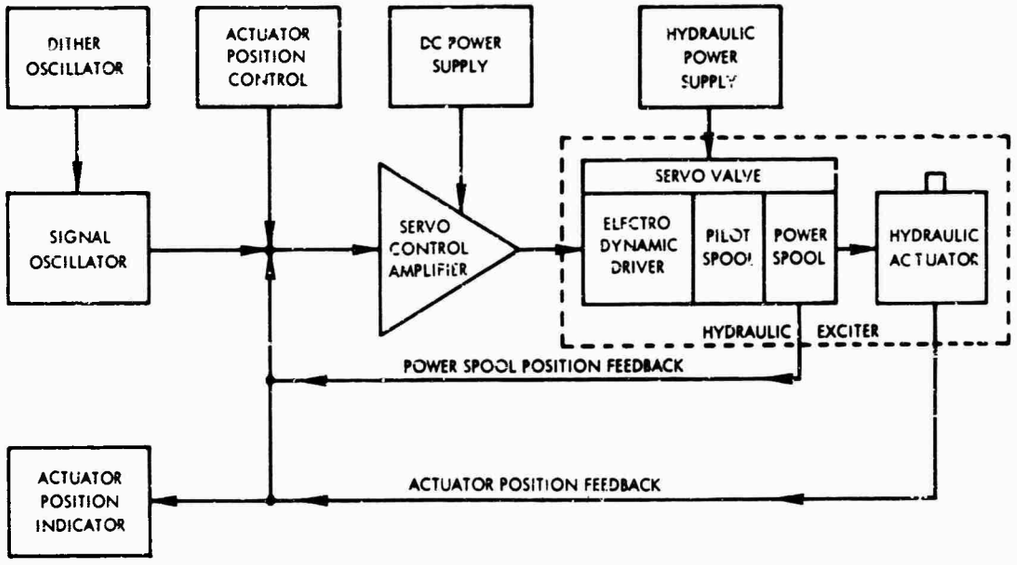

Fig. 2 - Block diagram, hydraulic exciter system

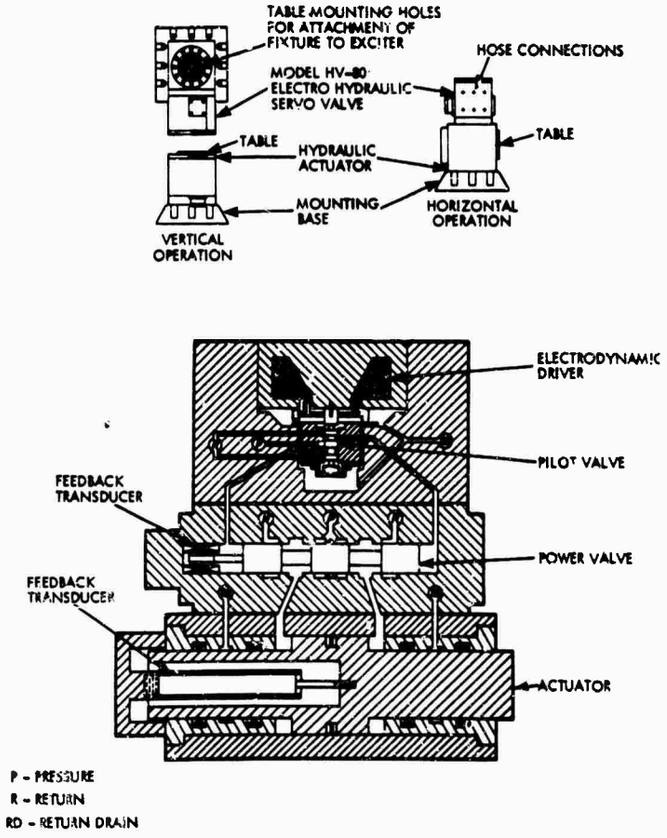

Fig. 3 - Hydraulic exciter operational schematic

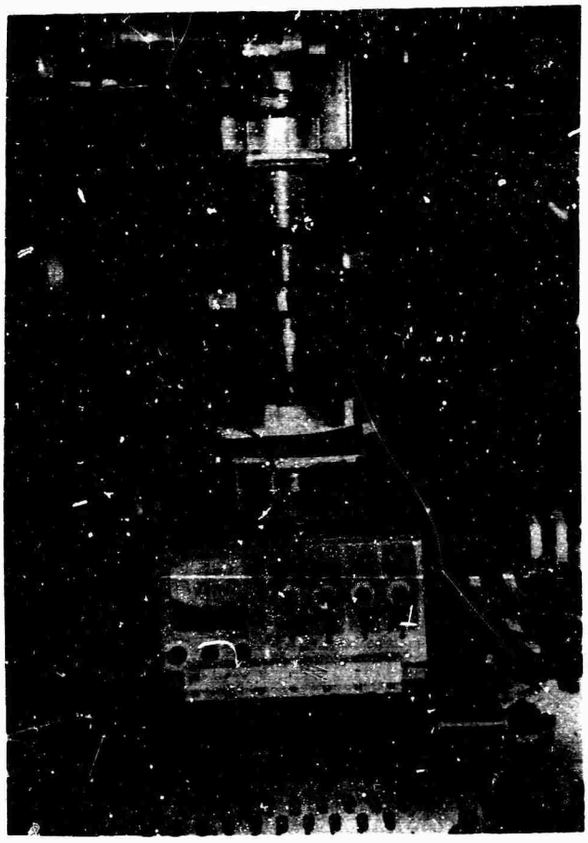

Fig. 4 - Hydraulic rotary joint

Fig. 5 - Hydraulic exciter on inertial mass with 15-lb load

TEST PROCEDURE

Off-Board Tests

Prior to installating the exciter on the centrifuge for combined environment testing, a series of tests were conducted with the exciter mounted on an inertial mass (50,000 lb) as shown in Fig. 5. These tests, designated as off-board tests, were conducted to make the system operational, verify that the exciter met contract specifications, and determine general operational characteristics of the system including the servoamplifier and hydraulic power supply. Following this shakedown operation, acceleration waveform distortion was investigated with the actuator and servo valve positioned in various orientations and under different combinations of vibratory accelerations and exciter table loads. These off-board test actuator-servo valve orientations are described as follows:

1. Condition 1 – Actuator vertical, power spool vertical, and pilot spool horizontal;

2. Condition 2 – Actuator vertical, power spool vertical, and pilot spool horizontal; and

3. Condition 3 – Actuator horizontal, power spool horizontal and parallel to the actuator, and pilot spool vertical.

The servo valve body containing the power spool and pilot spool was manufactured as a single unit with the two spools mutually perpendicular.

The exciter was operated at vibratory accelerations of 10, 20, and 30 g, and the table load ranged from bare table (no load) to a 30-lb mass load. The following parameters were held constant for the off-board series of tests:

1. Actuator hydraulic supply pressure was 1500 psig;

2. Pilot valve supply pressure was 1300 psig;

3. Actuator return pressure was 400 psig;

4. Pilot return pressure was 0 psig; and

5. Test frequency range was from 20 to 500 cps.

A supply pressure of 3000 psig was used for initial system checkout. However, all succeeding tests were conducted at 1500 psig since exciter performance was essentially the same at this lower pressure. In addition, the 1500-psig pressure caused less wear on the rotary joint seals during subsequent on-board tests. The dither oscillator maintained a constant frequency of 1073 cps. Dither amplitude was adjusted to a level sufficient to overcome actuator and power spool stiction. Accelerometers were attached to the exciter table (end of actuator piston) using an aluminum block weighing 2 lb 6 oz. The weight of the block and accelerometers was neglected, and this condition was regarded as bare table operation.

Acceleration waveform distortion measurements were made using a Hewlett-Packard Model 330 B distortion analyzer. (Acceleration waveform distortion used herein is defined as the ratio in percent of the rms value of combined harmonics, including dither oscillation, to the fundamental frequency.) Inaccurate distortion measurements occurred at frequencies less than 20 cps due to limitations of the distortion analyzer, and consequently no data were measured below this frequency. Exciter performance limited the maximum operational frequency to 500 cps. Test data were recorded on magnetic tape and also monitored on an oscillograph and an oscilloscope.

On-Board Tests

A preliminary series of acceleration waveform distortion tests were conducted to determine the actuator-servo valve orientation which produced optimum exciter-centrifuge system performance. For these tests, termed on-board tests, the exciter was mounted in the horizontal position on the centrifuge and operated with the thrust axis first parallel with and then perpendicular to the longitudinal axis of the centrifuge arm. Figure 6 illustrates the coordinate system established for the exciter table in which the Z-axis corresponded to the actuator thrust axis. The coordinate axes for the centrifuge basket accelerometers, also shown in Fig. 6, will be discussed later. Since the servo valve could be rotated 90 deg with respect to the actuator, the following four on-board actuator-servo valve orientations were achieved with respect to the centrifuge arm:

1. Condition 1 — Actuator thrust axis horizontal and parallel to the centrifuge arm, power spool horizontal and perpendicular to the actuator, and the pilot spool vertical (Fig. 6);

2. Condition 2 — Actuator thrust axis horizontal and parallel to the centrifuge arm, power spool horizontal and parallel to the actuator, and the pilot spool vertical;

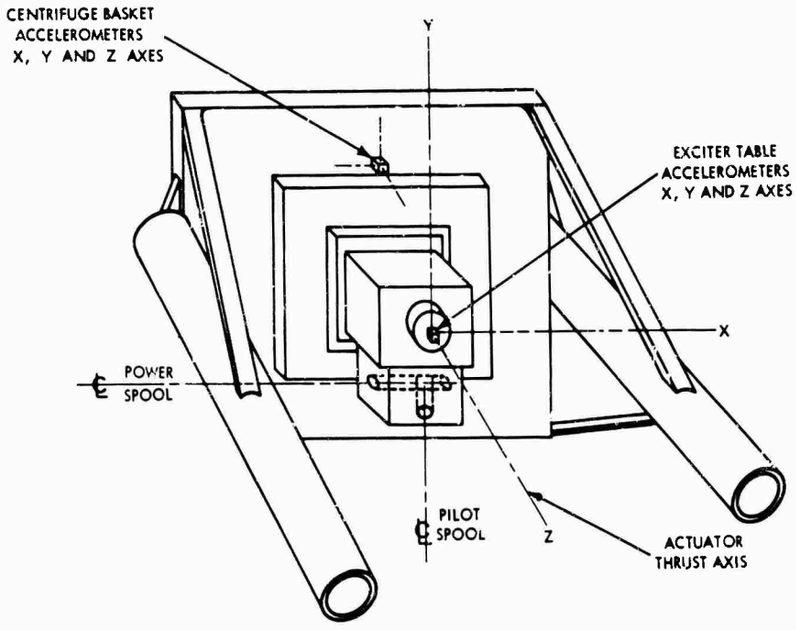

Fig. 6 - Three coordinate axes, exciter table and centrifuge basket accelerometers

3. Condition 3 — Actuator thrust axis horizontal and perpendicular to the centrifuge arm, power spool horizontal and parallel to the actuator, and the pilot spool horizontal; and

4. Condition 4 — Actuator thrust axis horizontal and perpendicular to the centrifuge arm, power spool vertical and perpendicular to the actuator, and the pilot spool horizontal.

To compare test results for these on-board actuator-servo valve orientations and to obtain a relationship with the off-board series of tests, the following parameters were held constant:

1. Actuator hydraulic supply pressure was 1500 psig;

2. Pilot valve supply pressure was 1200 psig;

3. Actuator return pressure was 400 psig;

4. Pilot return pressure was 0 psig;

5. Test frequency range was from 20 to 500 cps;

6. 10-g vibration level;

7. 10-g sustained acceleration level; and

8. Bare actuator table.

Initial survey tests were conducted for static condition (centrifuge in stationary mode) followed by a 10-g sustained acceleration test produced by centrifuge rotation. Test measurements taken during sustained acceleration runs were limited to a minimum number to prolong the life of the rotary joint seals. These preliminary on-board acceleration waveform distortion tests indicated condition 1 orientation of the actuator and servo valve yielded the most satisfactory set of results. All subsequent on-board tests were conducted for this condition.

The remaining distortion tests were conducted at 10-g vibratory acceleration, varying sustained acceleration levels from stationary mode to 20 g with table loads ranging from bare table to 15 lb. Figure 7 shows the exciter being prepared for a 15-lb table load test. Table loads greater than 15 lb were not attempted because at low frequencies pronounced mechanical rattling resonance occurred in the centrifuge deck plates, hatches, and slip ring covers.

The concluding series of on-board tests consisted of determining centrifuge response and exciter cross-axis acceleration to a sinusoidal vibration sweep for bare table and a 15-lb load at a 20-g sustained acceleration level. Outputs from the three accelerometers installed on the centrifuge basket (Fig. 6), as well as the three accelerometers on the exciter table, recorded the response of the centrifuge in the

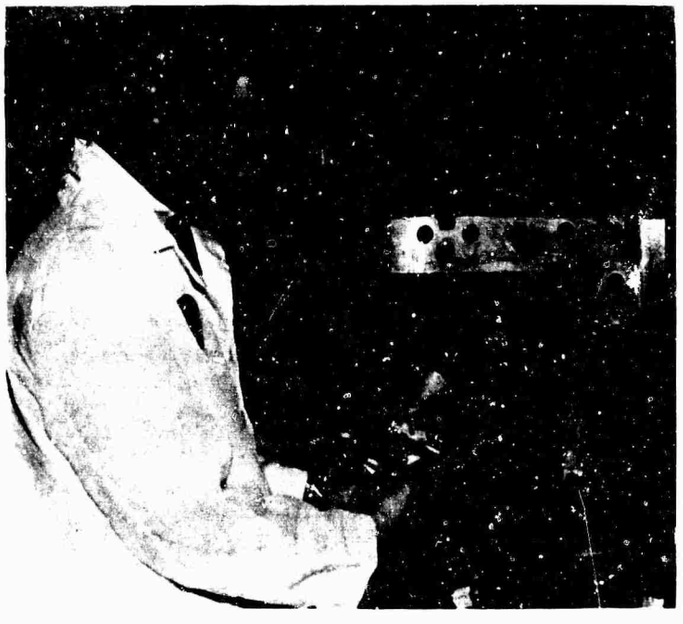

Fig. 7 - Hydraulic exciter on 20-ft diameter centrifuge with 15-lb load

X-, Y-, and Z-axes and also exciter table cross talk. The frequency was swept from 20 to 500 cps at a scanning speed of 4.7 octaves/min. These sinusoidal sweeps were not started until the centrifuge was brought up to a 20-g steady-state acceleration. Figure 8 shows the instrumentation setup used for on-board response tests and for acceleration waveform distortion tests.

Fig. 8 - Instrumentation setup for on-board tests

Previous experience with the hydraulic rotary joint revealed seal leakage problems. Therefore, the body of the joint and connecting hydraulic lines were instrumented with externally attached thermocouples to determine the temperature-time rise during rotation.

TEST RESULTS AND DISCUSSION

Off-Board Tests

Initial exciter evaluation indicated force output and actuator velocity were satisfactory. Displacement distortion values were less than 5 percent. However, acceleration waveform distortion was considerably higher, and therefore, this parameter was selected to evaluate exciter performance. Off-board acceleration waveform distortion data are presented in Figs. 9 through 13 showing percent of distortion as a function of exciter frequency. The maximum peak distortion ranged from 50 to 92 percent,

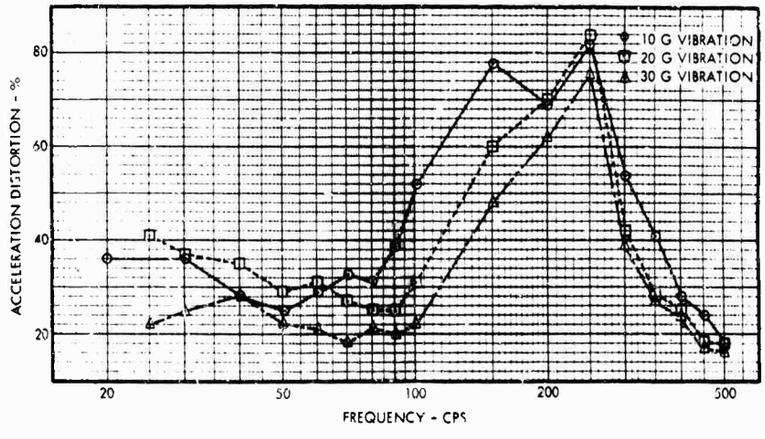

Fig. 9 - Off-board condition 1 acceleration distortion, bare table

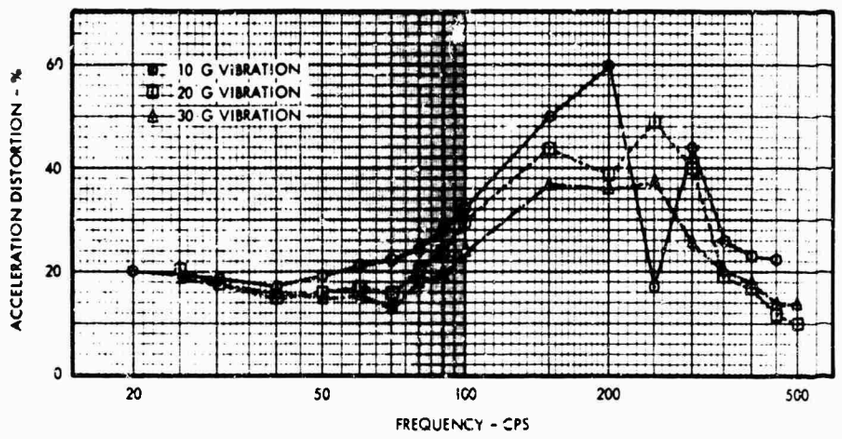

Fig. 10 - Off-board condition 1 acceleration distortion, 15-lb load

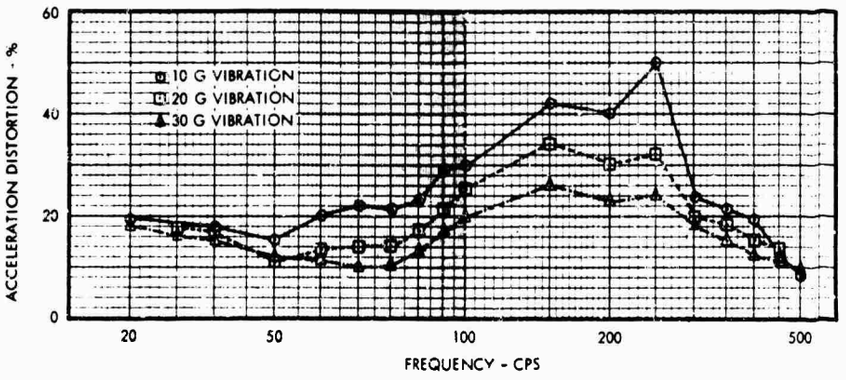

Fig. 11 - Off-board condition 1 acceleration distortion, 30-lb load

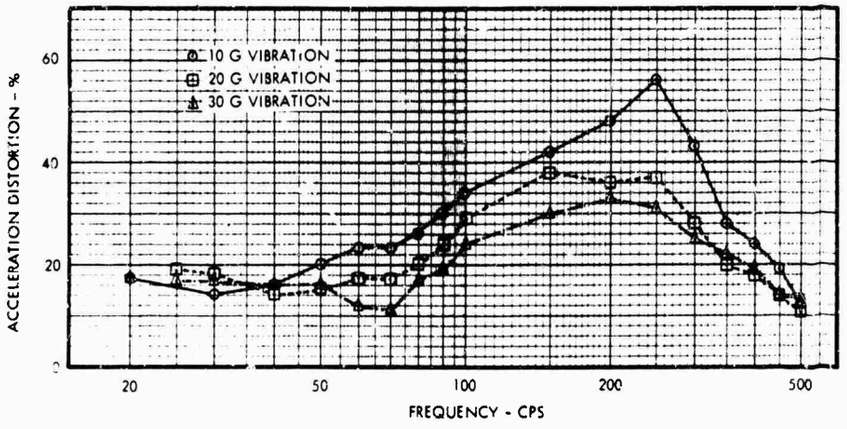

Fig. 12 - Off-board condition 2 acceleration distortion, 30-lb load

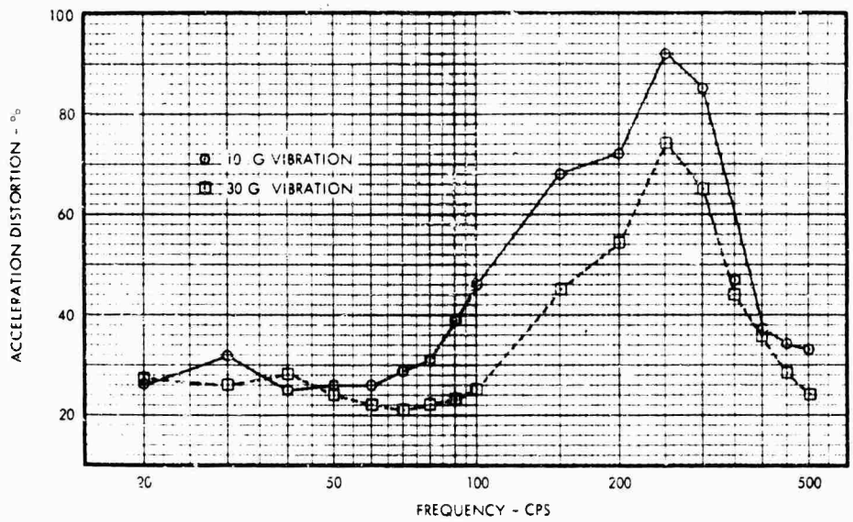

Fig. 13 - Off-board condition 3 acceleration distortion, 30-lb load

occurring at 250 cps. Minimum distortion values were recorded for frequencies below 90 cps. Examination of the distortion curves also shows that an increase of exciter vibration level resulted in a decrease in acceleration distortion. Similarly, increasing the exciter table load also reduced distortion. A comparison of distortion magnitude for the same table load and at the same vibration level reveals that condition 1 actuator-servo valve orientation levels are lower than those of condition 2. Figure 13 represents a set of test data for condition 3. This exciter orientation, in which the thrust axis was horizontal with the exciter supported in a cantilevered position, produced extremely high peak distortion, 1 . 92 percent for 10-g vibration and 74 percent for 30-g vibration.

On-Board Tests

Results from the first series of on-board tests, consisting of bare table acceleration waveform distortion surveys for the four actuator-servo valve orientations, are shown in Figs. 14 through 17. These curves indicate that on-board condition 1 exciter orientation produced distortion measurements substantially lower than the other three conditions for both the stationary mode and 10-g sustained acceleration. Peak distortion for condition 1 (Fig. 14) reached 36 percent which was considerably lower than all off-board 10-g vibration level test results. For frequencies below 100 cps, condition 1 distortion increased slightly with 10-g sustained acceleration. At frequencies above 100 cps, the distortion levels for stationary and 10-g rotational acceleration modes were comparable. Condition 2 distortion, which reached a peak of 60 percent for the 10-g sustained acceleration mode (Fig. 15), was higher than condition 1 distortion throughout the entire frequency range. Distortion measured under sustained acceleration also remained higher than the stationary mode values for all but two test points. Conditions 3 and 4, shown in Figs. 16 and 17, respectively, produced erratic distortion curves for the stationary and rotational modes. For both of these conditions, the actuator thrust axis was perpendicular to the longitudinal axis of the centrifuge arm. Because of the lower mechanical impedance of the centrifuge to vibration in a direction perpendicular to the centerline of the centrifuge arm, the feedback of structural motion to the exciter amplified distortion levels. The distortion curves for condition 4 followed a scattered pattern in which a phase shift appears to have occurred between the stationary and rotational test runs. The power spool, positioned in a vertical attitude in this exciter orientation, was possibly influenced by the centrifuge vertical plane rocking mode. As previously stated, the results of the above survey tests indicated that the condition 1 exciter orientation produced the most satisfactory performance for the four conditions tested and, therefore, the remaining on-board tests were conducted using this orientation.

The next series of tests was also conducted to determine acceleration waveform distortion characteristics. For these tests, table loads were varied from bare table to 15 lb. In addition, the tests were conducted for stationary

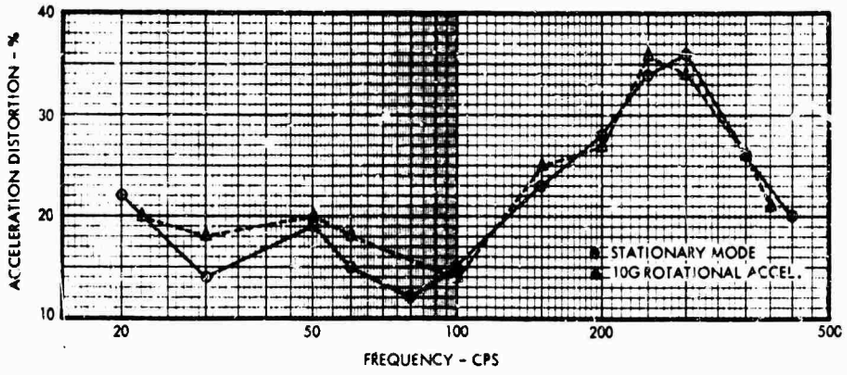

Fig. 14 - On-board condition 1 acceleration distortion, bare table

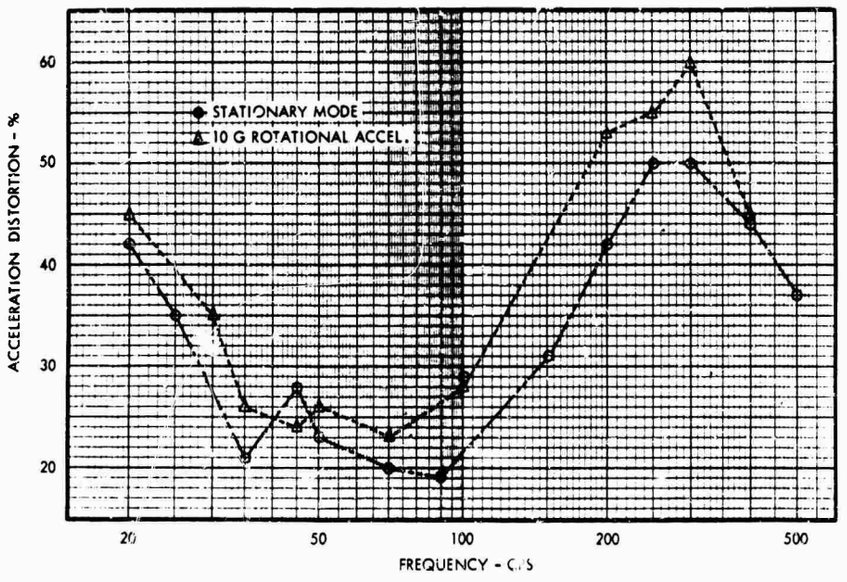

Fig. 15 - On-board condition 2 acceleration distortion, bare table

mode and 10- and 20-g sustained acceleration while maintaining a constant 10-g vibratory level. Figures 18 through 21 show that the major distortion peaks occurred at about 100 cps, and minor peaks were measured at approximately 45 and 400 cps. Distortion readings decreased with an increase in table load in the region of 200 to 300 cps. The curves also indicate that distortion increased proportionally with centrifugal acceleration at the higher end of the frequency range. However, because of the irregularity of the curves, the effect of centrifugal acceleration was difficult to determine for frequencies below 100 cps.

Prior to initiating the above tests, the servoamplifier output signal was checked and was found to be distorted. The actuator and power spool feedback loops were adjusted to improve the signal waveform. After the tests were completed, a comparison of Figs. 14 and 18 revealed poor repeatability. Since the distortion curve pattern in Figs. 18 through 21 remained generally consistent, the lack of repeatability was attributed to the changes in the feedback loop bandpass adjustment. Other variations of the system contributed to repeatability problems. Variations such as servo valve sizing and hydraulic fluid temperature caused perturbations of exciter performance.

Test data for the final series of on-board tests are presented in Figs. 22 through 33. These tests were made to determine three-dimensional

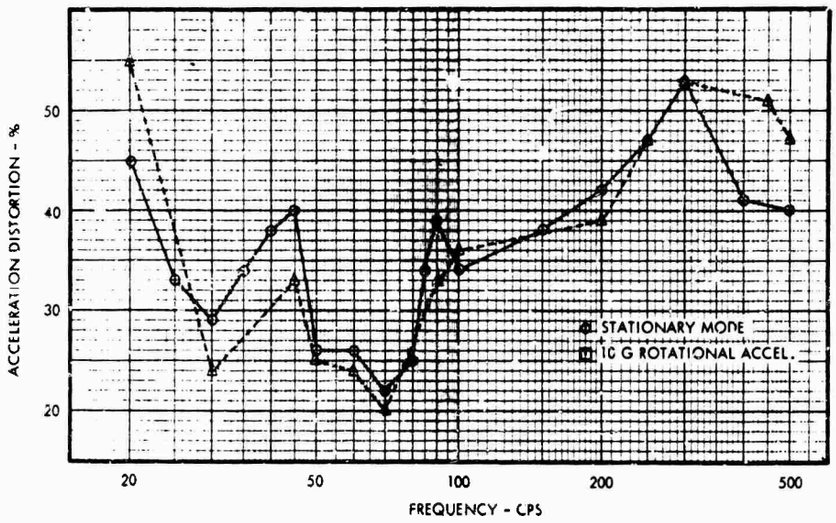

Fig. 16 - On-board condition 3 acceleration distortion, bare table

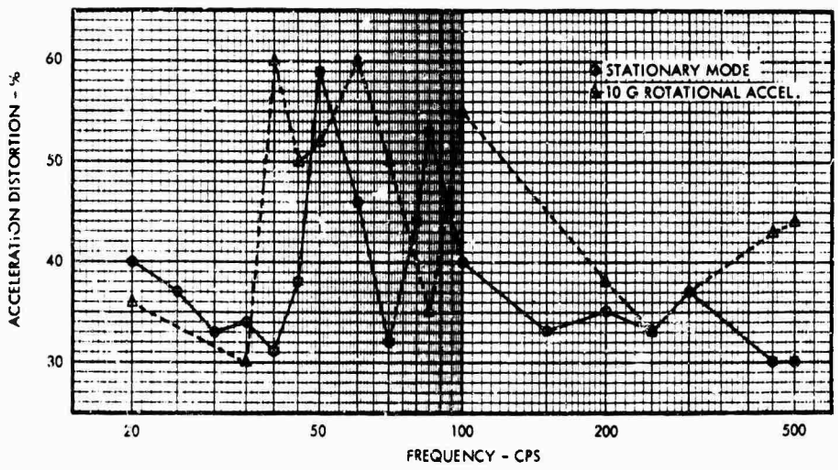

Fig. 17 - On-board condition 4 acceleration distortion, bare table

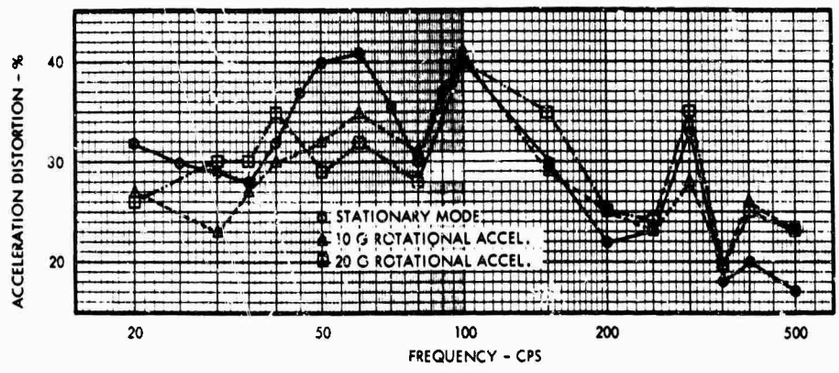

Fig. 18 - On-board condition 1 acceleration distortion, bare table

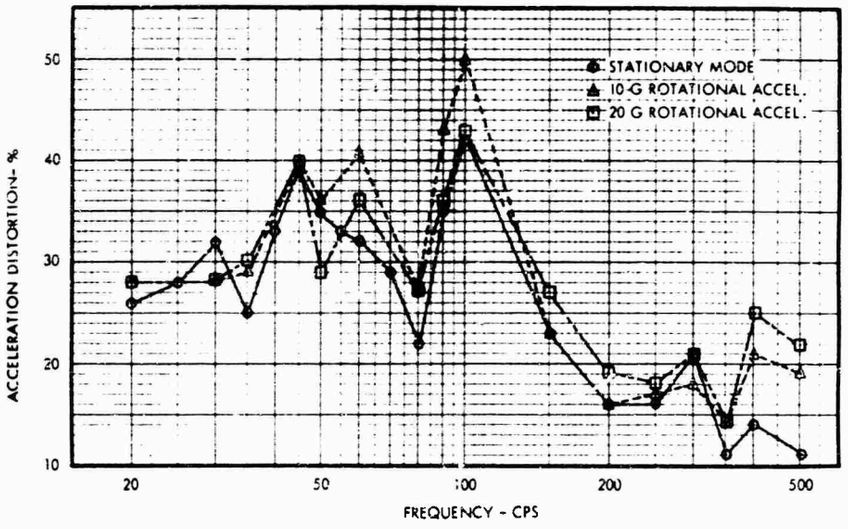

Fig. 19 - On-board condition 1 acceleration distortion, 5-lb load

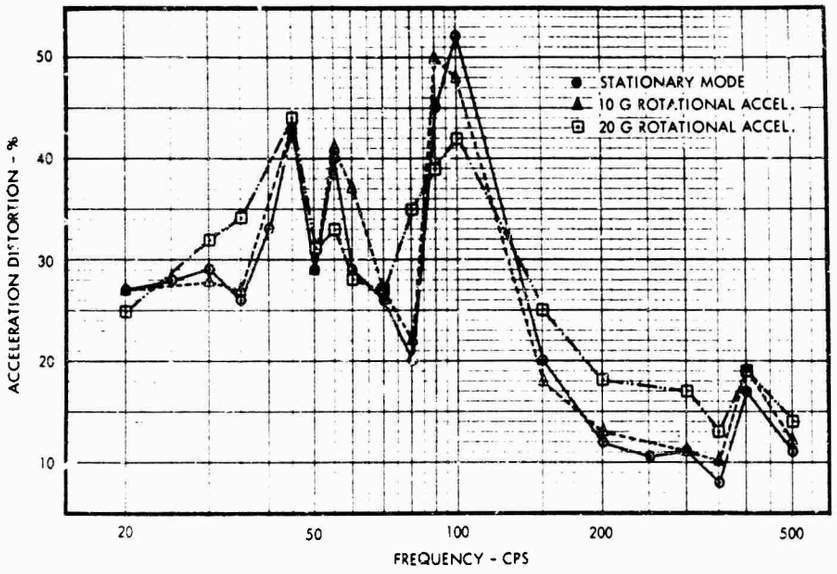

Fig. 20 - On-board condition 1 acceleration distortion, 10-lb load

centrifuge response to a sinusoidal vibration sweep as a function of frequency. Accelerometers installed on the exciter table also recorded exciter accelerations in the X-, Y-, and Z-axes for a constant input level. Response levels were obtained for bare and 15-lb table load conditions. All curves plotted in Figs. 22 through 33 represent unfiltered acceleration waveform data. For bare table frequency sweeps (Figs. 22 through 27), the exciter vibration level in the thrust axis varied between 13 and 22 g. All three centrifuge accelerometers recorded peak accelerations at frequencies below 125 cps with the Z-axis reaching a maximum of 5.6 g at 111 cps. Comparison of centrifuge accelerations in the remaining two axes shows considerable variation in the Y-axis. Exciter cross-axis acceleration also recorded peak values at lower frequencies. For example, the exciter X-axis accelerometer recorded a level of 3.8 g at

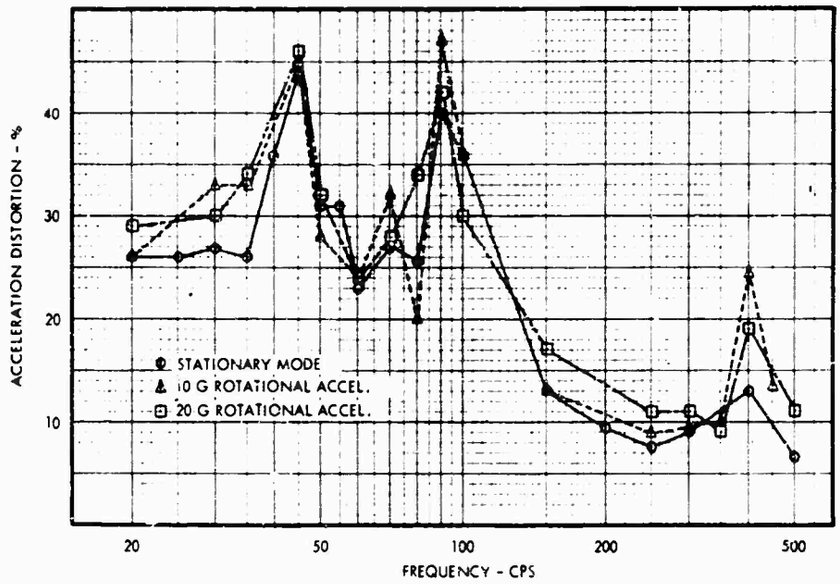

Fig. 21 - On-board condition 1 acceleration distortion, 15-lb load

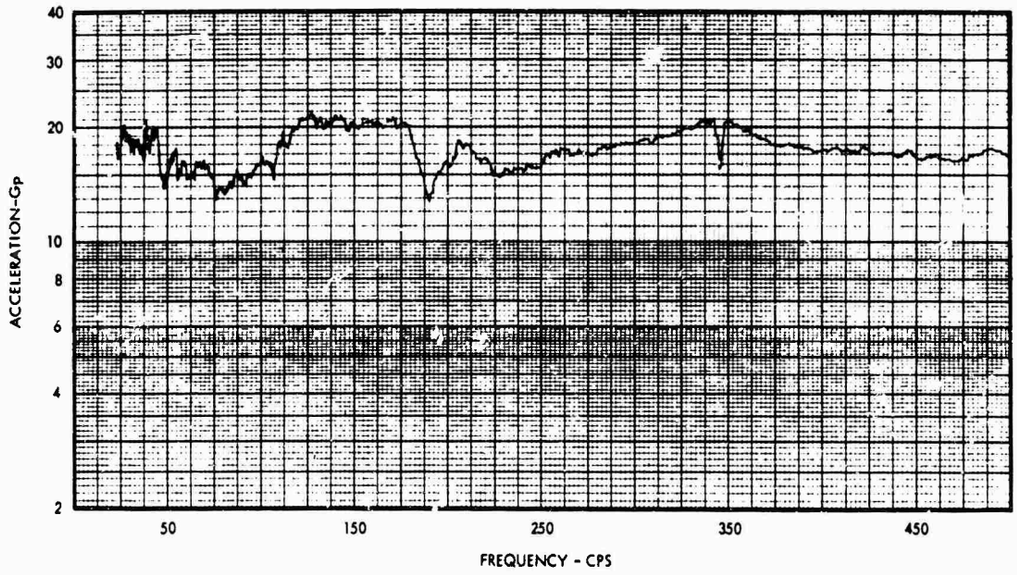

Fig. 22 - Table acceleration, Z-axis, bare table

60 cps but decreased to less than 0.5 g from 150 to 500 cps.

The 15-lb table load frequency sweeps (Figs. 28 through 33) produced much higher centrifuge acceleration response levels than the bare table sweeps. Except for the X-axis, centrifuge peak acceleration levels for the loaded condition were approximately twice as high as bare table levels. The centrifuge X-axis average level was of the same order of magnitude for bare table as for the 15-lb load condition. The exciter Y-cross-axis acceleration peaked to 13 g at 109 cps, which was greater than the X-axis peak cross talk by a factor of 3. As shown by Figs. 22 and 28, it is apparent that in the Z-axis, the exciter maintained a more constant input acceleration level with the 15-lb table load as compared to the bare table configuration.

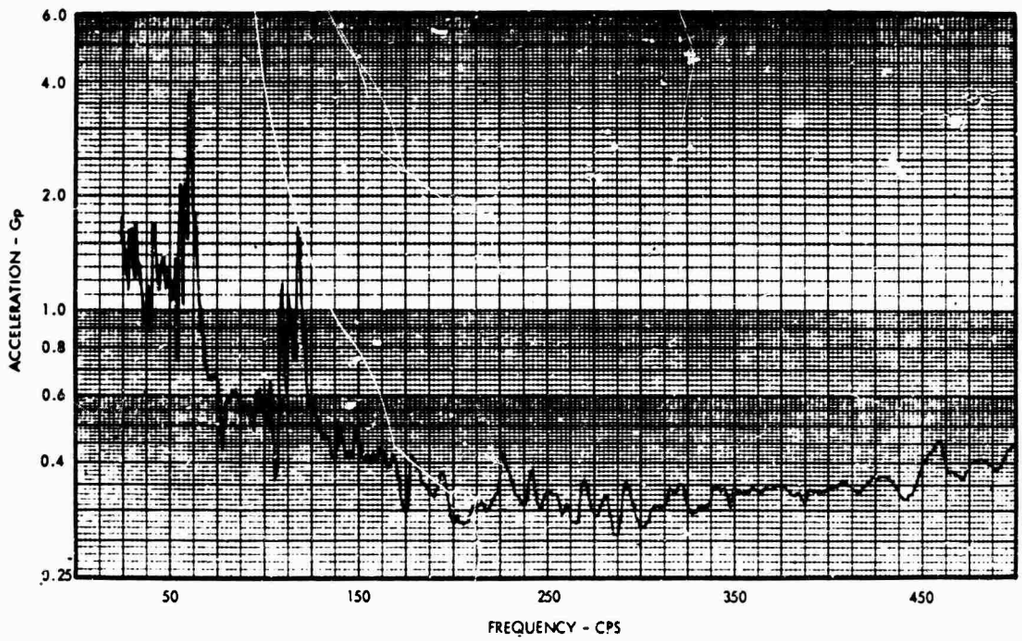

Fig. 23 - Table acceleration, X-axis, bare table

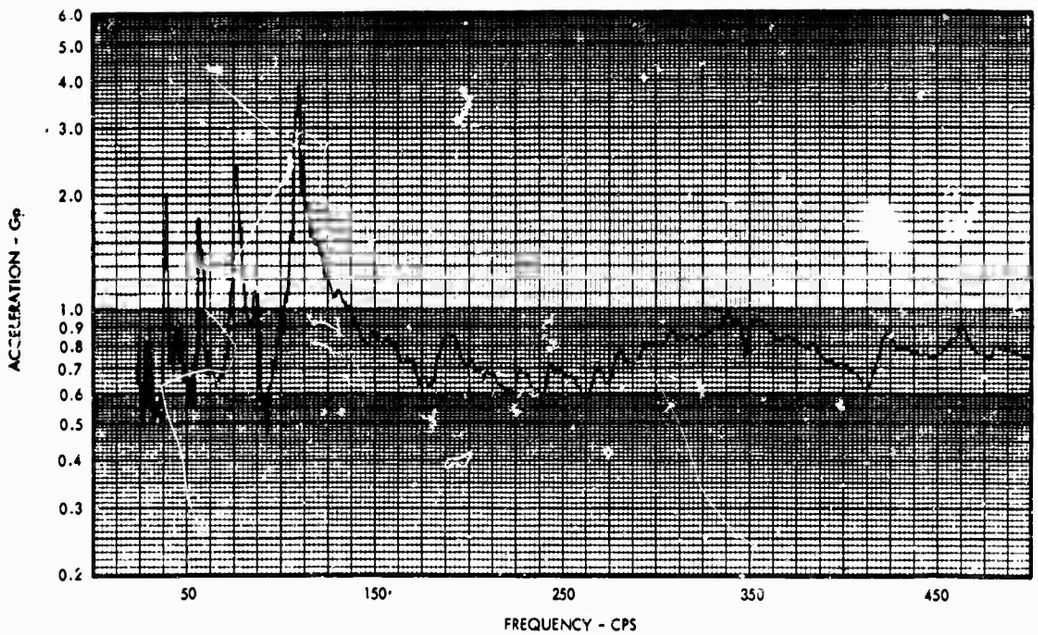

Fig. 24 - Table acceleration, Y-axis, bare table

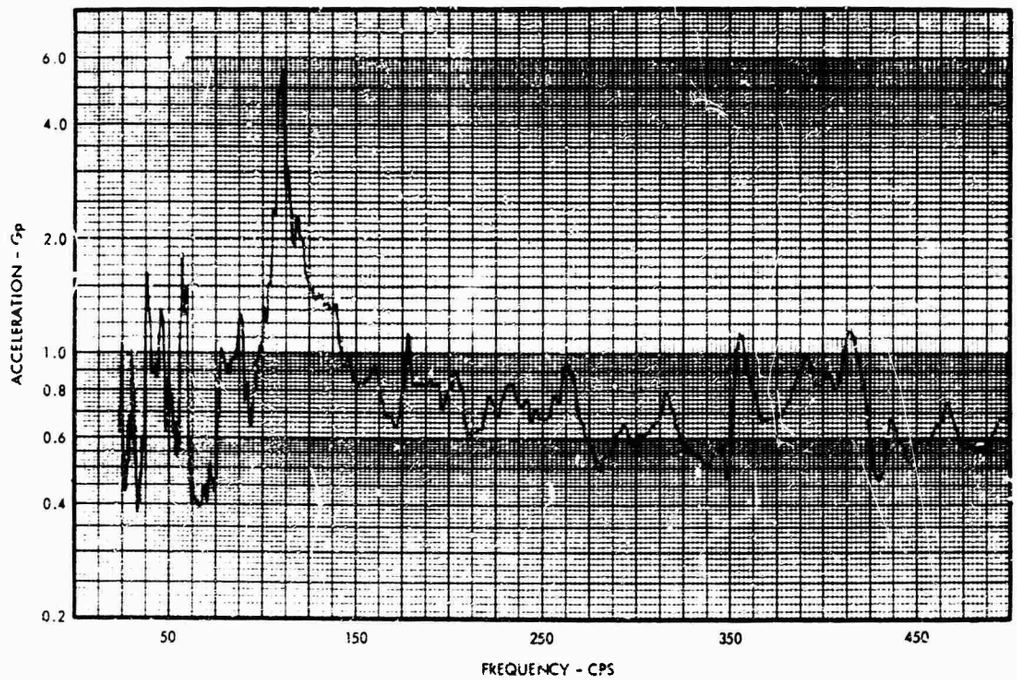

Fig. 25 - Centrifuge response, Z-axis, bare table

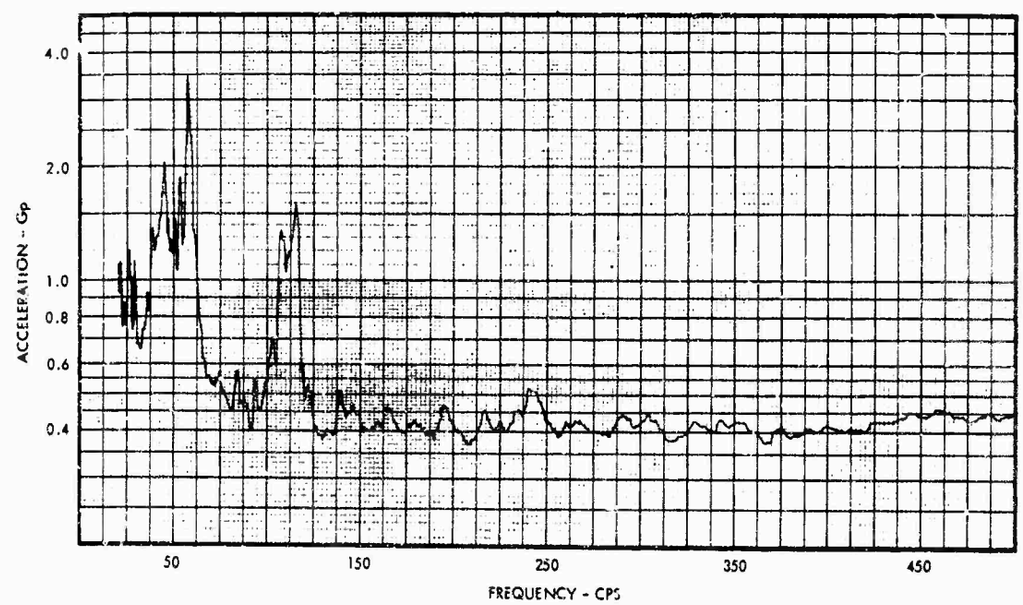

Fig. 26 - Centrifuge response, X-axis, bare table

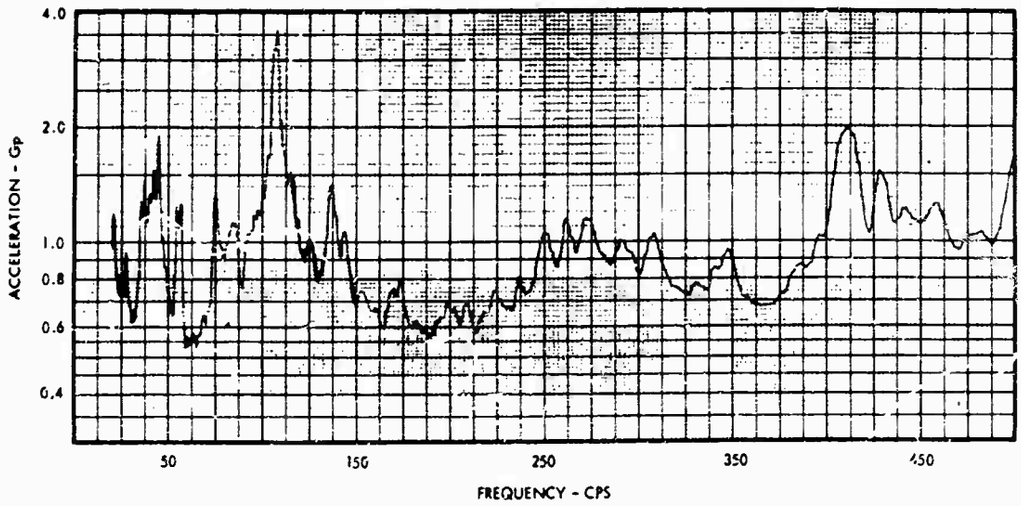

Fig. 27 - Centrifuge response, Y-axis, bare table

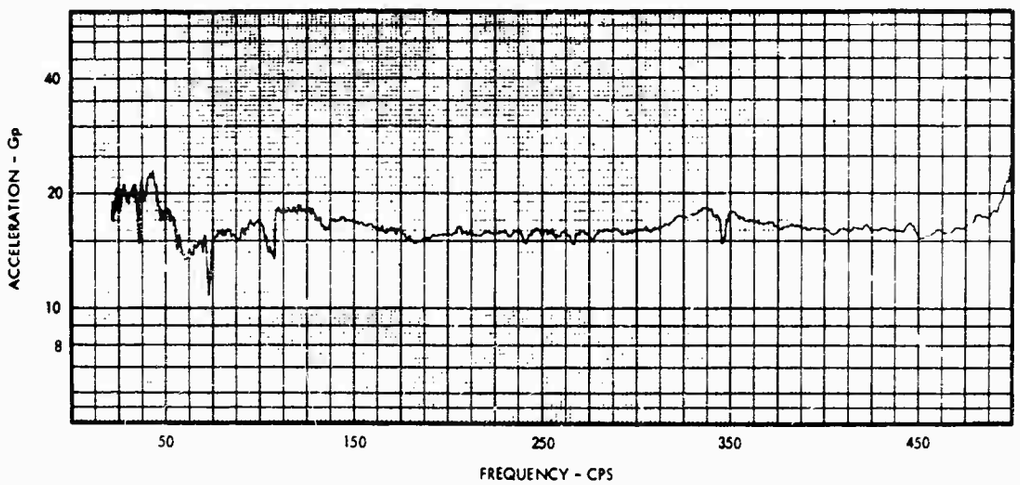

Fig. 23 - Table acceleration, Z-axis, 15-lb load

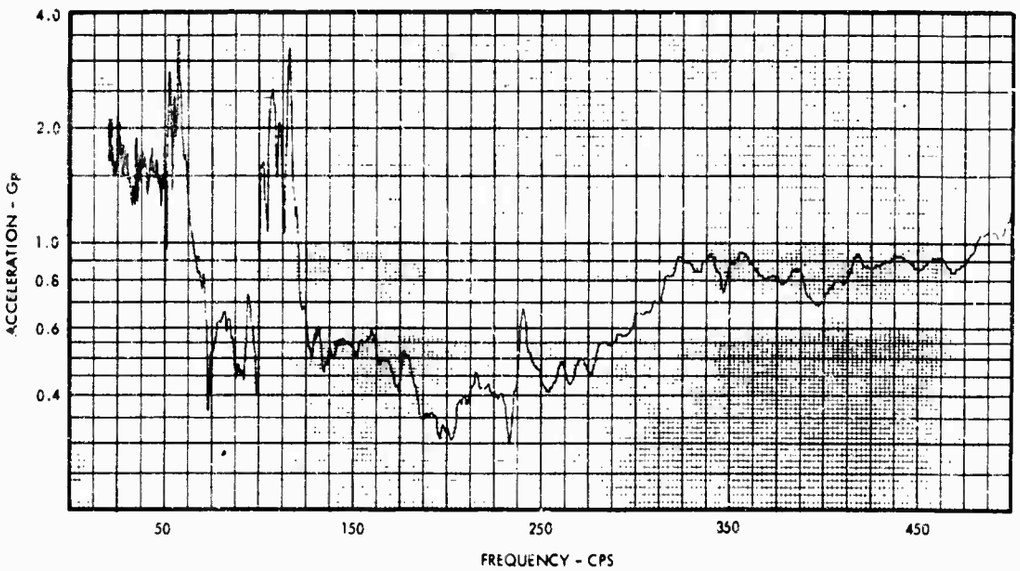

Fig. 29 - Table acceleration, X-axis, 15-lb load

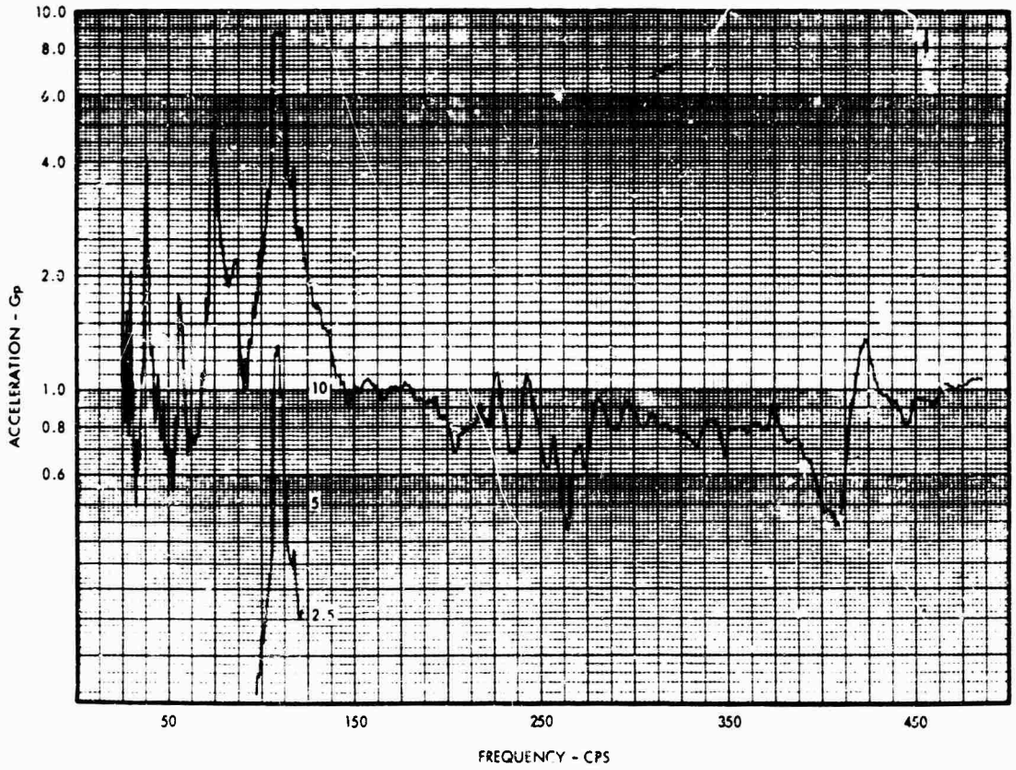

Fig. 30 Table acceleration, Y-axis, 15-lb load

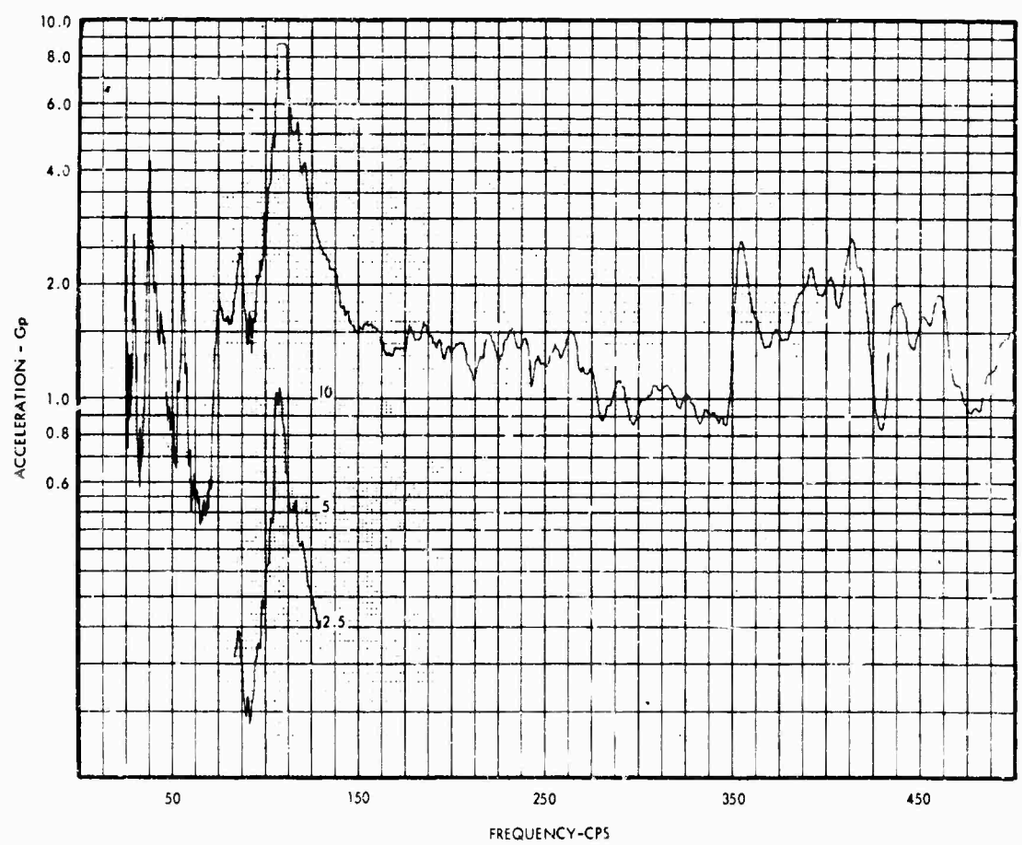

Fig. 31 - Centrifuge response, Z-axis, 15-lb load

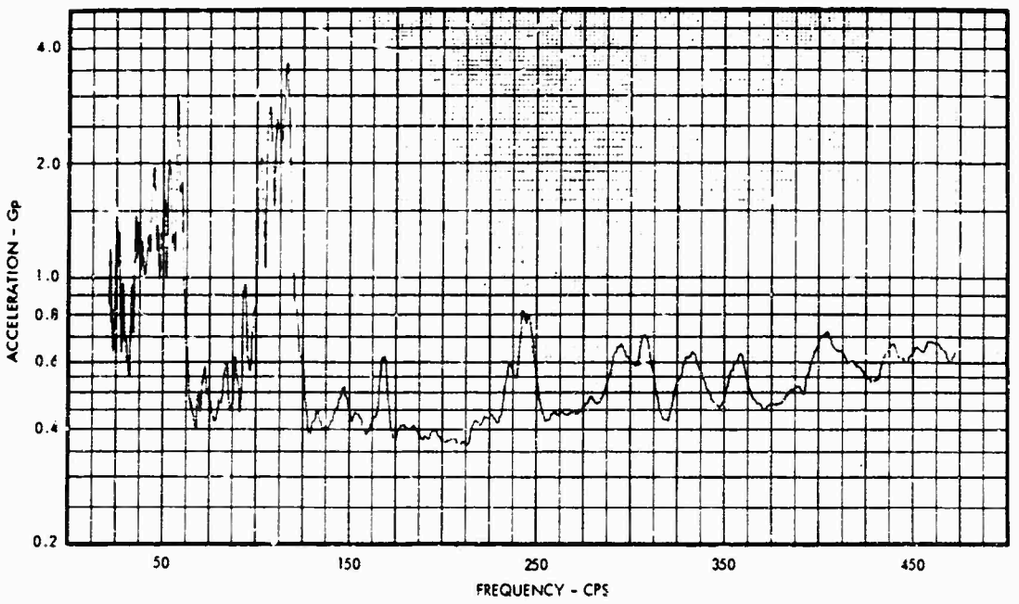

Fig. 32 - Centrifuge response, X-axis, 15-lb load

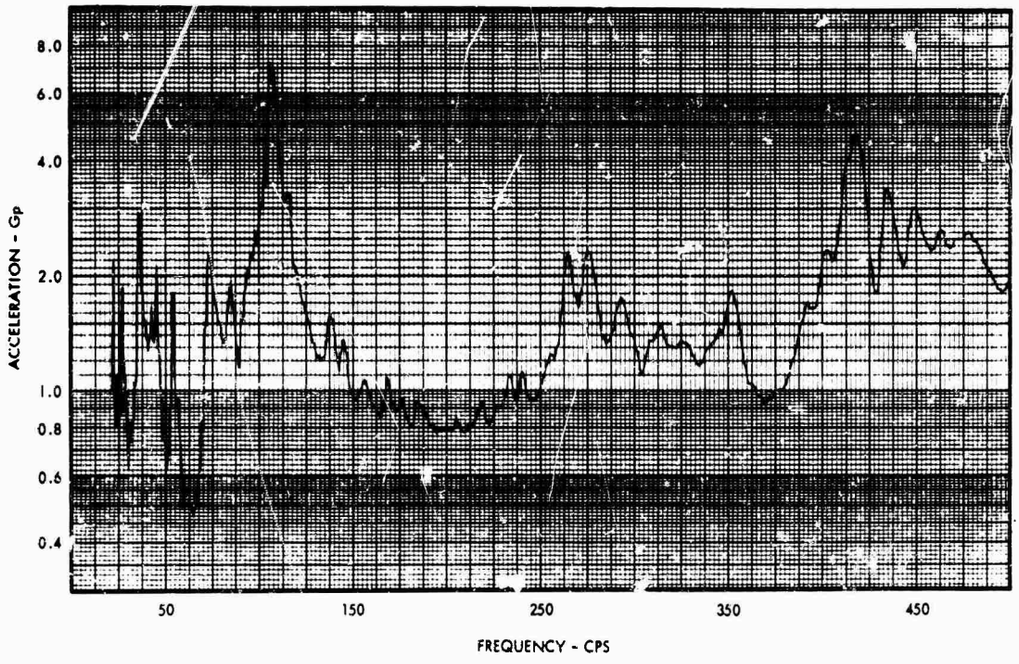

Fig. 33 - Centrifuge response, Y-axis, 15-lb load

During on-board testing, mechanical resonance of hydraulic lines installed on the centrifuge and resonance of centrifuge deck plates and slip ring covers significantly influenced accelerations measured at the exciter table and the centrifuge structure. Part of this problem was caused by the length of hydraulic lines from the power supply to the exciter which added to the difficulty of isolating line vibrations.

The results of the temperature rise test of the hydraulic rotary joint during a typical centrifuge operation are illustrated in Fig. 34. The curve shows the rotary joint temperature increased from 35°C to 55°C (95°F to 131°F) in 19 min of rotation at 56 rpm. The temperature rise was caused mainly by the friction of the internal seals. This temperature measurement was taken on the external surface of the joint, a

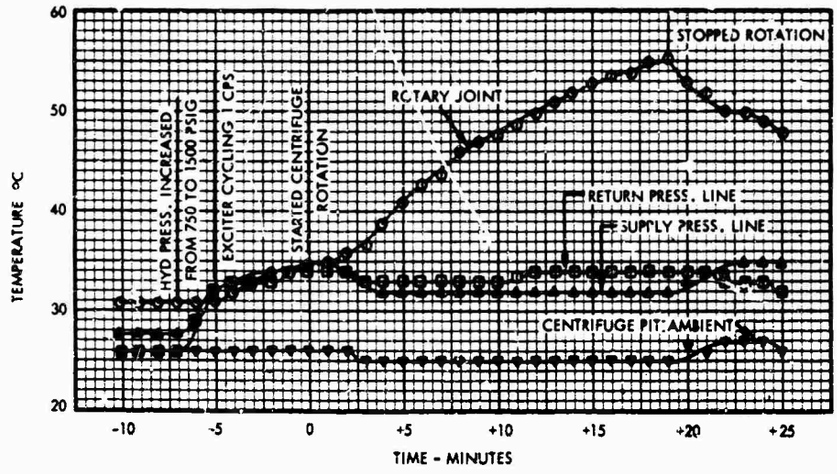

Fig. 34 - Hydraulic rotary joint temperature vs time

1-in. thick steel cylinder. The maximum internal temperature which the seals experienced was estimated at 60°C (140°F). Extrapolation of the temperature curve indicated that a leveling-off of the external temperature would occur at approximately 59°C (138°F) for prolonged joint rotation.

New seals were installed in the rotary joint prior to the start of on-board testing. Centrifuge rotation time was recorded to determine the amount of wear time on the seals. At the conclusion of on-board rotation tests, 7 hr 53 min operating time accrued. The rotary joint was then removed from the centrifuge, disassembled and inspected. The seals on both sides of the pressure annulus were scored and abraded, and failure appeared to be imminent. It was apparent that backup ring failure occurred first. Without the required support of backup rings, the pressure seals extruded into the gap between the spindle and cylinder, resulting in seal abrasion. In addition, backup ring particles lodged in the rotary joint bearings causing rough operation when rotated by hand.

CONCLUSIONS

The performance characteristics of a combined vibration and sustained acceleration system were investigated utilizing a hydraulic exciter mounted on a centrifuge. Performance of the exciter when combined with sustained acceleration depended to a significant extent on the orientation of the actuator-servo valve with respect to the plane of centrifugal rotation. The most satisfactory test results indicated that exciter performance was optimum for the following orientation: actuator thrust axis horizontal and parallel to the centerline of the centrifuge arm, power spool horizontal and perpendicular to the actuator, and pilot spool vertical. In this orientation, sustained acceleration acted in a direction perpendicular to both the power spool and pilot spool. An investigation of transverse exciter operation, i.e., thrust axis horizontal and perpendicular to the centrifuge arm, revealed relatively high distortion levels. This was attributed to the lower mechanical impedance of the centrifuge arm in the plane of rotation. Sustained acceleration caused an increase in exciter distortion particularly for the higher range of test frequencies, but at lower frequencies test results were too erratic to draw a definite conclusion. It should be noted that all on-board acceleration waveform distortion tests were conducted for very light exciter table loads. Improved exciter performance probably would have been demonstrated with heavier table loads if centrifuge rattling distortion could have been more effectively suppressed.

Centrifuge acceleration response recorded during frequency sweep tests showed the effect of low-frequency resonant conditions. The exciter table accelerometer reflected a considerable variation of input level, especially for bare table sweep tests. Correlation of centrifuge response levels with accelerations recorded at the exciter table demonstrated a distortion coupling effect which developed during centrifuge rotation. The Coriolis phenomenon, which produced an acceleration vector in the plane of centrifuge rotation, was also observed. The anticipated decrease in this acceleration as vibration frequency increased was more apparent for the bare table condition than for the 15-lb load condition. This was due to high resonance peaks

which occurred for the loaded condition and obscured the true magnitude of Coriolis acceleration.

Limitations of the exciter-centrifuge system imposed a restriction on the range of test parameters, i.e., exciter table load and vibration and sustained acceleration level. Since these parameters were constrained, a broad investigation of sustained acceleration effects on the hydraulic exciter was also limited. These limitations resulted from problems involving resonance of hydraulic lines and centrifuge components, distortion of feedback signals, and marginal capability of the rotary joint.

Combining vibration and sustained acceleration created interactions of the integrated exciter-centrifuge system, thus increasing the magnitude of operational difficulties. The experience gained in combined environment operation was invaluable in revealing potential LPS design problem areas and will be utilized in the operational development of the Launch Phase Simulator.

ACKNOWLEDGMENTS

The author wishes to thank the personnel of the Structural Dynamics Branch of Goddard Space Flight Center for their contributions and assistance.

REFERENCES

1. E. J. Kirchman, "Launch Phase Simulator," AIAA Publication CP-11, Nov. 1964

2. Richard E. Sipfle, "Hydraulic Shakers," Fluid Power International, Jan. 1964

DISCUSSION

Mr. Thomas (AFFDL, W-PAFB): We have done some preliminary work of this type at Wright Field on a very old centrifuge using an electrodynamic shaker. Have you compared your results using the hydraulic shaker with an electrodynamic shaker from the standpoint of the reactive mass involved with the shaker body?

Mr. Skolka: We had an earlier test using an electrodynamic driver. The reactive mass you are referring to is the centrifuge structure itself; we used the same centrifuge for both tests. The results of the electrodynamic shaker were much improved with regard to acceleration distortion, which was the major test parameter checked.

* * *

AVERAGING FUNDAMENTAL VIBRATION CONTROL SIGNALS: A THEORETICAL STUDY*

W. W. Shurtleff
Sandia Co.poration
Albuquerque, New Mexico

This report presents a theoretical evaluation of three methods of vibration feedback control signal averaging. The evaluation criteria employed are phase sensitivity, fundamental averaging, and accuracy and linearity of average. Experimental results confirm the theoretical superiority of the tracking filter and operational amplifier averaging technique over resistive and time-sharing averaging techniques.

W. W. Shurtleff

INTRODUCTION

One important parameter in vibration testing is the feedback signal between the transducer on the vibration table and the servo controller (Fig. 1). If this signal is not a true indication of the vibration table acceleration or velocity, the specimen being tested may be undertested, overtested, or even destroyed.

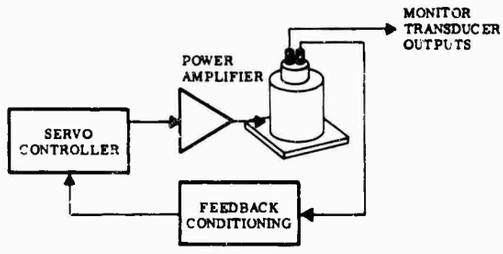

Fig. 1 - Vibration control diagram

There are at least three reasons why a feedback transducer may not give an accurate signal. First, the table driving hardware may be imperfect and cause unequal accelerations on the table top. Second, the test specimen may have been incorrectly placed so that its center of mass did not coincide with the center of mass of the table-jig combination; this also causes unequal accelerations, depending on the mass of the component. Finally, the transducer's characteristics may change during a test, thereby causing a change in feedback signal. Any one of these reasons is justification for looking for a better technique of feedback control than the present method of single point sensing.

One suggested solution of this problem is to put a number of transducers around the table top and average their outputs to get a feedback signal. This method should give a signal which is equal to the acceleration or velocity of the table top and, therefore, of the test specimen if a perfectly rigid jig is used. Also, if one transducer should change or even open circuit, the others will continue to give approximately a true average output; the accuracy of this approximation is a direct function of the total number of channels being averaged.

This report discusses and compares three appropriate and obvious techniques that can be used for averaging the feedback signals: (a) resistive averaging, (b) time-sharing averaging, and (c) averaging by using tracking filters and an operational amplifier. Each one of these

*This work was supported by the United States Atomic Energy Commission.

techniques will be theoretically analyzed. Experimental data are presented for the two best techniques.

COMPARISON CRITERIA

The three techniques will be compared according to the following criteria: phase sensitivity, fundamental averaging, and accuracy and linearity of average. Each of these criteria arise from the nature of the feedback signal and from the methods of vibration testing; these criteria are discussed in more detail below.

Phase Sensitivity

If different areas of a vibration table top are experiencing different accelerations, they are also out of phase. If these out-of-phase signals are linearly added, there will be cancellation. Presently this is an undesired feature of a feedback signal. However, there may be applications in the future where it is desired to operate on the real or imaginary components of the feedback signal. In this case the feedback will have to be phase sensitive.

Fundamental Averaging

There is a requirement in vibration testing that the controller respond only to the fundamental component of the feedback signal. This means that if the controller is providing a signal of X cps to the power amplifier which drives the shaker, the feedback signal should be composed only of the X-cps signal from the feedback transducer and not of distortion components generated by the amplifier-driver combination. The averager must, therefore, only average on the fundamental frequency vibration component.

Accuracy and Linearity of Average

This requirement is self-explanatory. The average must be accurate to have any meaning, and it also must be independent of frequency since frequency is varied from about 10 cps to 3 kc.

ANALYSIS OF AVERAGING TECHNIQUES

Resistive Averaging

Mathematically, resistive averaging techniques can be expressed as:

$$\text{Average} = \overline{v(t)} = \frac{1}{n}\sum_{i=1}^{n} A_i \sin(\omega t + \theta) , \quad (1)$$

where there are n inputs to the averager. Expanding and grouping of terms gives:

$$\overline{v(t)} = \frac{\sin \omega t}{n}\sum_{i=1}^{n} A_i \cos \theta_i + \frac{\cos \omega t}{n}\sum_{i=1}^{n} A_i \sin \theta_i . \quad (2)$$

These are the "real" and "imaginary" components of the averaged feedback signal.

A simple case of two inputs is a good example:

$$v(t) = \frac{1}{2}\left[A_1 \sin \omega t + A_2 \sin(\omega t + \theta_2)\right] . \quad (3)$$

Let $A_1 = A_2$ and $\theta_2 = 180°$. Therefore,

$$\overline{v(t)} = \frac{A_1}{2}(\sin \omega t - \sin \omega t) = 0 , \quad (4)$$

showing that there is a chance that the signals will vectorially cancel due to phase difference and result in damage to the vibration driver and/or test specimen.

Another method using resistive averaging is first to rectify the signal and then to average it. Assuming the inputs are of the form

$$v_i(t) = A_i \sin(\omega t + \theta_i) \quad (5)$$

and they are half-wave rectified and integrated from zero to $1/f$, the result is only a dc term [1]:

$$v_i'(t) = \frac{A_i}{\pi} . \quad (6)$$

If an operational amplifier averaging circuit is used and the $v(t)$'s are averaged, the resultant average is a true average:

$$\overline{v'(t)} = \frac{1}{n}\sum_{i=1}^{n} A_i . \quad (7)$$

This method is excellent if the incoming sine waves are composed of only the fundamental frequency as in the tracking filter – operational amplifier technique.

Time-Sharing Averaging

The time-sharing averager uses sampling techniques. The signals come from the

transducers into the multiplexer which continuously presents each input in turn to the tracking filter. The tracking filter derives the fundamental component of this complex signal, and it is then averaged by either a true averaging circuit or a true rms averaging circuit as illustrated in Fig. 2. The following mathematical development of the multiplexing process shows that this averaging method is useful only in limited cases.

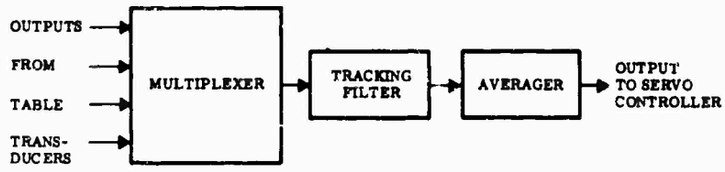

Fig. 2 - Time-sharing averager feedback conditioning

Inputs — All inputs to the time-sharing averager are assumed to have the same fundamental frequency and can be expressed as a sum of sinusoids

$$v_n(t) = \sum_{m=1}^{\infty} A_{mn} \sin (m\omega t + \theta_n) , \qquad (8)$$

where n is the number of the input and m is the number of the harmonic. All terms need not be present.

Multiplexing — The multiplexing is assumed to have rectangular time periods (zero rise and fall time) so the input and output signals per period are identical. The time each input is connected to the output is given by

$$t_n = 1/S , \qquad (9)$$

where S is the switching rate.

Tracking Filter — The rise time (100 percent) of the tracking filter is found empirically [2] to be

$$t_{100\%} = 1/B , \qquad (10)$$

where B is the bandwidth of the bandpass filter in the tracking filter. The time for $t_{100\%}$ in the literature [3] is given as $4/B$ to allow for overshoot and settling time, but this makes little difference in the development of the averaging process.

Averager — Two forms of averaging will be discussed: true averaging and true rms averaging. In true averaging the fundamental will be assumed to go through a half-wave rectifier into a low-pass filter. The Fourier series for a half-wave rectified signal is [1]

$$v_n(t) = \frac{A_n}{\pi} + \frac{A_n}{2} \sin (\omega t + \theta_n) - \frac{2A_n}{3\pi} \cos (\omega t + \theta_n) . \qquad (11)$$

The true average is

$$\overline{f_1(t)} = \frac{1}{4RC} \int_0^{4RC} v_n(t)\, dt , \qquad (12)$$

where RC is the time constant of the low-pass filter. The true rms average is

$$[V_{rms}]^2 = \frac{1}{T} \int_0^T v(t)^2\, dt \qquad (13)$$

and is usually derived from the nonlinear portions of biased diodes. T is dependent on the filter in the averager.

Signal into Averager — The amplitude of the signal into the averager is determined by the rise time of the tracking filter. A typical example of this modification of the amplitude is shown in Fig. 3. Mathematically, this modification can be approximated as follows:

$$A_{in} = A_n(1 - e^{-4Bt}) . \qquad (14)$$

If $t = t_n = 1/S$,

$$A_{in} = A_n(1 - e^{-4B/S}) . \qquad (15)$$

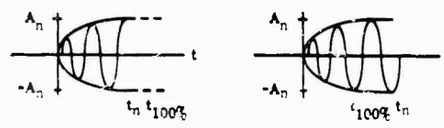

Fig. 3 - Inputs to averager

This modifying term takes care of the case where the initial charge of the filter is zero. Addition of other cases would only complicate the results and would not add much information.

Average —

1. True average. Using Eq. (1) and averaging over each of the inputs will give:

$$\overline{f_1(t)} = \frac{(1 - e^{-4B/S})}{4RC} \int_0^{4RC} v_n(t)\, dt \qquad (16)$$

and

$$v_n = \frac{A_n}{\pi} + \frac{A_n}{2} \sin(\omega t + \theta_n) - \frac{2A_n}{3\pi} \cos(\omega t + \theta_n) . \qquad (17)$$

Assuming there are D inputs to the averager each 4RC averaging time, a relationship can be found between D and 4RC:

$$\frac{D}{S} = 4RC . \qquad (18)$$

Also,

$$4RC = \sum_{n=1}^{D} \frac{4RCn}{D} - \frac{4RC(n-1)}{D} . \qquad (19)$$

Therefore,

$$\overline{f_1(t)} = \frac{S}{D}(1 - e^{-4B/S}) \sum_{n=1}^{D} \int_{\frac{4RC(n-1)}{D}}^{\frac{4RCn}{D}} v_n(t)\, dt$$

$$= \frac{S}{D}(1 - e^{-4B/S}) \left\{ \sum_{n=1}^{D} \frac{A_n 4RC}{D\pi} + \frac{A_n}{2\omega} \times \left[\cos\left(\frac{4RC\omega(n-1)}{D} + \theta_n\right) - \cos\left(\frac{4RC\omega n}{D} + \theta_n\right) \right] \right\} . \qquad (20)$$

If the frequency is sufficiently high, the terms with $1/\omega$ are negligible and we arrive at a simpler form:

$$\overline{f_1(t)} = \frac{(1 - e^{-4B/S})}{D} \sum_{n=1}^{D} \frac{A_n}{\pi} . \qquad (21)$$

This is the correct average of the inputs into the averager with the condition that the input frequency is high enough and B/S >> 1. Otherwise the average is a function of frequency, phase, tracking filter bandwidth, and signal amplitude.

2. True rms average

$$[v_{rms}]^2 = \frac{(1 - e^{-4B/S})}{T} \sum_{n=1}^{D} \int_{t_{n-1}}^{t_n} v(t)^2 dt . \qquad (22)$$

$$T = \sum_{n=1}^{D} t_n - t_{n-1} . \qquad (23)$$

$$v_n(t) = A_n \sin(\omega t + \theta_n) . \qquad (24)$$

$$[v_{rms}]^2 = \frac{S}{D}(1 - e^{-4B/S}) \sum_{n=1}^{D} \frac{A_n^2}{2} \left[\frac{T}{D} + \frac{1}{2\omega} \sin \times \left(\frac{T}{D}(n-1) + \theta_n \right) - \frac{1}{2\omega} \sin\left(\frac{T}{D} n + \theta_n \right) \right] . \qquad (25)$$

Again assuming high frequency, the last two terms can be neglected giving

$$[v_{rms}]^2 = \frac{(1 - e^{-4B/S})}{2D} \sum_{n=1}^{D} A_n^2 . \qquad (26)$$

which is a true rms average, if B/S >> 1. If the last terms cannot be neglected, the true rms average is a function of frequency, phase, and amplitude.

Tracking Filter and Operational Amplifier Averaging Technique

This technique is the third and most important of the techniques discussed. It works in the same manner as the rectified resistive averaging except that rectification is done in a tracking filter and, therefore, the dc signal is proportional to only the amplitude of the fundamental signal (Fig. 4). An explanation of

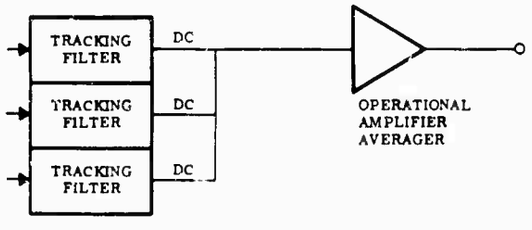

Fig. 4 - Operational amplifier averager

tracking filter operation can be found in Spectral Dynamics Corp. tracking filter manuals.

1. Input:

$$v_n(t) = \sum_{m=1}^{\infty} A_{nm} \sin(\omega_m t + \theta_n), \quad (27)$$

where m is the number of harmonic.

2. DC output of tracking filter:

$$v_{out} = \frac{A_{n_1}}{\pi}. \quad (28)$$

3. One example of an operational amplifier is found by summing the inputs at the summing point of the operational amplifier and using a feedback signal equal to π/n_1 giving an average of

$$\overline{v(t)} = \frac{1}{n_1} \sum_{n=1}^{n_1} A_{n_1}. \quad (29)$$

Review

The formulas for each of the averaging techniques are reviewed in the following listing:

1. Resistive:

$$\overline{v(t)} = \frac{1}{n} [A_1 \sin \omega t + A_2 \sin(\omega t + \theta_2) + \cdots + A_n \sin(\omega t + \theta_n)]. \quad (30)$$

2. True average:

$$\overline{v(t)} = \frac{S}{D}(1 - e^{-4B/S}) \left[\sum_{n=1}^{D} A_n \left(\frac{4RCn}{D} + \frac{1}{2\omega} K(\theta_n \omega) \right) \right]. \quad (31)$$

3. True rms average:

$$[\overline{v(t)}]^2 = \frac{S}{D}(1 - e^{-4B/S}) \left[\sum_{n=1}^{D} \frac{A_n^2}{2} \left(\frac{T}{D} + \frac{1}{2\omega} K_1(\theta_n \omega) \right) \right]. \quad (32)$$

4. Tracking filter-operational amplifier average:

$$\overline{v(t)} = \frac{1}{N} \sum_{n=1}^{N} A_n. \quad (33)$$

TESTS OF AVERAGING TECHNIQUES

The two most important of the above techniques (true rms time-sharing and operational amplifier averaging) have been tested in the laboratory. The test setups are illustrated in Figs. 5 and 6. The tests that were done were of linearity, phase sensitivity, and fundamental averaging. The results of these tests are condensed in Figs. 7, 8 and 9.

CONCLUSIONS

Comparisons of the time-sharing and the operational amplifier systems can best be shown by Table 1. It is obvious that the operational amplifier system is the better of the two methods of averaging.

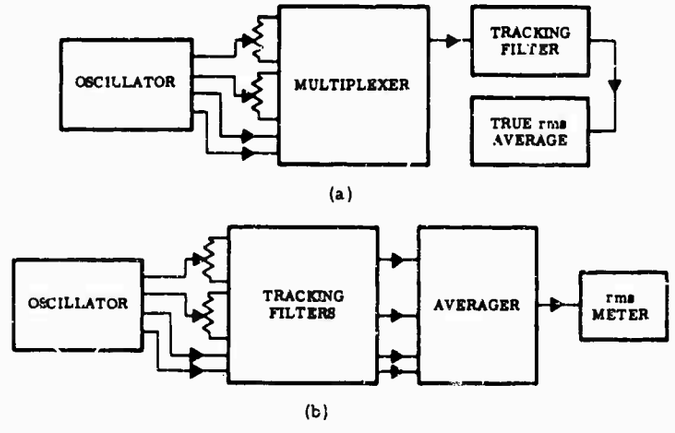

Fig. 5 - Block diagrams of experiments: (a) time-sharing averager, and (b) operational amplifier averager

(a)

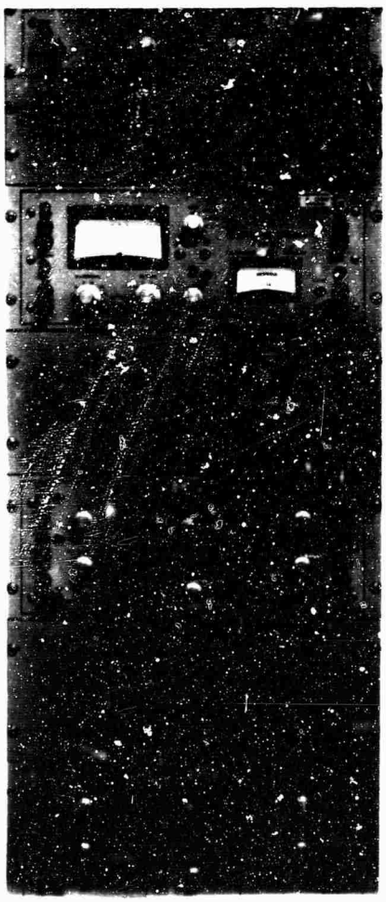

(b)

Fig. 6 - (a) Multiplexing system, and (b) spectral dynamics averaging system

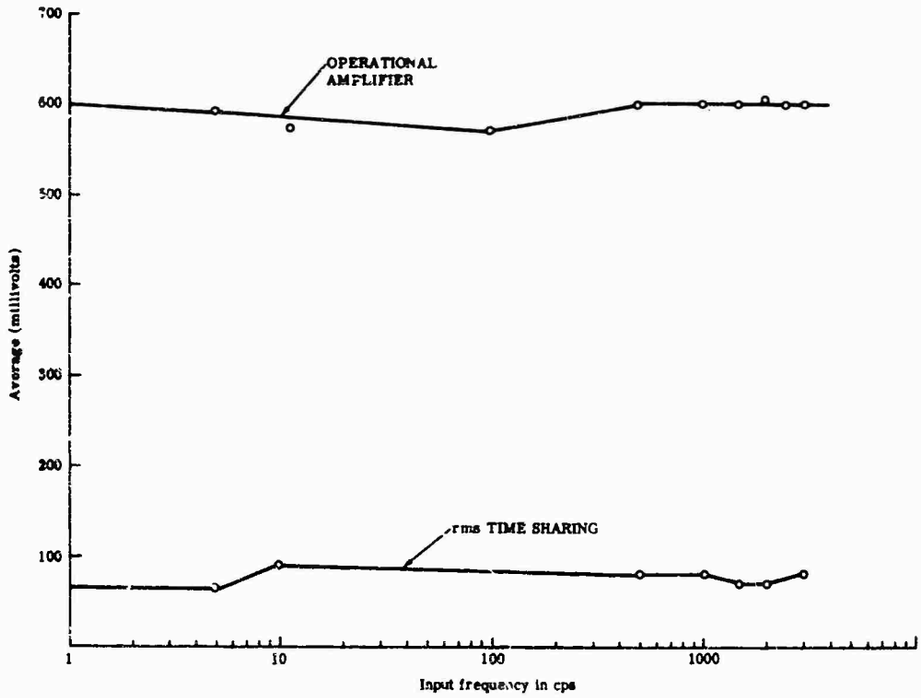

Fig. 7 - Average vs frequency of inputs

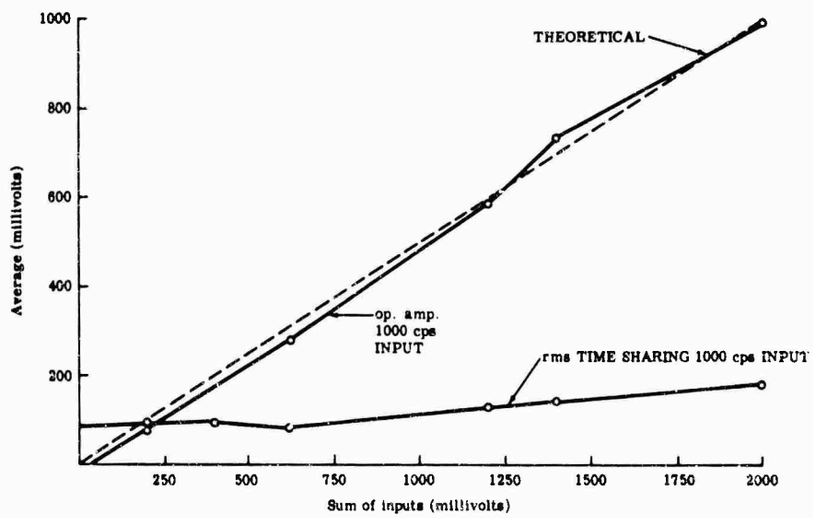

Fig. 8 - Average vs sum of inputs

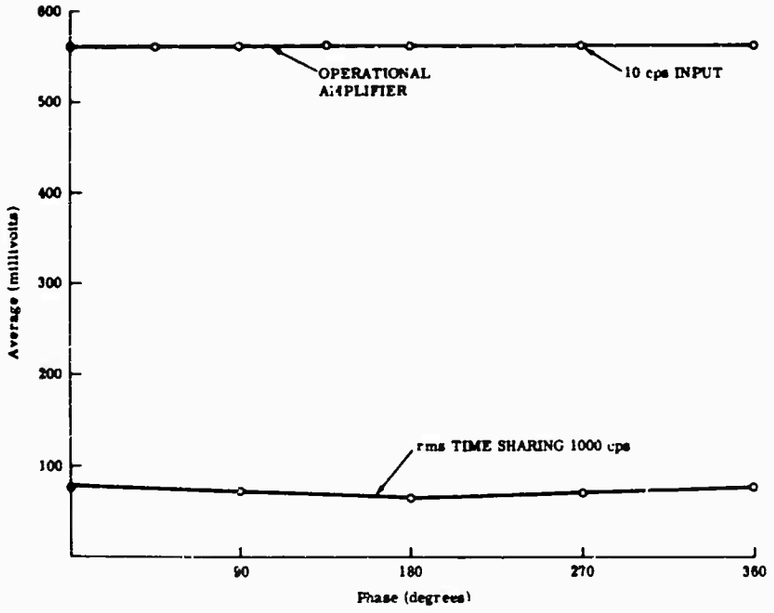

Fig. 9 - Average vs phase difference of inputs

TABLE 1
Comparison of Systems

Criterion	Time Sharing		Operational Amplifier	
	Theoretical	Experimental	Theoretical	Experimental
Phase	Except at high frequency, $v(t)^2$ is a function of phase.	A function of phase. Maximum error equal to 25 percent.	Not a function of phase.	Not a function of phase.
Fundamental	Averages on nw where w is the fundamental frequency.	Does not average on fundamental.	Averages on fundamental.	Averages on fundamental.
Linearity	Linear at high frequencies.	Linear at high frequencies. Low level due to high scanning frequency and characteristics of multiplexer.	Linear	Linear

REFERENCES

1. Erwin Kreyszig, Advanced Engineering Mathematics, Wiley, New York, 1962
2. J. D. Tebbs, "Time Shared Average," Sandia Corp. Organization 7335 informal memo
3. L. R. Burrow, Jr., "Some Analog Methods for Power Spectral Density Analysis," Instrument Soc. Am. 20th Ann. Conf. Preprint No. 1.5-3-65-1

* * *

CONTROL TECHNIQUES FOR MULTI-SHAKER VIBRATION SYSTEMS*

Richard A. Arone
Wyle Laboratories
Huntsville, Alabama

and

Paul A. Brock
Sine Engineering Company
Granada Hills, California

The problems associated with the control of a multi-shaker operation during sinusoidal and random vibration testing are complex because of the severe, unpredictable, and sometimes nonlinear effects of large structures under test, as well as possible differences in the individual shaker servo components. This paper discusses possible methods for performing these tests and outlines the requirements for equipment and basic operating characteristics of an automatic vibration control system used for an eight-shaker vibration test program.

INTRODUCTION

Wyle Laboratories, Huntsville Facility, is currently conducting a high-force vibration test program for North American Aviation on the Saturn V vehicle, S-II structures. The program involves both sinusoidal and random vibration testing utilizing an eight-Hydrashaker system capable of delivering 400,000 force-lb into specimens 33 ft in diameter, 30 ft high, and weighing in excess of 50,000 lb. Figure 1 shows the vibration test area and specimens.

Although several testing programs have been performed using multi-shaker systems, the complete control of eight individual hydraulic shakers is new. Previous experience has shown that such obvious methods as multiple random control systems cannot even operate with, to say nothing of completely controlling, some types of structures. Other methods must, therefore, be examined as an aid to final selection of a specific method of controlling a given specimen under a particular method of excitation.

Because of the extremely high cost of the test specimens, every possible consideration must be made to insure that they are not overtested. A major structural failure due to overtest could result in failure of the whole testing program. For this reason, every effort must be made to provide a control capability which will allow limitation of test levels to prevent overtest.

DEFINITION OF SINUSOIDAL CONTROL SYSTEM PARAMETERS

The general concept most often used in defining control system input parameters is that of locating the control sensors at points which can be identified as interfaces between main structural elements. If it is assumed that flight tests of the vehicle produced information defining acceleration levels at this interface, a reasonable simulation of the flight environment may be obtained by vibrating the structure at this interface and controlling the levels at the interface to those encountered in flight. It is possible and highly probable, however, that it may not be possible to produce and/or control these levels at all frequencies of interest. This problem arises from three causes:

*This paper was not presented at the Symposium.

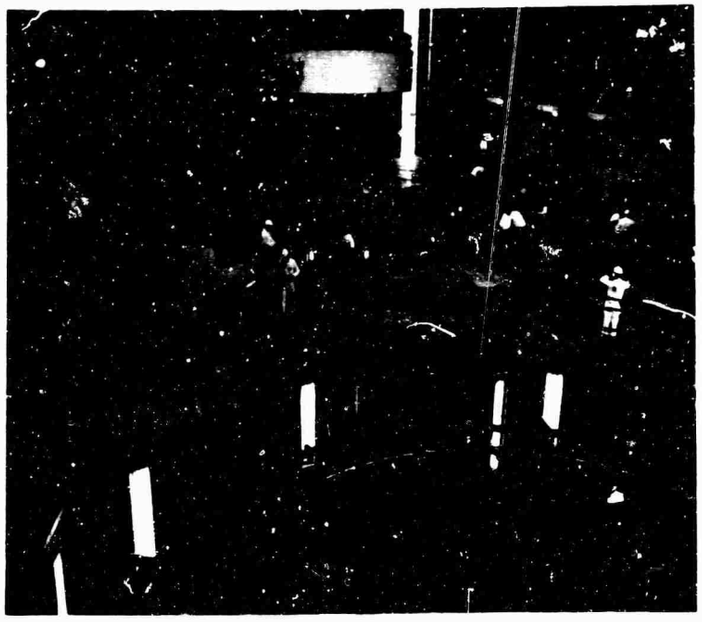

Fig. 1 - High-force vibration test area

1. The shaker and fixture system may present a mechanical impedance vastly different from that provided by the interfacing flight structure and may thus affect the performance of the test structure extremely differently than that of the flight structure. These differences are caused by the fact that point sources (multiple shakers) are used to drive the specimen rather than distributed sources, such as aerodynamic buffeting, and any fixturing or restraints terminate in points rather than being continuous loads (long shell structures). The choice of control points, therefore, can be strongly affected by the actual structures and fixturing involved. That is to say, the motion of total test specimen is controlled as much by the configuration of the fixturing and restraints as it is by the choice of control locations.

2. The control systems are generally limited to a specific number of control points. The behavior of the specimen between these points is somewhat dependent on the location of these control points. Proper choice of these locations (most probably by "cut and try" methods) will tend to make the vibration between the control points predictable, but only to a limited degree.

3. Unless information other than control level amplitudes and phase are used as a basis for control, the shakers and/or control accelerometers may interact (crosscouple), producing signals which cause large errors in test level.

SINUSOIDAL CONTROL SYSTEM CHARACTERISTICS

A sinusoidal control system is designed specifically to provide signals into the Hydra-shaker control amplifiers which will maintain a specific amplitude and phase control of acceleration signals at the control accelerometers. Any control system operating on a single shaker will have certain dynamic limitations. These limitations are related to frequency sweep speed, filter bandwidths, compressor time constants, structural resonances, etc. The analyses presented in this paper describe these limitations as they relate to the Spectral Dynamics Corporation (SDC) servo control system. Figure 2 shows the control system located in the high-force instrumentation control room.

The control system, when used in controlling several shakers coupled together in some way, may incur other dynamic limitations to shaker control. These limitations are due to crosscoupling, that is, the introduction of energy from one shaker into the control accelerometer of another shaker by the coupling between. If this crosscoupled energy tends to increase the amplitude of the structure at a control point to a greater degree than the shaker amplitude specifically referenced to that channel, the control system will completely turn off the reference shaker. Since the energy is coming from some other shaker than the reference, the control of the specimen is lost.

Fig. 2 - High-force instrumentation control room

It is important that this problem be carefully investigated because (a) the specimen may be overtested in sinusoidal tests, and (b) the information gained in the analysis of the sinusoidal control system can be used as a basis for analysis of the random control system.

POSSIBLE SOLUTIONS TO SINUSOIDAL CONTROL PROBLEMS

Crossfeed as Solution to Multi-Shaker Interaction

Under crosscoupling conditions, when a control accelerometer is receiving most of its input energy from a shaker which is not referenced to the subject control accelerometer, the controller will turn off the shaker referenced to that control accelerometer. When this occurs, the subject controller cannot affect the amplitude or phase of the signal at the control accelerometer. If some of the signal information from the other controlling channels is crossfed into the controller of interest, that controller will always get an input signal and will never completely turn off. There are three possible advantages of the crossfeed method of correction:

1. During shut-off conditions, because of crossfeed, the phase controller can still be active. This means that when the signal comes back up, the phase of that signal will be correct.

2. When controllers are completely turned off, they tend to saturate, a condition which causes a delay in their turn-on cycle. The crossfeed tends to keep the controller from going into this saturated condition, thus speeding recovery time.

3. The crossfeed from the active channel tends to reduce the level of all of the other channels, thus reducing the overtest level.

Average Selection Control Systems

Equipment is available which can produce the arithmetic average of several signals. If, in the case of shaker systems, the outputs of all the control accelerometers are averaged, this amplitude signal can be distributed as a control signal for all shakers. The advantage of this system is that the high levels at certain control points, caused by crosscoupling, will tend to suppress the most active driver level so that the specimen may not be unduly stressed.

Peak Selection Control Systems

This control method utilized a system which detects the accelerometer signal having the highest amplitude level and delivers this signal to the compressor systems as the control signal. The highest level existing in the system is the control level. Overtest cannot exist, except in the case of especially poor choice of accelerometer locations.

Average Selection with Peak Override

An average signal may be used for control when the specimen is not responding in an extreme fashion. When extreme levels exist in only a few locations, however, the average signal will not reduce those extreme levels sufficiently to prevent severe overtest. By combining averaging methods with a peak selector system, it is

possible to control not only on the average during normal testing, but also any extreme signals when they exceed the average by pre-selected amounts. The test may, therefore, be run at the defined test levels, except during those times when the specimen response is such that damage may result. At those times, the level will be reduced to protect the specimen.

Individual Peak Override Controls

The SDC control system is designed so that two input signals may be used as control references; the system selects the larger of these two inputs. This capability may be used in the following ways:

1. The second input can be connected to the accelerometer signal from an adjacent shaker control point. If that other control point is receiving energy from the first shaker, so that the level at the second control point exceeds the level at the first shaker control point, the controller will reduce the level of the first shaker to suppress the excitation to the second control point.

2. The second control input may be driven from an accelerometer adjacent to the first control accelerometer so that if one accelerometer fails or comes off, the control signal is not lost.

3. The first control input may be driven from an averaging system to control average level of acceleration. The second channel is connected to a control accelerometer adjacent to the one used for averaging signal. The sensitivity of that channel is adjusted to a level somewhat higher than that of the average so that if that control signal becomes excessive, the excessive signal will control rather than the average signal.

4. It may be desirable to place the second control accelerometer on the shaker head rather than on the fixture so that, in the case of decoupling of the load from the shaker head, the maximum shaker output may be limited to protect the shaker from acceleration overload or to limit shaker displacement.

5. The second input can be connected to the force signal from the shaker and the sensitivity of that channel can be adjusted to a specific force level so that if the force of the shaker becomes excessive, the channel will control on the force signal and limit the input to the specimen.

DYNAMIC CHARACTERISTICS OF AMPLITUDE AND PHASE CONTROL SYSTEM

Figure 3 shows in block diagram form a single channel of the servo control system. Several of the parts of this system have limited frequency response characteristics which affect the behavior of the total system. The effect of these frequency responsive elements is to control the phase and amplitude of the carrier (fundamental shaking frequency) signal provided by the control system. These response effects are related to system performance in the following ways:

1. The instantaneous phase of the control signal is modified so that without correction the movement of various shakers in the system may be in opposite directions. The effect of the phase controller is to eliminate these instantaneous phase differences so that all shakers will be moving in the same direction at the same time.

2. The mean levels of the shaker amplitudes are modified by the responses so that the same force or acceleration levels are not found at all control points. These effects are related to the phase and amplitude of the envelope of the carrier as detected and averaged rather than the instantaneous values of the carrier itself. The pertinent effects of the frequency responsive elements from this standpoint are related to their effect on the phase and amplitude of the detected envelope (modulation).

The main frequency responsive elements are the Hydrashaker and its servoamplifier, the dynamics of fixture and specimen, the tracking filter, the smoothing (compressor speed) of the amplitude detector and controller, and any smoothing used in the phase detector and controller. Of these, only two can be controlled by the test engineer: the compressor speed and the tracking filter bandwidth. The other items are controlled by the equipment manufacturer or are uncontrolled and undefined responses of fixture and specimen. This section defines the capability of controlling the total system by selecting those controllable parameters to optimize the control of the system for certain specified limits assumed for those items which are beyond the control of the test engineer.

The following parameters are considered available to the test engineer as variables:

1. Tracking filter bandwidths of 10 and 50 cps; and

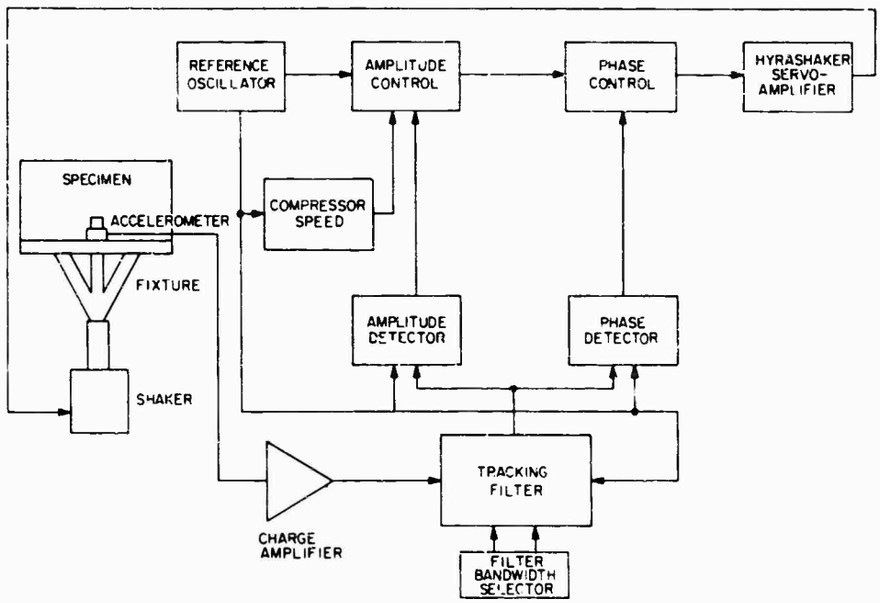

Fig. 3 - Single channel of SDC servo control system

2. Compressor speeds of 10 to 3000 db/sec (RC time constants of 16 to 0.05 sec).

The following parameters are considered fixed by equipment manufacturers or test specifications:

1. Phase control speed of 300 deg/sec;

2. Fundamental response of Hydrashakers, the important effects of which will be considered as part of the fixture and specimen responses; and

3. The oscillator sweep speed which is specified.

The following assumptions are made with respect to specimen, fixture, and Hydrashaker responses, since prior to testing they cannot be defined:

1. For the purposes of this analysis no crosscoupling is assumed; that is, each shaker system is evaluated as an individual system.

2. The Q (amplification factor) of any resonance does not exceed 100.

3. All structural effects are linear with amplitude.

4. The upper frequency limit of testing is 300 cps.

DISCUSSION OF PHASE CONTROL RESPONSES

The control of phase is required because of two factors: (a) the Hydrashaker and its servoamplifier have an acceleration output to voltage input phase response which is a function of frequency; and (b) structural resonances and antiresonances produce extreme phase changes as the driving frequency is swept through their natural frequencies. Of these two responding systems, only the second will be considered since the phase changes due to structural responses can occur at much faster rates than do Hydrashaker responses.

One possible source of phase control response limitation is the tracking filters, since these filters appear within the phase control loop. If it is assumed that the narrowest filter of 10 cps bandwidth is used at the highest test frequency, the response may be defined in a manner similar to a resonant system, that is, by determining an equivalent Q:

$$Q = \frac{f_c}{BW} = \frac{300}{10} = 30 ,$$

where f_c is the center frequency of the filter and BW is the bandwidth of the filter (-3 db). This Q is substantially less than the maximum of 100 assumed for structural responses. In addition, it may be assumed that the narrow filter will not be used at higher than 100 cps,

providing an equivalent Q of 10 which is much below the possible structural responses. This factor will, therefore, be ignored for this part of the analysis.

As the driving frequency is swept through a resonance or antiresonance, a phase change of 180 deg from mechanical output at low frequencies to that at the higher frequencies is observed. Of this change, 90 deg will occur within the 3-db bandwidth of the resonance. Assuming a maximum Q of 100, we thus have a 90-deg change in 1 percent of the resonance frequency. If the sweep rate is 1 octave/min 1 percent of the center frequency of an octave would be swept through in 1/100 min or 0.6 sec. Since this change corresponds to a maximum of about 90 deg, the phase rate becomes:

$$\frac{90 \text{ deg}}{0.6 \text{ sec}} = 150 \text{ deg/sec}.$$

Since the system capability is 300 deg/sec, no loss of phase control should result even for such extreme situations as Q's of 100.

DISCUSSION OF AMPLITUDE CONTROL RESPONSES

In any amplitude control system utilizing tracking filters for elimination of noise and harmonics, there are two predominant time constants: the response time of the amplitude controller (compression speed) and the response time of the tracking filter. Basic control system theory requires that these time constants provide less than a 180-deg phase shift of the control signals around the control loop when the control gain around the loop is near unity. This situation may be achieved by making the compression speed as slow as possible. It is desirable, however, to make the compression speed as fast as possible so that the amplitude may be controlled as quickly as possible.

The addition of bandwidth limiting elements, such as structural resonances and tracking filters or both, tend to limit the allowable compression speed because these elements add phase lags to the control loop which tend to make it unstable. SDC suggests that, as a rule, the maximum compression speed should not exceed eight times the bandwidth of tracking filters. The selection of filters of 10 and 50 cps implies, therefore, maximum compression speeds of 80 and 400 db/sec, respectively. Since the filter networks used in tracking filters are multipole crystal lattice networks, their envelope phase response characteristics change much more rapidly with time than simple second order resonances. SDC suggests that the response times (an indication of phase response) of these crystal filters is on the order of 4/BW (4 sec divided by filter bandwidth) as compared to about 1.2/BW (1.2 sec divided by bandwidth) for a simple second order resonant system. If tracking filters are used, the destabilizing effects of resonant structural elements can be ignored if their bandwidths are more than one-third of the tracking filter bandwidths. The regions in which these resonances become important will be evaluated below, following the discussion of the effects of the tracking filter.

It was assumed previously that the possibility exists for resonances having Q's as high as 100. This Q implies an amplitude change of 100 or 40 db. It has also been shown that the expected sweep rates are 1 octave/min or 1/100 of a given frequency in 1/100 min (i.e., 0.6 sec). The amplitude will have moved from 0.7 of the peak through the peak and back to 0.7 of the peak in this time. At 1 octave away, the response is down approximately 0.7/Q of the peak value. Thus, the changes are typically 3db/0.3 sec = 10 db/sec near the peak and 43 db/60 sec = 2/3 db/sec at the skirts. Even the slowest chosen compression speed appears adequate to control the system on the basis of these criteria.

It is necessary to evaluate the effect of resonances on the control loop stability, since a Q of 100 implies bandwidths much narrower than that allowable for system stability based on the phase lag effects discussed above. It is extremely doubtful that Q's greater than 30 would be experienced below 20 cps. If a criteria of compression speeds equal to 24 (the SDC figure of eight times the bandwidth multiplied by the ratio of response times of a second order system to a crystal filter) times the bandwidth be employed for defining the maximum compression speed limit due to resonances, at 5 cps the maximum allowable speed is:

$$24BW = \frac{24 f_c}{Q} = \frac{24 \times 5}{30} = 4 \text{ db/sec},$$

at 20 cps, it is

$$24BW = 24 \times \frac{f_c}{Q} = \frac{24 \times 20}{30} = 16 \text{ db/sec},$$

and at 100 cps, it is

$$24BW = \frac{24 \times f_c}{Q} = \frac{24 \times 100}{100} = 24 \text{ db/sec}.$$

Since these compression speeds, although conservatively calculated, represent some extreme limitations to the control capability, the actual Q's should be carefully determined before any high-level tests are attempted.

RANDOM VIBRATION CONTROL METHODS

Random Averaging

The random averaging vibration control system is shown in Fig. 4. Basically, this method consists of averaging the eight control accelerometers and feeding the average PSD spectrum and level into an automatic analyzer/equalizer random control console. The random control console is used to adjust the input signal to provide proper equalization of acceleration levels within the confines of the test spectrum. The output signal from the random control console is fed into each of the eight amplitude servo control units, which provide a specified overall vibration level into each of the eight-Hydrashaker systems. In this instance the spectral density of the random control signal is equal to the average of the spectral densities of the input signals at each frequency. Thus, the average of the spectral densities of the input signals can be controlled to a prescribed shape.

The three principal units in the random averaging control system are the averager, the analyzer/equalizer, and the amplitude servos.

Random Averager – The random averager will accept as many as ten input signals from signal conditioning amplifiers. The output signal of the unit is equal to the average of the spectral densities of the input signals at each frequency. The unit has the useful property of being phase-insensitive. Instantaneous averaging devices do not produce a spectral density which is the average of the spectral densities of the inputs because reinforcement and cancellation may occur.

During random vibration, each of the input signals is gated to the output for a fixed period of time. The gate period is selected so that it is large compared to the inverse of the analyzer filter bandwidth and small compared to the averaging time of the networks following the detectors in the spectral analyzer. These conditions can be met simultaneously, because the product of the averaging time and the analyzer filter bandwidth must be fairly large to insure adequate accuracy in a statistical sense for the analyzer. Figure 5 shows in block diagram form the basic operation of the averager.

Automatic Analyzer/Equalizer Random Control Console – The automatic analyzer/equalizer random control console provides the necessary shaping of the input signal to reproduce the random vibration level requirement within the test specifications. The vibration spectrum can be programmed before power is applied to the shakers. When operation is initiated, proper servo dynamic conditions are automatically maintained as programmed.

The random console incorporates a meter readout and control slider adjustment for each bandpass channel, enabling on-line observation of the random spectrum and single channel adjustments.

Amplitude Servo – The amplitude servo is used in the random control system to provide

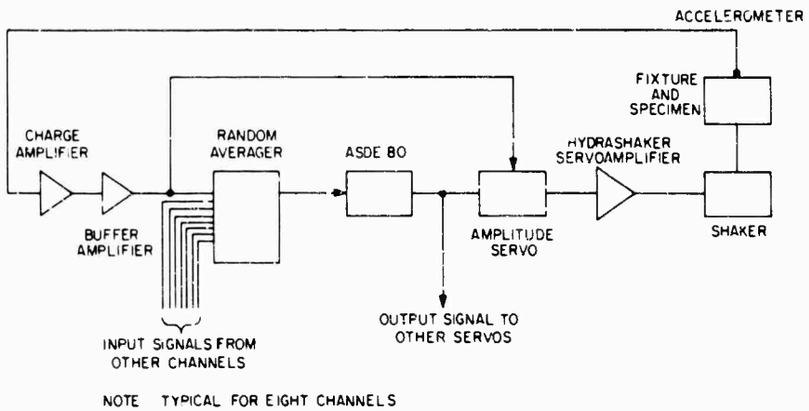

Fig. 4 - Block diagram of random vibration control system

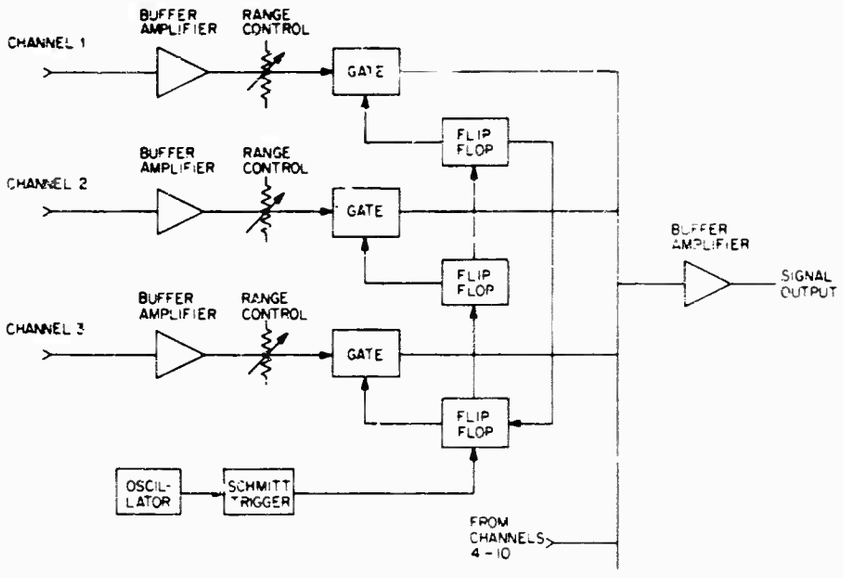

Fig. 5 - Block diagram of random averager

individual gain control for each shaker and metering for that channel. The amplitude servos are set to provide equal g rms levels into the eight-shaker system.

Discussion of Method – Averaging, though certainly an improvement over single accelerometer control, can allow overtesting to take place since one input may increase while another decreases. In such a case, the average would tend to remain the same, but a portion of the specimen is subjected to excessive g levels. Conversely, selection and control on the highest g level present would cause portions of the specimen to be undertested. However, the combined information from the several control points would represent the general response of the specimen.

For the averaging method, a random averaging device which essentially samples each of the input control signals for a short duration of time and feeds the signal to an automatic random analyzer/equalizer is used. The detector circuits in the automatic random analyzer do the actual averaging. Simple instantaneous addition of the random input signals would not yield a signal having the desired averaged spectrum because of phase coherence. Cancellation problems are eliminated when the signals are detected in the automatic analyzer.

Multiple Automatic Random Control Consoles

The use of multiple automatic control consoles provides the most versatile arrangement for multiple shaker operation in that each shaker is driven by its own random console. Independent spectrum programming is thus permitted, and this affords the most practical method of shaping a vibration profile.

The automatic random control consoles could be combined into a single eight-channel system, with limited frequency range. This system would incorporate eight sets of filters with 20 filters per set to cover the required frequency range. Equalization controls and power spectral density readout meters would be located on the front of the unit to form a linear group of equalizer controls and analyzer readout meters. A single noise generator would drive the entire 160 equalizer channels.

For the eight shakers, there would be effectively eight random control consoles and eight control accelerometers. The multiple random control console would be programmed so that each analyzer/equalizer channel provided the necessary shaping of the input signal to reproduce the random vibration level requirement within the test specifications.

The multiple random control console would give the desired random level and spectrum at the control points located around the input to the specimen, provided the crosscoupling between the control points is not excessive. As crosscoupling increases, a point would be reached where the random spectrum at some of the control points would be out of specification and uncontrolled. Monitoring the analyzer outputs

of the multiple random control console would immediately reveal which control accelerometers are being controlled to the test specification and which are uncontrolled.

Single-Point Equalization

The single-point equalization method basically uses a single control accelerometer and an automatic analyzer/equalizer random control console. For multiple shaker operation, the output of the random control console is fed into a power amplifier containing multiple individually gain-controlled outputs. Each output of the amplifier is then fed to its particular shaker system.

During random vibration testing, the input signal from a single accelerometer is shaped in the automatic random control console to provide the random vibration test spectrum. The overall random vibration levels at each of the shakers are adjusted in the power amplifier so that the shaker output levels are equal. Essentially, utilizing this method the exciters produce an equal vibration level to the specimen, with a spectrum resulting in the proper vibration test spectrum at the single control point.

This method has been used for random testing of large structures. A four-shaker system was employed and during the random vibration testing, the four exciters were adjusted to the same rms output level, as monitored by an accelerometer on each exciter. Spectrum and overall level control was established from one accelerometer fed into an automatic analyzer/equalizer random control console.

This system proved to be a satisfactory method of control with no severe shortcomings. The use of this method, however, assumes that the single control point selected on the specimen is representative of the complete input to the specimen. This does not necessarily hold true and is subject to the distribution characteristics of the test specimen. Since these characteristics are generally unknown, the selection of such a representative point is a difficult task. Most often, the representative point is at best a compromise.

Commutated Tape Recorder Equalization

This method involves recording the outputs of all eight control accelerometers on a tape recorder. A single automatic random control console, in conjunction with a switching system, would correct the spectrum level on one channel and then switch to the next. The system would dwell on each channel for a set period of time. The tape would then be played back to the vibration system, providing the proper vibration spectrum.

This is essentially an open-loop control method and assumes that the system dynamic parameters do not change from the time the recording is made until the playback is complete. The Hydrashaker vibration system, however, is subject to change in operating conditions with time and does not reach the high degree of time stability required by this method.

* * *